

**SUSTAINED RELEASE MICROPARTICLES FOR PULMONARY
DRUG DELIVERY**



ROBERT OWEN COOK

A THESIS SUBMITTED FOR THE DEGREE OF DOCTOR OF PHILOSOPHY

2004

**DEPARTMENT OF PHARMACEUTICS, UNIVERSITY OF LONDON
SCHOOL OF PHARMACY, 29/39 BRUNSWICK SQUARE, LONDON,
WC1N 1AX, UK.**



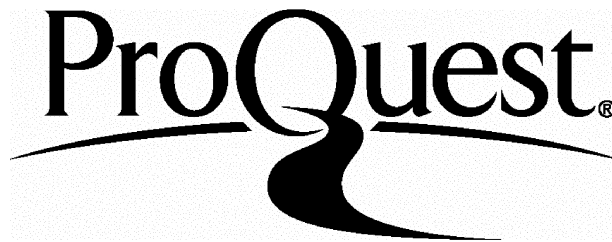
ProQuest Number: U186520

All rights reserved

INFORMATION TO ALL USERS

The quality of this reproduction is dependent upon the quality of the copy submitted.

In the unlikely event that the author did not send a complete manuscript and there are missing pages, these will be noted. Also, if material had to be removed, a note will indicate the deletion.



ProQuest U186520

Published by ProQuest LLC(2016). Copyright of the Dissertation is held by the Author.

All rights reserved.

This work is protected against unauthorized copying under Title 17, United States Code.
Microform Edition © ProQuest LLC.

ProQuest LLC
789 East Eisenhower Parkway
P.O. Box 1346
Ann Arbor, MI 48106-1346

Acknowledgements

I would like to sincerely thank my academic supervisor, Professor Ian W. Kellaway, for his guidance and encouraging discussions throughout the research project. I would also like to acknowledge Dr. Rupi K. Pannu, my industrial supervisor at AstraZeneca, for her interest throughout the project and assistance with several practical issues.

AstraZeneca R&D Charnwood is gratefully acknowledged for sponsoring this research project.

I am very grateful to the technical staff at the University, in particular Dave for all of the SEM work, Keith for resuscitating equipment on a number of occasions, and Lionel and John for constructing the horizontal diffusion cell.

Thanks to the postgraduate students in the group and department who made the last three years thoroughly enjoyable, in particular Jean-Luc and Alastair.

I would like to thank my parents for their unwavering support throughout, and finally, Jessica for all of her motivation and optimism during my research and especially for making the transatlantic move to London.

Abstract

In this study, several formulation approaches for generating sustained release (SR) microparticles suitable for pulmonary deposition are described. The model drug chosen for investigation was the hydrophilic β_2 -adrenoceptor agonist, Terbutaline Sulphate (TS), used in the treatment of asthma. A particular challenge to achieving suitable sustained release profiles arose from the high water solubility and ionised state of TS.

Initial investigations focused on generating TS microcrystals, which would be subsequently coated with a SR excipient. A controlled crystallization method was developed in which TS was crystallized from an anti-solvent, which contained particle size restricting growth retardants. Significantly smaller crystals were obtained in the presence of growth retardants relative to crystallization without retardants. However, the smallest crystals obtained (3.6 μm) were too large for progression, as the application of a SR coat to such crystals would have increased particle size beyond that suitable for inhalation.

The next investigation assessed TS release from a polysaccharide matrix particle containing molecularly dispersed active. Drug release was measured (HPLC) using a custom-built diffusion cell, designed to mimic release at the pulmonary epithelium. Release profiles showed that a degree of SR was possible from polysaccharide-based particles; although, SR was not sufficient for further development.

Finally TS nanoparticles, obtained from an emulsion-template process, were encapsulated (spray-drying) within hydrophobic microparticles of respirable particle size. Several optimised formulations of this type provided promising *in-vitro* sustained release of the active at a variety of drug loadings and in a range of release media. The most useful SR excipient chosen for further development was hydrogenated palm oil, which was observed to coat the nanoparticles effectively. *In-vitro* deposition profiles were determined for a selection of formulations using an Andersen Cascade Impactor, and it was shown that deposition profiles were formulation-dependant and of size ranges suitable for pulmonary deposition.

Chapter 1: Introduction	12
1.1 Pulmonary Drug Delivery	13
1.1.1 Anatomy, Physiology and Histology	14
1.1.2 Particle Deposition in the Airways	16
1.2 Pulmonary Disease and Therapeutics	21
1.2.1 Asthma	21
1.2.2 Chronic Obstructive Pulmonary Disease	23
1.2.3 Other Medical Conditions Treated by the Pulmonary Route	24
1.3 Pulmonary delivery device technology	26
1.3.1 Nebulisers	26
1.3.2 pMDI Device Technology	29
1.3.3 DPI Device Technology	33
1.4 Aerosol Particle Generation	36
1.4.1 Crystallization/Micronisation	36
1.4.2 Spray-Drying	37
1.4.3 Supercritical Fluids	38
1.5 Sustained Release	39
1.6 Pulmonary Sustained Release	43
1.6.1 Advantages of Pulmonary Sustained Release	43
1.6.2 Barriers to Pulmonary Sustained Release	44
1.6.3 Methods of Achieving Pulmonary Sustained Release	46
1.6.3.1 Modulation of Dissolution Rate - Salts, Co-precipitates and conjugates	46
1.6.3.2 Liposomes	47
1.6.3.3 Microparticles	49
1.6.3.4 Nanoparticles	51
1.7 Research Scope	51
Chapter 2: Controlled Crystallization of Terbutaline Sulphate	52
2.1 Introduction	53
2.2 Materials	56
2.2.1 Model Drug	56
2.2.2 Growth Retardants	56
2.2.3 Solvents	57
2.3 Methods	57
2.3.1 Crystallization	57
2.3.2 Drying	58
2.3.3 Crystal Sampling	58

2.3.4	Laser Diffraction Particle Sizing	59
2.3.5	Sample Visualisation	59
2.4	Results and Discussion	60
2.4.1	Controls	60
2.4.2	Controlled Crystallization of TS with PVP as Growth Retardant	61
2.4.3	Controlled Crystallization of TS with PAA as retardant	64
2.4.4	Controlled Crystallization of TS with Polysorbate 80 as Retardant	64
2.4.5	Controlled Crystallization of TS with poloxamers as retardant	64
2.4.6	Optimisation of Crystallization Conditions	68
2.5	Conclusion	70
Chapter 3: Polysaccharide Matrix Microparticles		71
3.1	Introduction	72
3.1.1	Matrix Microparticle Excipients I: Chitosan (CS)	72
3.1.2	Matrix Microparticle Excipients II: Sulphated Polysaccharides	73
3.2	Materials	75
3.2.1	Model Drug	75
3.2.2	Matrix Excipients	75
3.2.3	Solvents/Chemicals	75
3.3	Methods	76
3.3.1	Determination of the Concentration of TS by High Performance Liquid Chromatography (HPLC)	76
3.3.1.1	HPLC Conditions/Equipment	76
3.3.1.2	Mobile Phase Preparation	76
3.3.1.3	TS Working Standard Solution (1.0 µg/mL)	78
3.3.1.4	Chromatography	78
3.3.1.5	HPLC System Performance	78
3.3.2	Production of CS/TPP/TS Microparticles	80
3.3.3	Production of Sulphated Polysaccharide Microparticles	81
3.3.4	Design of Horizontal Diffusion Cell for Drug Diffusion Assay	82
3.3.5	Operation of Horizontal Diffusion Cell for Drug Diffusion Assay	82
3.3.6	Determination of TS/Polysaccharide Microparticle Drug Loading	84
3.4	Results and Discussion	85
3.4.1	Determination of the Concentration of TS by High Performance Liquid Chromatography (HPLC)	85
3.4.2	Suitability of Horizontal Diffusion Cell	86
3.4.3	TS Release from CS/TPP Microparticles	86

3.4.4	TS Release from Sulphated Polysaccharide Microparticles I: CGN	90
3.4.5	TS Release from Cation Cross-linked CGN Microparticles	94
3.4.6	TS Release from Sulphated Polysaccharide Microparticles II: DexS	100
3.4.7	TS Release from Sulphated Polysaccharide Microparticles III: ChonS	104
3.5	Conclusion	106
Chapter 4: Formulation of TS Nanoparticles		107
4.1	Introduction	108
4.2	Materials	110
4.2.1	Model Drug	110
4.2.2	Nanoparticle Formulation	110
4.3	Methods	110
4.3.1	w/o Emulsion Preparation	110
4.3.2	Freeze-Drying (Lyophilisation)	111
4.3.3	Nanoparticle Purification	111
4.3.4	Particle Size Characterisation	113
4.3.5	Determination of Viscosity of Suspending Medium used in PCS	115
4.3.6	Particle Morphology Characterisation	116
4.3.7	Determination of Effectiveness of Surfactant Washing Procedure and TS Content of Nanoparticles	116
4.3.8	X-Ray Powder Diffraction (XRPD)	116
4.3.9	Determination of Glass Transition Temperature Using Differential Scanning Calorimetry (DSC)	118
4.4	Results and Discussion	119
4.4.1	Initial TS Particle Formulation From w/o Emulsions	119
4.4.2	TS Nanoparticle Production	120
4.4.3	Surfactant Removal from TS Nanoparticles	124
4.4.4	Morphological Characterisation of TS Nanoparticles	125
4.4.5	Physicochemical Characterisation of TS Nanoparticles	126
4.5	Conclusion	129
Chapter 5: Hydrophobic SR Microparticles Containing TS Nanoparticles		130
5.1	Introduction	131
5.2	Materials	135
5.2.1	Model Drugs	135
5.2.2	Hydrophobic Matrix Forming Excipients	135

5.2.3	Phospholipids	135
5.2.4	Solvents	136
5.2.5	Release Media	136
5.3	Methods	137
5.3.1	Spray-drying	137
5.3.2	Sustained Release Microparticle Characterisation	139
5.3.3	Assessment of TS Release from Sustained Release Microparticles	139
5.3.4	Assessment of TS Release from Sustained Release Microparticles into Simulated Lung Media	139
5.3.5	Differential Scanning Calorimetry (DSC)	141
5.3.6	Dynamic Contact Angle (DCA) Measurement	142
5.3.7	Dynamic Vapour Sorption (DVS)	142
5.3.8	Content Uniformity	143
5.3.9	X-Ray Powder Diffraction (XRPD)	143
5.3.10	Visualisation of TS Nanoparticle Distribution Within Hydrophobic Microparticles	143
5.3.10.1	Focused Ion-Beam (FIB) sectioning	144
5.3.10.2	Confocal Laser Scanning Microscopy (CLSM)	145
5.4	Results and Discussion I: Lipid Excipients	146
5.4.1	Spray-drying TS Nanoparticles with GB as Hydrophobic Matrix Excipient	146
5.4.2	Spray-drying TS Nanoparticles with GB/TP as Hydrophobic Matrix Excipients	149
5.4.3	Entrapment of SS and IB Nanoparticles in Hydrophobic Microparticles	151
5.4.4	Effect of Feed Solvent on Hydrophobic Microparticle Size	151
5.4.5	Physicochemical Characterisation of Lipid Microparticles	158
5.4.6	Effect of Storage upon Particle Size of Lipid Microparticles	163
5.4.7	Effect of Release Media Temperature upon TS Release	165
5.5	Results and Discussion II: Hydrogenated Oil Excipients	169
5.5.1	Assessment of TS Release from HPO Microparticles	169
5.5.2	Effect of Release Media upon TS Release	172
5.5.3	Factorial Design Experiment for Particle Size Optimisation	173
5.5.4	Content Uniformity	176
5.5.5	Comparison of HPO Formulation to GB:TP Formulation I: DCA	177
5.5.6	Comparison of HPO Formulation to GB:TP Formulation II: DVS	178
5.5.7	Stability of HPO Microparticles	179

5.5.8	Visualisation of TS Nanoparticle Distribution Within Hydrophobic Microparticles	182
5.6	Conclusion	186
Chapter 6: Aerosol Development for HPO Microparticles		187
6.1	Introduction	188
6.2	Materials	189
6.2.1	Candidate SR Formulation	189
6.2.2	HFA propellants	189
6.2.3	Additional Chemicals	189
6.3	Methods	190
6.3.1	Procedure for Filling PET Bottles with HFA Propellant	190
6.3.2	Determination of HPO Solubility in HFA Propellants	190
6.3.3	Assessment of Aerodynamic Particle Size	191
6.3.4	Filling, Operation and Validation of Penn-Century DP-4 Insufflator	192
6.3.4.1	Filling and Assembly	193
6.3.4.2	Determination of Emitted Dose (ED)	193
6.3.5	High Speed Photography	193
6.3.6	Assessment of Particle Deposition using Andersen Cascade Impaction (ACI)	193
6.3.6.1	ACI Operation Procedure	195
6.3.6.2	Calculations of FPF, MMAD and GSD	196
6.4	Results and Discussion	197
6.4.1	Formulation of HPO Microparticles into HFA Propellants	197
6.4.2	Determination of HPO Solubility in HFA Propellants	199
6.4.3	Assessment of Aerodynamic Particle Size	200
6.4.4	Validation of Penn-Century DP-4 Insufflator	200
6.4.5	Assessment of Particle Deposition using Andersen Cascade Impaction (ACI)	202
6.4.6	Improvement of Aerosol Performance for SR-TS formulation	204
6.5	Conclusion	211
Chapter 7: General Discussion and Future Directions		213
7.1	General Discussion	214
7.2	Future Directions	219
Appendix		222
References		232

List of Figures

- 1.1.1: Schematic of Weibel lung morphology model
- 1.1.2.1: Relationship between particle size and FEV₁
- 1.1.2.2: Major mechanisms of aerosol deposition in the lung
- 1.1.2.3: Relationship between aerosol particle size and regional deposition
- 1.3.1: Dispersion mechanism for (1) Jet nebuliser and (2) Ultrasonic nebuliser
- 1.3.2: Schematic of (1) pMDI device and (2) metering valve design
- 1.3.3: DPI delivery devices: (1) Turbohaler (2) Nektar pulmonary inhaler
- 1.4.1: Schematic of air-jet mill
- 1.5.1: Effect of drug release profiles on drug plasma concentration versus time:
- 1.5.2: Schematic of rate-controlled transdermal drug delivery patch
- 1.6.3.2: Section of liposome wall

- 2.1.1: Adapted solubility-supersaturation diagram for crystallization
- 2.1.2: Controlled crystallization theory
- 2.4.1.1: TS crystallised from absolute ethanol without retardant
- 2.4.1.2: Micronised TS
- 2.4.2.1: Correlation between PVP concentration and Crystal Yield
- 2.4.2.2: TS crystal aggregates crystallised from 0.25% w/v PVP in absolute ethanol
- 2.4.2.3: Effect of Increased wash volume on crystal aggregates
- 2.4.2.4: TS crystallized from 0.1% w/v PVP in 50:50 absolute ethanol:acetone
- 2.4.5.1: TS crystallized from 4% L44 w/v in absolute ethanol
- 2.4.5.2: TS crystallized from 10% w/v L64 in absolute ethanol
- 2.4.5.3: Correlation between Poloxamer HLB and Particle Size Cut-off diameters
- 2.4.5.4: TS crystallized from 2% L64/2% L101 in absolute ethanol

- 3.1: Pulmonary sustained release formulation aims:
 - 3.1.1.1: Chemical structure of CS
 - 3.1.1.2.1: Structures of CGN (1) *Kappa* CGN: (2) *lambda* CGN (3) *iota* CGN
 - 3.1.1.2.2: Gelation mechanism of *kappa* CGN
 - 3.1.1.2.3: Gelation mechanism for *iota* CGN
 - 3.3.1.1: General HPLC set-up:
- 3.3.2: Appearance of CS/TPP following particle production method
- 3.3.4.1: Image of horizontal diffusion cell showing sampling ports
- 3.3.4.2: Simplified schematic for horizontal diffusion cell
- 3.3.6: Determination of Maximum TS release from microparticles
- 3.4.1: Sample HPLC chromatogram
- 3.4.3.1: 50:50 TS:CS microparticles (milled product)
- 3.4.3.2: 10:90 TS:CS microparticles (milled product)

- 3.4.3.3: Effect of TS:CS ratio upon drug release from CS microparticles
- 3.4.3.4: Effect of drug loading on first order release constant, k
- 3.4.4.1: 10:90 CGN 109 microparticles (milled product)
- 3.4.4.2: 10:90 CGN 911 microparticles (milled product)
- 3.4.4.3: Effect of CGN type on TS release
- 3.4.4.5: 'Early time' plot for % TS release vs. $\sqrt{\text{time}}$ for drug release from CGN
- 3.4.4.6: 'Late time' drug release kinetics
- 3.4.5.1: Effect of crosslinking kappa CGN with potassium ions, on TS release
- 3.4.5.2: Effect of crosslinking iota CGN with calcium ions, on TS release
- 3.4.6.1: Effect of membrane choice upon TS release
- 3.4.6.2: Effect of DexS (different molecular weights) on TS release
- 3.4.7.1: Spray dried TS/ChonS microparticles
- 3.4.7.2: Effect of ChonS process method on TS release

- 4.1: Methodology for nanoparticle production
- 4.3.1.1: Emulsification
- 4.3.1.2: Freezing step
- 4.3.4: Typical set-up of PCS instrument
- 4.3.5: U-tube viscometer, with relevant standardised lettering
- 4.4.1: TS particles generated from early emulsification studies
- 4.4.2.1: Effect of surfactant concentration on TS particle size
- 4.4.2.2: Effect of Homogenisation speed on TS particle size
- 4.4.2.4: Effect of TS concentration in aqueous phase on TS particle size
- 4.4.2.4: PCS particle size distribution generated for optimised TS nanoparticles
- 4.4.4.1: Freeze-dried w/o emulsion
- 4.4.4.2: Washed TS nanoparticles Image shows good correlation with PCS data
- 4.4.4.3: TEM image of TS nanoparticles
- 4.4.5.1: Spray-dried pure TS from aqueous solution
- 4.4.5.2: Diffractograms of crystalline micronised, and amorphous TS
- 4.4.5.3: Diffractograms of crystalline micronised and nanoparticulate TS
- 4.4.5.4: DSC traces of crystalline micronised and nanoparticulate TS

- 5.1: Droplet-Particle drying rate curve
- 5.3.1: Outline and photograph of spray dryer
- 5.3.10.1: FIB process schematic
- 5.4.1.1: Light microscopy image of GB formulation (66% w/w TS content)
- 5.4.1.2: GB spray-dried formulation (66% w/w TS content)
- 5.4.1.3: GB spray-dried formulation at 59 °C inlet temperature
- 5.4.1.4: Spray-dried GB microparticles (14.1% w/w TS content)
- 5.4.2.1: Effect of GB:TP ratio upon drug release microparticles

- 5.4.3:** Sustained release of IB and SS
- 5.4.4.1:** Particle size vs. DCM content in spray-drying feed
- 5.4.4.2:** TS containing GB:TP 60:40 microparticles spray-dried from DCM
- 5.4.4.3:** TS containing GB:TP 60:40 microparticles spray-dried from 50:50 CFM:DCM
- 5.4.4.4:** Variation of TS release from GB:TP 60:40 microparticles
- 5.4.4.5:** Effect of storage upon TS release from GB:TP 60:40 microparticles
- 5.4.5.1:** DSC thermal profile for freshly prepared lipid microspheres
- 5.4.5.2:** DSC thermal profiles – effect of storage
- 5.4.6.1:** Freshly prepared GB:TP 60:40 microparticles (stored in freezer)
- 5.4.6.2:** Oven-stored GB:TP 60:40 microparticles
- 5.4.6.3:** Oven-stored lecithin-free GB:TP 60:40 microparticles
- 5.4.7.1:** Effect of temperature on TS release from GB:TP 60:40 microparticles
- 5.4.7.2:** Effect of temperature on TS release from lecithin-free microparticles
- 5.5.1.1:** SEM image for HPO microspheres, (13.0% w/w TS content)
- 5.5.1.2:** Effect of drug loading on TS release from HPO microparticles
- 5.5.2:** Effect of release media on TS release from HPO microparticles
- 5.4.4:** Content uniformity for three batches of HPO microparticles
- 5.5.7.1:** DSC thermal profiles of HPO-based formulations
- 5.5.7.2:** Diffractogram of HPO
- 5.5.7.2:** Diffractograms of spray-dried blank HPO and HPO/TS microparticles
- 5.5.8.1:** FIB sectioned cluster of TS/HPO microparticles
- 5.5.8.2:** CLSM of nanoparticle encapsulation within HPO microparticles
- 5.5.8.3:** CLSM fluorescence scan through individual microparticles

- 6.3.4:** Penn-Century model DP-4 dry powder insufflator.
- 6.3.6:** ACI schematic
- 6.4.1.1:** Flocculation in HFA formulations of SR-TS microparticles
- 6.4.1.2:** Photomicrographs of spray dried HPO following exposure to HFA
- 6.4.4:** Delivery efficiency from DP-4 insufflator for different formulations
- 6.4.5:** Delivery of SR-TS from DP-4 Insufflator (high speed photography)
- 6.4.6.1:** ACI profile for SR-TS with 5 ml and 3 ml air bolus volume
- 6.4.6.2:** ACI profile for SR-TS formulations with increasing w/w DPPC content
- 6.4.6.3:** Effect of DPPC content on TS release profile
- 6.4.6.4:** Effect of 5% v/v ACT in DCM feed, upon ACI deposition profile

Abbreviations/Symbols

ACI	Andersen cascade impactor	MMAD	Mass median aerodynamic diameter
ACT	Acetone	mPa s	Millipascal seconds
AM	Alveolar macrophage	M_t	Amount of drug remaining at time t
APS	Aerodynamic particle sizer	MW	Molecular weight
CFC	Chlorofluorocarbon	NP	Nasopharyngeal
CFM	Chloroform	OED	Oligoester derivative
CGN	Carrageenan	OLA	Oligolactic acid
ChonS	Chondroitin sulphate	OP	Oropharyngeal
CLSM	Confocal laser scanning microscopy	P	Pulmonary
COPD	Chronic obstructive pulmonary disease	PAA	Poly(acrylic acid)
CS	Chitosan	PCS	Photon correlation spectroscopy
CST	Cholesterol	PEG	poly(ethylene glycol)
CV	Coefficient of variation	PET	poly(ethylene tetraphthalate)
d_a	Aerodynamic diameter	PLA	poly(lactic acid)
DCA	Dynamic contact angle	PLGA	poly(lactic-co-glycolic acid)
DCM	Dichloromethane	pMDI	Pressurised metered dose inhaler
DexS	Dextran sulphate	PVP	poly(vinylpyrrolidone)
d_g	Geometric diameter	PW	Paraffin wax
d(H)	Hydrodynamic diameter	RH	Relative humidity
DIC	Differential interference contrast	RPM	Revolutions per minute
DPPC	Dipalmitoylphosphatidylcholine	SCF	Supercritical fluid
DSC	Differential scanning calorimetry	SD	Standard deviation
DSPC	Distearoylphosphatidylcholine	SEM	Scanning electron microscopy
DPI	Dry powder inhaler	SILF	Simulated interstitial lung fluid
DPPE	Dipalmitoylphosphatidylethanolamine	SLN	Solid lipid nanoparticle
DVS	Dynamic vapour sorption	SS	Salbutamol sulphate
ECD	Effective cut-off diameter	SSLF	Surfactant simulated lung fluid
ED	Emitted dose	SR	Sustained release
FEV₁	Forced expiratory volume in 1 sec	SR-TS	Candidate SR formulation
FIB	Focused ion beam (microscopy)	T	Tailing factor
FPF	Fine particle fraction	t₅₀	Half-time (for drug release)
GB	Glyceryl dibehenate	T_g	Glass transition
GPR	General purpose reagent	TB	Tracheobronchial
GSD	Geometric standard deviation	TEM	Transmission electron microscopy
HAL	Halothane	TP	Tripalmitin
HFA	Hydrofluoroalkane	TPP	Tripolyphosphate
HLB	Hydrophile-lipophile balance	TS	Terbutaline sulphate
HPLC	High performance liquid chromatography	TSI	Twin stage impinger
HPO	Hydrogenated palm oil	UV	Ultra-violet
HSO	Hydrogenated soybean oil	VMD	Volume median diameter
IB	Ipratropium bromide	v_{ts}	Terminal settling velocity
IR-TS	Pure, micronised TS	WHO	World Health Organisation
Kcps	Kilocounts per second	w/o	Water-in-oil (emulsion)
LM	Light microscopy	XRPD	X-ray powder diffraction
M	Mouth	z_{ave}	Z-average diameter
M_∞	Total drug release		

Chapter 1: Introduction

1.1 Pulmonary Drug Delivery

The lung is a very attractive target for drug delivery as it is the end organ for the treatment of local diseases or is an administration route for systemic treatments (Labiris and Dolovich, 2003a). Therefore, delivery of drugs by inhalation has become the most popular administration route for the treatment of the majority of patients suffering from respiratory disease, e.g. asthma (Gonda, 2000). Pulmonary delivery also presents future opportunities for safe, painless drug delivery to the systemic circulation, in particular for proteins, peptides (reviewed by Adjei and Gupta, 1997) and gene therapy (reviewed by Brigham, 1997), which would represent landmark alternatives to injection (Brown, 2002). Table 1.1 highlights the advantages of pulmonary drug delivery.

Successful therapy with any inhaled drug is the culmination of four key events: (1) the identification of a safe and efficacious active pharmaceutical ingredient (drug), (2) incorporation of this drug into a stable formulation or carrier system, (3) design and fabrication of a device to administer the formulation, and (4) access to and correct use of the device by the patient (Dalby and Suman, 2003).

Advantages

Local

- Rapid delivery of medicine to the target organ, e.g. asthma
- Ease of administration
- Achieve high local concentrations of drug, minimise systemic side effects
- Reduction in dose required relative to oral administration (10-20% required)
- Increasing availability of reliable delivery systems

Systemic

- Large surface area for absorption
 - Thin diffusional layer for absorption
 - High bioavailability
 - Avoidance of gastrointestinal tract/first pass metabolism
 - Rapid absorption without need for penetration enhancers e.g. insulin
 - Natural presence of proteolytic inhibitors
-

Table 1.1: Advantages of local and systemic (in particular for proteins/peptides) pulmonary drug delivery.

1.1.1 Anatomy, Physiology and Histology

A basic understanding of lung anatomy and physiology is required in order to understand the opportunities and difficulties associated with delivering drugs to the lung (Altiere and Thompson, 1996).

The primary function of the respiratory system is to exchange O₂ (required to support energy-generating chemical reactions) and CO₂ (produced during these reactions as waste) between the atmosphere and the blood (Sherwood, 1993). To serve these functions, the respiratory system processes approximately 10-25 m³ of air per day (Hinds, 1999).

The respiratory system may be divided conveniently into three regions (Task Group on Lung Dynamics, 1966): (1) the nasopharyngeal (NP) region consisting the nasal cavity, mouth and pharynx, (2) the tracheobronchial (TB) region which consists of non-alveolated airways, lined with smooth muscle to maintain and control airway patency, from the trachea down to the terminal bronchioles, and (3) the pulmonary (P) region which is defined as the respiratory bronchioles, alveolar ducts and sacs. This region is the location of gas exchange.

Beginning at the mouth/nasal cavity, the respiratory tract extends through the pharynx (throat) and down to the trachea. At the base of the trachea, the airway divides into two main branches - the left and right bronchi - which enter the left and right lung, respectively. Within each lung, the airway continues to divide, which produces new generations of airway tubes of progressively narrower diameter, but of greater number and total cross-sectional area. The pulmonary tissue is therefore specialised to present the maximum possible surface area for gas exchange. Ultimately there are about 300 million alveoli in the lung, each having a diameter of 300 µm (Sherwood, 1993). The pulmonary capillary density is such that each alveolus is almost encircled by a continuous sheet of blood and the total surface area of the alveolar region averages 102 ± 21 m² (Stone *et al.*, 1992).

Several models of airways branching have been developed; however, the most frequently applied model is the symmetrical dichotomously branching airway of the Weibel lung morphology, (Figure 1.1.1, Weibel, 1963).

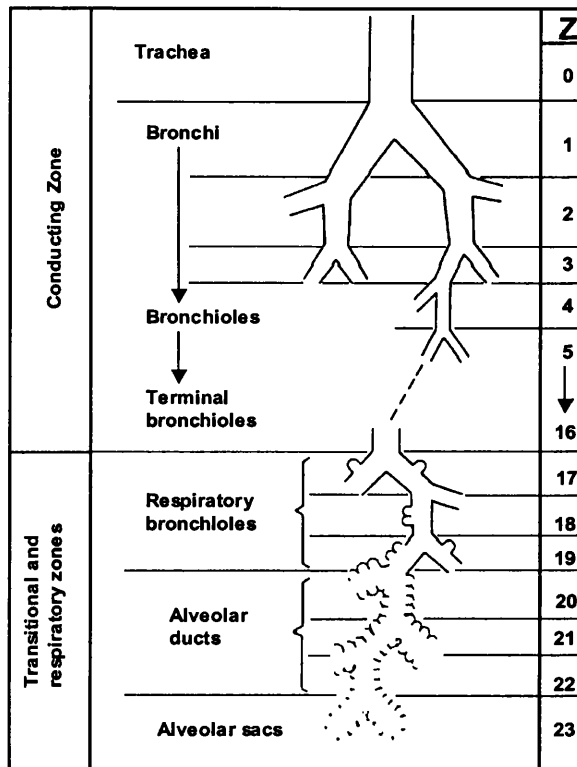


Figure 1.1.1: Schematic of Weibel lung morphology model, showing simplified layout of the respiratory tract. Conducting airways are those involved in air flow (Weibel, 1963). Key: Z = airway generation (branching).

The 'symmetry' of the model infers that after each generation, each pair of airways is identical. The 'dichotomy' indicates that there are 2^Z airways in each generation e.g. for generation, Z=23 there are 8.4 million airways. The TB regions are numbered in order (0-16) from the trachea to the terminal bronchioles. Airway generations Z = 1, 2, 3, 4 represent the main, lobar, segmental and subsegmental bronchi, respectively. The P region is further divided into three generations of partially alveolated respiratory bronchioles (Z = 17-19), three generations of alveolar ducts (Z = 20-22) and finally the alveolar sacs.

The cellular profile changes throughout the pulmonary system, conferring different properties to each region (Martini, 2004). The epithelium lining

inferior portions of the pharynx is stratified squamous epithelium, similar to that of the oral cavity. The upper airway is lined with pseudostratified, ciliated columnar epithelium with many goblet cells that secrete mucus. These secretions form a thick (~5 μm) mucus blanket which serves to prevent dehydration, aid saturation of incoming air with water and trap and remove foreign particles (Section 1.6.2). The cell size gradually decreases in proportion with the decreasing airway diameter (Altieri and Thompson, 1996). In the smaller bronchioles, pseudostratified epithelium is replaced by cuboidal epithelium with scattered cilia. The gaseous exchange surfaces of the alveolar are required to be thin-walled in order to maximise the gaseous diffusion rate between blood and air. Two cell types comprise the alveolar epithelium (Sherwood, 1993): (1) Type I pneumocyte alveolar cells are approximately 0.1 - 0.5 μm thick and cover 97% of the alveolar surface, providing surface for gas exchange and (2) Type II pneumocyte alveolar cells which secrete pulmonary surfactant, a complex phospholipoprotein mixture that reduces alveolar surface tension and prevents alveolar collapse due to lung elasticity and alveolar wall tension changes during inspiration. Two resident cells also populate the lung, alveolar macrophages (Section 1.6.2) and mast cells that are involved in clearance and inflammatory responses, respectively.

1.1.2 Particle Deposition in the Airways

Aerosols for pulmonary inhalation are given by mouth, as the majority of nasally administered particles are effectively deposited within the nose and pharynx. When an aerosolized drug product is inhaled, aerosol particles will deposit in different regions of the respiratory tract (from mouth through to alveoli), dependent on a number of factors, e.g. particle size and density, lung morphology, breathing pattern and aerosol velocity.

Particle size is the primary determinant of where particle deposition will take place either in the NP (this region for oral inhaled medication is represented as the oropharyngeal (OP) region), TB or P region (Gonda, 1981). Particle size for inhalation is typically characterized by the aerodynamic diameter, d_a ,

which is the diameter of a unit sphere with the same settling velocity as the particle in question (Task Group on Lung Dynamics, 1966). In practice, pharmaceutical inhalations are polydisperse with lognormal distributions. The Mass Median Aerodynamic Diameter (MMAD) and Geometric Standard Deviation (GSD) characterize such aerosol distributions. MMAD is the value for d_a , above or below which 50% of the mass of aerosol resides (Gonda, 1985) and takes into account particle size, density and shape factors. GSD is the square root of d_a at the 84.13% cumulative value divided by the 15.87% cumulative value. Theoretically, a GSD value of 1 refers to a perfectly monodisperse system; although in practice, <1.22 is accepted as monodisperse for pharmaceutical aerosols (Fuchs and Sutugin, 1966).

The optimal aerodynamic size range for particle deposition in the lung is 0.5-5 μm (Dalby *et al.*, 1996); however, Newhouse (1998) stated that a size range of 1-3 μm was more clinically relevant. A number of studies in the literature support the use of small particle size drug aerosols (reviewed by Dolovich, 2000). For instance, Rees *et al.*, (1982) demonstrated that a terbutaline sulphate with a particle size distribution under 5 μm produced enhanced bronchodilation and greater lung penetration, relative to particle sizes greater than 5 μm . More specifically, Zanen *et al.*, (1996) investigated the relationship of particle size to clinical response in patients with severe airway obstruction (Figure 1.1.2.1) and found that the optimal particle size for salbutamol and ipratropium aerosol inhalations were 2.8 μm .

The ideal particle size also depends on the intended region for which the therapeutic aerosol is required to target (McDonald and Martin, 2000). For instance, delivery of zanamivir for influenza is suited to the upper respiratory tract; whereas, another antiviral used for treatment of *Pneumocystis carinii* infection, pentamidine, is required to penetrate the alveolar spaces at the site of infection. For asthma, the receptors for β -agonists are found throughout the respiratory system, from the large central airway through to the small lower TB regions and therefore, wider aerosol delivery is required (Martonen and Yang, 1996).

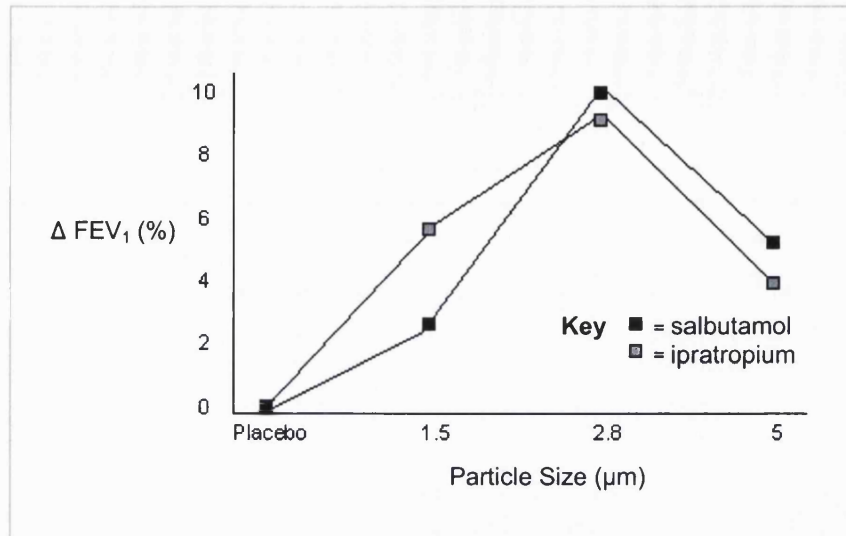


Figure 1.1.2.1: Relationship between particle size and Forced Expiratory Volume in one second, FEV₁, an indicator of lung function. Maximum pharmacodynamic effect was achieved with a particle size of 2.8 μm (adapted from Zanen *et al.*, 1996).

Once administered, therapeutic aerosols are entrained into the air stream. Particle trajectory and deposition is affected by particle size and airstream velocity (determined by tidal volume (500 ml to 3050 ml) and the breathing frequency (14-40 breaths/min)). Three principal mechanisms (Figure 1.1.2.2) govern particle deposition in the respiratory tract - inertial impaction, sedimentation and diffusion (Gonda, 1992). The first two mechanisms are governed by d_a . Diffusion, which accounts for a small fraction of the dose, is influenced by the geometric diameter, d_g . Two additional minor mechanisms, interception and electrostatic deposition, are only important in specific situations (Hinds, 1999) and will not be discussed herein.

During inhalation the airstream negotiates a number of directional changes from the mouth to the alveolar region. At each direction change, particles will continue on in their original direction for a short distance instead of following the air stream. When a particle continues and hits the airway epithelium, the process is known as inertial impaction, and is particularly apparent for larger particles, $>5 \mu\text{m}$ (higher momentum and therefore greater stopping distance).

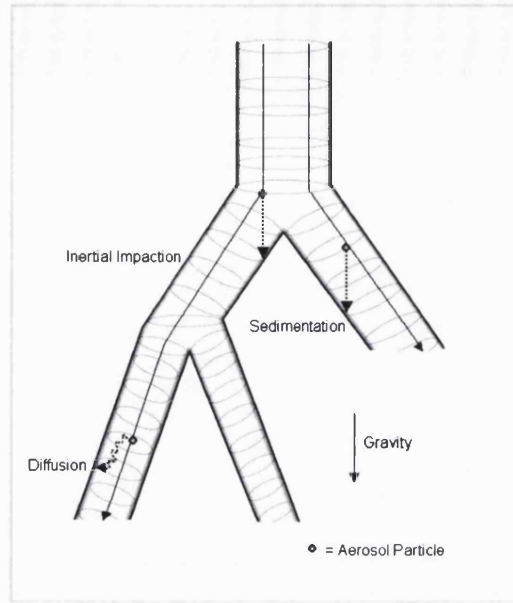


Figure 1.1.2.2: Major mechanisms of aerosol deposition in the lung.

The majority of inertial impaction occurs at the back of the throat and at the first division of the trachea (the 'carina'). Losses of therapeutic aerosols by impaction at the back of the throat can reach in excess of 70% dose (Martonen and Yang, 1996) and are responsible for localized side effects, e.g. candidiasis and dysphonia for inhaled corticosteroids.

Sedimentation of aerosols takes place under the force of gravity. The process typically occurs in the smaller airways where airflow is slower (Gonda, 1981), and therefore particles are subjected to gravitational force for longer periods of time. A sphere of particle diameter, D and density, d , under the influence of gravitational force, will have a terminal settling velocity, v_{ts} , governed by Stokes law (equation 1.1.2).

$$v_{ts} = \frac{d \times D^2 \times g}{18\eta}$$

Equation 1.1.2: Stokes Law for particle settling: g = gravitational acceleration, η = viscosity of the air. A slip correction factor, C_c , is typically applied to the numerator for small particles which 'slip' through the air (Gonda, 1992).

As for inertial impaction, the probability of sedimentation increases with particle size and becomes increasingly important for particles $>1 \mu\text{m}$ (Davies, 1966). In addition, when pulmonary residence time is increased (e.g. breath holding), particles travel further and are therefore more likely to settle, which maximizes therapeutic deposition.

Deposition by diffusion is important for submicron particles ($<1 \mu\text{m}$, Martonen and Yang, 1996). Brownian motion of particles (generated by random bombardment of gas molecules) drives the diffusion process, the rate of which is indirectly proportional to particle size, and causes particles to move from high concentration (airway) to low concentration, where they deposit on the epithelium. Hence for very small particles, the highest probability of deposition occurs in the lung periphery with its small airway dimensions, as conditions further up in the airway fail to deposit the particles (Schulz, 1998) This is the proposed advantage for nanoparticle delivery for systemic therapy as drug absorption from these peripheral regions is high.

Several deposition models have been developed for predicting aerosol deposition in man. Two advanced models, which are widely used, are the International Commission on Radiological Protection (ICRP) and National Council on Radiation Protection and Measurement (NCRP) models (reviewed by Hinds, 1998). Figure 1.1.2.3 displays a typical relationship between regional deposition and particle size, calculated from a mathematical model of mass deposition (Rudolph and Kobrich, 1994). The model shows that the ideal size for targeting the bronchiolar region (between bronchial and alveolar) is 2-3 μm .

It must be noted that however effective a delivery device and formulation is at generating an aerosol of ideal particle size for pulmonary deposition may be, deposition in the airways will always be affected by a variety of patient or physiological factors (Gonda, 1992). For instance, detrimental factors are: inadequate inspiratory flow rate, excessive inspiratory flow rate, inability to operate device correctly (poor counselling/coordination) and lung function of the patient (disease states affect deposition).

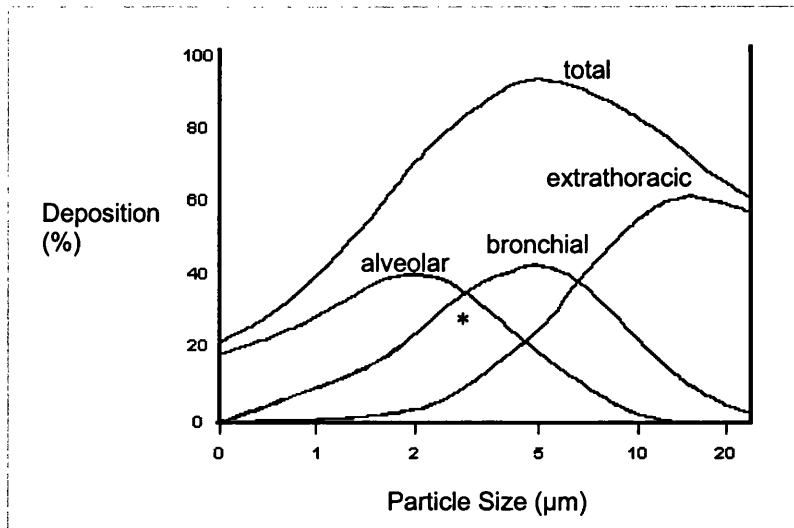


Figure 1.1.2.3: Relationship between aerosol particle size and regional deposition. * = bronchiolar region. Adapted from Rudolph and Kobrich (1994).

1.2 Pulmonary Disease and Therapeutics

1.2.1 Asthma

Asthma is the most common respiratory crisis encountered in UK clinical practice (McFadden and Hejal, 1995) and often starts in childhood. According to the World Health Organization (WHO), there are 100-150 million asthmatics globally and in the United States, for example, annual asthma care costs exceed US\$6 billion (WHO, 2000). The condition is associated with increased bronchial hyper-reactivity to a number of stimuli. An asthma attack, characterized by severe breathlessness and wheezing, is caused by narrowing of the airways due to three factors (Hope *et al*, 1999): (1) bronchial muscle contraction, (2) airway inflammation (caused by mast cell and basophil cell degranulation, which releases inflammatory mediators e.g. prostaglandins and leukotrienes), and (3) mucus formation which causes airway blockage.

Treatment of asthma consists of symptom control as opposed to cure (Caramori and Adcock, 2003). Acute asthma exacerbations are treated with inhaled short acting beta₂-adrenoceptor stimulants, e.g. salbutamol sulphate or terbutaline sulphate. Management of chronic asthma in the UK has

essentially remained unchanged over the past three decades (Lipworth, 1999) and follows guidelines set by the British Thoracic Society *et al.*, (1997). Typical therapeutic strategies make use of regular short beta₂-adrenoceptor stimulants, together with a combination of one or more drugs (listed in Table 1.2.1) and aims to reduce the number of asthmatic episodes and improve lung function.

Therapeutic Class	Examples
Long acting beta ₂ -adrenoceptor stimulants	Salmeterol xinafoate, formoterol fumerate
Antimuscarinic bronchodilators	Ipratropium bromide, oxitropium bromide Triotropium bromide (long-acting)
Inhaled corticosteroids	Beclometasone dipropionate, budesonide, fluticasone propionate
Cromolyns	Sodium cromoglycate, nedocromil sodium
Leukotriene receptor antagonists (oral)	Montelukast sodium, zafirlukast
Theophylline (oral)	Theophylline, aminophylline
Oral corticosteroids	Prednisolone*

Table 1.2.1: Medication used in the treatment of asthma, in addition to short acting beta₂-adrenoceptor stimulants. *used as 'rescue' therapy for periods of severe asthma.

Treatment of asthma is localized to the lung by inhalation, which therefore requires lower doses (mcg) than the oral route (mg) to produce the same pharmacological effect. A benefit of the lower dose is the reduced incidence of side effects such as tremor for oral salbutamol and adrenal suppression for oral prednisolone. Also, direct delivery to the site of action also results in rapid onset of action relative to oral delivery (ideal for acute treatment).

A relatively new treatment for asthma is the development of monoclonal antibodies e.g. omalizumab, which target Immunoglobulin E (IgE) and stop the inflammatory cascade. IgE is responsible for moderating response to allergens such as house dust mites, pollen and spores, and is therefore associated with exacerbations of asthma. Administration of the antibody to IgE reduces the requirement for steroids in asthma treatment (Buhl, 2003) and highlights the entry of macromolecule treatment for asthma, as opposed to traditional low molecular weight drugs.

1.2.2 Chronic Obstructive Pulmonary Disease (COPD)

COPD is a collective term for a number of diseases e.g. chronic bronchitis and emphysema, which are characterized by a progressive airflow limitation in the lung. The condition is one of the most common causes of morbidity and mortality in the world (Barnes, 2003), and further increases in the prevalence and mortality of the disease are predicted for the coming decades (Hurd and Pauwels, 2002). Symptoms of COPD include cough, sputum production, dyspnoea, wheeze and fever, which are precipitated by chronic inflammation and recurrent infection. The disease increases with age and depends on risk factors such as genetic disposition, oxidative stress and smoking history (Puchelle and Vargaftig, 2001). In fact, for smokers in particular, only two interventions have been shown to increase survival for those that develop COPD - stopping smoking (nicotine replacement therapy has proven useful) and long term oxygen therapy (Roche, 1999).

Chronic bronchitis results in an increase in thickness of the bronchiolar lining from inflammation and hyperplasia of the mucus glands (Green and Harris, 1998). These factors also result in hypersecretion of mucus that either partly or completely plugs the airway, especially as mucus clearance by the cilia is typically impaired by chronic insult to the lung, e.g. smoking. As a result, a degree of bronchoconstriction develops together with frequent infections, as mucus can harbour bacteria. Emphysema typically occurs with chronic bronchitis and causes dilatation of the respiratory bronchioles and alveolar sacs through destruction of the walls lining the airways. Pathophysiological changes are due to reduced alpha1-antitrypsin activity, an enzyme that protects the epithelium from auto-digestion by proteolytic enzymes.

COPD has a reversible element, and symptoms may be treated with beta₂-adrenoceptor stimulants and antimuscarinic bronchodilators (Polatli *et al*, 2002). Studies between the two therapeutic classes have shown both to be equally effective and a combination of two drugs from both classes is typically used, as the effects are synergistic (British Thoracic Society, 1997).

The extent of reversibility varies from patient to patient and depends on how far the disease has progressed. In the case of emphysema, due to the lag between onset and diagnosis, the condition is unlikely to have a significant reversible element. Although corticosteroids reduce inflammation and improve lung function in asthmatic patients, little benefit is derived in COPD, and they should not be used frequently (Barnes, 2003).

1.2.3 Other Medical Conditions Treated by the Pulmonary Route

Table 1.2.3 highlights the variety of drugs available on the UK market for inhalation. Despite obvious domination by drugs with intended local action, a vast amount of research is taking place in the biotechnology field for systemic delivery, such that the potential of pulmonary delivery remains to be fully realized (McDonald and Martin, 2000). The most revolutionary product in late-stage development for pulmonary delivery is inhaled insulin, which is being developed by several companies, each with proprietary technology. Patton *et al.*, (1999) has reviewed the technological and safety aspects for pulmonary delivery of insulin.

Condition	Drug Class	Examples	Delivery Mechanism		
			pMDI	DPI	N
Asthma	β_2 -agonists	salbutamol sulphate	*	*	*
		terbutaline sulphate	*	*	*
		fenoterol hydrobromide	*		
		salmeterol xinafoate	*	*	
		formeterol fumerate		*	
	Anticholinergics	ipratropium bromide	*	*	*
		oxitropium bromide	*	*	
		tiotropium bromide	*		
	Corticosteroids	beclomethasone dipropionate	*	*	*
		budesonide	*	*	*
		fluticasone propionate		*	
		mometasone furoate			
	Other	sodium cromoglycate	*	*	*
		nedocromil	*		
Cystic Fibrosis	Mucolytics	dornase alfa (rhDNAase)			*
		acetylcysteine			*
	Aminoglycosides	tobramycin			*
<i>P. aeruginosa</i> Infection/ bronchiectasis	Polymyxins	colistin			*
<i>P. carinii</i> infection	Antiviral	pentamidine			*
Influenza	Antiviral	zanamivir		*	
Respiratory syncytial virus	Antiviral	ribavirin			*
Respiratory distress syndrome	Surfactant	beractant poractant alfa			
Anaesthesia	Inhalational Anaesthetics	desflurane enflurane halothane isoflurane seroflurane nitrous oxide			
Cigarette Withdrawal	Nicotine replacement	nicotine			

Table 1.2.3: Drugs administered by the inhalation route.. Key: pMDI: pressurised Metered Dose Inhaler. DPI: Dry Powder Inhaler. N: Nebulised formulation. (source: BNF, 2003). Surfactants for respiratory distress syndrome are delivered by endotracheal tube. Inhalatory anaesthetics are administered using calibrated vaporisers with air/oxygen/nitrous oxide-oxygen as carrier gas. Nicotine vapour is inhaled from a nicotine-impregnated plug in a plastic tube.

1.3 Pulmonary delivery device technology

There are three conventional methods of inhalation drug delivery to the lung, the nebuliser, pressurised metered dose inhaler (pMDI) and dry powder inhaler (DPI). The major differences between the devices are shown in Table 1.3. To be acceptable for clinical use, a device must meet 5 basic criteria (Dalby *et al.*, 1996).

- generate an aerosol ideally in the size range 0.5-5 μm
- provide reproducible dosing
- protect the physicochemical stability of the drug
- offer portability and inconspicuousness during use
- be simple to operate with minimal training.

Device	Particle Size Range (μm)	Dose Range	[air]	Means of delivery to lung	Formulation	Exit velocity from device
Nebulizer	0.5-5	100-200 $\mu\text{g}/\text{min}$	Low	Passive	Solution/ Suspension	Fast (30 m/s)
pMDI	1-10	0-250 μg	High	Active	Solution/ Suspension	Variable
DPI	1-10	1-20 mg	High	Passive/ Active	Dry powder	Slow

Table 1.3: Differences between conventional inhalation devices (adapted from Hickey, 2003).
[air] = aerosol concentration in the air during administration.

1.3.1 Nebulisers

Nebulisers are devices that disperse drug solutions (and suspensions) into aerosol droplets, and have been in use for over a century (Grossman, 1994). They form a niche in the market for delivery of large quantities of drugs. For example, pentamidine isetionate requires treatment of 600 mg daily for three weeks (BNF, 2003), a dose that is unattainable with pMDI or DPI devices. Despite devices appearing bulky and time consuming, patient acceptance is high (Barta *et al.*, 2002), and as they require minimal coordination they are particularly suited for elderly and young patients. Preservatives in aerosol

formulations have been implicated in paradoxical bronchospasm (Summers *et al.*, 1991) and as such are typically formulated as preservative-free unit-dose sterile preparations. Viscosity and surface tension are also controlled, as these factors have implications for droplet formation from solution. Nebulisers also represent useful delivery systems for proteins and peptides, since aqueous solutions suitable for atomization are easier to formulate than pMDI or DPI systems (Dalby *et al.*, 1996). Other noteworthy examples of delivery from nebulisers include liposomes containing sodium cromoglycate (Taylor *et al.*, 1989) and ciclosporin (Arppe, *et al.*, 1998) as well as nanoparticle delivery of beclometasone dipropionate (Ostrander *et al.*, 1999) or budesonide (Jacobs and Muller, 2002).

There are two classes of nebulisers currently in use, air-jet and ultrasonic (Figure 1.3.1). The air-jet nebuliser requires a portable compressor or central air supply to generate high-speed airflow through a nozzle, which entrains and disperses the liquid into aerosol droplets (Venturi effect). The aerosol generated is coarse; therefore, a carefully positioned airflow controller or 'baffle' is used in order to allow impaction of the large drops. Smaller, respirable droplets then leave the nebuliser and are inhaled by the patient. Ultrasonic nebulisers use a piezoelectric transducer to generate the aerosol from an open liquid reservoir and avoid the requirement for an external air supply. Pressure waves from the piezo vibrator move towards the surface where they constructively interfere and create an ultrasonic fountain. The lower sections of the fountain are inherently unstable and disperse into a respirable aerosol cloud. Again, baffles are used to entrap larger droplets and return them to the bulk solution. Ultrasonic nebulisers generate relatively large droplets (>2 μm) and therefore may be inappropriate for applications that require aerosol penetration to the deep lung (Newman *et al.*, 1987). Heat generation occurs during ultrasonic nebulisation, which can degrade heat labile substances – due to this problem, the use of the ultrasonic type device with rhDNAase is prohibited (BNF, 2003).

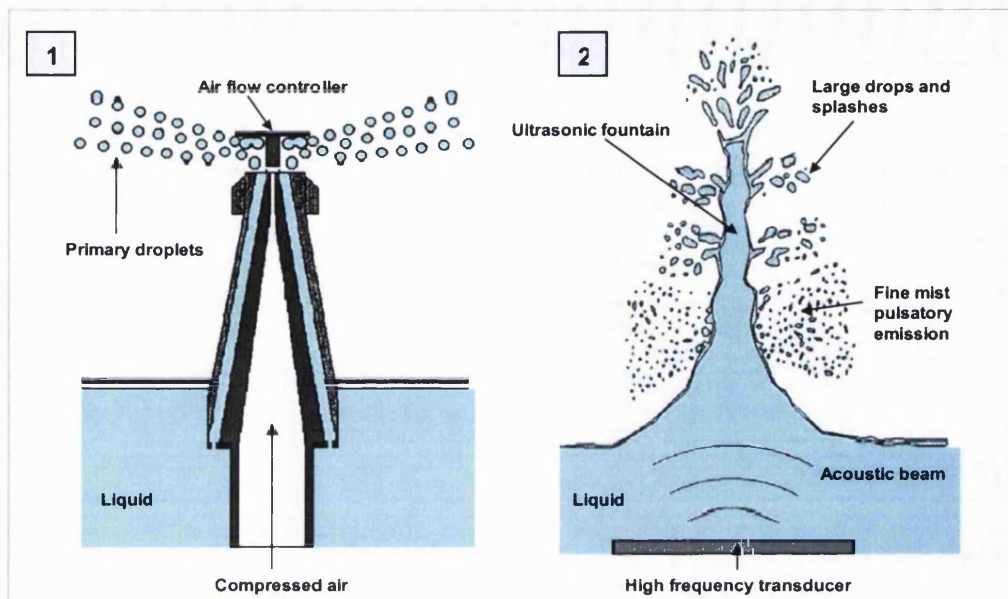


Figure 1.3.1: Dispersion mechanism for (1) Jet nebuliser and (2) Ultrasonic nebuliser.

The chief disadvantage of nebulisers is that since the liquid aerosol is generated continuously, a large proportion is wasted (>50%) during the patient's expiratory cycle. To counteract this, feedback systems have been developed, which only allow the nebulised aerosol to be generated during the first half of the patient's inspiratory cycle (Knoch and Finlay, 2003).

Recently, novel handheld nebuliser technology has been developed (e.g. Aerodose™ inhaler, Aerogen Inc., Mountain View, CA, USA, and the AERx™ system, Aradigm Corp., Hayward, CA, USA). Both nebulise liquids through micromachined holes in plates. The resulting MMAD values are suitable for deep pulmonary inhalation, and as such the technology is being developed to formulate systemically acting compounds such as insulin. Along with greater portability, a range of patient features can be also incorporated into the design - for instance, sensors in the AERx system detect optimal flow rates for delivery, and then aerosol release is triggered.

1.3.2 pMDI Device Technology

The pMDI is the most widely used inhaler owing to its convenience and approximately 600 million inhalers are distributed annually (Brown, 2002). pMDIs are devices that incorporate a propellant (pressurized) to generate a metered dose of an aerosol through an atomization nozzle. The phase out of chlorofluorocarbon (CFC) propellants (ozone depleting) with more environmentally friendly hydrofluoroalkane (HFA) propellants has provided opportunities to develop and further optimize pMDI device technology (Smith, 2002). Bioequivalence between CFC and HFA formulation has been shown frequently in large randomized controlled studies, e.g. ipratropium bromide (Taylor *et al.*, 2001) and salbutamol sulphate (Lumry *et al.*, 2001). In some cases, reformulation into HFA propellants has enhanced device performance - for instance, a beclomethasone dipropionate solution HFA improves peripheral lung deposition (Leach *et al.*, 1998).

Drug substances are typically formulated in HFA-propellants as solutions or dispersed as surfactant-stabilised drug suspensions. Drug solubility in the propellant limits the choices for formulating solutions, although solubility can be achieved by adding a co-solvent, such as ethanol. Solution pMDIs offer the theoretical advantage of greater dose uniformity compared to suspensions (McDonald and Martin, 2000) but suffer from disadvantages such as supersaturation and crystallization at low temperatures (Dalby *et al.*, 1996). All surfactants that had previously been used in CFC products display poor solubility in HFA propellants (Vervaet and Byron, 1999). Alternative surfactants proposed are poly(ethylene glycol) (PEG), propoxylated PEGs, and perfluoroalkanoic acids (Dalby *et al.*, 1996). For ideal suspension formulations, upon shaking the formulation must be immediately redispersible across the product lifespan in order to provide homogeneous and accurate dosing. Low surfactant concentrations are also recommended to reduce drug solubility in the propellant and thus avoid Ostwald ripening (redistribution of partially soluble drug into solution, then recrystallization back onto remaining particles, resulting in particle growth).

The pMDI device has three essential components (Figure 1.3.2): the canister, metering valve and actuator (Dalby *et al.*, 1996). The canister is fabricated from aluminium, which may be coated with a variety of agents, such as anodized aluminium or perfluoroalkoxyalkane coatings to prevent container-formulation interactions. Alternatively, novel containers have been developed from plastic-coated glass offering the advantage of transparency (Hormes and Swift, 2002), which allow the patient to gauge remaining doses. The canister typically provides a product reservoir of sufficient volume to deliver 200 doses. The metering valve (Figure 1.3.2) is designed to release a fixed, reproducible amount of product during each actuation. The dose is the product of the metering chamber volume (typically 25-100 μL) and concentration of drug in the reservoir, assuming homogeneous drug content (Dalby *et al.*, 1996). During manufacture, the valve is crimped to the canister and product is often filled through the valve stem under high pressure.

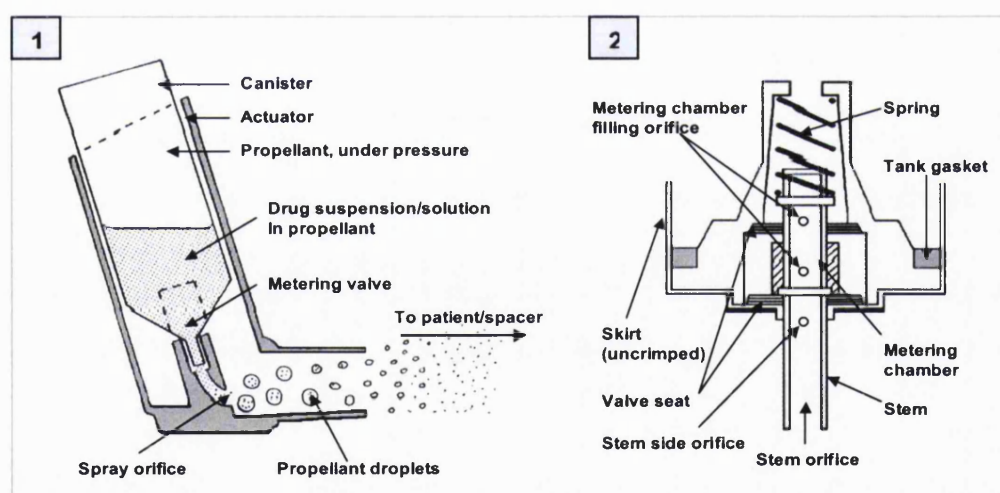


Figure 1.3.2: Schematic of (1) pMDI device and (2) metering valve design.

A further function of the valve, or more specifically the elastomeric seal between the valve and the canister, is to prevent the ingress of moisture and air into the canister, and prevent escape of the propellant by evaporation - all of which can severely affect product performance. New elastomeric seals specifically for HFA propellants have been introduced recently (Colthorpe, 2003) which have solved the problems arising from the use of CFC-type seals for HFA inhalers, such as unacceptable water ingress and inadequate

valve integrity (Tiwari *et al.*, 1998). FDA draft guidelines (FDA, 1998) also require testing for leaching of extractable chemicals, some carcinogenic, from plastic and elastomeric components of the valve - although recent data has shown that the levels are unlikely to pose significant risks to human health (Howlett *et al.*, 2002).

The actuator, typically moulded plastic, serves to facilitate valve opening (actuation) and also to direct the aerosol spray into the patient's mouth. A tight fit between the valve stem and actuator is required to prevent product leakage. Spray orifice diameter is important, since droplet size leaving the orifice is proportional to the diameter (Clark, 1992). For instance, Polli *et al.*, (1969) showed a decrease in MMAD from 11 to 3.2 μm when orifice diameter was reduced from 0.61 mm to 0.46 mm. For a solution based beclometasone dipropionate pMDI, fine particle dose was significantly increased with a reduction in orifice diameter (0.42 to 0.25 mm) due to lower throat deposition (Gabrio *et al.*, 1999), although MMAD was only reduced by 0.3 μm in this case. Excessive reduction in orifice diameter however can lead to physical blockage with the use of suspension pMDIs (Dalby *et al.*, 1996). The short distance between the mouthpiece and the oropharynx, together with the high exit velocity of the aerosol results in large deposition in the throat (Newman *et al.*, 1981). Investigations into aerosol plume velocities by Gabrio *et al.*, (1999) showed that exit velocity was lower for HFA-227 compared to HFA-134a and CFC-12 due to lower vapour pressure (456 kPa vs. 666 and 652 kPa respectively) - this suggests that HFA-227 based formulations might exhibit less throat deposition.

Also, given the short time between actuation and inhalation, one of the major recognized drawbacks of the pMDI device is the requirement for the patient to coordinate these events (Smith, 2002). Breath-actuated devices, which automatically actuate a dose upon patient inhalation, eliminate the reliance on patient coordination for effective aerosol delivery (Hampson and Mueller, 1994). In fact, a cohort study which included over 5000 patients showed that breath actuated devices provided better symptomatic control than standard

pMDIs, and reduced extra medication requirements and visits to general practitioners or outpatient clinics (Price *et al.*, 2003).

Also, there are a variety of spacers (which attach to the actuator mouthpiece), which provide additional volume prior to aerosol inhalation by the patient. The additional time gained before inhalation reduces the requirement for coordination, and is useful for younger patients. In a recent study, Williams III *et al.*, (2001) showed that for all five spacer devices tested, throat deposition was reduced and fine particle fraction (FPF, % of particles in an appropriate size for pulmonary deposition) was increased for inhalation of HFA-based steroid formulations.

The convenience of the pMDI is emphasized by the fact that the majority of medicines on the UK market for inhalation have a pMDI presentation (Table 1.2.3). As with nebulisers, pMDIs are being evaluated as a device for future delivery of proteins and peptides since primary and secondary structure is conserved in the propellant environment (Adjei, 2003). For instance, adenosine deaminase (used in treatment of adenosine deaminase deficiency) has shown compatibility with HFA upon storage for 3 months at 4 °C and 25 °C with no change in enzyme activity. MMAD (1.6 - 2.5 µm) and FPF (>60%) were also suitable for deep pulmonary delivery of the protein (Brown *et al.*, 2002).

In other developments, hollow porous particles, Pulmospheres™, have been formulated into HFA-pMDIs and have shown excellent dispersion properties. The propellant penetrates within particles, thus preventing rapid creaming or sedimentation of particles, a common problem in pMDI technology, which causes dose inaccuracy. A Pulmosphere™/salbutamol HFA dispersion shows stability for four hours as opposed to 30 seconds with a commercial salbutamol HFA formulation (Dellamary, 2000).

1.3.3 DPI Device Technology

DPI development has undergone enormous activity recently in terms of device technology (Smith, 2002) - this has occurred in line with the phase-out of CFC propellants. There are three major types of device (Dalby *et al.*, 1996): unit dose, multi-unit-dose and multidose reservoirs. All devices are portable and designed such that upon patient inhalation through the device, airflow is sufficient to aerosolize the formulation out from the device. Therefore, DPIs requires less coordination than pMDIs. Some authors cite that a drawback of this approach is the variability of patient inspiratory flow rate, which in some cases (young, elderly and advanced disease states) may not be sufficient to aerosolize the powder (Smith, 2002). However, it is argued that patients can still generate a high inspiratory flow even in an acute situation (e.g. asthma attack, Borgstrom *et al.*, 2002).

Unit-dose devices were introduced over 30 years ago (Bell *et al.*, 1971). They contain the dry powder formulation in a capsule (gelatin), which, once loaded into the device, is either pierced or broken prior to inhalation, e.g. triotropium bromide capsules for the Spirava[®] Handihaler[®] device (Boehringer Ingelheim, Bracknell, Berkshire, UK,). Alternatively, in multi-unit-dose presentations, strips or disks of blister packs containing drug are inserted into the device. Prior to inhalation the blister is moved into an actuation position and opened, e.g. blister packs of blended salmeterol xinafoate/fluticasone propionate in the Seretide[®] Accuhaler[®] (GlaxoSmithKline, Brentford, Middlesex, UK). Finally, there are multidose reservoir systems such as the Turbohaler[®] device (Figure 1.3.3, AstraZeneca, London, UK) which meter doses from a powder hopper. There is also an array of next generation devices that are designed primarily for systemic delivery of peptide/protein powders - e.g. the Nektar Pulmonary Inhaler[®] (Figure 1.3.3, Nektar Inc., San Francisco, CA, USA) which actively actuates and disperses the dose into an aerosol cloud prior to patient inhalation, thus providing an aerosol that is independent of inspiratory flow.

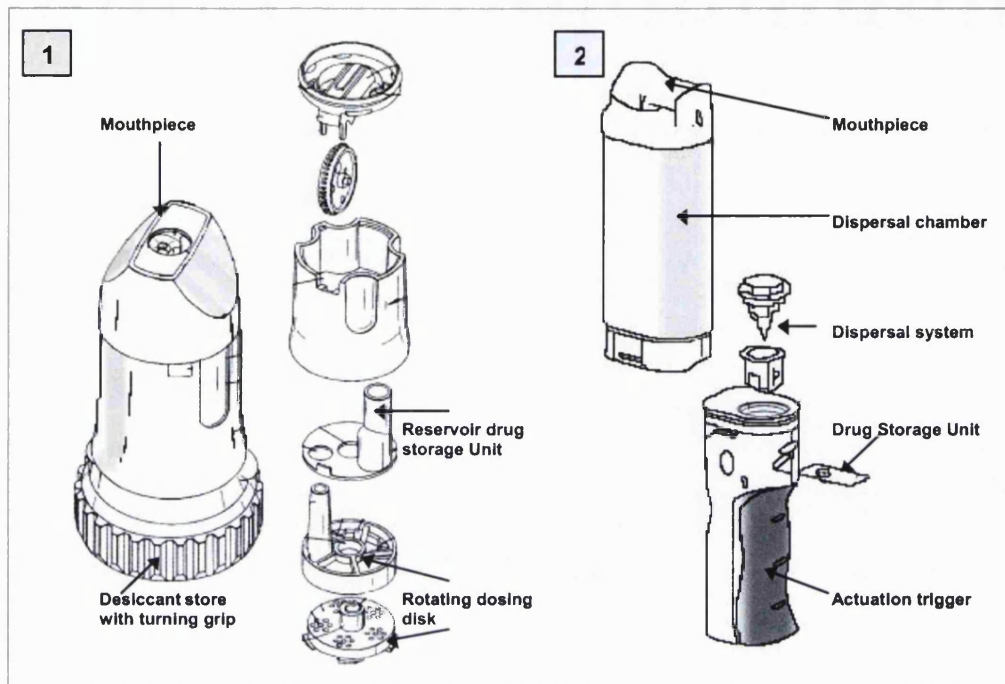


Figure 1.3.3: DPI delivery devices: (1) Turbohaler® (AstraZeneca) and (2) Nektar Pulmonary Inhaler® (Nektar). (Adapted from US device patents 6655380 and 6257233 respectively).

All DPIs have four common components: a dose-metering mechanism, an aerosolisation mechanism (typically the patient themselves), a deaggregation mechanism, and an adaptor/mouthpiece to direct the aerosol into the patient's mouth (Dalby *et al.*, 1996).

Reproducible dose metering is essential for DPI technology. Factory-metered devices (unit dose/multiple unit dose) are expensive to manufacture but provide consistent dosing performance. Reservoir formulations (device-metered) are cost effective to manufacture but may deliver variable dosing (Malton *et al.*, 2003). DPI devices are designed to minimise resistance through the device in order to maximize air velocity and lift the powder into the airstream for inhalation. Some devices cause the powder to impinge on the device surface, thereby deaggregating the powder (Parry-Billings *et al.*, 1999) or in the case of the Turbohaler®, long spiral flow tubes through the device cause drug aggregates to break up under high shear forces (Ashurst and Malton, 2003). However, these tubes produce a high resistance within

the device against which some patients find it difficult to inhale (Dalby *et al.*, 1996).

The formulation of dry powders for inhalation is also critical for DPI performance. As discussed previously, particles should be $< 5 \mu\text{m}$ (MMAD) for efficient lung delivery. Particles in this size range tend to be cohesive, due to van der Waals' and electrostatic forces (Corn, 1966), resulting in poor flow, poor handling during processing and inadequate dispersion (aerosol adhesion is reviewed in detail by Zeng *et al.*, 2001). In the case of Turbohaler[®] formulations, micronised drug is spheronised to form large uniformly sized agglomerates and permit accurate dose metering (Wetterlin, 1988). However, dose metering in this way for more potent drugs requiring low doses would compromise accuracy (Malcolmson and Embleton, 1998). The alternative, and commonly used practice, is to blend micronised drug with coarse carrier particles (50-100 μm), which results in the drug particles being uniformly distributed over the surface of the particle. Lactose is the excipient of choice for the carrier particle as it is physiologically inert. Powder flow is greatly enhanced in drug/lactose blends, and accurate dosing is possible. The high air velocity through the device during inhalation detaches micronised drug from the lactose surface, and the lactose carrier particles impact in the oropharynx region. Inevitably, a proportion of drug remains attached to the carrier particle and causes localised side-effects and reduced respirable fractions. Therefore, a variety of investigations have been performed with the aim of improving drug particle detachment from the carrier during inhalation and improvement in FPF. Examples of these include: (1) addition of a ternary phase, e.g. microfine lactose or L-leucine, in order to occupy high energy sites which otherwise would have strongly attracted drug (Staniforth, 1996), (2) low drug:carrier ratios and small ($<32 \mu\text{m}$) carrier particle size (Steckel and Muller, 1997), (3) use of lactose carrier particles with fused partially amorphous lactose fines (Al-hadithi *et al.*, 2002) and (4) use of recrystallized lactose carrier materials (Larhrib *et al.*, 2003). Mouthpiece design, as is the case for pMDI devices, is typically a tube through which the patient inhales the formulation and should be selected

from a material of low electrostatic potential to reduce drug deposition in the device (Dalby *et al.*, 1996).

Historically, DPIs occupied only a small portion of the market (<10%), although recently, use of the device has grown and is taking a significant part of the pMDI market (Dalby and Suman, 2003) - this is particularly true for the dry powder combination product Seretide[®] (GSK). The simplicity of use, together with indicator systems to allow the patient to see how many doses are remaining, are establishing DPIs as major competitors to the pMDI market (Borgstrom *et al.*, 2002). The majority of improvements in DPI technology have arisen from novel powder formulation technology (Section 1.4), however there are a number of new devices. The novelty of the devices lies in their different mechanisms of efficient powder aerosolisation. For instance, the aforementioned Nektar Pulmonary Inhaler[®] uses compressed gas to actively aerosolize the powder into a spacer chamber, and the Spiros[®] Inhaler (Dura Pharmaceuticals Inc., San Diego, Ca, USA) uses a battery powered motor to drive an impeller which provides mechanical energy to enable excellent powder dispersion (Han *et al.*, 2002).

1.4 Aerosol Particle Generation

1.4.1 Crystallization/Micronisation

Crystallization is the process in which molecules assemble into a solid mass, characterised by a regular internal structure and planar external geometry. Crystallization from solution, described in detail in Section 2.1, is the major method of preparing drug crystals in the pharmaceutical industry. Following production however, the crystals rarely have the correct particle size suitable for inhalation so further processing is required. Air-jet milling (Figure 1.4.1) has been the method of choice for particle size reduction or 'micronisation' of inhaled drugs for a number of years (Zeng *et al.*, 2001). Bulk crystals are fed into a hopper and entrained into opposing jets of high velocity compressed air - their resultant impact causes fracture and size reduction to <10 µm (Hickey, 2003).

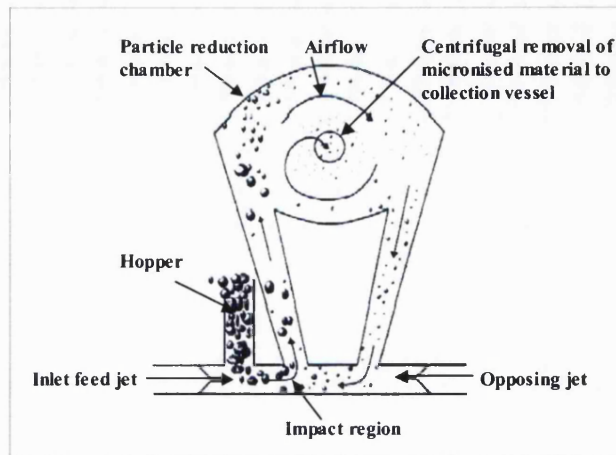


Figure 1.4.1: Schematic of air-jet mill. Particles are entrained into a compressed air jet and flow into the particle reduction chamber at high velocity, where they impact the wall and fracture. Particles then flow downwards where they are entrained into an opposing compressed air jet, and fired at the particles entering the system causing more fracture and size reduction. Once sufficiently small, micronised material is removed by centrifugal flow into a collection vessel (Adapted from Hickey, 2003).

Micronised material is cohesive (Corn, 1996) and therefore powders are either spheronised (controlled aggregation of micronised particles) or blended with lactose (Section 1.3.3) in order to produce dry powder for inhalation. Micronisation is a high-energy attrition process that can induce instability (amorphous regions) at the surface (Ward and Schulz, 1995), such that alternative powder generation techniques may well be advantageous.

1.4.2 Spray Drying

Spray-drying represents an alternative method to crystallization/micronisation for particle generation and provides flexibility in terms of particle size, distribution, shape, density, surface characteristics, flowability and dispersibility (Sacchetti and van Oort, 1996). The process is described in detail in section 5.1. Application of spray-drying to respiratory formulation has been described in various reports, for instance disodium cromoglycate (Vidgren *et al.*, 1987) and salbutamol sulphate (Chawla *et al.*, 1994); however, no spray-dried products are currently marketed for respiratory drug delivery.

Spray-drying is useful for heat-sensitive molecules such as proteins or peptides. Several companies use this technology to produce protein/peptide formulations since stability in the solid state is typically greater than liquid formulations (e.g. formulations for nebulisers). For instance, Nektar Inc. (San Carlos, CA, USA) has developed a variety of spray-dried formulations in which therapeutic products (e.g. insulin, proteinase inhibitors and tobramycin) are stabilized in amorphous glass microparticles (Pulmosol™ technology, Clark, 2003).

In other developments, Edwards *et al.*, (1997) identified that dispersibility of a spray-dried powder could be improved by increasing the geometric particle size ($>10\ \mu\text{m}$) and reducing the particle density ($<0.4\ \text{g cm}^{-3}$), whilst maintaining the aerodynamic particle size in the respirable range. This technology has been used to develop formulations for epinephrine, salbutamol, insulin and human growth hormone (Batycky *et al.*, 2003).

1.4.3 Supercritical Fluids (SCFs)

Over the last 5 years, the use of SCF technology to generate particles of controlled morphology, surface properties and size has increased (Hickey, 2003). SCFs occur at conditions above the critical temperature and pressure (at which liquid and gas have equal density). CO_2 has a low critical temperature ($31\ ^\circ\text{C}$), toxicity and price and is not flammable, making it one of the most popular SCFs for preparing drug particles at conditions close to ambient temperature. Supercritical fluids can be viewed as typical recrystallization solvents; therefore, they can be used to precipitate drugs in a crystallization step or be used like traditional solvents in spray-processing. In gas antisolvent or supercritical antisolvent processing, the SCF is used as an antisolvent to precipitate drug from the solvent in which it was initially dissolved (Sacchetti and Van Oort, 1996). Alternatively, when SCFs are used as a solvent, drug is dissolved in the SCF and the pressure is rapidly dropped, resulting in flash SCF removal and rapid precipitation of finely dispersed drug - this process is termed Rapid Expansion of Supercritical Solutions. Solvent- and anti-solvent-based SCF processing, and their

potential for use in particle design, are the subject of a recent literature and patent review (Jung and Perrut, 2001).

Shekunov *et al.*, (2003) prepared salmeterol xinafoate powders using SCF technology and blended the particles with carrier lactose. This blend offered superior dispersion properties compared to a micronised drug/lactose blend. FPF (<4.4 μm) was 57.8% for the SCF prepared drug compared with micronised drug (25.2%). This result, in spite of larger geometric particle size for the SCF prepared drug, was due to a lower bulk density, reduced sphericity and reduced surface energy compared to micronised drug. For formulation of an inhaled protein dry powder, Sievers *et al.*, (1996) developed a supercritical CO_2 -assisted nebulisation process for the preparation of rhDNAase in which 73% of the enzyme particles generated were of particle size <3.1 μm . These results, amongst many others, highlight the potential value of SCF technology to prepare inhaled medications that are superior to powders produced from standard micronisation processes.

1.5 Sustained Release (SR)

The vast majority of drugs administered to the body are expected to be absorbed effectively and exert their activity rapidly - a prime example of this requirement is the use of analgesics, in which pain control is required immediately. However, many drugs only confer a short duration of therapeutic activity as they are rapidly cleared from the body. The consequence is frequent dosing schedules, which are inconvenient (and in the case of injections, painful) for patients and result in problems with medication compliance. The presence of high drug concentrations following dosing may also lead to unwanted side effects or toxicity. In addition, control over the medical condition can be lost during periods of low drug concentration prior to subsequent dosing, which could have profound consequences, e.g. convulsions in epileptics, angina in ischaemic patients or bronchoconstriction in asthmatics.

Clearly, drugs may not confer maximal therapeutic benefit to the patient unless the correct amounts can be delivered to the target area/organ at the right time, for the right duration, and at levels that minimize side-effects (Robinson, 1978). Accordingly, a vast amount of work has been performed in developing pharmaceutical formulations that modify or slow the release of the drug molecule into the body in order to achieve these goals.

A variety of phrases are used to define modified drug release formulations. 'Sustained release' shall be used throughout this work and relates to any dosage form that provides medication over an extended time (Jantzen and Robinson, 2002) - this term is also interchangeable with prolonged release. 'Controlled release' specifies dosage forms that attempt to control therapeutic drug concentrations in the target tissue. 'Repeat action' refers to dosage forms that contain multiple doses of drug that are designed to release over periodic intervals. 'Delayed release' occurs when there is a defined interval between drug administration and release, e.g. enteric-coated tablets, which release their contents following transit through the stomach.

Drug release from formulations follows one of three main kinetic profiles (Figure 1.5.1); however this is not limiting, as complex formulations may show alternative kinetics. Immediate-release conventional formulations typically show rapidly increasing plasma concentrations of drug which peak soon after administration. This elevated concentration is transient and falls in accordance with clearance from the plasma. Sustained release profiles may follow 'first-order' kinetics in which the release rate is directly proportional to the amount remaining in the formulation at the time of sampling. Controlled release formulations may exhibit 'zero-order' kinetics where drug is continually released at the same rate, giving rise to constant plasma levels.

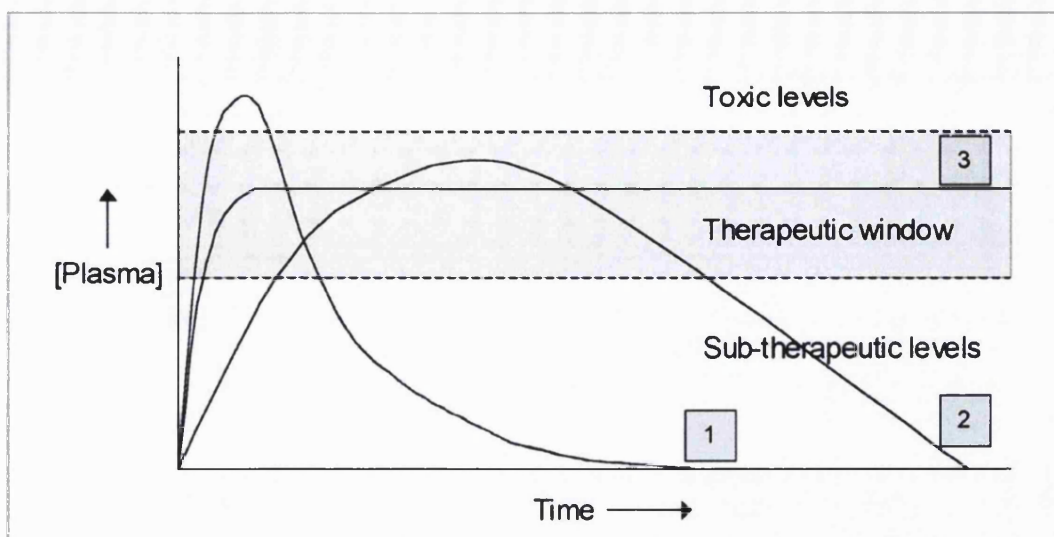


Figure 1.5.1: Effect of drug release profiles on drug plasma concentration versus time: 1 = conventional immediate release formulation, with toxic dose administered: 2 = sustained release profile (first order): 3 = controlled release profile (zero-order).

There are a large number of strategies for modified release for most routes of administration, e.g. oral tablets/capsules, transdermal patches, subcutaneous implants, ocular inserts. Several review texts provide excellent insight into a number of these formulations (Robinson, 1978; Wise, 2000; Rathbone *et al.*, 2003). Two methods of sustaining drug release are: (1) dissolution controlled systems and (2) matrix diffusion controlled systems (Jantzen and Robinson, 2002).

Dissolution is the process by which drug molecules enter solution from the solid phase, and is affected by saturated solubility in the solution, surface area exposed to the solution, temperature, pH and viscosity. Therefore a number of drugs have intrinsic sustained release as conferred by their low aqueous solubility, e.g. griseofulvin and indomethacin. To achieve a dissolution controlled process, the salt form of the drug can be altered to reduce aqueous solubility, the drug can be complexed with resins (ion-exchange) or the drug can be dispersed in, or coated/encapsulated by, a poorly soluble excipient which slowly dissolves, thus delaying dissolution of the drug (Lee and Robinson, 1978).

Matrix diffusion controlled systems provide an inert barrier to drug release through which the drug must move from a high concentration to low concentration (diffusion). There are two sub-divisions, reservoir systems with matrix barriers and matrix systems with dispersed drug. Firstly, reservoir systems contain a core of drug (the 'reservoir') surrounded by a diffusion controlling membrane (Figure 1.5.2). An example of this class is transdermal drug delivery from a patch e.g. 72 hour delivery of fentanyl from Durogesic[®] (Janssen-Cilag Ltd, High Wycombe, Buckinghamshire, UK). A rate controlling membrane (polymeric e.g. EVA copolymer) between the skin and the drug reservoir provides a diffusional barrier that sustains drug release.

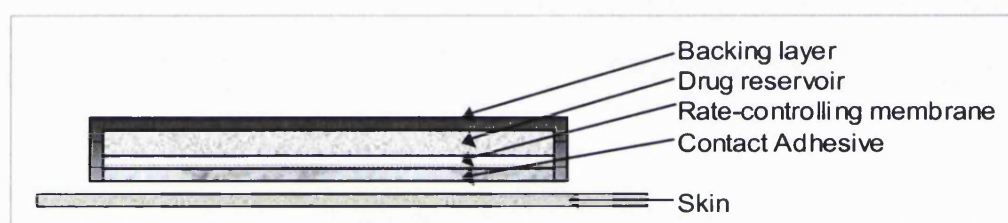


Figure 1.5.2: Schematic of rate-controlled transdermal drug delivery patch.

Conventional tablets may also be coated with polymers to provide sustained release formulations (e.g. theophylline tablets with poly(ϵ -caprolactone) coatings (Lin and Lee, 2003) or Carbopol[®] coatings (Muramatsu *et al.*, 2000)).

Secondly, drugs can be homogeneously dispersed through the entire matrix, and release is then proportional to the rate of drug diffusion through the matrix. Again, transdermal delivery serves as an example. Instead of using a rate controlling membrane with a reservoir of drug, the drug can simply be dispersed/dissolved into a thicker layer of specialized adhesive (e.g. poly(isobutylene)) which serves two functions: (1) adhesion to the skin and (2) provision of sustained release by controlling diffusion of drug through the layer and into the skin (Venkatraman and Gale, 1998).

1.6 Pulmonary Sustained Release

1.6.1 Advantages of Pulmonary Sustained Release

The advantages for SR drug delivery to the respiratory tract are listed in Table 1.6.1 (Zeng *et al.*, 1995a; Hardy and Chadwick, 2000).

Advantage
Extended duration of action
Improved compliance
Reduction in drug use
Improved management of therapy
Reduction in side effects
Potential cost savings

Table 1.6.1: Advantages of pulmonary SR formulations.

A sustained release preparation will provide available drug over an extended period, which may enhance the control of disease states, e.g. asthma symptoms. In particular, short acting beta₂-adrenoceptor stimulants have a short plasma half-life (4-6 hours) and require frequent dosing. This makes these agents ideal candidates for SR preparations.

Malo *et al.*, (1989), showed that four times daily treatment of asthma (provision of more constant drug levels) with a corticosteroid resulted in less nocturnal cough, attacks and relapses when compared to a twice daily schedule, with no change in the side effect profile. However, excessive dosing frequency is a well-documented cause of non-compliance in patients (Derom and Thorsson, 2002). In another study, inhaler under-usage was greater with four times daily versus twice daily treatment (57.1% vs. 20.2%, Mann *et al.*, (1992)). Even with twice daily dosing, only 40% of patients actually complied with the administration protocol, even after extensive education at the study onset (Chmelik and Doughty, 1994), which highlights the problem of compliance even at low dosing frequency. An inhaled sustained release formulation, ideally administered once-daily, may therefore

provide benefits to non-compliant patient groups owing to the convenience of reduced dosing-frequency.

Asthma is usually worse at night - which corresponds to the trough of the circadian rhythm for bronchial patency (0400 hours, D'Alonso *et al.*, 1999) and coincides with the greatest airway hyperreactivity to allergens and other stimuli (Smolensky *et al.*, 1987). It is desirable that bronchodilator therapy results in an overall 24-hour improvement in bronchial patency or at least provides cover for the nocturnal decline. Sustained release drug delivery may provide this cover and improve therapy, especially if administered at bedtime to cover the night 'no-dose' period.

General improvements in therapy, management of disease progression and reductions in hospital admission rates may result from sustained release preparations. These advantages are anticipated to provide significant cost savings to health providers (Saks and Gardner, 1997) and, more importantly, overall benefits to the patient.

1.6.2 Barriers to Pulmonary Sustained Release

Once inhaled particles deposit in the airways, they are exposed to different lung fluids and clearance mechanisms. The nature of both depends on the region of deposition (Hickey, 2003). Particles subject to clearance will be unable to act as a reservoir for sustained drug release.

Within the TB airways, particles deposit on a thick mucus layer (2-8 μm , Mercer *et al.*, 1992) and are subject to mucocilliary clearance. The mucocilliary escalator consists of a mucus layer that is propelled upwards towards the pharynx at a rate of 2-5 cm min^{-1} (Courrier *et al.*, 2002), by the rhythmic beating of underlying cilia, which protrude into the mucus layer. Particles are then swallowed. Particles with sufficient solubility in the mucus, however, will dissolve and enter the systemic circulation before being carried out of the lung. Taylor and Gumbleton (2002) clearly highlighted the effects of particle deposition in the central airway - mucocilliary clearance was

calculated to be responsible for a dramatic reduction in relative bioavailability from 53% to 1.25% for deposition in airway generation $Z=15/16$ and $Z=2$ respectively (Weibel model, Figure 1.1.1). Kreyling *et al.*, (1999), showed there was 50-95% clearance from the canine airway for 2.5 μm monodisperse polystyrene particles within 24 hours. The remaining fraction, present for an additional 48 hours, had deposited in the non-respiratory bronchioles and alveoli. Therefore, these regions are to be targeted for longer-term pulmonary residence.

The mucociliary escalator does not reach the peripheral lung compartment, and as such, particles deposit on thin layers of alveolar lining fluid/pulmonary surfactant. Clearance from this region is not fully understood (Kreyling and Scheuch, 2000). A significant concern for SR microparticle delivery to the peripheral airways is the potential of the particles to encounter alveolar macrophages (AMs) (Ng *et al.*, 1998), which play a significant role in alveolar clearance. Foreign particles adhere to the macrophages through electrostatic or specific (receptor mediated) interactions. The particles are then endocytosed and subject to lysosomal degradation or clearance to the upper respiratory tract as the cells migrate to the mucocilliary escalator. AMs also release chemokines, which recruit further immune cells to enter the airway space. Whilst these effects are beneficial for targeting an infected macrophage population, e.g. rifampicin treatment for tuberculosis (O'Hara and Hickey, 2000; Sharma *et al.*, 2001), macrophage uptake must be avoided in order to increase SR particle residence times. Administering particles with a large geometric diameter has been shown to reduce the tendency for macrophage uptake. Makino *et al.*, (2003) have also shown a relationship for uptake and particle size; polystyrene microsphere uptake was greatest for 1 μm spheres, evident for 0.5 μm and 6 μm spheres, but minimal for 0.2 μm and 10 μm particles. Indeed, Edwards *et al.*, (1997) concluded that enhanced bioavailability of insulin from inhaled large porous particles ($> 5 \mu\text{m}$) was due to a reduction in phagocytosis. Surface chemistry of the inhaled particles also affects the magnitude of macrophage uptake. Dipalmitoylphosphatidylcholine (DPPC), the major constituent of lung surfactant, has been shown to reduce alveolar macrophage uptake of

particles. Evora *et al.*, (1998) prepared poly(D, L, lactic-co-glycolic acid) (PLGA) microparticles comprising ~10% DPPC and incubated them with AMs for 1 hour. AMs internalised significantly less PLGA-DPPC particles than the PLGA (DPPC-free) particles (26.2 ± 13.9 versus 65.1 ± 15.9), as demonstrated by confocal microscopy. Jones *et al.*, (2002) also incubated PLGA particles with surface adsorbed DPPC in media containing AMs, and also showed a reduction in microsphere uptake.

In conclusion, the lung has very efficient clearance mechanisms for foreign particles, which are likely to jeopardise the potential of a SR formulation to release drug over extended periods. Therefore pulmonary formulations for sustained release must (1) have a small MMAD and high FPF in order to minimise central/TB deposition and bypass the effects of mucocilliary clearance and (2) possess surface characteristics which will reduce AM recognition, uptake and clearance.

1.6.3 Methods of Achieving Pulmonary Sustained Release

By modifying the formulation of inhaled drugs, it may be possible to achieve sustained release. A pulmonary formulation that provides SR would generally require the drug to be incorporated into a particle suitable for delivery from an inhaler. To date however, no commercial SR formulation for pulmonary administration has been marketed. This section reviews some ways in which SR has been achieved in research and development.

1.6.3.1 Modulation of Dissolution Rate - Salts, Co-precipitates and Conjugates

Reducing the rate of dissolution is a potential means of achieving sustained release. For example, Jashnani *et al.*, (1992) showed that the stearate salt of salbutamol displayed a significantly slower dissolution profile than both salbutamol base and sulphate in phosphate buffer at 37 °C. The authors concluded that a stearate-rich layer covered the poorly soluble salt during dissolution studies, which may provide SR in the lung lining fluid. Hickey and Byron (1986), prepared solid co-precipitates of a water-soluble

fluorescein dye in magnesium hydroxide and showed a sustained release profile of the dye. However, both of these studies determined release from a powder compact, which would be expected to give rise to substantially slower release profiles than individual respirable particles, due to the enormous difference in surface area for contact with the dissolution medium. Conjugation of drug molecules with macromolecules has also been shown to provide SR. For instance, Williams and Taylor (1992) conjugated the acid of disodium cromoglycate with dextran (10000MW) and showed that SR was proportional to drug content, with half-lives of the drug conjugate ranging from 40 to 290 min.

1.6.3.2 Liposomes

There is a wealth of literature regarding liposomal drug delivery to the lung. Liposomes (Figure 1.6.3.2) are vesicles, which are formed when phospholipid molecules associate into bilayers in the presence of excess water or salt solution (Florence and Attwood, 1988). Phospholipids typically chosen are endogenous to pulmonary surfactant and therefore represent a biocompatible and non-toxic delivery system. Liposomes can be prepared in sizes applicable to pulmonary administration, and control over pulmonary retention time can be achieved by manipulating formulation variables (Fielding and Abra, 1992).

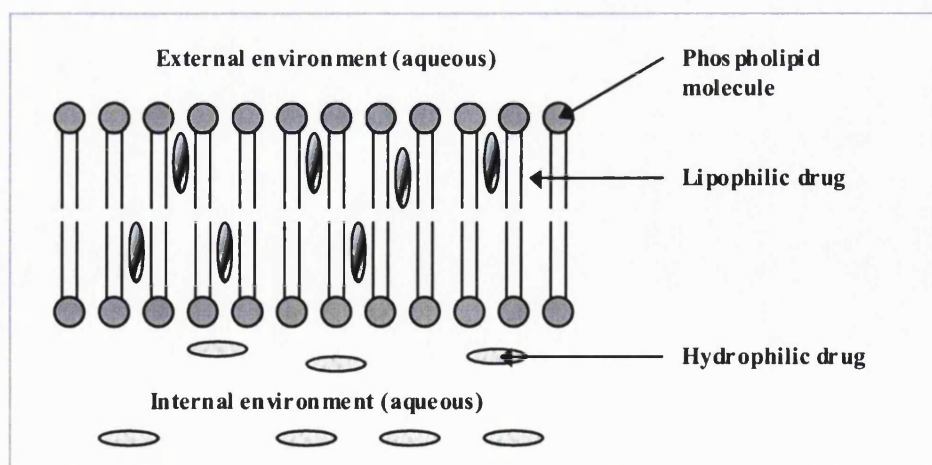


Figure 1.6.3.2: Section of liposome wall - phospholipid bilayer is continuous and forms a vesicle. Hydrophilic and hydrophobic drugs can be entrapped in the aqueous core or within the lipid bilayer, respectively.

A variety of hydrophilic and hydrophobic drugs have been incorporated into liposomes; Kellaway and Farr (1990) and Courrier *et al.*, (2002), have reviewed drugs specifically for pulmonary administration. These include: analgesics, antibiotics, anticancer agents, antioxidants, corticosteroids, glucocorticoids, gene therapy agents, immunosuppressants, interferons, insulin and other proteins and peptides.

The concept of liposomal SR delivery to the respiratory tract was proven by Juliano and McCullough (1980). The researchers showed that a chemotherapy agent arabinoside had a longer half-life for release in the lung than free drug (8 hours versus 1 hour, respectively). Retention within the lung provided more specific inhibition of DNA synthesis and minimization of systemic exposure (therefore a reduction in gastrointestinal and myelotoxic side-effects). McCalden *et al.*, (1989), administered liposomal orciprenaline to guinea pigs. Liposomes comprising saturated long-chain phospholipids and cholesterol were able to prolong the release of orciprenaline (half life = 20 hours versus 1.4 hours for free drug), provide protection against histamine bronchoprovocative challenge at 12 hours and reduce side effects (tachycardia and hypotension) compared to free drug. Taylor *et al.*, (1989) administered liposomal (DPPC:cholesterol 1:1) disodium cromoglycate to healthy volunteers. Detectable levels of cromoglycate were measured at 25 hours, whereas an equivalent dose of drug inhaled as a solution could not be detected. This investigation clearly showed the applicability of liposome mediated pulmonary SR in humans. Antifungal agents have poor lung penetration, thus Gilbert (1996) delivered amphotericin liposomes to mice and showed that effective protection against *Cryptococcus neoformans* challenge was evident 14 days post administration.

The poor efficiency of current nebulisers to deliver liquid aerosol to the deep lung might limit the success of SR therapy as deposition in the upper airways leads to rapid clearance (Barker *et al.*, 1994). Also, the nebulisation process can disrupt liposomes, resulting in release of the encapsulated drug. Liposomes are also unstable during storage, even at low temperature, which limits their practicality as commercial formulations (Taylor and Farr, 1993).

However, two developments may provide solutions to these problems. Firstly the development of more portable handheld nebulisers that produce smaller aerosol droplets will target the peripheral lung more effectively (Section 1.3.1). Secondly, some success has been derived from dry liposome powders for inhalation which may aid stability, e.g. for corticosteroids (Darwis and Kellaway 2003).

1.6.3.3 Microparticles

Microparticles include microspheres, microcapsules and irregular shaped particles, and as they can be prepared as dry particulates, confer greater *in vitro* and *in vivo* stability over aqueous liposomal formulations (Courrier *et al.*, 2002). Production of microparticles is desirable as altering a number of process parameters can easily control particle size.

Zeng *et al.*, (1995b) developed albumin microspheres for the delivery of tetrandine, an anti-silicotic agent used for the treatment of occupational silicosis. A respirable fraction (<6.4 μm) of 11-18% was reported for the formulation, which although low, provides greater lung drug concentrations than those achieved with conventional oral dosing. Li *et al.*, (2001) also used albumin microspheres to entrap ciprofloxacin, and showed *in vitro* SR profiles of the antibiotic over 12 hours.

Non-inhalational formulations of polymeric SR microparticles can be prepared in a size range for passive lung targeting (> 7 μm , Selek *et al.*, 2003). Upon injection, targeting of terbutaline sulphate/PLGA microspheres to the lung was achieved, although specificity was low as a slightly greater amount of microspheres targeted the liver. This method for SR delivery to the lung has a number of drawbacks: (1) drug loading is very low (1-4% w/w) which would require large amount of SR microparticles to be administered, (2) daily injections to asthmatic patients is not acceptable given current inhalation practice and (3) delivery to the systemic circulation is unnecessary and will lead to side effects. However, targeting of lung tumours by this method with anti-cancer agents could well be efficacious.

PLGA and poly(L-lactic acid) (PLA) microparticles have also been delivered directly to the lung for SR applications. Lai *et al.*, (1993) reported prolonged protection against bronchoconstriction challenge in rats, at least 12 hours post-administration with PLGA/isoproterenol microspheres. In addition, El-Baseir and Kellaway (1998) entrapped beclomethasone dipropionate and nedocromil sodium in PLA microparticles and showed SR *in vitro* for 8 days and 6 days respectively.

However, pulmonary administration of PLA microspheres to rabbits was associated with inflammation at sites adjacent to microparticle deposition. Neutrophil count was significantly raised at 24 hours together with incidence of haemorrhage (Armstrong *et al.*, 1996). PLA and PLGA microparticles also show significant reduction in cell viability compared with lipid particles in cell based toxicity screens (Muller *et al.*, 1996), and long residence due to slow degradation (Dunne *et al.*, 2000) might lead to polymer accumulation in the lung, especially with daily administration.

A reduction in the amount of PLGA may provide acceptable biocompatibility. For instance, Singh *et al.*, (2002), pulsed laser coated budesonide microparticles with nano-thin layers of PLGA, and still achieved an *in vitro* time taken for 50% drug release (t_{50}) of 60 minutes, relative to 1.2 minutes for uncoated drug. Alternatively, oligolactic acids (OLA), that have a shorter biological half-life than PLA, may be more suitable than PLA/PLGA for pulmonary delivery (Labiris and Dolovich, 2003b). Edwards *et al.*, (1997) originally achieved *in vivo* sustained release of insulin in rats with large porous particles fabricated from PLGA, and showed less macrophage uptake and immune response to the larger particles relative to non-porous controls. However, current formulation strategies for SR porous particle technology employ non-polymeric endogenous excipients, e.g. phospholipids/albumin/lactose, which may be more suitable for commercialization as excipient clearance is more favourable (Ben-Jebria, *et al.*, 1999; Dellamary *et al.*, 2000; Basu *et al.*, 2001). Also, oligoester derivatives (OEDs) have provided *in vivo* SR - for instance, 24-hour plasma levels in rats have been acquired with for leuprolide/OED particles (Alcock *et al.*, 2002).

1.6.3.4 Nanoparticles

Nanoparticles may also provide SR, although due to the high surface area to volume ratio, SR is typically only achieved with hydrophobic molecules or physically entrapped macromolecules. Solid lipid nanoparticles (SLNs) provide SR for a variety of drugs (Muller *et al.*, 2000); however, their use in pulmonary drug delivery is yet to be exploited. Kawashima *et al.*, (1999) formulated PLGA nanoparticles containing insulin that provided reduction in glucose plasma levels for over 48 hours. Chitosan-PLGA nanoparticles have also shown promise in SR peptide delivery to the respiratory tract, as they are mucoadhesive, which extends residence time and duration of action to over 24 hours (Takeuchi *et al.*, 2001).

1.7 Research Scope

At present there are a variety of highly effective drugs on the market for the treatment of respiratory conditions. However, there are no SR products on the worldwide market for pulmonary drug delivery despite active research in the field for over 20 years.

The purpose of this research was to develop, optimise and characterise novel microparticle formulations for the SR of terbutaline sulphate. Terbutaline sulphate was selected as a model drug for its hydrophilic nature and relatively short duration of action, making it an ideal candidate for SR formulation development. However, this particular drug represented a considerable challenge to SR formulation owing to its high water solubility (>30% w/w). No pharmacopoeial methods exist for assessing drug release from SR particles in the respiratory tract, therefore one of the aims of the project was to develop suitable *in vitro* testing apparatus and another aim was to test the formulations in release media which were representative of the lung. Once SR profiles were accomplished and release mechanisms determined, the final purpose of the research was to evaluate *in vitro* aerosol performance, to ensure that the formulation was suitable for delivery to the peripheral lung where extended residence is expected.

Chapter 2: Controlled Crystallization of Terbutaline Sulphate (TS)

2.1 Introduction

Crystallization is the process in which molecules assemble into a solid mass, characterised by a regular internal structure and planar external geometry. Three stages are required for crystallization to occur: supersaturation, nucleation and crystal growth (Mullin, 1993).

Supersaturation is an essential requirement for all crystallization procedures as it drives the transition from solution to the solid state. The difference between the elevated actual concentration and its solubility at the same temperature is the supersaturation of the solute in a given system (David and Giron, 1998). Miers and Isaac (1907) developed a diagrammatic representation (Figure 2.1.1) of the relationship between solubility, supersaturation and crystallization. The diagram explains the tendency of a supersaturated system to undergo spontaneous crystallization.

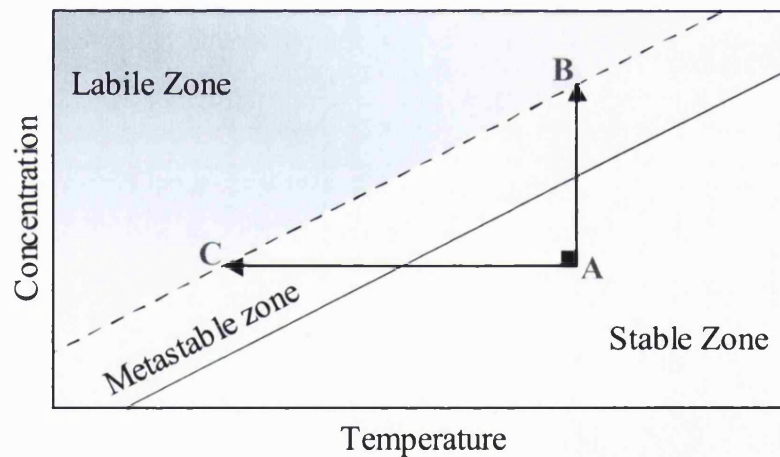


Figure 2.1.1: Adapted solubility-supersaturation diagram. Black diagonal line represents the solubility curve. Upper broken diagonal line represents supersaturation curve, above which is the labile/supersaturated zone where spontaneous crystallization is probable. Between the two lines is the metastable zone where spontaneous crystallization is improbable unless the system is seeded by another crystal and growth occurs. Crystallization is impossible in the stable zone as the solute remains in solution. Moving from A to B represents evaporation and A to C represents cooling. Both processes, commonly used in industrial crystallization, move the system to the labile zone where crystallization is possible.

Before crystallization can occur, there must exist in solution a number of minute solid bodies that act as centres of crystallization i.e. nuclei/seeds (Mullin, 1993). Nucleation may either occur spontaneously or be induced artificially. For spontaneous nucleation a cluster of constituent molecules need to coagulate, resist the tendency to redissolve and become oriented in a fixed lattice. Whether or not the newly formed cluster grows or redissolves is dependant upon the free energy of the process which, in turn, is directly linked to particle size. Particles smaller than a critical size (r_c) will dissolve and particles larger than the critical size will continue to grow. Artificial nucleation occurs when seed crystals or impurities are added to a supersaturated system, the addition of which promotes further nucleation.

Crystal growth is a complex process that takes place once stable nuclei are formed, which leads to further deposition of solute molecules onto the growing crystal faces. Numerous models for crystal growth are excellently reviewed in Mullin (1993), and David and Giron, (1998).

Crystallization from solution is the most widely used method for obtaining solid pharmaceutical agents (Kachrimanis and Malamataris, 1999; Shekunov and York, 2000), and is typically achieved by evaporation or cooling or by the addition of a poor solvent (solvent-change). Crystallization engineering techniques employ alternative crystallization conditions in order to obtain raw materials with improved properties (York, 1992). Controlled crystallization is a potential method of engineering drug microcrystals through manipulation of the crystallization process. Additives such as long chain polymers or surface-active agents have a tendency to adsorb at the crystal-solvent interface and affect crystal growth kinetics. The most common observation for the effect of additives on crystallization is a reduction in crystal size, often associated with a growth rate decrease (Canselier, 1993).

The use of polymers to inhibit the growth of crystals was investigated by Simonelli *et al.*, (1970). This study examined the effect of poly(vinyl pyrrolidone) (PVP) on sulphathiazole crystallization. The authors found that

the presence of polymer affected two key processes, crystal growth rate and crystal growth pattern (Figure 2.1.2).

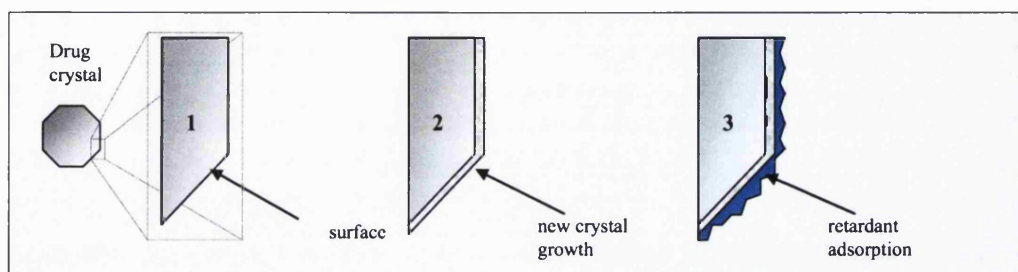


Figure 2.1.2: Controlled crystallization theory: 1 = Appearance of growing crystal surface outline, 2 = Normal crystal growth (smooth linear lines) in the absence of retardant, 3 = Control of crystal growth by retardant adsorption to growing crystal face. The adsorption creates a net covering the crystal surface, which changes both crystal growth rate and crystal growth pattern.

Crystal growth rate is retarded by the amount of PVP adsorbed onto the growing crystal face. This slows the diffusion rate of sulphathiazole to the crystal surface from bulk solution. PVP may bind to the surface in a net-like film that disrupts the crystal growth pattern. Crystal growth then only occurs as protrusions through gaps in the film. However, due to higher curvature of these protrusions the minimum supersaturation ratio for growth increases. As the amount of PVP bound increases, the net becomes tighter reducing protrusion radii, such that the minimum supersaturation ratio increases to a point where crystal growth is completely inhibited.

Investigations of the interactions between drug and PVP were also performed by Ziller and Rupprecht (1988). The results showed, in agreement with Simonelli *et al.*, (1970) that the inhibitory effect of PVP on drug crystallization was primarily attributable to protective PVP layers adsorbed on the crystal face, especially in active site regions (areas of crystal growth). The hydrophilic-hydrophobic property of a polymer influences drug crystallization by an adhesive force between drug and polymer (Suzuki and Sunada, 1998) such that judicious polymer choice will maximise this adhesive force and exert

greater control over the crystallization process. An alternative model for control of crystallization is the direct adsorption of PVP onto crystal nuclei (Ma *et al.*, 1996), which represents an explanation for total growth inhibition rather than rate retardation.

The following research aims to show the effect of PVP, and other additives, upon the crystallization of TS. At additive levels lower than that required to cause growth inhibition, a reduction in crystal size might be possible. The required TS particle size target is <2 μm , which would be appropriate for subsequent coating with a sustained release matrix (1-2 μm expected coat thickness). In order to develop a pulmonary sustained release formulation, the overall particle size must be kept below 5 μm (Gonda and Byron, 1978) to obtain particulates suitable for pulmonary deposition.

2.2 Materials

2.2.1 Model Drug

The hydrophilic drug, terbutaline sulphate (TS), was generously supplied in micronised form by Investigational Products at AstraZeneca R&D Charnwood (Loughborough, Leicestershire, UK). A brief description of TS is provided in Table 2.2.1. The same batch (Lot 4104H) was used throughout the research.

2.2.2 Growth Retardants

Poly(vinyl pyrrolidone) (10000MW), Poly(acrylic acid) (PAA, 2000MW) and Polysorbate 80 were purchased from Sigma-Aldrich Company Ltd. (Gillingham, Dorset, UK). Pluronic[®] poloxamers and reverse poloxamers were kindly supplied by BASF Corp. (Mount Olive, NJ, USA) as research samples.

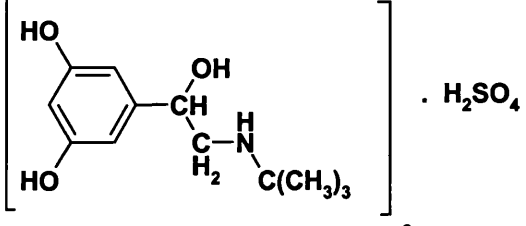
Physical Form	White to off-white greyish crystalline powder with faint odour of acetic acid.
Molecular Weight	548.6
Molecular Structure and Formula	 $(C_{12}H_{19}NO_3)_2 \cdot H_2SO_4$
Solubility	Freely soluble in water (1 in 4), Slightly soluble in 95% ethanol, Practically insoluble in acetone, chloroform, dichloromethane, and diethyl ether.
Melting Point	Approximately 250 °C with decomposition
Storage	Protect from light in airtight containers at 15-25 °C

Table 2.2.1: Terbutaline Sulphate (TS) characteristics

2.2.3 Solvents

All solvents used were at least GPR grade. Ethanol 96% and absolute ethanol were provided by Hayman Ltd. (Witham, Essex, UK). Acetone, butan-1-ol, chloroform, diethyl ether and methanol were obtained from VWR International Ltd. (Poole, Dorset, UK) and cyclohexane, hexane, octan-1-ol and tetrahydrofuran from Sigma-Aldrich Company Ltd. Deionised water was obtained from an Option 4 water purification system (Elga Ltd., High Wycombe, Buckinghamshire, UK).

2.3 Methods

2.3.1 Crystallization

An excess (>40% w/v) of TS was added to 0.01 M H₂SO₄ (aq), and then magnetically stirred on a RT10 Power stirrer (IKA Werke GmbH., Staufen, Germany) for 24 hours in order to obtain a saturated drug solution. The liquid was then filtered through a 47 mm diameter 0.1 µm nylon membrane filter

(Whatman International Ltd., Maidstone, Kent, UK) using a Buchner funnel to remove undissolved drug.

Anti-solvent systems were prepared prior to initiating crystallization experiments. The desired amount of growth retardant was directly weighed (5-figure balance) into a 100 mL volumetric flask, and then made up to volume with solvent. Saturated TS (aq), 0.4 mL, was then added to 20 mL anti-solvent during magnetic stirring (600 rpm, constant speed) in a crystallization vessel. The vessel was then covered with Parafilm[®] M film (Pechiney Plastic Packaging Inc., Chicago, IL, USA) to prevent solvent evaporation. Stirring was then continued for a defined time and speed until TS crystals were obtained. Crystals were subsequently separated from the anti-solvent by vacuum filtration through a 0.1 μm nylon membrane filter. Once collected, the crystals were rinsed with three 25 mL aliquots of pure anti-solvent. When temperature reduction was required, samples were placed in a sodium chloride/ice bath on top of the magnetic stirrer and the antisolvent systems were acclimatised for one hour in the bath until stable temperature was achieved (± 0.5 °C). Temperature increases were achieved in similar fashion, but through the use of a warm water bath. All crystal studies were performed in triplicate.

2.3.2 Drying

Unless otherwise stated, the TS crystals were placed in a model D100 oven (WTB Binder GmbH, Tullingen, Germany) for 12 hours at 50 °C.

2.3.3 Crystal Sampling

In order to obtain representative samples of the crystal population, segments of the dry mass (total = 10 mg) were taken. Breaking the dry mass into a powder prior to sampling would have introduced bias by allowing segregation of individual crystals within the powder.

2.3.4 Laser Diffraction Particle Sizing

Laser diffraction was performed using a Malvern Instruments Mastersizer X (Malvern Ltd., Worcestershire, UK) in order to obtain a numerical indication of particle size. The instrument operates with a He-Ne 632.8 nm laser diffraction source and operates over a 0.5 - 900 μm particle size range. A Malvern MS7 magnetically stirred small volume (15 mL) diffraction cell was thoroughly cleaned prior to use to avoid cross-contamination and then filled with filtered chloroform. Approximately 10 mg TS crystals were sonicated for 60 seconds (XB6 Ultrasonic Bath, Grant Instruments Ltd., Royston, Herts, UK) in 0.5% w/v Span 85 in chloroform (5 mL) to aid sample dispersion. The sample was then pipetted dropwise into the MS7 cell until a suitable obscuration value was achieved (preferably 10-15%). A mathematical model or 'presentation' was used to generate a particle size distribution from the diffraction data and the machine was run in polydisperse mode. Accurate refractive indices for the TS particles (value obtained from AstraZeneca R&D Charnwood) and medium (Chloroform, 1.456) are required for the analysis. The sizing process was repeated three times for each sample to ensure reproducibility. Means were then taken for the following values: $D(v, 0.1)$, 10% particle size cut-off; $D(v, 0.5)$, 50% particle size cut-off, also known as the Volume Median Diameter (VMD); $D(v, 0.9)$, 90% particle size cut-off.

2.3.5 Sample Visualisation

Samples were visualised with light microscopy (LM) and scanning electron microscopy (SEM) where appropriate. SEM analysis was performed by Mr. D. McCarthy of the SEM service at the University of London, School of Pharmacy. Samples were immobilised on metal stubs by brushing the crystals over a piece of double-sided adhesive carbon tape. The sample was then sputter-coated with gold atoms using a K550 machine (Emitech Ltd., Ashford, Kent, UK) and then visualised using a XL20 electron microscope (Philips, Eindhoven, Netherlands).

2.4 Results and Discussion

2.4.1 Controls

All crystals produced from controlled crystallization experiments were compared with a control particle size distribution (Table 2.4.1). This distribution was obtained from TS crystallization in absolute ethanol without growth retardant. Crystallization was evident after 15 minutes of stirring. Any reduction in size from this distribution in the test experiments was taken to indicate growth retardant mediated control over the crystallization process. Also included for reference in this table is the particle size distribution of pure, micronised TS, as received from AstraZeneca.

Sample	D(v, 0.1) (μm)	D(v, 0.5) \pm SD (μm), VMD	D(v, 0.9) (μm)	Span \pm SD
Control	2.37	6.49 \pm 1.2	18.3	2.46 \pm 0.89
TS micronised	0.95	2.96 \pm 0.067	6.56	1.90 \pm 0.045

Table 2.4.1: Particle size distributions of reference samples.

Span = indicator of spread given by: $(D(v, 0.9) - D(v, 0.1)) / D(v, 0.5)$.

Figures 2.4.1.1 and 2.4.1.2 are scanning electron micrographs of the control TS crystals and micronised TS respectively. The control crystals appear to be long, thin and plate-like in appearance. Micronised TS has an appearance typical of milled material with slightly rounded edges to the particles.



Figure 2.4.1.1: TS crystallised from absolute ethanol without retardant.



Figure 2.4.1.2: Micronised TS.

2.4.2 Controlled Crystallization of TS with PVP as Growth Retardant

Crystallization was initially attempted with 96% v/v ethanol as anti-solvent. Despite agitation with a glass rod (to promote nucleation) and overnight refrigeration (to reduce solubility), no crystallization took place either in the presence or absence of PVP. It is expected that the presence of 4% v/v water in the 96% v/v ethanol was sufficient to maintain TS solubility thus preventing crystal formation.

Diethyl ether was chosen as the next anti-solvent since it is a less polar solvent than ethanol. In a 50:50 diethyl ether:96% v/v ethanol system, crystallization occurred but with very low yield. The presence of PVP as growth retardant led to the formation of resinous matter (thought to comprise of PVP, terbutaline and water) that lined the glass crystallization vessel.

Absolute ethanol was the first anti-solvent in which crystals were successfully produced. As indicated in Figure 2.4.2.1, the presence of PVP in the crystallization media, led to a concentration-dependant reduction in TS yield.

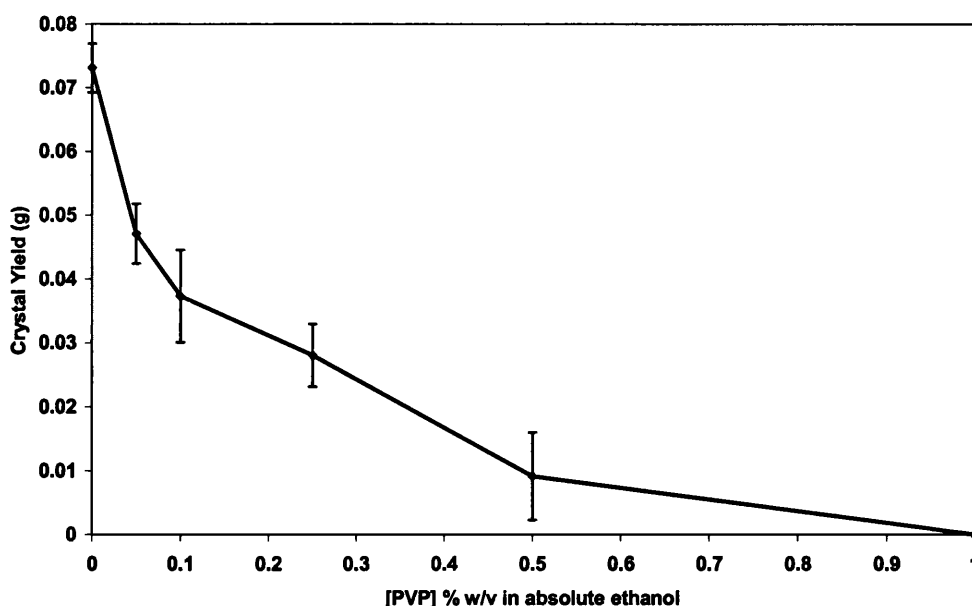


Figure 2.4.2.1: Correlation between PVP concentration and Crystal Yield. As PVP concentration increases, yield was reduced. At 1% w/v PVP, crystallization was completely inhibited ($n=3 \pm SD$).

The presence of 0.25% w/v PVP in the system reduced the yield by approximately 60% relative to the absence of PVP, indicating the dramatic capacity for PVP to exert influence over the crystallization process. It is also worthy to note that time for crystallization to initiate increased with a rise in PVP concentration (15 minutes for 0% w/v PVP, >12 hours for 0.5% w/v PVP) - this effect was also observed by Raghavan and co-workers for the crystallization time of hydrocortisone acetate in the presence of PVP (Raghavan *et al.*, 2001).

At 1% w/v PVP, no crystallization was observed, which indicates that nucleation was possibly inhibited (Ma *et al.*, 1996), thus preventing growth.

No correlation was found, between increasing PVP concentration and particle size as it was not possible to size unit crystals. This was confirmed by scanning electron microscope images that showed large randomly sized aggregates of crystals. Crystals obtained from 0.25% w/v PVP in absolute ethanol (shown in Figure 2.4.2.2) had a VMD equal to 18.7 μm , which showed that it was not possible to de-aggregate the crystal mass to unit crystals during preparation for particle sizing.

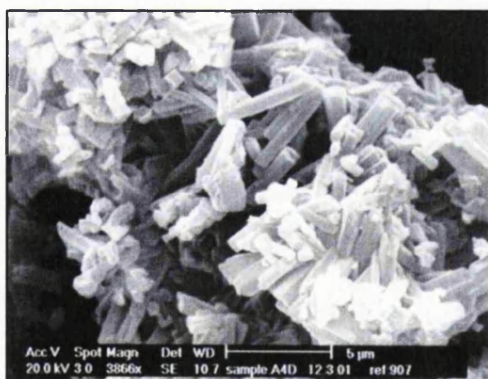


Figure 2.4.2.2: Large TS aggregates, crystallised from 0.25% w/v PVP in absolute ethanol. Unit crystal size appears to be <5 μm .

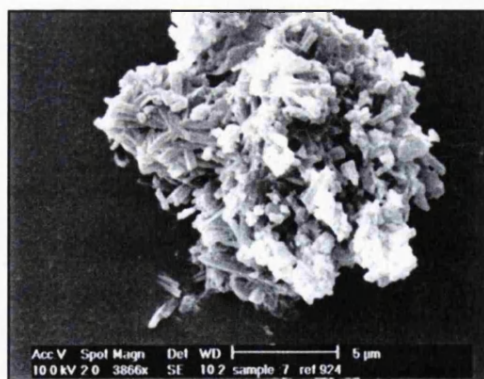


Figure 2.4.2.3: Increased wash volume (25 mL vs. 75 mL). Aggregation still apparent.

Increasing the volume of absolute ethanol used to rinse the crystals from 25 mL to 75 mL in attempt to de-aggregate the crystals did not reduce aggregation (VMD = 15.0 μm , Figure 2.4.2.3). Drying the crystals in a

vacuum oven (as opposed to hot air drying, which may have fused the crystals), and particle sizing in absolute ethanol (rather than chloroform as dispersant) likewise showed no effect on the observed aggregation. Although individual crystals appeared to be of a suitable size for progression, aggregation was found to be a limiting factor. These aggregates are classed as polycrystalline granules that consist of monocrystals attached by rigid joints made up from the same bonds as within the crystals themselves (David and Giron, 1998). Garekani *et al.*, (2000) also demonstrated comparable aggregation with the crystallization of paracetamol in the presence of PVP. Individual paracetamol crystals had a size of 1-2 μm , but, as in this case, were present as 10-40 μm granules.

Crystallization was also performed in acetone-absolute ethanol co-solvents. Figure 2.4.2.4 highlights crystals obtained from 0.1% w/v PVP in 50:50 absolute ethanol:acetone system. Despite a further reduction in individual crystal size (a large proportion of crystals are visibly of submicron size), aggregation was greatly increased in these systems. At all levels of PVP investigated, the $D(v, 0.9)$ values exceed 50 μm compared to absolute ethanol systems where the $D(v, 0.9)$ values did not exceed 40 μm . This clearly highlighted the extent of aggregation in the acetone containing systems. The lower solubility of TS in the acetone/ethanol system, relative to ethanol, was likely to promote higher initial levels of supersaturation where the presence of too many seed crystals leads to overcrowding and the development of highly aggregated particles (Mullin, 1993).

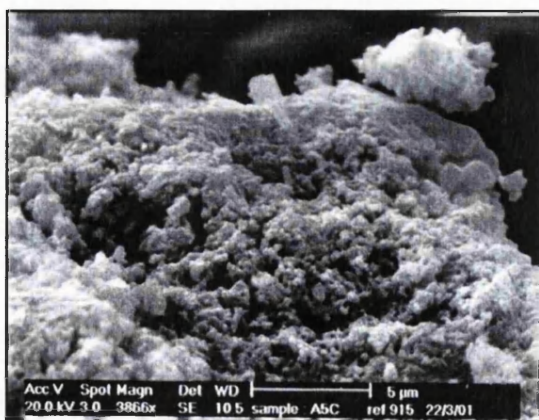


Figure 2.4.2.4: Fused TS crystallized from 0.1% w/v PVP in 50:50 absolute ethanol:acetone.

2.4.3 Controlled Crystallization of TS with PAA as retardant

Aggregation tendency was reduced with the use of PAA as shown by the decrease in VMD sizes relative to PVP systems. For 1% and 2% w/v solutions of PAA in absolute ethanol the VMD values \pm SD were $6.03 \pm 0.032 \mu\text{m}$ and $5.75 \pm 0.32 \mu\text{m}$, respectively. The presence of PAA produced crystal populations that had less inter-batch variability in size (reduction in standard deviation), which suggested crystal size was tightly controlled by the polymer. However, the size of crystals generated in the presence of PAA was not significantly reduced (t-Test, $p > 0.05$) compared to the control population.

2.4.4 Controlled Crystallization of TS with Polysorbate 80 as Retardant

As for PAA, the nonionic surfactant, Polysorbate 80, had no significant effect on limiting TS crystal size during crystallization relative to control.

2.4.5 Controlled Crystallization of TS with Poloxamers as Retardants

Poloxamers are non-ionic polymeric surfactants which are based on triblock copolymers of poly(ethylene oxide) (hydrophilic) and poly(propylene oxide) (hydrophobic) (see Appendix A for structure and nomenclature). Variation of the block copolymer structure gives rise to a range of surfactants with a variety of properties and characteristics (Alexandridis *et al.*, 1994). TS crystal size was significantly controlled (t-Test, $p < 0.05$) by a number of poloxamer/absolute ethanol systems. The particle size data for the most effectively controlled systems are shown in Table 2.4.5. No clear trends however were observed for the effect of poloxamer concentration on particle size across the range of surfactants studied (poloxamers L101, L44, L64, 10R5 and 17R2, 17R4 and 25R4).

% w/v poloxamer	D(v, 0.1) (μm)	VMD ± SD (μm)	D(v, 0.9) (μm)	Span ± SD	t-Test vs. control (p)
4% L44	1.63	4.26 ± 1.2	9.95	1.95 ± 0.18	0.034
10% L64	1.70	4.14 ± 0.067	8.92	1.74 ± 0.099	0.028
2% L64 / 2% L101	1.61	3.57 ± 0.34	7.45	1.64 ± 0.062	0.015

Table 2.4.5: Particle size distributions of controlled crystallization samples, n=3.

The systems containing 4% L44 (Figure 2.4.5.1) and 10% w/v L64 (Figure 2.4.5.2) generated particle sizes that represented 34% and 36% size reductions in VMD relative to control.



Figure 2.4.5.1: TS crystallized from 4% L44 w/v in absolute ethanol.



Figure 2.4.5.2: TS crystallized from 10% w/v L64 in absolute ethanol.

It was clear from particle size data and SEM evidence (Figures Figure 2.4.5.1 and 2.4.5.2) that extensive aggregation (that was apparent in PVP batches) was absent with the use of poloxamers. Unit size however was larger and this arose from a reduction in affinity for the growing crystal surface relative to that of PVP. The mechanism of growth retardation for poloxamers has similarities with that of PVP, as poloxamer molecules adsorb to the surface (Tanninen *et al.*, 1992; MacKellar *et al.*, 1994). However, the free surfactant chains protruding into solution were likely to provide a more efficient steric barrier to the approach of additional solute molecules and/or other crystals in suspension. This protective barrier has been shown to prevent aggregation (El-Bary *et al.*, 1990; Canselier, 1993), possibly by disrupting the joint formation responsible for polycrystalline granule formation. The morphology

of the crystals produced from poloxamer containing systems was typically prismatic, as opposed to the flat, plate-like appearance of the control batch (Figure 2.4.1.1). This change in habit evolved from different extents of adsorption (due to molecular characteristics) on different crystal faces (Raghavan *et al.*, 2001). The crystals appeared smoother than the control batch - typical of crystallization from surfactant systems (Canselier, 1993). Crystallization in the absence of surfactants yielded crystals that were prone to fragmentation due to crystal collisions (evident in Figure 2.4.1.1) and the absence of the protective barrier, thus altered crystal appearance was observed.

TS crystal particle size was affected by the hydrophile-lipophile balance (HLB) of the poloxamer (Figure 2.4.5.3). Median crystal particle size was limited by surfactants having high (>12) HLB values, which was anticipated for a highly hydrophilic drug such as TS. This finding was in agreement with work by MacKellar *et al.*, (1994), which found that suppression of crystal size for a model drug was more pronounced with increased hydrophilicity of the surfactant. It was hypothesised that the hydrophilic poly(ethylene oxide) chains adsorbed to hydrophilic/polar faces of the crystals and prevent growth. The control over particle size was enhanced with increased hydrophilicity of the poloxamer. This theory was further supported by the fact that the hydrophobic poly(propylene oxide) chain of the poloxamer preferentially locates towards ethanol relative to the hydrophilic poly(ethylene oxide) chain (Ivanova *et al.*, 2001).

Poloxamer surfactants with HLB values greater than 16 may exert greater control over particle size. However, the poor solubility characteristics of these high HLB surfactants in absolute ethanol precluded their use in the investigation.

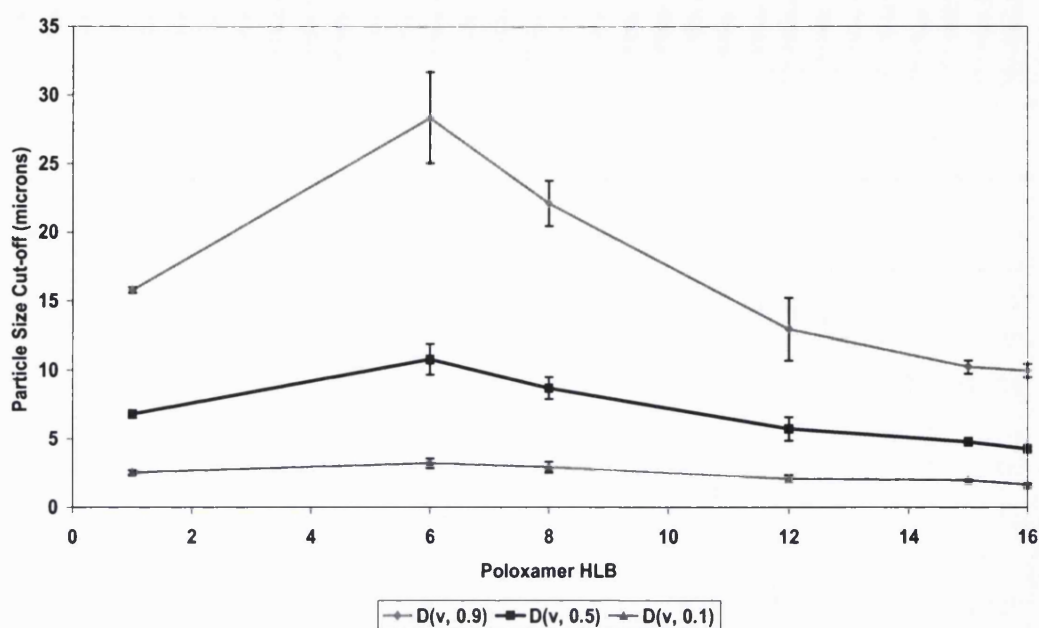


Figure 2.4.5.3: Correlation between Poloxamer HLB and Particle size cut-off diameters. (n=3, Poloxamer concentration = 4% w/v) Greatest size retardation achieved at high HLB.

Conversely, low HLB values (< 12) promoted an increase in particle size (except for HLB = 1, where size was not significantly different to control); for example, crystallization from a 1% w/v poloxamer 17R2 (HLB = 6) system, VMD was equal to 11.1 μm (significantly larger than control, $p < 0.01$). This signified that the presence of these surfactants created an environment in which crystal growth was promoted, possibly through the facilitation of mass transfer to the growing surface (Canselier, 1993).

The combination of a high HLB (L64, HLB = 15) surfactant with a low HLB (L101, HLB = 1) surfactant controlled TS crystal size to the greatest degree (Figure 2.4.5.4). At all concentrations of this surfactant combination investigated, particle size was significantly limited. The use of a 2% w/v L64/2% w/v L101 system in absolute ethanol gave 45% size reduction relative to control. However, the mechanism behind the synergism between low and high HLB poloxamers remains uncertain as when used alone, the low HLB poloxamer generated crystals sizes that were not significantly different from control.



Figure 2.4.5.4: TS crystallized from 2% w/v L64/2% w/v L101 in absolute ethanol.

2.4.6 Optimisation of Crystallization Conditions

The 2% w/v L64/2% w/v L101 in absolute ethanol system gave rise to the smallest TS crystals obtained. This system was therefore optimised for solvent selection, temperature of crystallization, stirring speed and time, with the overall aim to limit particle size further. Table 2.4.6.1 shows the effect of changing the solvent characteristics by varying alcohol selection. Increasing the hydrophobicity of the non-solvent, by selecting higher molecular weight alcohols, served to increase particle size.

The effect of temperature on the crystallization conditions is shown in Table 2.4.6.2. As the temperature was increased from 0 °C to 22.5 °C (laboratory temperature), the particle size reduced from 7.1 to 3.6 μm respectively (regression coefficient = 0.989). At 30 °C however, the relationship was reversed and the particle size increased relative to 22.5 °C. This effect may have arisen through solvent evaporation from the crystallization media (solvent condensation on sides of vessel and Parafilm[®] cover was visible), which altered TS solubility and promoted crystal growth. Variations of crystallization temperature therefore offered no advantage on the smallest particle size obtained previously.

Investigations to optimise this system for particle size by altering crystallization time and stirring speed were also unsuccessful as the particle sizes obtained did not show improvement below 3.6 μm, as achieved in earlier studies.

% w/v poloxamer	Additional solvent*	D(v, 0.1) (µm)	VMD (µm) ± SD	D(v, 0.9) (µm)	Span ± SD
2% L64 /2% L101	methanol	-	-	-	-
2% L64 /2% L101	ethanol	1.61	3.57 ± 0.34	7.45	1.64 ± 0.062
2% L64 /2% L101	butan1-ol	2.42	5.50 ± 0.89	10.89	1.54 ± 0.034
2% L64 /2% L101	octan-1-ol	3.00	6.39 ± 0.96	11.24	1.29 ± 0.12

Table 2.4.6.1: Effect of solvent system on particle size distributions of controlled crystallization samples (n=3). No crystallization occurred the methanol-based system.

* additional antisolvent represents 50% of stated solvent mixed with absolute ethanol.

% w/v poloxamer	Temp (°C)	D(v, 0.1) (µm)	VMD (µm) ± SD	D(v, 0.9) (µm)	Span ± SD
2% L64 /2% L101	0	2.78	7.08 ± 0.85	15.97	1.86 ± 0.12
2% L64 /2% L101	7.5	2.38	6.21 ± 0.57	13.90	1.85 ± 0.12
2% L64 /2% L101	15	2.06	4.64 ± 0.36	9.74	1.65 ± 0.10
2% L64 /2% L101	22.5	1.61	3.57 ± 0.34	7.45	1.64 ± 0.062
2% L64 /2% L101	30	2.06	4.78 ± 0.41	9.87	1.63 ± 0.057

Table 2.4.6.2: Effect of temperature on particle size distributions of controlled crystallization samples (n=3).

2.5 Conclusion

The effect of a variety of polymers and surfactants on the crystallization of terbutaline sulphate was significant. For systems containing PVP as growth retardant, microscopic evidence indicated that individual TS crystal size was substantially reduced in all cases investigated. However, the final product was collected in a highly aggregated state, which was not suitable for use.

Poloxamer-based systems did not limit TS particle size to the same extent as PVP, but the crystals showed little aggregation and were therefore re-dispersible. The optimal particle size obtained was 3.6 μm . A detailed investigation into the interaction between the poloxamer surfactants and the growing TS crystal faces may provide opportunities for further growth retardation and generate pure drug particles in a size range suitable for inhalation. This would provide a favourable alternative to the current industrial manufacturing practice of crystallization followed by micronisation/milling. The latter step is an expensive, high-energy process, which can generate defects in the crystal surface and regions of surface amorphicity thus altering product performance (Ward and Schultz, 1995).

Recently, work by Steckel and coworkers involving similar controlled crystallization techniques has highlighted the application of the technique for generating micronised particles (sodium cromoglycate and fluticasone propionate, Steckel *et al.*, (2003a) and (2003b), respectively). Once spray-dried directly from the crystallization suspension, the particles were suitable for dry powder inhalation.

The aim of 1-2 μm required for further processing of the crystals into a sustained release dosage form, however, was not achieved. Coating crystals possessing a median diameter of 3.6 μm would have placed the final particle size beyond that of which is suitable for pulmonary deposition. This work was halted in favour of direct incorporation of TS into a matrix particle (Chapter 3) and TS nanoparticle generation followed by coating with a sustained release excipient (Chapters 4 and 5).

Chapter 3: Polysaccharide Matrix Microparticles

3.1 Introduction

Controlled crystallization of TS did not meet the required particle size limit of $<2\ \mu\text{m}$. A molecular dispersion of drug within a polysaccharide matrix particle is a potential way of achieving SR (Thanoo *et al.*, 1992). This method may circumvent the coating step, which would have been required for the crystallization method (Figure 3.1). The principal aim of the following investigation was to incorporate TS within a polysaccharide matrix particle. Polysaccharide chains may also be complexed with a counter-ion in order to modify particle density and achieve a greater control over drug release through the matrix.

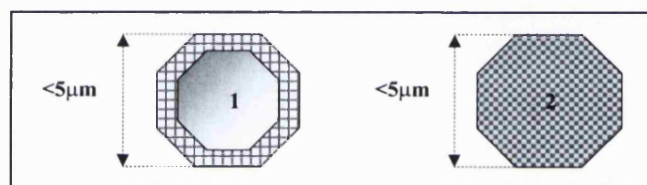


Figure 3.1: Pulmonary SR formulation aims:
(1) Controlled crystallization of drug followed by application of matrix coat.
(2) Direct incorporation of drug into matrix.

3.1.1 Matrix Microparticle Excipients I: Chitosan (CS)

The matrix-forming agent chosen for preliminary experiments was CS. CS (Figure 3.1.1), a biodegradable cationic polysaccharide, which forms gels with multivalent anions; this property is responsible for the polymer's ability to retard drug release. The use of CS in the pharmaceutical field was extensively reviewed in the literature (e.g. Kaş, 1997) and has been used for a variety of drug delivery applications. Particle sizes of the reviewed CS microspheres are frequently in excess of $5\ \mu\text{m}$. Spray-drying methods, however, have produced CS microspheres in the desired size range for pulmonary delivery (Williams III *et al.*, 1998) and which were compatible with pMDI formulations.

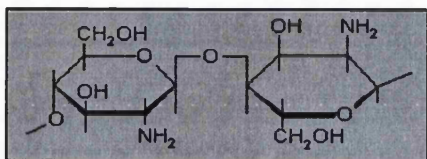


Figure 3.1.1: Chemical structure of CS.

3.1.2 Matrix Microparticle Excipients II: Sulphated Polysaccharides

Carrageenan (CGN) is a biodegradable marine hydrocolloid polysaccharide, which has been used in tableting controlled release applications (reviewed by Bhardwaj *et al.*, 2000). CGN (Figure 3.1.2.1) contains sulphate groups that will potentially interact with TS. Anionic excipients may offer control over the early release of soluble basic drugs through ionic interactions (Ranga Rao *et al.*, 1990). Three types of CGN were selected for investigation, *lambda* CGN (non-gelling), and *kappa* CGN and *iota* CGN (both gelling).

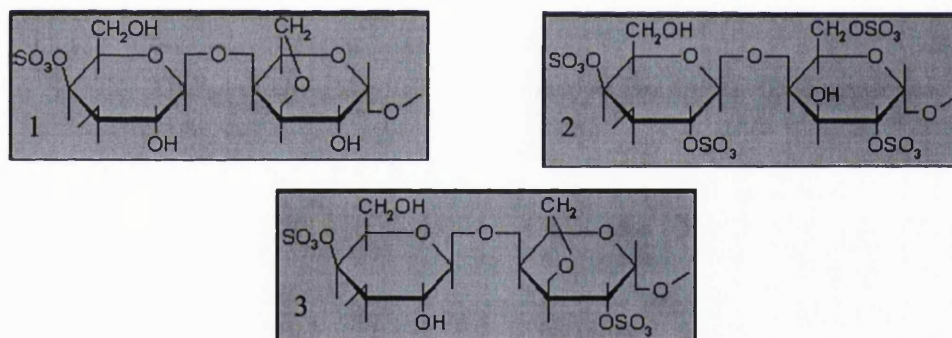


Figure 3.1.2.1: Structures of CGN. (1) *Kappa* CGN; (2) *lambda* CGN. (3) *iota* CGN. The ester sulphate content is 18-25% for *kappa*, 30-40% for *lambda* CGN and 25-34% for *iota* CGN.

Kappa and *iota* CGN form gels when the helix of a single CGN molecule comes into close proximity to an identical CGN molecule to form a double helix (Bubnis, 1998). *Kappa* CGN forms its most rigid gels with potassium ions (Figure 3.1.2.2) and *iota* CGN with calcium ions (Figure 3.1.2.3). Increasing gel rigidity is expected to increase retention of TS within the particle, thus extending release profiles.

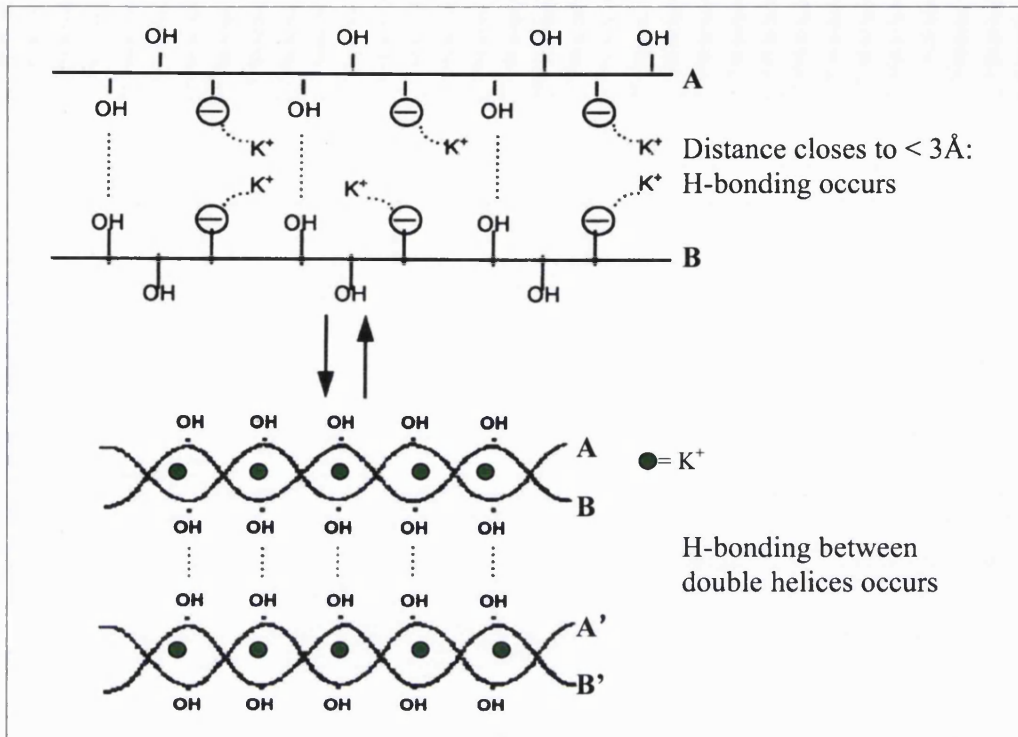


Figure 3.1.2.2: Gelation mechanism of *kappa* CGN. Potassium ion addition to CGN solution results in helix formation (neutralisation of sulphate groups on polysaccharide chains A and B). Two helices (AB/A'B') can then H-bond and aggregate forming a rigid gel.

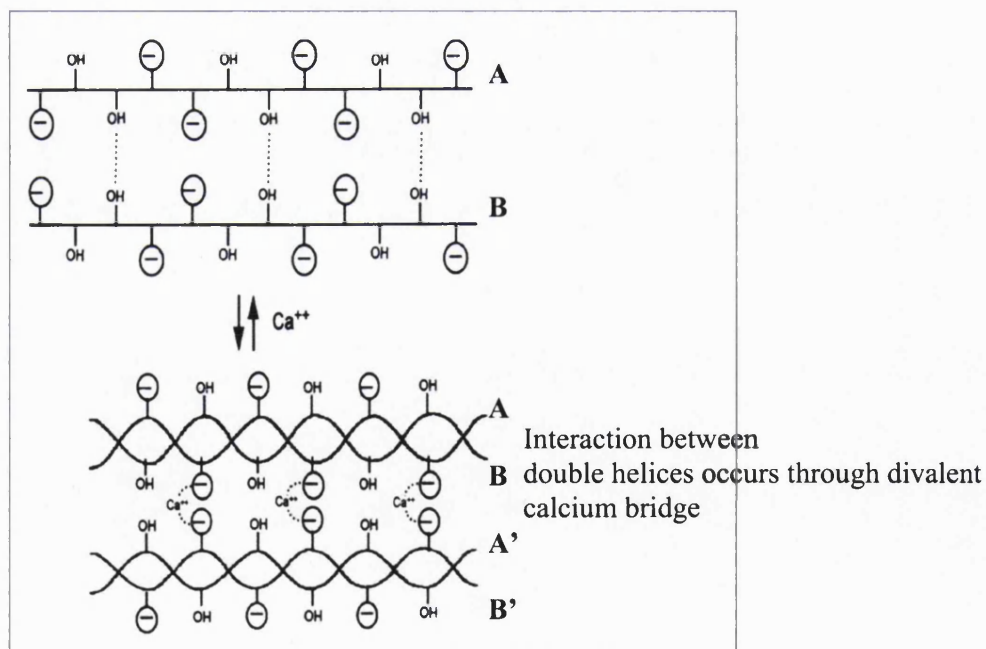


Figure 3.1.2.3: Gelation mechanism for *iota* CGN. Neutralisation of sulphate groups allows *iota* chains to hydrogen bond and form double helices (AB). Helices aggregate (AB/A'B') through divalent calcium bridges and form a loose 3-D network that can control water mobility (adapted from Bubnis, 1998).

As alternative excipients to CGN, the lower molecular weight sulphated polysaccharides, dextran sulphate (DexS), and chondroitin sulphate (ChonS) were also investigated. DexS has been safely administered by inhalation to dogs in a study to examine its effects on tracheal mucocilliary clearance (Sudo *et al.*, 2000) and may therefore be more appropriate for pulmonary delivery.

3.2 Materials

3.2.1 Model Drug

The hydrophilic drug, terbutaline sulphate (TS), was supplied in micronised form (Lot 4104H) by Investigational Products at AstraZeneca R&D Charnwood (Loughborough, Leicestershire, UK).

3.2.2 Matrix Excipients

CS (400000MW, medium molecular weight), penta-sodium triphosphate (tripolyphosphate, TPP) and ChonS (17000MW) were purchased from Fluka Chemicals Ltd. (Gillingham, Dorset, UK). Three types of CGN, (*kappa*, Gelcarin[®] GP-911; *lambda*, Viscarin[®] GP-109 and *iota* Gelcarin[®] GP-379) were a generous gift from FMCBiopolymer Inc. (Philadelphia, PA, USA). Cross-linking agents, potassium chloride and calcium chloride, were acquired from Fisher Scientific Ltd. (Loughborough, Leicestershire, UK). DexS (10000MW and 500000MW) was bought from Sigma-Aldrich Company Ltd. (Gillingham, Dorset, UK) and 40000MW DexS was donated by Dextran Products Ltd. (Scarborough, ON, Canada).

3.2.3 Solvents/Chemicals

All chemicals and solvents for liquid chromatography were HPLC grade unless otherwise noted. Water was deionised through an Option 4 water purification system (Elga Ltd., High Wycombe, Buckinghamshire, UK). Absolute ethanol was obtained from VWR International Ltd. (Poole, Dorset,

UK). Potassium dihydrogen orthophosphate, dipotassium hydrogen phosphate and orthophosphoric acid were used for mobile phase and buffer preparation and were purchased from Fisher Scientific Ltd. The pH meter used in buffer preparation (model pH 211, Hanna Instruments Ltd., Leighton Buzzard, Bedfordshire, UK) was calibrated in accordance with the manufacturer's guidelines using pH 4 (phthalate) and pH 7 (phosphate) buffers obtained from Fisher Scientific Ltd.

3.3 Methods

3.3.1 Determination of the Concentration of TS by High Performance Liquid Chromatography (HPLC)¹

3.3.1.1 HPLC Conditions/Equipment

The reversed-phase, isocratic assay of TS concentration was based on a validated method developed at AstraZeneca R&D Charnwood (Needham, 2000). Chromatography conditions (Table 3.3.1.1) were constant for each experiment. The HPLC equipment was assembled from components (Figure 3.3.1.1).

3.3.1.2 Mobile Phase Preparation

For each litre of stock 1.0 M phosphate buffer, 136 g potassium dihydrogen orthophosphate was accurately weighed, then dissolved in 900 mL deionised water. Orthophosphoric acid was added to adjust to required pH and then the buffer was made up to 1000 mL. When not required, the stock buffer was refrigerated (<4 °C) to prolong shelf-life.

50 mL of 1.0 M phosphate was diluted to 1000 mL with water to prepare each litre of 0.05 M phosphate buffer. This was mixed well and filtered. (0.05 M

¹ Brief details disclosed. For specific HPLC method, please contact AstraZeneca R&D Charnwood, who will release test method on a case-by-case consideration.

phosphate buffer was used to dilute samples to within the calibration range, and also for blank injections).

Column	Kromasil C18
Mobile phase	Phosphate buffer/Ethanol
Sample diluent	0.05 M phosphate buffer
Mobile phase filter	0.2 µm cellulose nitrate
Flow Rate	1.5 mL/min
Injection Volume	100 µL
Column Temperature	45 °C
Detection Wavelength	210 nm
Approximate Run Time	5 min

Table 3.3.1.1: HPLC run conditions.

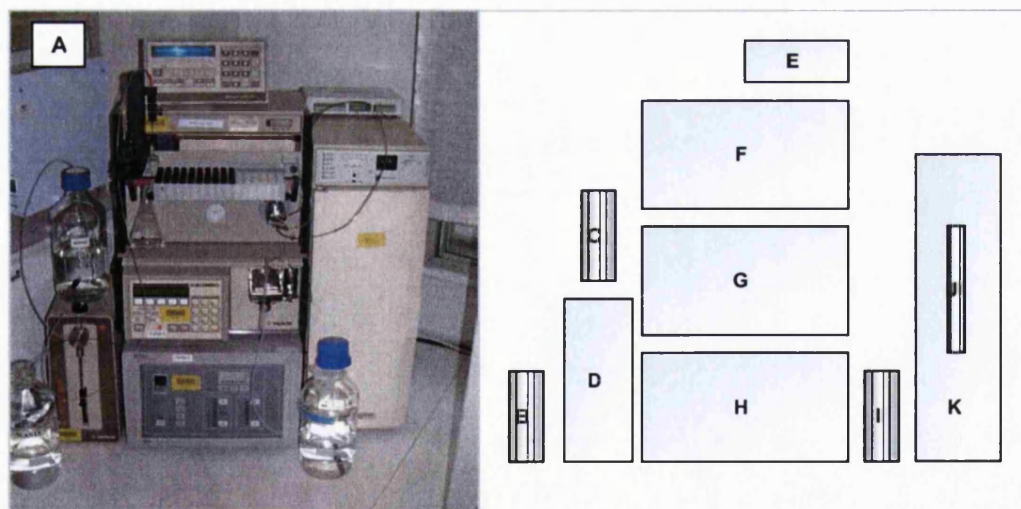


Figure 3.3.1.1: General HPLC set-up: Key: A: equipment Image. B: waste collection bottle. C: sample loop rinse bottle (50:50 water/methanol) D: Gilson 401 sample dispenser (Gilson Inc., Middleton, WI, USA). E: Gilson 506C software interface. F: Gilson 231 programmable auto-injector. G: Gilson 307 isocratic HPLC pump. H: Applied Biosystems 759A variable wavelength UV detector (Norwalk, CT, USA). I: mobile phase bottle. J: column. K: Shimadzu CTO-6A column oven (Shimadzu Ltd., Milton Keynes, Bedfordshire, UK). The HPLC system was controlled with Gilson 711 control software, version 1.30.

For mobile phase, 1.0 M phosphate buffer was diluted to 900 mL with deionised water, pH was adjusted using orthophosphoric acid and made up to final volume (1000 mL). Absolute ethanol was added to a portion of this solution, and then the mobile phase was mixed well and filtered. Mobile phase was degassed for 15 minutes by placing the bottle in a sonicating bath (XB6 Ultrasonic Bath, Grant Instruments Ltd., Royston, Hertfordshire, UK).

3.3.1.3 TS Working Standard Solution (1.0 µg/mL)

Approximately 25.0 mg TS was weighed accurately (5-place balance) and rinsed into a 250 mL volumetric flask, and made up to volume with 0.05 M phosphate buffer. After mixing well, 2.0 mL of this solution was pipetted into a 200 mL volumetric flask, then diluted to volume with 0.05 M phosphate buffer. The process was repeated in order to obtain two identical working standards, A and B. TS working standard solutions were stored in a refrigerator when not required. Samples from TS release studies were typically diluted to the region of 0.5-1.0 µg/mL. As working standard solutions were used (single concentration point), a calibration curve was also constructed to ensure linearity within the assay range (example curve in Appendix B1).

3.3.1.4 Chromatography

To allow stabilisation, the UV detector and column oven were switched on at least 30 min prior to the initial run. Mobile phase solution was pumped through the system at 1.5 mL/min for 15 minutes before each run was initiated. Each run consisted of duplicate injections for each TS working standard solution (A+B), followed by the samples from the diffusion-cell experiments (maximum 20 samples between standard repeats). Each sample was tested in duplicate.

3.3.1.5 HPLC System Performance

The following steps were undertaken to ensure system validity. Blank injections of 0.05 M phosphate buffer, were routinely performed (following standard injections) to ensure that (1) the mobile phase was not

contaminated with drug/interfering peaks therefore providing an acceptable baseline and (2) carry over from the previous injection was not present.

Repeatability of Injection was assessed by six replicate injections and the coefficient of variation (CV) was calculated (Values >2% were not accepted). CV values are usually low for analytical techniques (Jones, 2002)).

The Tailing Factor, T (equation 3.3.1.5a), is a measure of peak symmetry and was calculated for the first standard. As peak asymmetry increases, for example if tailing occurs, integration and therefore precision becomes less reliable. Values are required to be less than 2; if values were greater than 2.0, a column washing procedure was performed (Appendix B2.1) and the tailing factor reassessed.

$$T = \frac{W_{0.05}}{2f}$$

Equation 3.3.1.5a: Tailing Factor. $W_{0.05}$ = width of peak at 5% height: f = Width between start of peak and peak maximum at 5% height.

Concordance of Standards was calculated as follows (equation 3.3.1.5b) as a check that the standard solutions (A, B) for quantification were prepared accurately.

$$\frac{A_{stdA}}{W_{stdA}} \times \frac{W_{stdB}}{A_{stdB}} = 1 \pm 0.02$$

Equation 3.3.1.5b: Calculation for standard concordance.

A_{stdA} = mean peak area (duplicate injection) standard A

A_{stdB} = mean peak area (duplicate injection) standard B

W_{stdA} = weight taken (mg) for standard A preparation.

W_{stdB} = weight taken (mg) for standard B preparation.

3.3.2 Production of CS/TPP/TS Microparticles

Work initially followed a method by Berthold *et al.*, (1996), for the aqueous preparation of CS microspheres as a drug carrier for prednisolone sodium phosphate. TPP was used to cross-link CS instead of sodium sulphate (as was used in the reference method). A rigid gel was produced after centrifugation, and following lyophilisation, no microspheres were observed (Figure 3.3.2). This method was also unlikely to trap a hydrophilic drug e.g. TS, as the drug will remain in the aqueous phase rather than precipitate with the chitosan microspheres (Bodmeier and Paeratakul, 1989). The method was therefore adapted as follows.

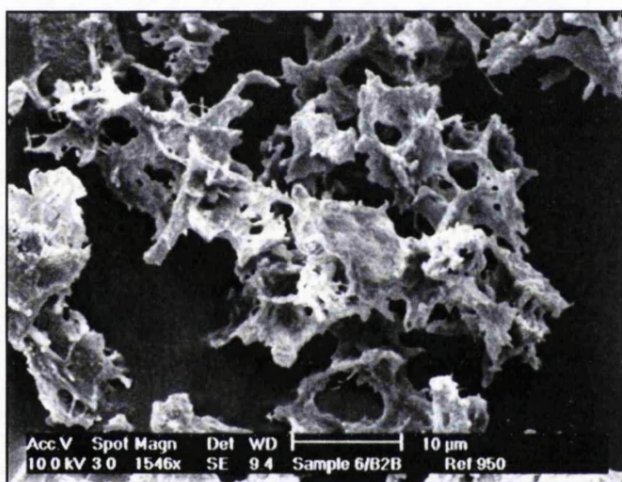


Figure 3.3.2: Appearance of CS/TPP following particle production method.

40 g of 0.25% w/v medium molecular weight CS (dissolved in 2% w/v aqueous acetic acid) was accurately weighed into a round-bottomed flask. 40 mL of 2.5% w/v TPP was added drop-wise (5 mL min^{-1}) during stirring with a blade stirrer (model RZR 50, Heidolph Instruments GmbH, Schwabach, Germany) at 2000 rpm and ultrasonication. After addition of TPP, stirring and sonication continued for 15 min. The resulting cross-linked CS solution was centrifuged at 3000 rpm for 15 min (3K30 Refrigerated Centrifuge, Sigma Laborzentrifuges GmbH, Osterode am Harz, Germany). The supernatant was discarded and the sediment re-suspended in 40 mL deionised water. The centrifugation step was repeated. The desired amount

of TS was subsequently added to the gel pellet and thoroughly mixed with a homogeniser (Ultra-turrax T25, IKA-Werke GmbH, Tullingen, Germany) at 9500 rpm. The CS/TPP/TS mixture was then frozen rapidly in liquid nitrogen and lyophilised (see section 4.3.2) for 24 hr (Drywinner 110, Heto-Holten A/S, Gydevang, Denmark). Freeze-dried powder was placed into a Certiprep Mixer vibratory ball mixer mill (Glen Creston Ltd., Stanmore, Middlesex, UK) with ten 4 mm glass balls, and micronised for 10 min. Micronised particles were visualised with SEM.

3.3.3 Production of Sulphated Polysaccharide Microparticles

Similar formulation methods were employed for all types of sulphated polysaccharide. Briefly, 0.1 g matrix excipient was dispersed in 9.9 g water in accordance with dispersion instructions recommended by FMC Biopolymer Inc. The excipient was sprinkled slowly into the vortex of magnetically stirred water. Aggregation occurred, and this was eliminated by gently heating the solution, which enabled the aggregates to wet and dissolve. The desired amount of TS was then added to the polysaccharide solution in order to achieve the correct ratio of TS:CGN. The cooled solution was frozen rapidly in liquid nitrogen and lyophilised for 24 hr. The freeze-dried powder was micronised according to the CS microparticles method. When cation cross-linked CGN microparticles were required, potassium chloride/calcium chloride was added to the TS solution prior to mixing with the polysaccharide solution. Finally, ChonS and DexS microspheres were produced using a spray-drying method adapted from Ganza-Gonzalez *et al.*, (1999), with the following conditions: Inlet temperature: 130 °C, Outlet temperature, 70 °C, Flow Rate 800 L hr⁻¹, Aspiration 65% and Pump Rate 15%. (Spray-drying as a technique for producing microparticles is discussed in detail in Chapter 5.)

3.3.4 Design of Horizontal Diffusion Cell for Drug Diffusion Assay

No pharmacopoeial methods are applicable for testing drug diffusion from powders designed for sustained drug release to the respiratory tract (McConville *et al.*, 2000). For instance, USP paddle systems are unsuitable for ascertaining release profiles that may be expected in the pulmonary space (Batycky, 2003). Accordingly, a custom-built diffusion cell was designed and built in-house (Figure 3.3.4.1 and 3.3.4.2). The cell was constructed from stainless steel and polished acrylic sheet (transparent to allow visualization of the receiver chamber). The aim of the horizontal diffusion cell design was to crudely mimic the *in vivo* scenario, such that the air-membrane-receiver layout imitated the airway space-epithelium-circulation.

3.3.5 Operation of Horizontal Diffusion Cell for Drug Diffusion Assay

Firstly, a 0.45 μm nylon membrane (Whatman International Ltd., Maidstone, Kent, UK) was hydrated in 0.05 M phosphate buffer, pH 7.4 for half an hour. Then 17.5 mL of degassed 0.05 M phosphate buffer, pH 7.4 was pipetted into the receiver compartment of the diffusion chamber (physiological pH, 0.05 M phosphate buffer has been used by others for pulmonary *in vitro* release studies (O'Hara and Hickey, 2000) and a magnetic stirrer bar was added. 0.05 M phosphate buffer, pH 7.4 was prepared by mixing 40.1 mL 1.0 M dipotassium hydrogen phosphate with 9.8 mL 1.0 M potassium dihydrogen orthophosphate, then making up to final volume of 1000 mL with deionised and distilled water. The cell was operated at ambient temperature.

The pore size of the membrane (0.45 μm) was chosen to (1) allow free diffusion of the drug into the receiver compartment and (2) prevent entry of microparticles. The hydrated membrane was carefully placed on to the surface of the phosphate buffer in the receiver compartment, to avoid introduction of air bubbles. The cell was then assembled and a magnetic stirrer was turned on at 240 rpm beneath the cell (speed constant throughout experiments). Test powder, 10.0 mg, was accurately weighed (5-figure balance) into a glass weighing boat (low powder adhesion). A stop-clock was started, and the dry powder was immediately sprinkled evenly on to the hydrated membrane.

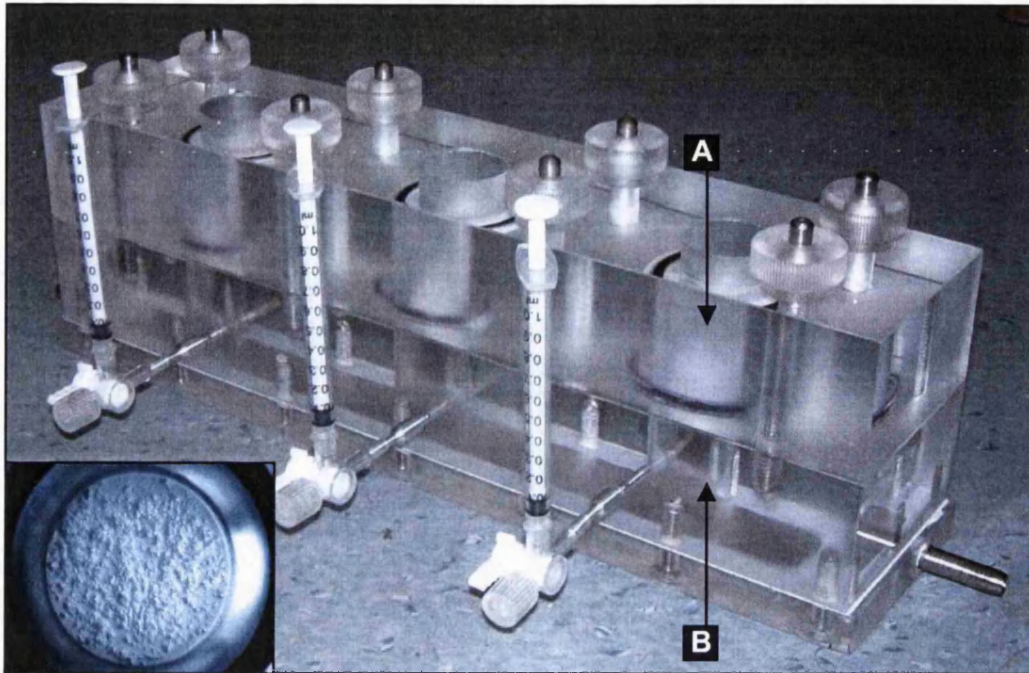


Figure 3.3.4.1: Image of horizontal diffusion cell showing sampling ports (connected to syringes): A = donor compartment (air), B = Receiver compartment, 17.5 mL, typically 0.05 M phosphate buffer, pH 7.4. **Inset:** Plan view down through donor compartment to membrane with particles present.

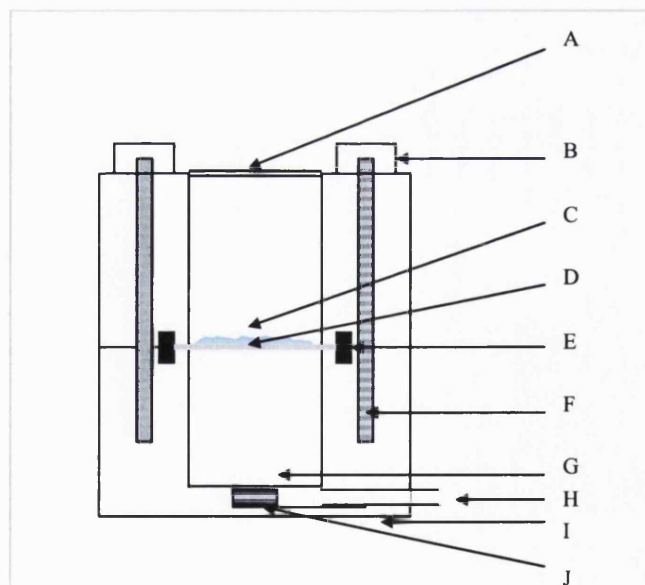


Figure 3.3.4.2: Simplified schematic for horizontal diffusion cell: A = plastic cover slip, B = fastening bolt, C = test powder, D = 0.45 μm nylon membrane (*pseudo-epithelium*), E = o-ring, F = screw fastening, G = 17.5 mL receiver cell, H = Sampling port, I = acrylic sheet body, and J = magnetic flea.

Samples (0.7 mL) were then taken from a three-way syringe port at allotted time intervals (3.75 min, 7.5 min, 15 min, 30 min, 60 min, 90 min, 135 min, 180 min). Fresh buffer was added carefully through the sample port to replace the sample taken. Ingress of air bubbles was minimised during this process since they collected under the membrane and impaired drug diffusion. The desired amount of sample was then taken with a 200 μL pipette from the 0.7 mL sample and diluted to the appropriate concentration within the HPLC calibration range. All test powder samples were tested in triplicate to ensure reproducibility.

3.3.6 Determination of TS/Polysaccharide Microparticle Drug Loading

Drug loading was determined by weighing accurately 10.0 mg of test powder into a 20 mL glass vial (Figure 3.3.6). 17.5 mL of 0.05 M phosphate buffer, pH 7.4, was then added to the vial, with a magnetic flea and the lid was sealed. Vials (triplicate) were placed on a magnetic stirrer for 24 hr. After this period, the solution was filtered through a 0.22 μL syringe filter (Whatman International Ltd., Maidstone, Kent, UK). Equal samples from each vial were taken, and thoroughly mixed, before diluting to the appropriate concentration for assay.

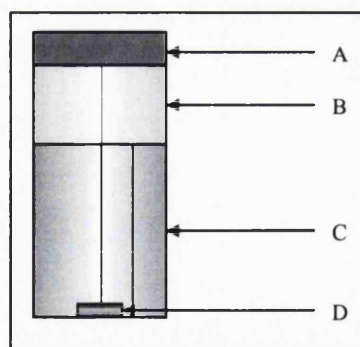


Figure 3.3.6: Determination of Maximum TS release from microparticles: A = Screw lid, B = Glass vial, C = 17.5 mL 0.05 M phosphate buffer, pH 7.4 + microparticles, D = Magnetic Flea.

Drug release data was therefore normalised by converting drug concentration assayed in solution (Section 3.3.5) to a percentage of the total drug release from the microparticles.

3.4 Results and Discussion

3.4.1 Determination of the Concentration of TS by High Performance Liquid Chromatography (HPLC)

Two calibration curves were generated across the range 0-2.0 µg/mL and are shown in Appendix B1. The regression coefficients for curve A and curve B were both 0.9996, which demonstrated excellent linearity. Drug content in samples was calculated by the ratio of sample peak area to the mean peak area for standards A and B (1.0 µg/mL). Samples were at all times diluted to concentrations within the original calibration range (<2.0 µg/mL, typically <1.5 µg/mL).

All validation steps carried out indicated satisfactory HPLC assay for TS. The baseline was flat with little deviation from 0 absorbance units (mV), except for the solvent front and TS peak which were separate (Example chromatogram shown in Figure 3.4.1). Blank injection (n=3) initially suffered sample carry over from the previous injection. The injection loop wash volume was increased to five times loop volume (500 µL) to eradicate the contaminating carry over. Limit of Detection (LOD) was 0.02 µg/mL and Limit of Quantification (LOQ) was 0.065 µg/mL.

Validation for repeatability of injection indicated acceptable accuracy of the sample loop injection system within the required limits (Needham, 2000). CV values of 1.33%, 1.01% and 1.42% were calculated for the system at initial system set-up, following service and before the final run, respectively.

Calculated tailing factors were typically less than 2, as required by the test method. Following assay of drug release from sulphated polysaccharides based microparticles, tailing became evident and frequent column washing was required (Appendix B2.1).

Concordance of standards was calculated and typically displayed repeatability (within the range 1.00 ± 0.02). When repeatability was greater than this value, the standard preparation was repeated.

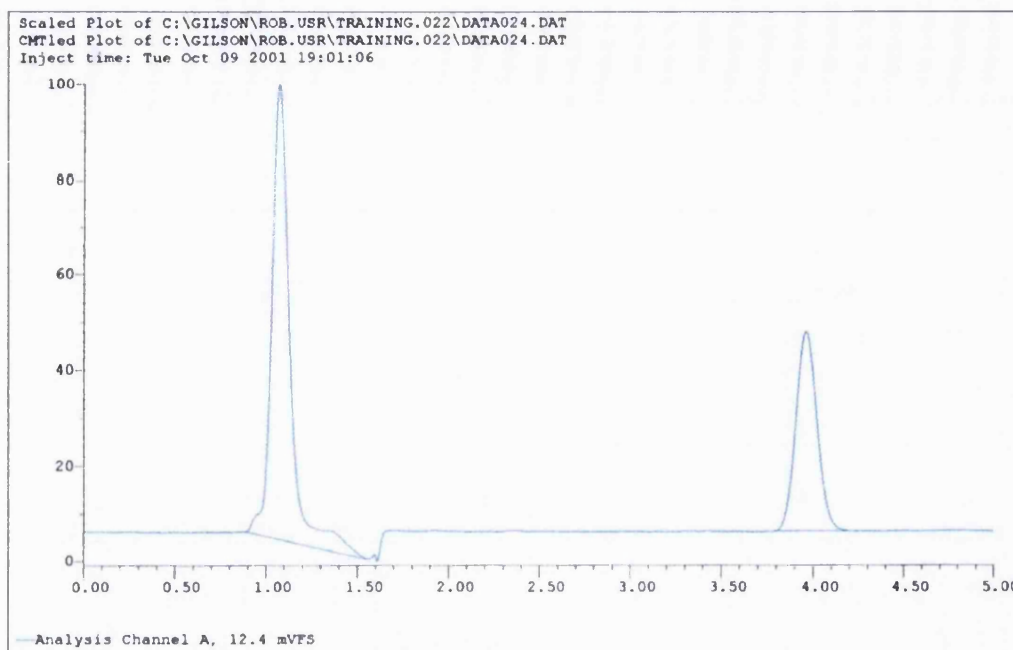


Figure 3.4.1: Sample chromatogram showing solvent front (1.10 min) and TS peak (3.95 min).

3.4.2 Suitability of Horizontal Diffusion Cell

The horizontal diffusion cell method for the determination of TS release was able to quantify drug diffusion into the receiver phase and distinguish release profiles from different formulations. The method was therefore accepted as a standard release methodology for the research project. The release of pure TS, in micronised form, was rapid (Table 3.4.3.1 and Figure 3.4.3.3). This speed of dissolution was expected due to high solubility and the ionised state of TS in the receiver phase (saturated solubility = 305 mg/mL), and confirmed that the hydrated 0.45 μm nylon membrane did not impede the transfer of TS into the receiver phase.

3.4.3 TS Release from CS/TPP Microparticles

Milling of the TS/CS/TPP matrix generated suitable particles for initial investigations as confirmed by SEM (Figures 3.4.3.1 and 3.4.3.2, particle size visibly $<5 \mu\text{m}$). Percentage TS release values from the CS/TPP microparticles are detailed in Table 3.4.3.1 and Figure 3.4.3.3.

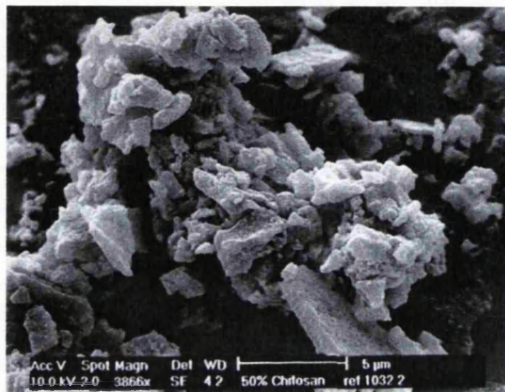


Figure 3.4.3.1: SEM image of 50:50 TS:CS microparticles (milled product).



Figure 3.4.3.2: SEM image of 10:90 TS:CS microparticles (milled product).

Time (min)	% TS release ± SD	% TS release (TS:CS 50:50) ± SD	% TS release (TS:CS 25:75) ± SD	% TS release (TS:CS 10:90) ± SD
0	0.00	0.00	0.00	0.00
3.75	49.5 ± 12.4	5.20 ± 5.10	11.5 ± 2.01	7.75 ± 0.99
7.5	73.2 ± 9.62	40.0 ± 5.61	23.8 ± 5.87	29.9 ± 15.5
15	86.8 ± 5.75	67.9 ± 3.03	55.3 ± 7.91	47.6 ± 11.8
30	91.6 ± 6.27	84.8 ± 1.35	77.9 ± 7.48	69.3 ± 6.13
60	96.2 ± 1.96	96.7 ± 3.58	86.9 ± 7.46	82.5 ± 7.37
90	97.3 ± 1.47	99.6 ± 4.26	85.7 ± 6.94	86.0 ± 7.25
135	97.3 ± 1.47	100 ± 5.06	92.5 ± 7.98	91.5 ± 5.41
180	97.3 ± 1.47	101 ± 6.67	90.5 ± 4.16	94.2 ± 7.62

Table 3.4.3.1: % release of TS into diffusion cell receiver compartment from pure TS and from TS/CS particles. Each value represents the mean from three experimental runs for that sampling interval (n=3).

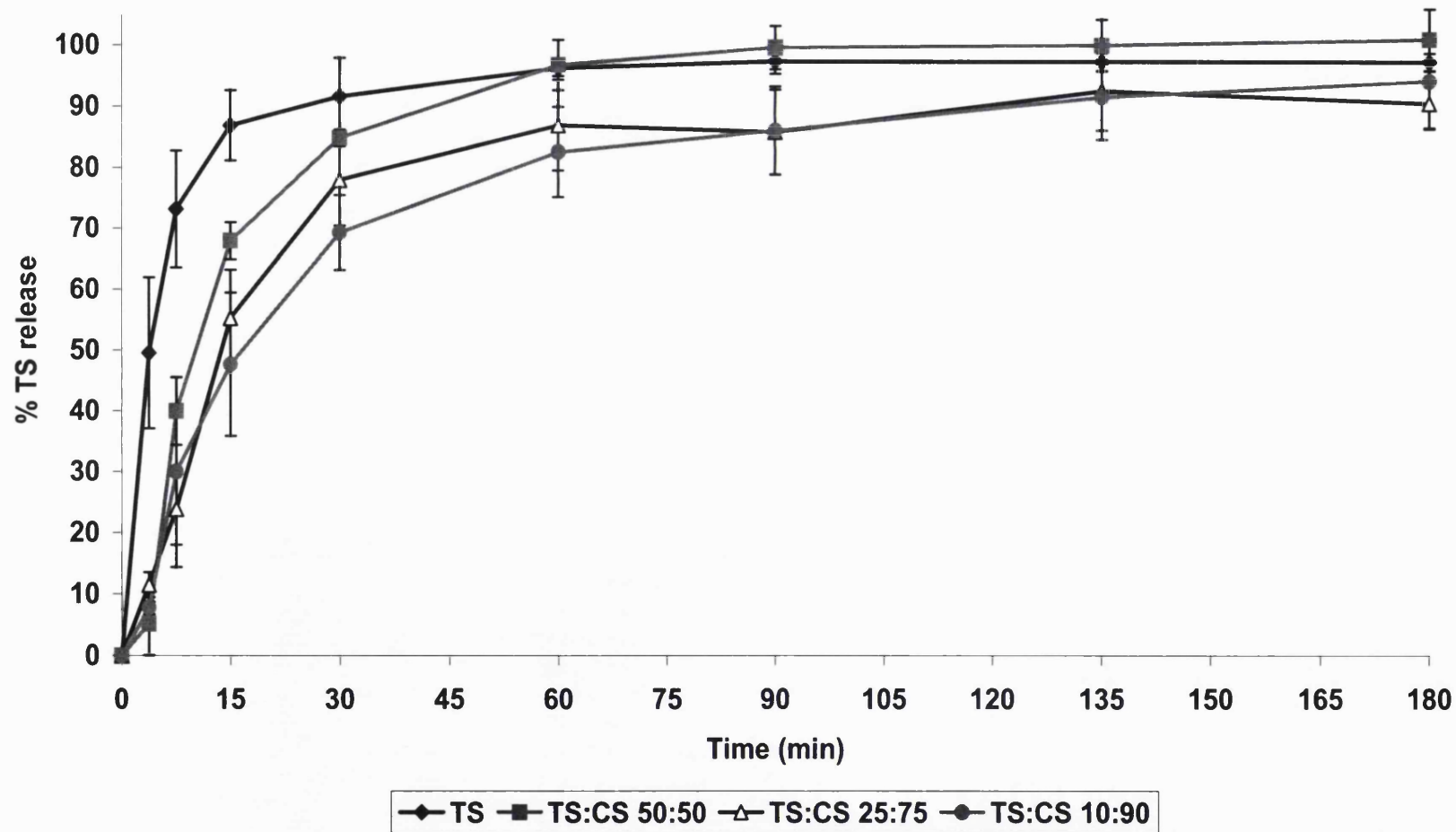


Figure 3.4.3.3: % TS release vs. time for pure micronised drug and the effect of TS:CS ratio upon drug release from CS microparticles (n=3 ± SD, 20 °C).

As evident from Figure 3.4.3.3, the shift in the release profile to the right from the pure drug release curve to the chitosan microparticles indicated a minor sustained release effect. The half-time, t_{50} , represents the time required to release 50% of the initial drug loading and this time can be used to calculate the first order rate constant, k (Equation 3.4.3).

$$t_{50} = \frac{\ln 2}{k}$$

Equation 3.4.3: Calculation of half-time, when first order rate constant, k is known.

Increasing the drug loading of the microparticles increased the release rate (Figure 3.4.3.4) for drug from the microparticle. This was expected as the diffusion rate increased at higher drug loadings, and a reduction in matrix material relative to drug provided less barrier to release. However, even at the lowest drug loading, 10% w/v, 47.6% of TS was released at 15 min which indicated substantial burst release, and release was complete at approximately 3 hr, which was not acceptable to meet the investigation objective.

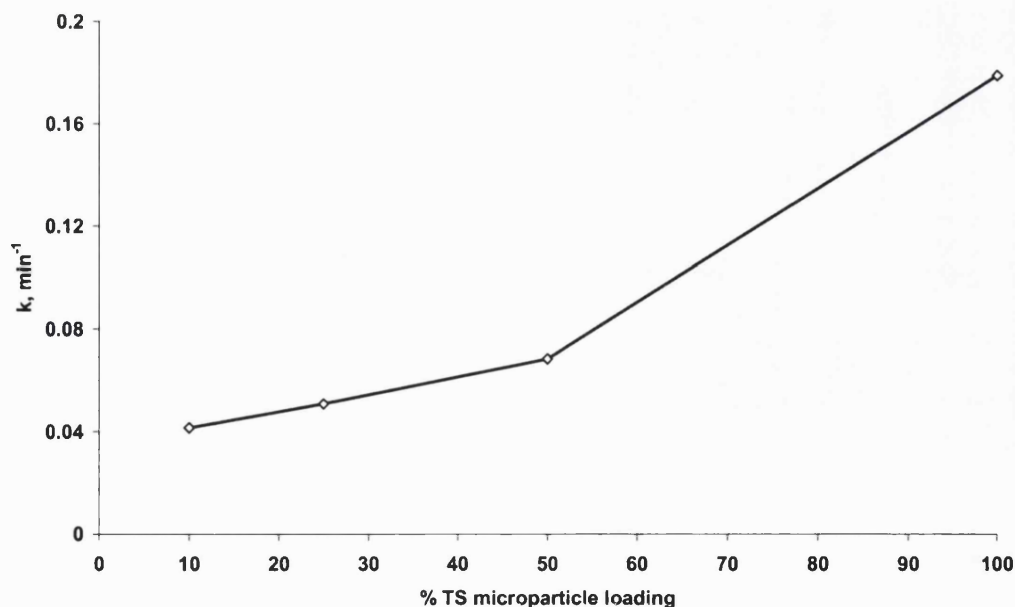


Figure 3.4.3.4: Effect of drug loading on first order release constant, k . Ideal sustained release first order release constants are between 0.001 and 0.002 ($t_{50} \sim 6-12$ hr).

These preliminary studies highlighted the inability of CS matrices, formulated using this method, to retard the release of TS. The rapid release resulted from rapid hydration of the matrix with subsequent rapid leaching (observed as burst release) of the drug (Thanoo *et al.*, 1991). Sawayanagi and co-workers (1982) concluded that drug release (indomethacin) through a CS matrix was controlled by pore size. The lyophilisation/milling processing was expected to create porosity and therefore alternative manufacturing, namely spray-drying, may create less porous particles which have more desirable SR properties. However release rates of model drugs (H₂-receptor antagonists) from spray-dried and cross-linked CS microspheres have also displayed fast release accompanied by a substantial burst effect (He *et al.*, 1999). An electrostatic interaction between drug (indomethacin) and chitosan has been shown to provide a mechanism for SR (Imai *et al.*, 1991). However, as both TS and CS are positively charged, there is no potential for interaction between matrix and excipient. The only barrier to SR is the formation of the hydrated chitosan gelled matrix. Whilst gelled formulations may be suitable for SR of large molecular weight drugs such as polypeptides or proteins, there is little provision for SR of low molecular weight hydrophilic drugs, as indicated in this case.

3.4.4 TS Release from Sulphated Polysaccharide Microparticles I: CGN

Investigations into the release of TS from sulphated excipient microparticles (Table 3.4.4) were initiated with two types of CGN, *lambda*-109 (Figure 3.4.4.1) and *kappa*-911 (Figure 3.4.4.2). The slowest release for TS from CS microparticles was achieved with a drug:excipient ratio of 10:90. This ratio was therefore selected for work with sulphated polysaccharides. The incorporation of TS into a CGN matrix significantly retarded the release of TS relative to free drug (Figure 3.4.4.3) and relative to the CS formulations. No burst release was noted for both CGN formulations, as evident for CS based particles. The absence of burst release and presence of SR, most likely arose from ionic interactions between the basic TS and ester sulphate groups on the polysaccharide backbone (shown for salbutamol sulphate by Bonferoni *et al.*, 1993).

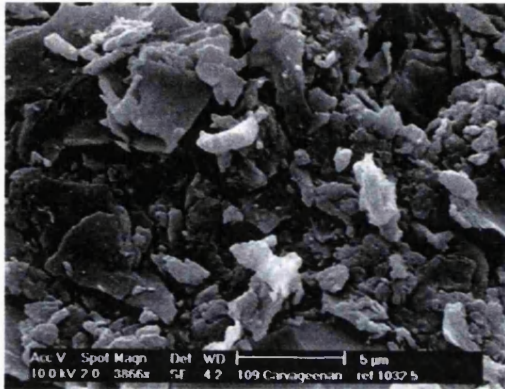


Figure 3.4.4.1: SEM image of 10:90 CGN 109 microparticles (milled product).

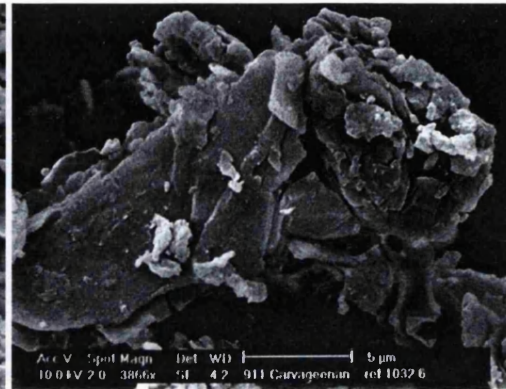


Figure 3.4.4.2: SEM image of 10:90 CGN 911 microparticles (milled product).

Both SEM images indicated that micronisation of TS/CGN was not as successful as TS/CS material (evidence of large particle sizes).

Time (min)	% TS release ± SD	% TS release (TS:CGN 109 10:90) ± SD	% TS release (TS:CGN 911 10:90) ± SD
0	0.00	0.00	0.00
3.75	49.5 ± 12.4	0.41 ± 0.708	0.00
7.5	73.2 ± 9.62	†7.74 ± 0.316	‡3.38 ± 3.03
15	86.8 ± 5.75	†18.0 ± 0.959	†12.2 ± 4.24
30	91.6 ± 6.27	‡30.8 ± 1.29	†29.2 ± 5.69
60	96.2 ± 1.96	‡48.5 ± 3.83	†51.7 ± 5.60
90	97.3 ± 1.47	†59.4 ± 6.60	†66.2 ± 4.58
135	97.3 ± 1.47	†68.6 ± 5.07	†78.3 ± 1.97
180	97.3 ± 1.47	‡80.1 ± 1.29	†85.6 ± 2.83

Table 3.4.4: % release of TS into diffusion cell receiver compartment from Pure TS and from TS/CGN particles (n=3). Significance calculated by t-Test for differences in release vs. pure drug release. Key: * = p <0.01, † = p <0.001, ‡ = p<0.0001. High levels of significant difference proved the ability of the horizontal diffusion cell to discriminate between formulations.

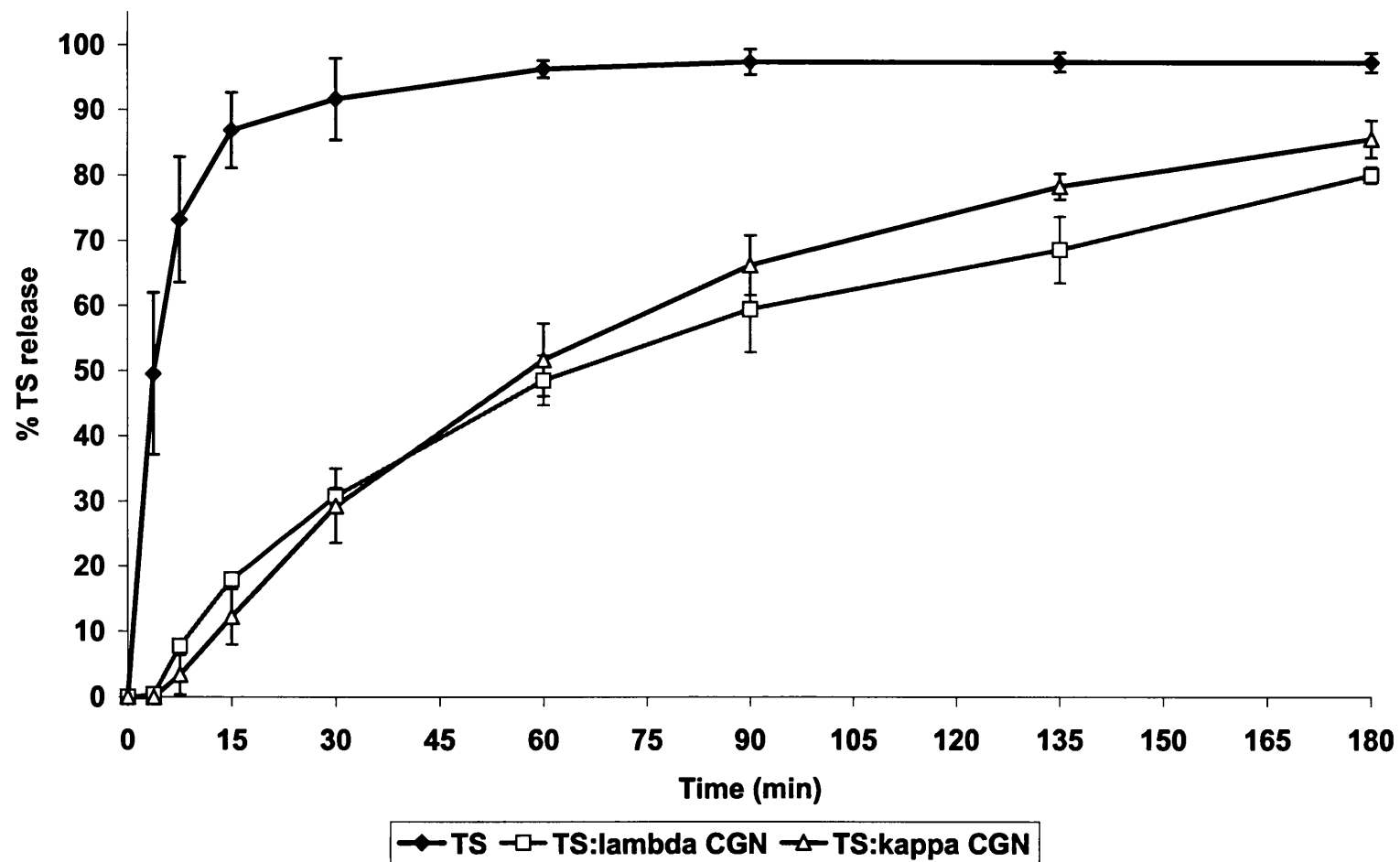


Figure 3.4.4.3: % TS release vs. time for pure micronised drug and for drug release from *lambda* and *kappa* CGN microparticles at (n=3 ± SD, 20 °C). TS:CGN ratio = 10:90.

There were differences in the release profiles observed for the two CGN types. *Lambda* CGN had a slight burst release effect. This occurred from the high ester sulphate content, which resulted in fast uptake of water by the particles. *Lambda* CGN contains 35%, and *kappa*, 25% ester sulphate content within the excipient (Bubnis, 1998). Relative to *kappa* CGN, sustained release of TS from *lambda* CGN was observed for slightly longer at the 135 min and 180 min intervals (t-Test, p< 0.05). This was expected given that there were more opportunities for ionic interaction between TS and the excipient as the drug travels from within the particle to the point of release at the particle surface.

Drug diffusion kinetics for release from matrix-type excipients containing uniformly dissolved drug, such as in the present example, are well documented within the literature (Lee and Good, 1987). Matrix-based systems typically show first order release which are indicated by continuously diminishing release rates since rate of release is dependent on the amount of drug, M, remaining at time, t (M_t). 'Early phase' release of drug for the first 60% of the total drug release (M_∞) follows Equation 3.4.4.1. However, measured release typically deviates from theory such that a 'late time' approximation for release of between 40% and 100% is required (Equation 3.4.4.2, Baker and Lonsdale, 1974). The equations provide overlap between 40 and 60% release, with each equation functioning throughout this range.

$$M_t / M_\infty = kt^{1/2}$$

Equation 3.4.4.1: Release kinetic equation for drug release from matrix systems, valid up to 60% release. k = constant, relating to drug diffusion through the matrix and matrix geometry.

$$M_t / M_\infty = 1 - \frac{8}{\pi^2} e^{-kt}$$

Equation 3.4.4.2: Kinetic equation for drug release from matrix systems, valid for final 60% drug release. k = constant, relating to drug diffusion through the matrix and matrix geometry.

For the first 60% drug release (equation 3.4.4.1), treatment of the *lambda* and *kappa* CGN data showed that release followed theoretical matrix diffusion kinetics (Figure 3.4.4.5). The regression coefficients were 0.9988 and 0.9899 for *lambda* and *kappa* CGN respectively. The slightly lower regression coefficient for *Kappa* CGN possible arises from the absence of a fast initial release due to the time lag associated with particle hydration. For the 'late time' approximation (40% release onwards, Figure 3.4.4.6) where release rate begins to fall exponentially and deviates from equation 3.4.4.1, release rates are shown to adhere to equation 3.4.4.2, with regression coefficients of 0.9568 and 0.9979 for *lambda* and *kappa* CGN respectively.

3.4.5 TS Release from Cation Cross-linked CGN Microparticles

Kappa and *Iota* CGN (not *lambda* – numerous sulphate groups prevent gel formation) are both gelling polysaccharides (Bubnis, 1998). Interactions between the polysaccharide chains result in the formation of a 3-D network that restricts water mobility within the particle, once hydrated. *Kappa* CGN was cross-linked with 1% and 2% w/w potassium chloride based on the total solid content. *Iota* CGN was cross-linked with milli-equivalent amounts of calcium ions relative to the potassium used for *kappa* CGN. Prior to lyophilisation, the CGN solutions that had been cross-linked formed rigid gels, whereas cation-free CGN formed a viscous solution.

Values for t_{50} and the associated release constants relative to pure drug are detailed in Table 3.4.5.1. All polysaccharide-based formulations significantly prolonged the t_{50} values relative to pure TS, indicating sustained release. As evident in Figures 3.4.5.1 and 3.4.5.2, cross-linking the matrices with cations shifted the release profile to the right with an associated increase in t_{50} values.

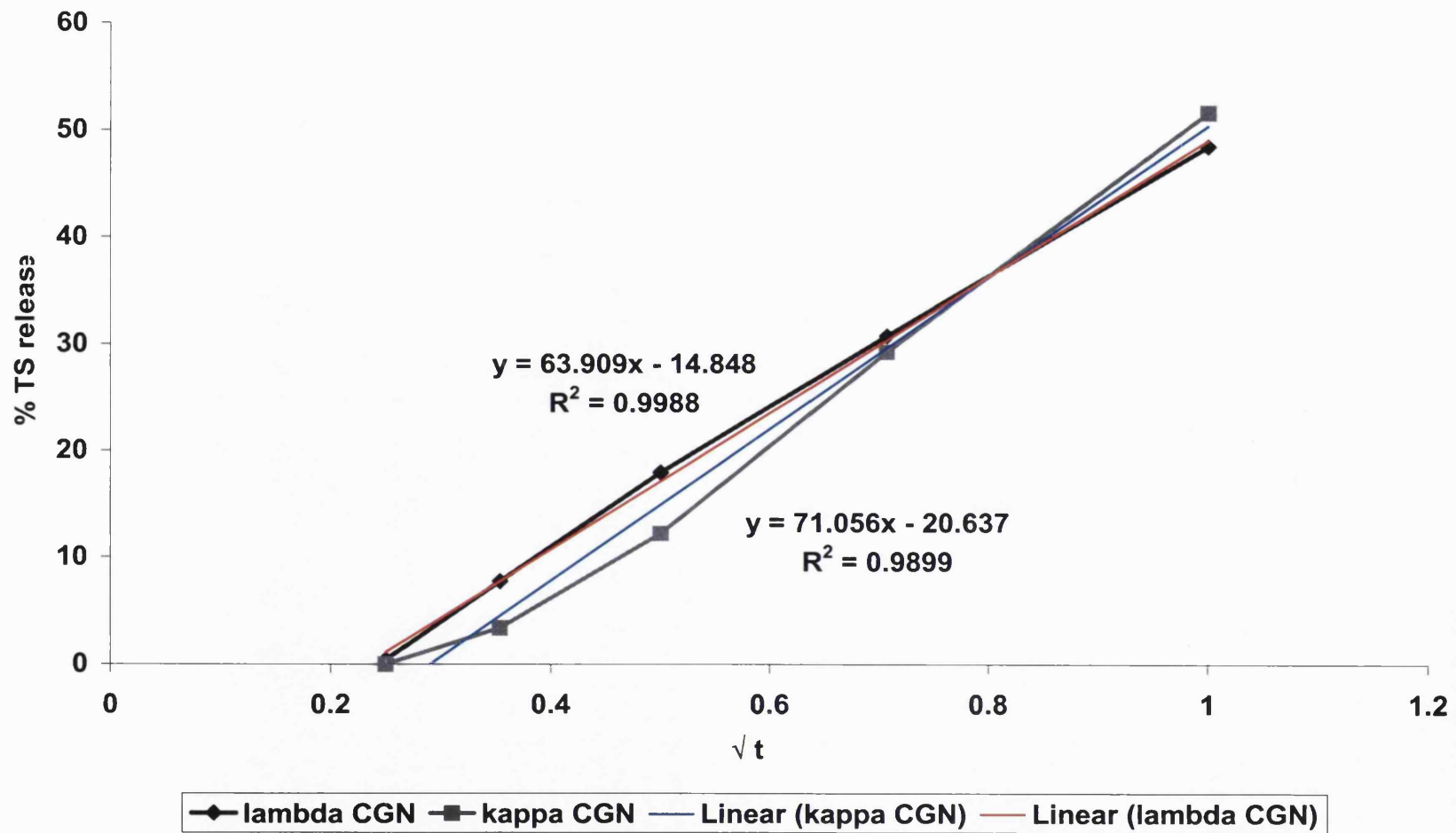


Figure 3.4.4.5: 'Early time' plot for % TS release vs. \sqrt{t} time for drug release from CGN microparticles, 7.5 min - 60 min. Straight line indicates adherence to matrix release kinetics for this time period.

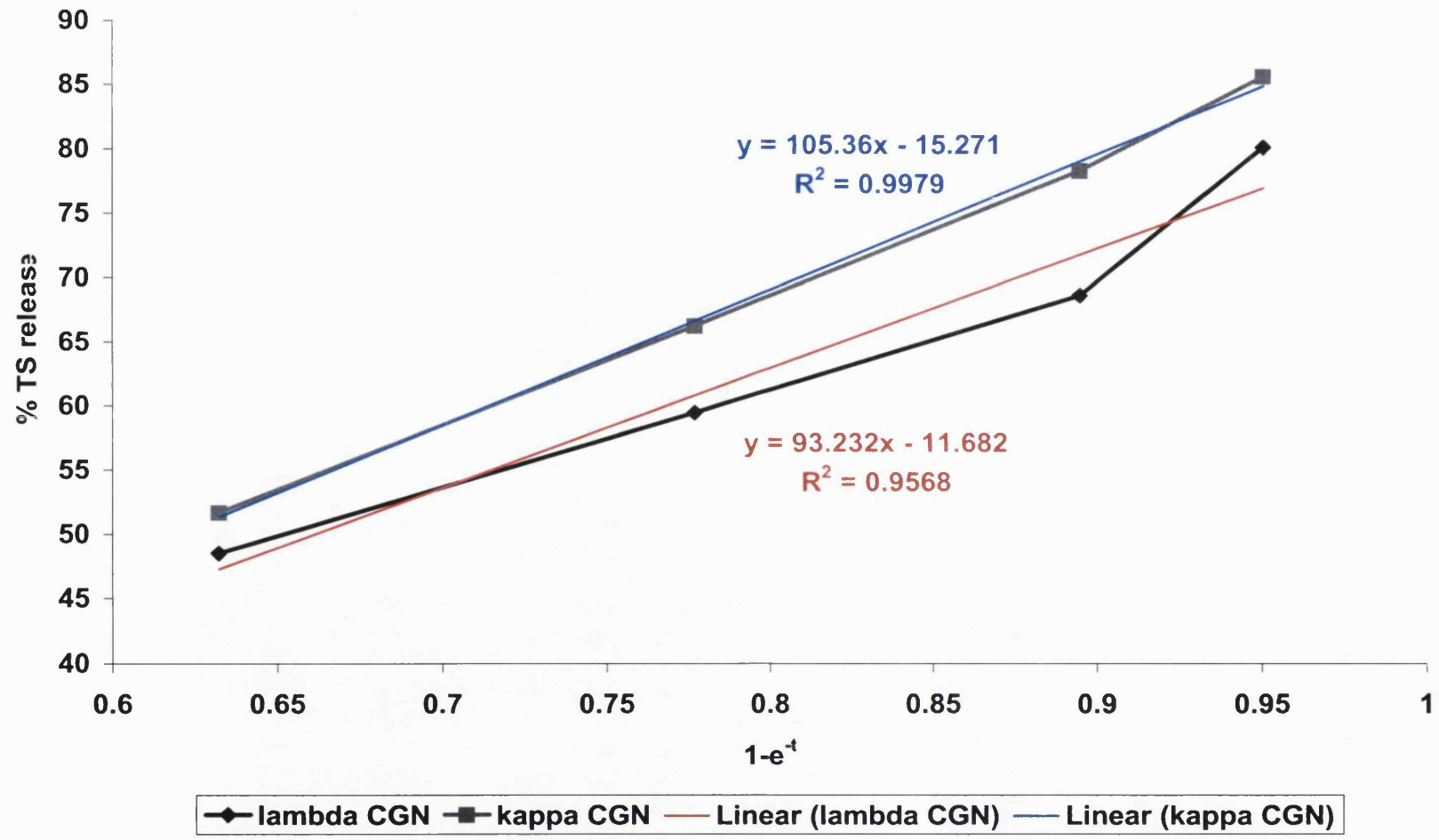


Figure 3.4.4.6: 'Late time' drug release kinetics based on equation 3.4.4.2. Straight line indicates adherence to late time kinetics.

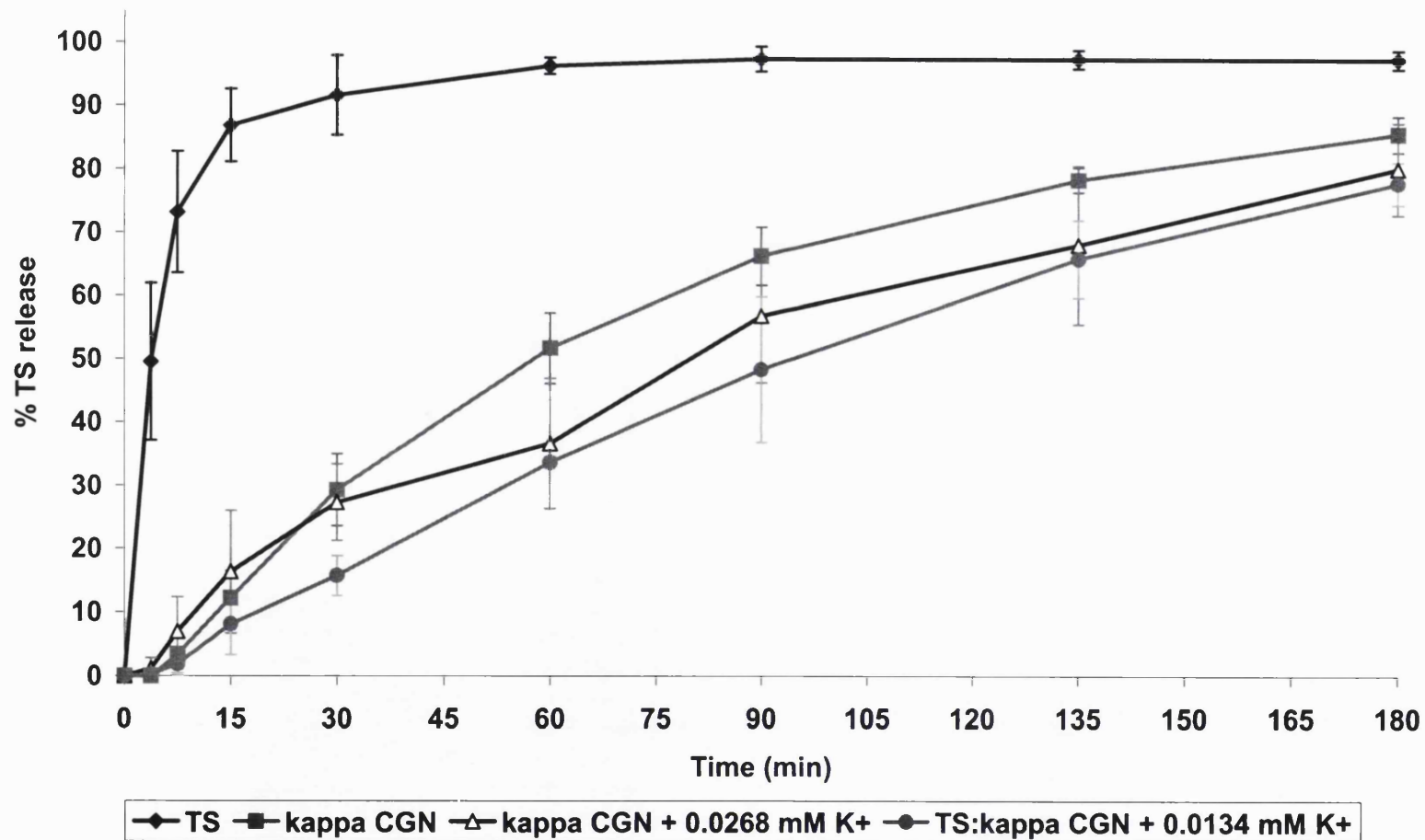


Figure 3.4.5.1: % TS release vs. time for pure micronised drug and for drug release from kappa CGN microparticles crosslinked with increasing amounts of potassium ions ($n=3 \pm SD$, 20 °C). TS:CGN ratio = 10:90.

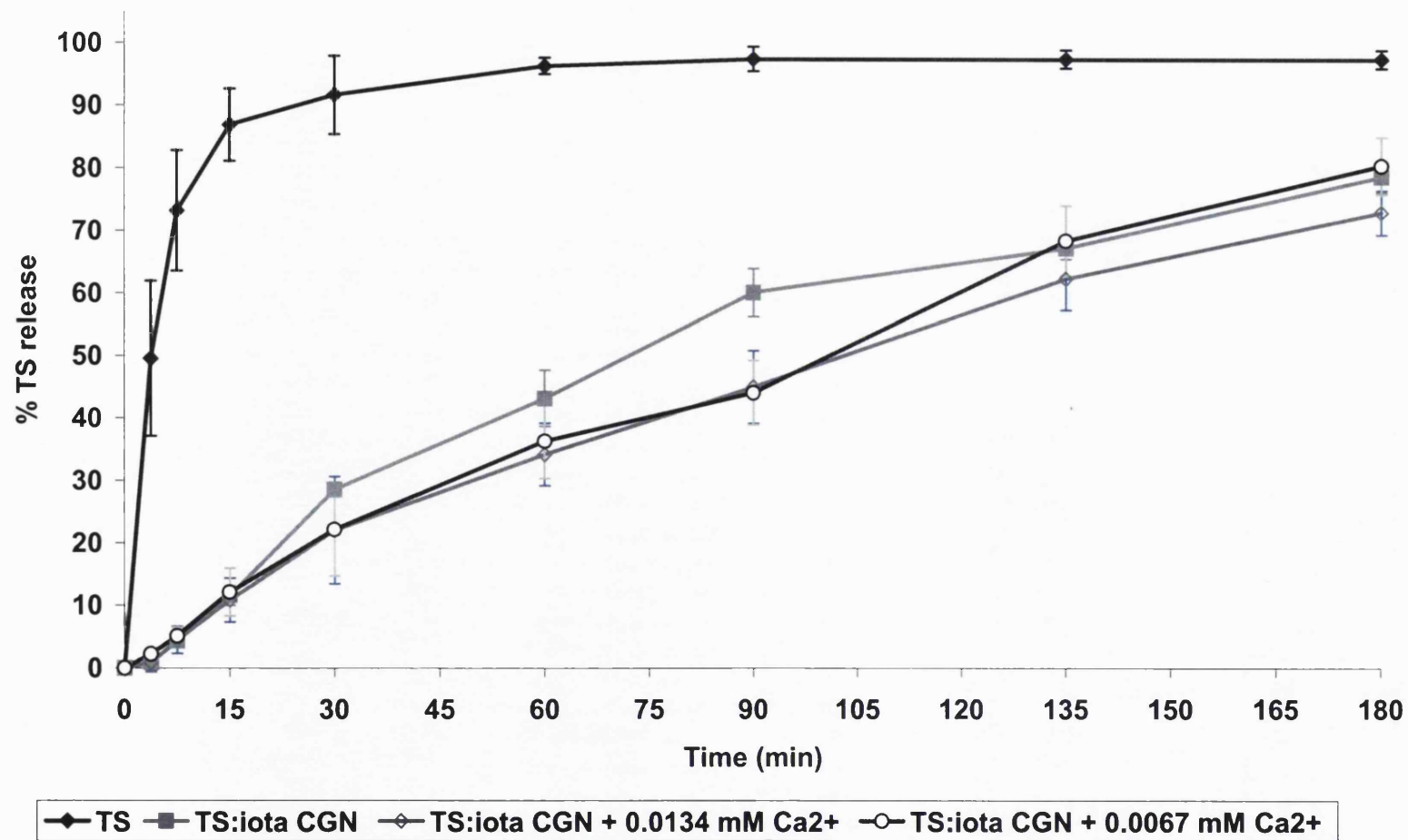


Figure 3.4.5.2: % TS release vs. time for pure micronised drug and for drug release from iota CGN microparticles crosslinked with increasing amounts of calcium ions ($n=3 \pm SD$, 20 °C).

Matrix	Cross-linking cation, (mM)	t_{50} (min) \pm SD	$k \pm$ SD	% TS release at 180 min \pm SD
TS (pure)	-	4.20 \pm 1.2	0.176 \pm 0.018	97.3 \pm 1.5
<i>kappa</i> CGN	0	58.4 \pm 8.2	0.0120 \pm 0.0018	85.6 \pm 2.8
<i>kappa</i> CGN	K ⁺ , 0.134	98.0 \pm 19	0.00727 \pm 0.0015	80.1 \pm 7.3
<i>kappa</i> CGN	K ⁺ , 0.268	83.4 \pm 13	0.00795 \pm 0.0018	77.8 \pm 3.4
<i>iota</i> CGN	0	71.8 \pm 7.8	0.00973 \pm 0.0011	78.5 \pm 2.5
<i>iota</i> CGN	Ca ²⁺ , 0.068	101 \pm 9.4	0.00693 \pm 0.00063	80.3 \pm 4.6
<i>iota</i> CGN	Ca ²⁺ , 0.134	102 \pm 10	0.00687 \pm 0.00074	72.8 \pm 3.5

Table 3.4.5.1: Summary for release characteristics from sulphated polysaccharide matrix microparticles.

Cross-linked polysaccharides had significantly longer t_{50} values relative to the non-cross-linked material (t-Test: $p < 0.05$ for *kappa* CGN and $p < 0.01$ for *iota* CGN). There was no significant increase in sustained release effect (shown for the t_{50} release values) from the particles when cross-linked at the higher cross-linking cation level. In fact, for *kappa* CGN, crosslinking at the higher potassium level appeared to promote faster release – this may have arisen from an excessive number of potassium ions interacting with the matrix, therefore reducing the ionic interaction between TS and the matrix. A maximal effect of cross-linking was attained at the lower cation concentration, with no further rises allowing for greater sustained release of TS. Finally, no significant difference (ANOVA: $p > 0.05$) was shown between the non-cross-linked and cross-linked groups for the amount released after 3 hr, highlighting the fact that the release rate following t_{50} was faster in the cross-linked groups.

Release from cross-linked matrix particles adhered (Table 3.5.4.2) to kinetics for matrix particles (Equation 3.4.4.1) over the first 60% drug release and to the 'late time' approximation for the final 60% release (Equation 3.4.4.2). This

adherence demonstrated that the crosslinked matrix microparticles also follow matrix diffusion kinetics, as shown previously for the non-crosslinked particles.

Matrix	'Early phase' regression coefficient	'Late phase' regression coefficient
<i>kappa</i> + 0.134 mM K ⁺	0.9799	0.9905
<i>kappa</i> + 0.268 mM K ⁺	0.9816	0.9507
<i>iota</i> + 0.067 mM Ca ²⁺	0.9969	0.9999
<i>iota</i> + 0.134 mM Ca ²⁺	0.9984	0.9955

Table 3.5.4.2: Regression coefficients for different CGN matrices.

Particles fabricated from the model sulphated polysaccharide CGN, whether cross-linked or not, have been shown thus far to provide a reasonable sustained release effect for TS. However, the high molecular weight of the CGN excipients (in the region of 350000MW) precludes their use as excipients for frequent pulmonary administration. Clearance from the respiratory tract for molecules of this size is negligible (Patton, 1996) and accumulation would occur.

3.4.6 TS Release from Sulphated Polysaccharide Microparticles II: DexS

The HPLC assay for TS deteriorated frequently (increase in tailing factor and retention time) with the measurement of TS release from CGN particles. By completing frequent washing procedures it was possible to maintain column performance. This problem was exacerbated when matrix particles fabricated from DexS were tested (retention time greatly increased and peak width >1 min, previously <20 sec). In order to quantify TS release from these particles, the 0.45 µm nylon membrane was replaced with a cellulosic 7000MW flat sheet dialysis membrane (Medicell International Ltd., London, UK). This

membrane prevented entry of the sulphated polysaccharide into the receiver phase and allowed satisfactory assay performance. However, the membrane pore size presented a barrier to TS diffusion (Figure 3.4.6.1). To allow comparison to previous data, it must be assumed that the 'real' release rates were faster than reported in the following graphs. All particles were produced in the TS:DexS ratio of 10:90. Figure 3.4.6.2 presents the release rates of TS from DexS microparticles. DexS 10000MW and 40000MW represent excipients suitable for pulmonary administration, whereas DexS 500000MW was chosen as it had a similar molecular weight as the CGNs investigated. Despite the highest molecular weight DexS displaying poor solubility in the release media, the release profiles showed that all DexS molecular weights gave rise to similar release profiles (large burst effect over first 60 min). ANOVA treatment of the data confirmed no significant difference ($p>0.05$) between the t_{50} values and % TS release at 180 minutes, which implied that release of TS from DexS microparticles was independent of excipient molecular weight. Visual assessment showed that all molecular weights of DexS particles had completely dissolved within 90 minutes - any residual SR in the final 90 minutes was likely to occur by ionic exchange between the sulphated polysaccharide above the dialysis membrane and the receiver phase below. The t_{50} values and release rates from DexS microparticles are shown in Table 3.4.6.

Matrix	t_{50} (min) \pm SD	$k \pm$ SD	% TS release at 180 min \pm SD
DexS 10000	28.6 \pm 6.3	0.0242 \pm 0.00037	99.3 \pm 8.61
DexS 40000	35.3 \pm 0.14	0.0196 \pm 0.0079	96.3 \pm 5.80
DexS 500000	25.6 \pm 1.1	0.0271 \pm 0.0023	96.0 \pm 2.24

Table 3.4.6: Parameters for TS release from DexS microparticles.

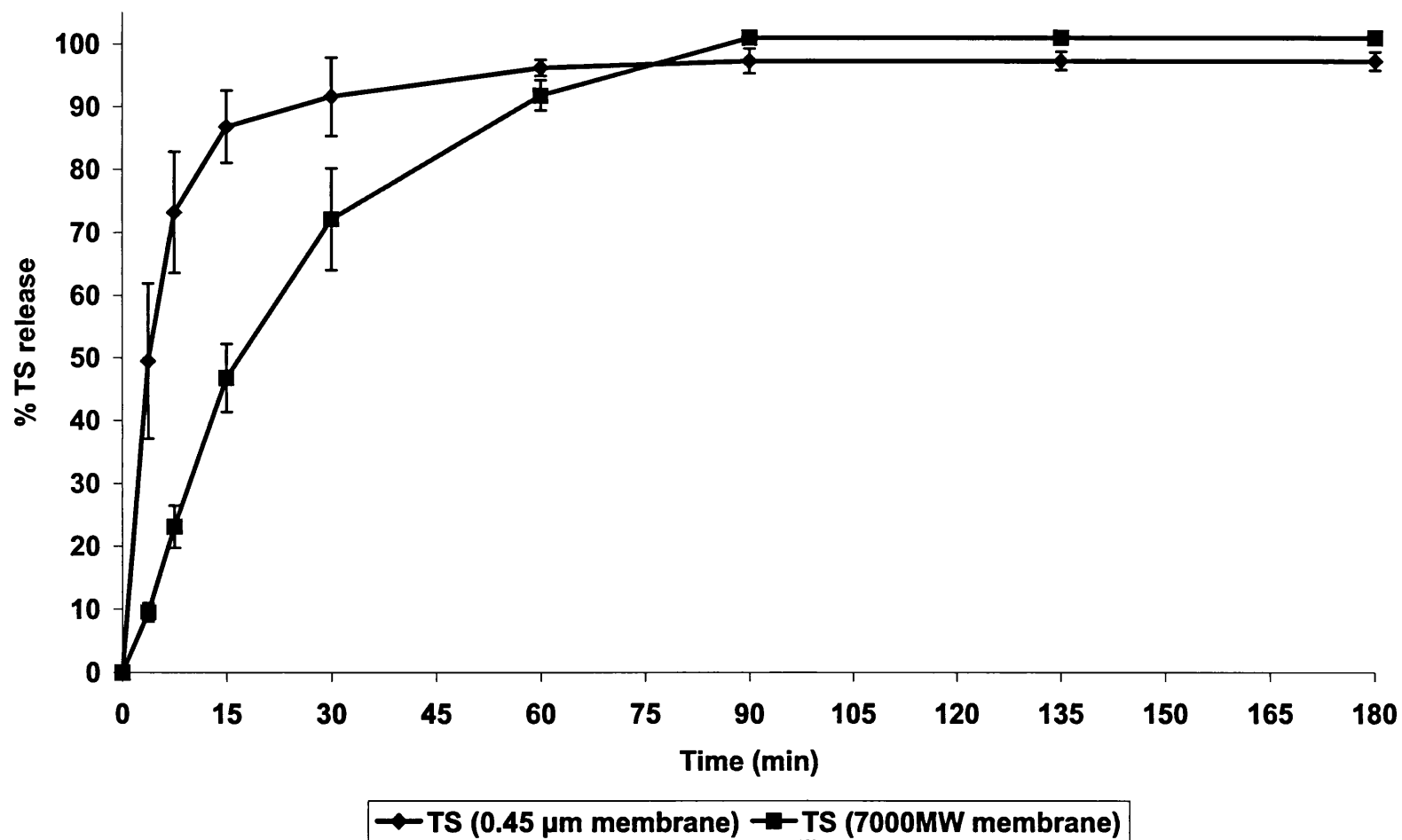


Figure 3.4.6.1: % TS release vs. time for pure micronised drug for release through (1) 0.45 µm nylon membrane and (2) a 7000MW cellulosic dialysis membrane (n=3 ± SD, 20 °C).

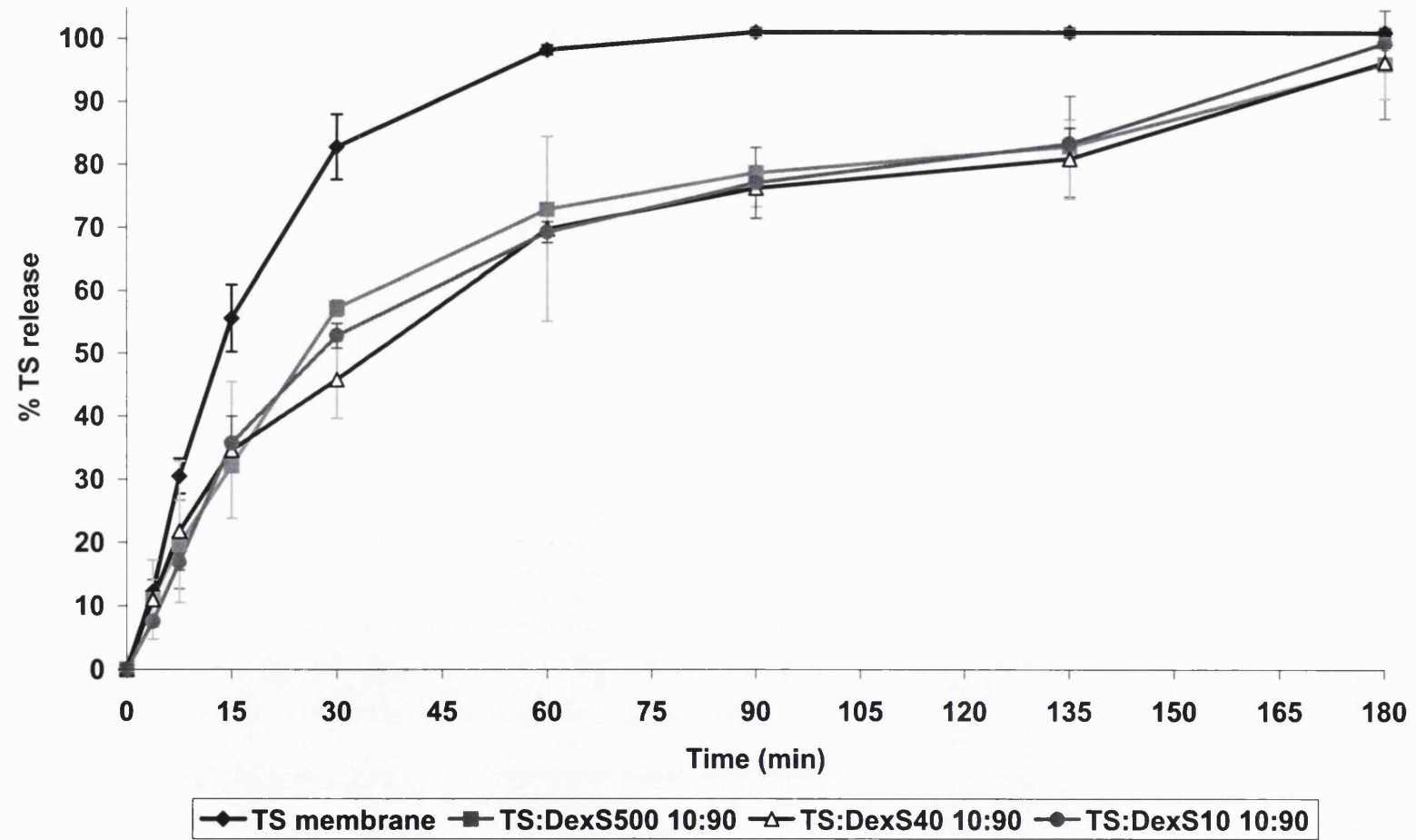


Figure 3.4.6.2: % TS release for pure drug through dialysis membrane and for formulations of DexS of different MW (x1000) (n=3 ± SD, 20 °C).

3.4.7 TS Release from Sulphated Polysaccharide Microparticles III: ChonS

The final excipient investigated for its potential to provide matrix-based SR of TS was ChonS, 17000MW. ChonS interfered with HPLC analysis such that a dialysis membrane was required again to prevent column deterioration. ChonS microparticles were produced by both milling and spray-drying (spray-dried product shown below in Figure 3.4.7.1). Release rates for both processes are shown in Figure 3.4.7.2.

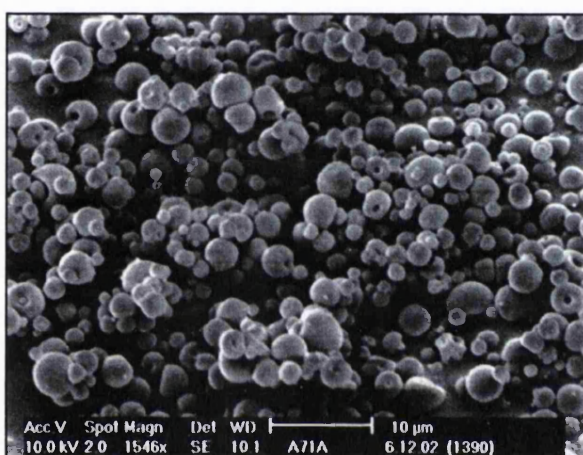


Figure 3.4.7.1: Spray-dried TS/ChonS microparticles. Spherical structure attained, VMD = 3.21 μm .

The significant effect of processing conditions on the release rates of TS from the ChonS microparticles is clearly seen in Figure 3.4.7.2. Milled material had a t_{50} value (value adjusted to release from nylon membrane) equal to 63.7 ± 10.0 minutes indicating SR, whereas spray-dried material release ($t_{50} = 14.3 \pm 4.2$ minutes) was not significantly different from pure drug dissolution (T-test, $p > 0.05$). Hydration of the milled material was observed to take longer, and this manifested as a TS release lag over the first 7.5 minutes. The difference in SR between the two processing conditions was likely to arise from (1) higher porosity of the spray-dried material allowing easier penetration of the release media into the particle and (2) differences in particle size (spray-dried VMD = 3.21 μm ; milled = 10.4 μm) allowed for greater surface exposure to the release media, with subsequent effects upon drug release and matrix dissolution in the spray-dried batch.

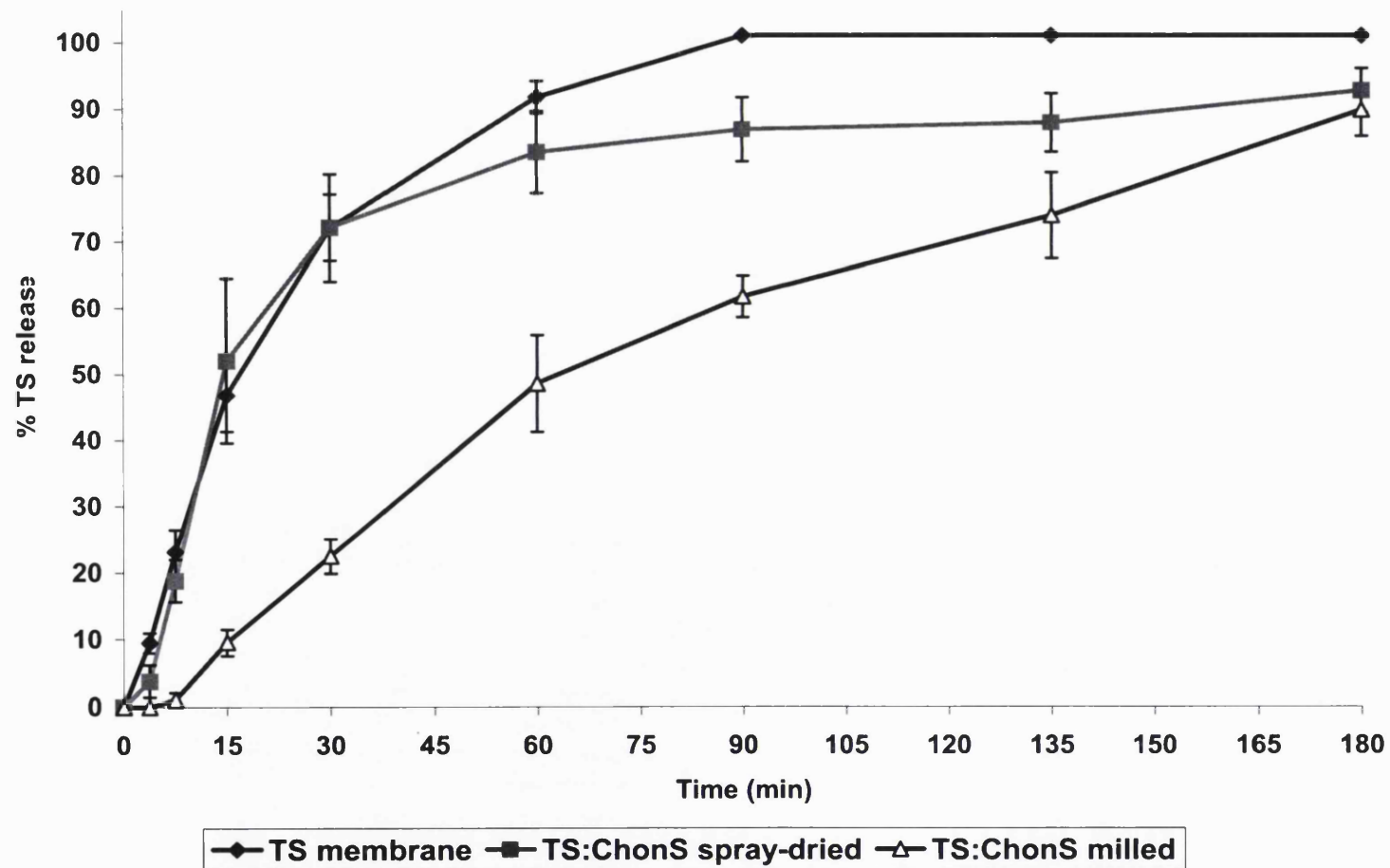


Figure 3.4.7.2: % TS release for pure drug through dialysis membrane and for ChonS formulations processed by method indicated (n=3 ± SD, 20 °C).

3.5 Conclusion

The entrapment of TS within matrix particles fabricated from sulphated polysaccharides provided a degree of SR, and in the majority of cases, release was shown to follow a matrix based diffusion process.

The mechanism of SR is two fold - firstly the particles must hydrate to allow molecular mobility of the dissolved drug, and this hydration generates a time lag in TS release. Secondly, the drug must diffuse out of the matrix into the release media. This diffusion process may be slowed by an ionic interaction between the positively charged drug and the negatively charged matrix when using sulphated polysaccharides. The absence of ionic interaction between TS and positively charged chitosan, resulted in fast release from such particles.

The greatest control over TS release was achieved with a sulphated polysaccharide, which was not appropriate for pulmonary deposition due to its high molecular weight. More acceptable lower molecular weight sulphated polysaccharides suffered from fast dissolution in the release media and showed only slight SR effects. The hydrophilicity of the matrix excipient was therefore a major drawback of this formulation approach. A spray-dried formulation (in a size appropriate for lung delivery) of the low molecular weight ChonS provided no sustained release relative to pure drug dissolution in the first hour of investigation.

In conclusion, no useful SR effects have been observed which warrant further investigation of sulphated polysaccharide particles.

Chapter 4: Formulation of TS Nanoparticles

4.1 Introduction

Nanoparticles by definition are submicron in size ($<1 \mu\text{m}$). It was the aim of this research, presented in this chapter, to generate nanoparticles of TS. Once formed, the particles would then be coated with a hydrophobic SR matrix - which was the intended secondary process for transforming TS crystals (generated from controlled crystallization, Chapter 2) into SR microparticles. In fact, coating of nanoparticles may offer distinct advantages over coating single crystals of pure drug. Breach of the SR coat in the latter case will result in immediate dissolution of the total payload. With nanoparticle entrapment however, breach of the coat will only expose single nanoparticles for dissolution, whilst the other nanoparticles within the matrix remain protected.

Chapter 3 highlighted the need for selecting SR matrix materials with greater hydrophobicity, e.g. lipids, to prevent rapid leaching of drug from the matrix. However, the hydrophilicity of TS precludes direct molecular incorporation into a hydrophobic matrix due to solubility problems during processing and incompatibility once dispersed in the matrix. For example, Westesen *et al.*, (1997), reported phase separation (drug crystallization) of molecularly dispersed drugs from lipid carriers. This highlighted potential stability issues associated with direct drug incorporation into lipophilic matrices, even with favourable drug solubility in the lipid. Therefore, it was decided to investigate ways of physically entrapping TS nanoparticles within the matrix.

There is little literature regarding the generation of pure hydrophilic drug nanoparticles. In the field of pharmaceuticals, nanoparticle generation is typically associated with (1) particle size reduction to increase dissolution and bioavailability of poorly water soluble drugs, for instance naproxen (Liversidge and Conzentino, 1995) or cyclosporine (Chen *et al.*, 2002) or (2) entrapment of actives in submicron colloidal systems, for example polymers (reviewed by Couvreur *et al.*, 1995) or lipids (reviewed by Muller, 2000).

For a hydrophilic drug, Dickinson *et al.*, (2001) developed a method in which nanoparticles could be fabricated from microemulsion templates. The nanoparticles were formulated successfully into a co-solvent modified

metered dose inhaler. However, the nanoparticles contained a high proportion of surfactant, which was undesirable for this investigation as this would further reduce the drug:excipient ratio in a SR product. An alternative formulation approach was therefore developed based on a simple water-in-oil (w/o) emulsion-template process. An emulsion is a liquid dispersion generally consisting of water and oil. The adsorption of a surfactant at the water-oil interface lowers the interfacial tension and allows the dispersal of the internal phase into droplets of small size (Florence and Attwood, 1988).

Generating nanoparticles for this investigation relied on the following theoretical method. Firstly, if high shear is applied during emulsification of a w/o emulsion, submicron aqueous droplets may be formed. Secondly, if these droplets are frozen rapidly the emulsion template may be maintained. Thirdly, providing there is sufficient drug loading of the aqueous phase to confer structural integrity, then following lyophilisation it may be possible to obtain solid drug nanoparticles (Figure 4.1).

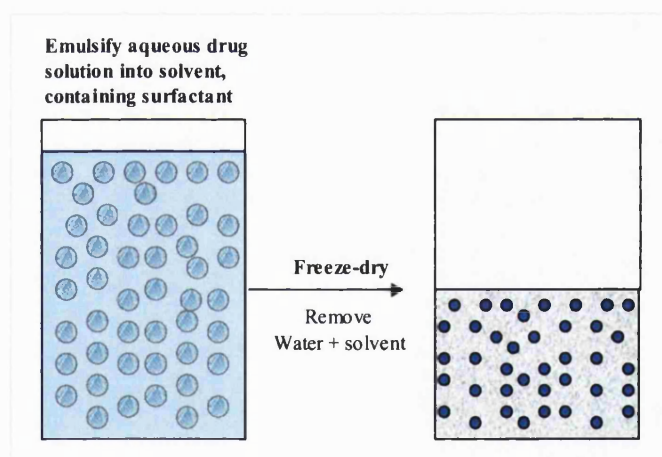


Figure 4.1: Methodology for nanoparticle production. Aqueous drug solution is emulsified into organic phase. Emulsion is rapidly frozen and water micro-droplet structure is maintained in the solid state - 'emulsion template.' Freeze-drying is then performed to remove water and solvent leaving behind a solid drug core, surrounded by surfactant.

A similar method, in which organic solvent was evaporated from the internal phase of an oil-in-water emulsion leaving an aqueous suspension of precipitated hydrophobic drug particles with a coating of surfactant, was developed by Sjostrom *et al.*, (1993a,b).

4.2 Materials

4.2.1 Model Drug

The hydrophilic drug, terbutaline sulphate (TS), was supplied in micronised form (Lot 4104H) by Investigational Products at AstraZeneca R&D Charnwood (Loughborough, Leicestershire, UK).

4.2.2 Nanoparticle Formulation

Sorbitan monostearate (Span 60), sorbitan trioleate (Span 85) and cineole were purchased from Sigma-Aldrich Company Ltd. (Gillingham, Dorset, UK). A research sample of Lecithin P100 was donated by Degussa Bioactives GmbH (Freising, Germany). Acetone (ACT), dichloromethane (DCM) and chloroform (CFM) were obtained from VWR International Ltd. (Poole, Dorset, UK) and water (HPLC grade) from Fisher Scientific Ltd. (Loughborough, Leicestershire, UK).

4.3 Methods

4.3.1 w/o Emulsion Preparation

Surfactant was accurately weighed on a 5-figure balance, into a 14 mL glass vial. Surfactants were chosen from the HLB range of 2-7, which stabilize w/o emulsions. The desired amount of solvent was weighed into the same vial, which was then sealed prior to vortexing (Rotamixer, Hook and Tucker Instruments Ltd., Croydon, Surrey, UK) until the surfactant had dissolved. The aqueous phase was prepared by weighing TS into a 7 mL vial and making up to final weight with water; final w:o ratio was maintained at 1:5 throughout the experimental work. The organic phase was then placed in contact with an UltraTurrax T25 homogeniser (IKA-Werke GmbH, Staufen, Germany). The aqueous phase was pipetted into the organic phase immediately after starting the homogeniser. Homogenisation was performed for 5 minutes to ensure thorough emulsification (Figure 4.3.1.1). N₂ (l) was poured into an insulated glass vessel that contained a fresh 14 mL glass vial

that was covered with perforated aluminium foil, also half-filled with N₂ (l). After completion of homogenisation, the emulsion was transferred with a pipette directly into the 14 mL vial and frozen rapidly (Figure 4.3.1.2).

4.3.2 Freeze-Drying (Lyophilisation)

The frozen vials were then transferred to a vacuum proofed 500 mL glass jar (Girovac Ltd., North Walsham, Norfolk, UK) and attached to a freeze-dryer (Drywinner 110, Heto-Holten A/S, Gydevang, Denmark). Freeze drying is a process in which materials are firstly dissolved in a solvent, e.g. water, and frozen. Secondly, solvent is removed by vacuum sublimation from the frozen mass, leaving behind a typically amorphous, solid product. The process and its pharmaceutical applications have been reviewed by Franks, (1998), in greater detail. The freeze-dryer was specifically purchased for its relatively low condenser operating temperature (-110 °C) that permitted retention of organic vapours. Freeze-drying was performed for a minimum of 12 h.

4.3.3 Nanoparticle Purification

The freeze-dried material consisted of TS nanoparticles encased in a mass of surfactant. This lyophilisate was then resuspended in a solvent in which TS was insoluble (to preserve nanoparticle structure) and in which the surfactant was freely soluble. The resultant suspension was then centrifuged at 15000 rpm (3K30 Refrigerated Centrifuge, Sigma Laborzentrifuges GmbH, Osterode am Harz, Germany) to sediment the nanoparticles. The solvent/surfactant solution was then decanted and the nanoparticles were collected. 50 mL Oakridge Teflon[®] centrifuge tubes (Nalge-Nunc Inc., Rochester, NY, USA) were selected for centrifugation owing to excellent solvent compatibility and ease of nanoparticle collection from the non-stick surface. The process was repeated as necessary.

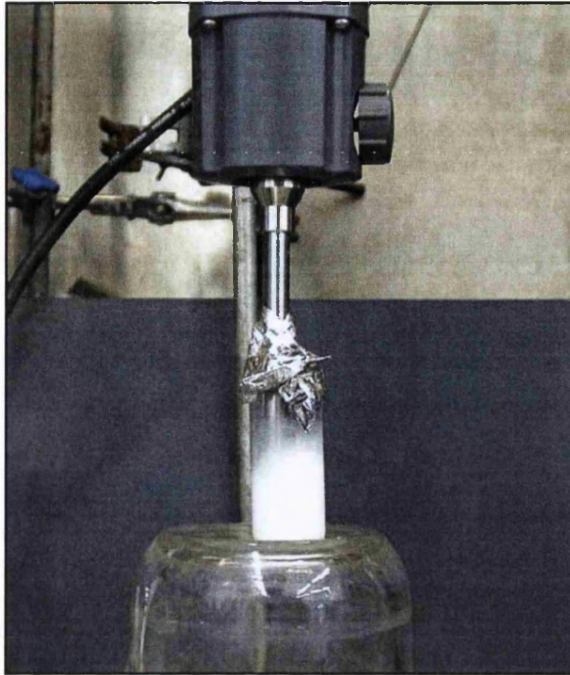


Figure 4.3.1.1: Emulsification step using homogeniser. Aluminium foil was in place to limit introduction of air into the emulsion (air caused build up of a thick emulsion on the vessel wall and isolated part of the emulsion from homogenisation).

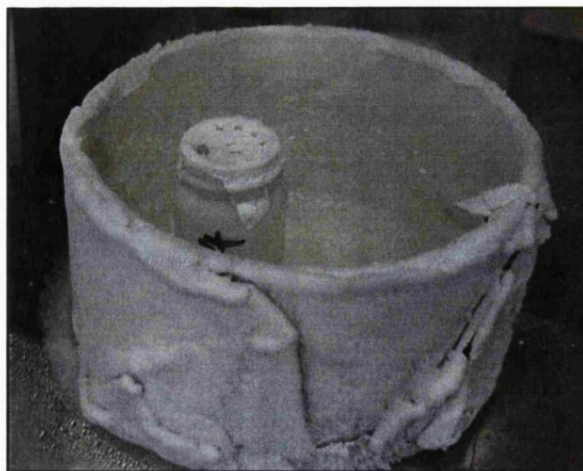


Figure 4.3.1.2: Freezing step in liquid nitrogen. The emulsion from Figure 4.3.1.1 was added to the vial with a pipette through one of the holes in the aluminium foil. Addition this way prevented the emulsion from expulsion out of the vial upon contact with liquid nitrogen.

4.3.4 Particle Size Characterisation

TS particles were sized by Laser Diffraction (Malvern Instruments Ltd. Mastersizer X, Malvern, Worcestershire, UK) by taking a mass of the lyophilisate (100 mg) and resuspending in CFM (5 mL). Particle sizing was carried out in accordance with section 2.3.4. Large quantities of sample were required to obtain acceptable obscuration values, which suggested that the particle size was beneath the lower operational limit of the machine (confirmed by overlap of the particle size distribution curve with the 0.5 μm size cut-off). In order to obtain reproducible size data, Photon Correlation Spectroscopy (PCS) was therefore used to provide an analysis of particle size.

PCS (also known as dynamic light scattering) measures fluctuations in the intensity of scattered light that results from particle movement (i.e. Brownian motion). A smaller particle is more subject to random bombardment by solvent molecules and therefore exhibits faster Brownian motion than larger particles. Accordingly, particle size is indirectly proportional to the rate of Brownian motion. As Brownian motion is affected by changes in temperature and viscosity, values for these factors must be known and controlled. The method is appropriate for characterising particles in the size range from a few nanoparticles to approximately 3 μm (Muller *et al.*, 2000).

The hydrodynamic diameter, $d(H)$, is the diameter of a sphere that has the same translational diffusion coefficient of the test particle and is given by the Stokes-Einstein equation (Equation 4.3.4).

$$d(H) = \frac{kT}{3\pi\eta D}$$

Equation 4.3.4: Stokes-Einstein Equation for calculation of hydrodynamic diameter. k = Boltzmann's constant, T = absolute temperature, η = viscosity, D = translational diffusion constant (calculated by instrument software).

A typical instrument set-up is shown in Figure 4.3.4. The instrument analyses the movement of scattered light and records a very complex and constantly

changing intensity pattern of 'speckles.' The rate of change of the intensity pattern depends on the particle size. For large particles, the intensity pattern signal changes slowly and therefore correlation between the signals is observed for a long time. However, for small particles moving rapidly the correlation disappears more rapidly. A 'correlator' within the computer measures the correlation of the signals versus time, and uses algorithms to generate a particle size distribution for the sample from this data. The distribution is typically characterised by a mean diameter (z-average diameter, z_{ave}) and width (polydispersity) for the size distribution.

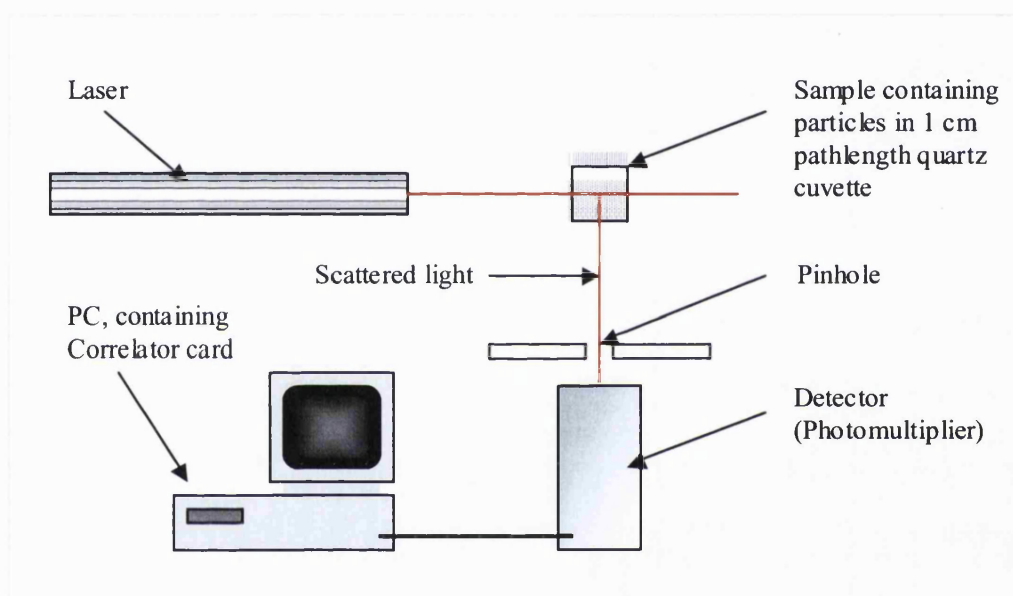


Figure 4.3.4: Typical set-up of PCS instrument.

For sample preparation, approximately 300 mg of lyophilisate was resuspended in 5 mL filtered CFM (filtered through 0.1 μm nylon membrane) and sonicated for 5 minutes. A 200 μL sample of the suspension was then dropped into a non-frosted quartz cuvette, containing 3 mL CFM. This sample concentration provided the required analytical count rate (>50 Kilocounts per second (Kcps)). The lid was placed on the cuvette and the sample inverted 5 times to ensure thorough mixing. The cuvette was then placed in the sample holder within the PCS machine and the lid closed. Once the machine had attained temperature stability (20 $^{\circ}\text{C}$) the machine started automatically. Each sample was sized in triplicate.

4.3.5 Determination of Viscosity of Suspending Medium used in PCS

An accurate value of viscosity is required to improve PCS accuracy as viscosity directly influences the rate of Brownian motion in liquids. The suspending media chosen for experiments was CFM (viscosity = 0.571 mPa s), however, surfactant was also present which will alter viscosity. Determination of dynamic viscosity was performed in accordance with Appendix 183 of the British Pharmacopoeia (2003), in a calibrated U-tube viscometer, Type O (Fisher Scientific Ltd., Loughborough, Leicestershire, UK).

CFM was used as supplied and a 0.31% w/v Span 60 in CFM solution was tested (concentration derived from sample preparation method). The viscometer (Figure 4.3.5) was placed in a glass walled water bath (Townsend and Mercer Ltd., Croydon, Surrey, UK) held at 20 °C.

The test solution was pipetted into the viscometer through tube L to slightly above mark G, using a pipette to minimise wetting of the glass wall. The solution was left for 10 minutes for temperature equilibration, the meniscus level was then adjusted to coincide with point G. The solution was then drawn up via suction to a point about 5 mm above point E. After releasing suction, the time for the meniscus to drop from the top edge of point E to the top edge of point F was measured. The dynamic viscosity, η , was calculated in millipascal seconds (mPa s) from Equation 4.3.5.

$$\eta = K\rho t$$

Equation 4.3.5: Calculation of dynamic viscosity, η , in mPa S. K = calibration constant of instrument (0.001029 (mm²/s)/s): ρ = mass/volume (g cm⁻³) obtained by multiplying relative density of fluid by 0.9982: t = time (s) for meniscus to drop from point E to point F.

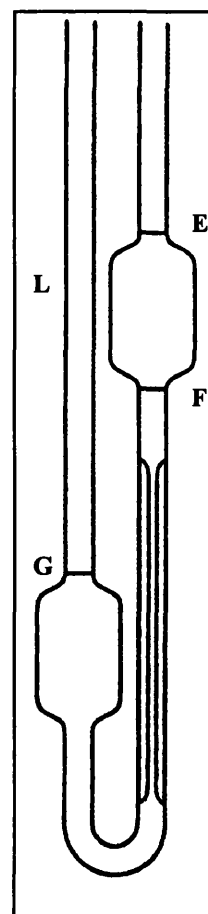


Figure 4.3.5: (Inset) U-tube viscometer, with relevant standardised lettering.

4.3.6 Particle Morphology Characterisation

TS nanoparticles were characterised with SEM prior to centrifugation and post centrifugation in an identical method to that of Section 2.3.5. Transmission Electron microscopy (TEM) was also performed, by Mr. D. McCarthy of the EM service at the University of London, School of Pharmacy. The majority of TEM preparation is aqueous based, which was not suitable for TS, as the particles would dissolve. TS nanoparticles were therefore suspended in a small amount of light mineral oil (obtained from Sigma-Aldrich Company Ltd., Gillingham, Dorset, UK) and immobilised on copper grids. The sample was then introduced into the vacuum port of the TEM instrument prior to visualisation. Photomicrographs were developed from the transmitted image.

4.3.7 Determination of Effectiveness of Surfactant Washing Procedure and TS Content of Nanoparticles

Following preparation of nanoparticles, purification (surfactant removal) was performed by centrifugation. During this step, the nanoparticles were sedimented and the surfactant dissolved into the organic supernatant. Experiments were performed to determine the number of centrifuge washes (15000 rpm at 18 °C) required for surfactant removal. Following decanting of the supernatant, the sedimented nanoparticles were dried overnight in a model D100 oven (WTB Binder GmbH, Tullingen, Germany) at 50 °C. Accurately weighed 20.0 mg samples were taken from the dry mass and dissolved in 0.05 M phosphate buffer and assayed for TS content using HPLC (Section 3.3.1).

4.3.8 X-Ray Powder Diffraction (XRPD)

Sublimation of water from the dispersed phase of the emulsion during lyophilisation left TS in the solid state. XRPD was employed to assess the nature of this solid state, i.e. amorphous, partially amorphous or crystalline.

When a focused x-ray beam interacts with a material, part of the beam is absorbed, refracted, scattered and most importantly for this technique, diffracted. In XRPD, x-rays are generated when a copper target is bombarded with accelerated electrons from a filament under high voltage (15-60 KV). The x-rays are then collimated and directed onto the sample. When an x-ray hits the sample, the diffraction distance between the planes of atoms (d-spacings) may be measured using Bragg's Law (Equation 4.3.8).

$$n\lambda = 2d\sin\theta$$

Equation 4.3.8: Bragg's Law. n = order of diffracted beam: d = distance between adjacent planes of atoms: λ = wavelength of incident x-ray beam (known): θ = angle of incidence of x-ray beam (this angle is varied at a controlled rate in order to generate an x-ray scan)

The characteristic set of d-spacings generated in a typical x-ray scan provides a unique fingerprint of the material. Diffraction of an x-ray beam depends on the type of atoms within the material and how these atoms are arranged geometrically. Regular repeating units of atoms, which form a crystal lattice, define crystalline materials. The crystalline form is characterised by a number of sharp, narrow peaks within the XRPD pattern (Briggner *et al.*, 1994). Materials made up from atoms that are not packed in a long range ordered fashion are said to be amorphous. If the solidification process (for example, spray-drying) is too rapid for the molecules to align in the correct form for a crystal, the material is likely to be amorphous.

A small amount of powder (30 mg) was gently compressed into an XRPD round disc sample holder, and the surface was smoothed to ensure no cracks or defects, using a flat Perspex[®] block. The sample was then loaded into a Philips PW3710 Powder Diffractometer, and the sample was analysed at the following conditions: Cu K α ($\lambda = 1.542 \text{ \AA}$) radiation, 5-30 $^\circ$ 2 θ , step size 0.02 $^\circ$, time per step 4 seconds (adapted from Columbano *et al.*, 2002). In order to determine the amorphous/crystalline nature of the TS nanoparticles, the nanoparticle diffraction pattern was compared to patterns for pure crystalline TS (as received from AstraZeneca) and pure amorphous TS (from a simple aqueous spray drying method adapted from Chawla *et al.*, (1994)).

4.3.9 Determination of Glass Transition Temperature Using Differential Scanning Calorimetry (DSC)

DSC analysis provides detailed information about both physical and energetic properties of pharmaceutical materials: for instance, polymorphism, phase transition, dehydration, decomposition, excipient compatibility and purity. The technique is accurate and can be performed with small sample sizes (< 5 mg) - for these reasons, DSC is frequently the thermal analysis technique of choice (Clas *et al.*, 1999).

DSC measures the amount of energy (heat) absorbed or released by a sample, as it is heated/cooled. The technique compensates for temperature differences between a reference pan and sample pan, the differences arising from thermal transitions within the sample (for example, melting or glass transition, T_g). Compensation occurs by varying the energy input required to keep both pans at the same temperature. The amount of energy required to maintain this equilibrium is directly proportional to changes occurring in the sample. Using this principle, energy differences between the pans were conventionally plotted against sample temperature (thermal profile).

Samples (1-5 mg) were accurately weighed using a microbalance into open aluminium pans (Kit No. 0219-0041, Perkin Elmer Inc., Shelton, CT, USA). Lids were then placed on the pans, and crimped to ensure a tight seal using a crimper press. An empty crimped pan was used as reference. Sample and reference pans were then loaded into a Pyris 1 Calorimeter (Perkin Elmer) equipped with an Intracooler 2-P cooling unit. Calibration was performed prior to each session with high purity indium and lead standards with known onset melting points. Nitrogen was used as purge gas throughout experimental work at a flow rate of 20 mL/min. The pans were left to reach thermal equilibrium within the calorimeter for 5 minutes. Scan rates of material were performed at standard temperature scan rates of 10 °C/min and at 200 °C/min (high speed temperature scan - developed by Perkin Elmer and referred to as HyperDSC™).

4.4 Results and Discussion

4.4.1 Initial TS Particle Formulation From w/o Emulsions

Early attempts to generate particles from w/o emulsions quickly indicated that there was insufficient surfactant present to stabilise small aqueous droplets in the emulsion. This was evident from laser diffraction data ($VMD = 11.2 \pm 0.63 \mu\text{m}$) and SEM images that showed relatively large TS clusters (Figure 4.4.1).

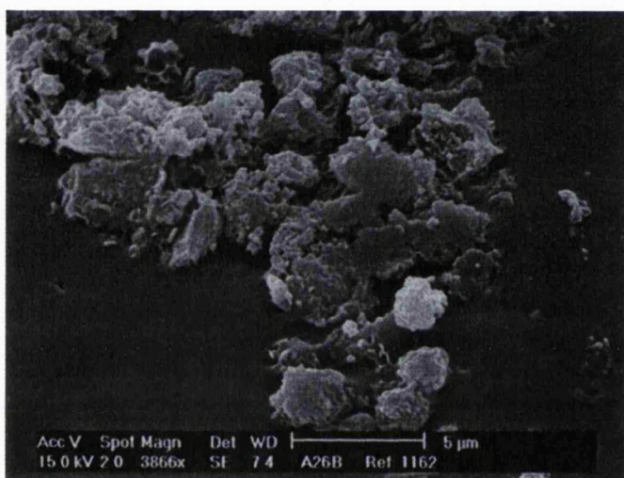


Figure 4.4.1: SEM image of TS particles generated from early emulsification studies. Image suggested lack of structural control attained.

In other preliminary experiments, Span 85 was ruled out for use as a surfactant, as the aqueous emulsion droplets rapidly coalesced and the emulsion separated. Coalescence is due to the interfacial barrier having insufficient strength to prevent formation of progressively larger droplets, and ultimately 'breaking' or complete separation of the emulsion (Im-Emsap, 2002). Lecithin (Epikuron P100) was also found to show poor w/o emulsification performance, as the HLB value (7) is at the limit necessary to stabilise such emulsions.

Span 60 was selected as an ideal surfactant ($HLB = 4.7$) as (1) the emulsion was visibly stable and (2) as the surfactant is solid at room temperature, it

provided a stable matrix during and after lyophilisation. The solid freeze-dried product was typically granular, which allowed for ease in handling. A further advantage of Span 60 is the hydrophobicity of the molecule, which prevented undesirable surfactant incorporation into the aqueous droplet, and therefore excess entrapment into the final TS nanoparticle.

4.4.2 TS Nanoparticle Production

TS nanoparticles were optimised by investigating the effects of surfactant concentration, homogenisation speed and TS content in the aqueous phase (Table 4.4.2.1).

Factor	Levels Investigated
Surfactant concentration, (w/w)	4%, 6%, 8%, 10%
Homogenisation speed, (1000 x rpm)	11, 13, 16, 19, 22, 24
TS concentration (w/w)	5%, 10%, 15%, 20%

Table 4.4.2.1: Factors and levels investigated for emulsion optimisation.

Light microscopy was used to examine the nature of the emulsion, however, as the droplets were submicron in size, visualisation of the dispersed aqueous droplets was impeded.

Figures 4.4.2.1-3 show the effect of the process variables upon particle size, as determined by PCS. Calculation of viscosity at 20 °C of the suspending media (n=5) gave a value of 0.585 mPa S (versus 0.571 for pure CFM), which was the input viscosity value used in PCS. Particle sizing by PCS provided reliable indications of particle size as indicated by a high value for a built-in quality indicator (% In Range >98) and correlograms that appeared smooth with a flat baseline (indicating absence of aggregates that skew the particle size distribution).

Figure 4.4.2.1 indicates that as the surfactant concentration in the organic phase increased, the particle size of the TS nanoparticles decreased. Increasing the amount of surfactant reduces the interfacial tension - therefore droplets are easier to break up into smaller droplets, and the tendency to recombine is reduced (Eccleston, 2002). Consequently, the resultant TS nanoparticles were smaller. This is in agreement with Sjoström *et al.*, (1995) who observed that cholesterol acetate particles were smaller when prepared from o/w emulsions with greater amounts of emulsifier. Further increases in surfactant concentration were not investigated due to limited surfactant solubility in the organic phase.

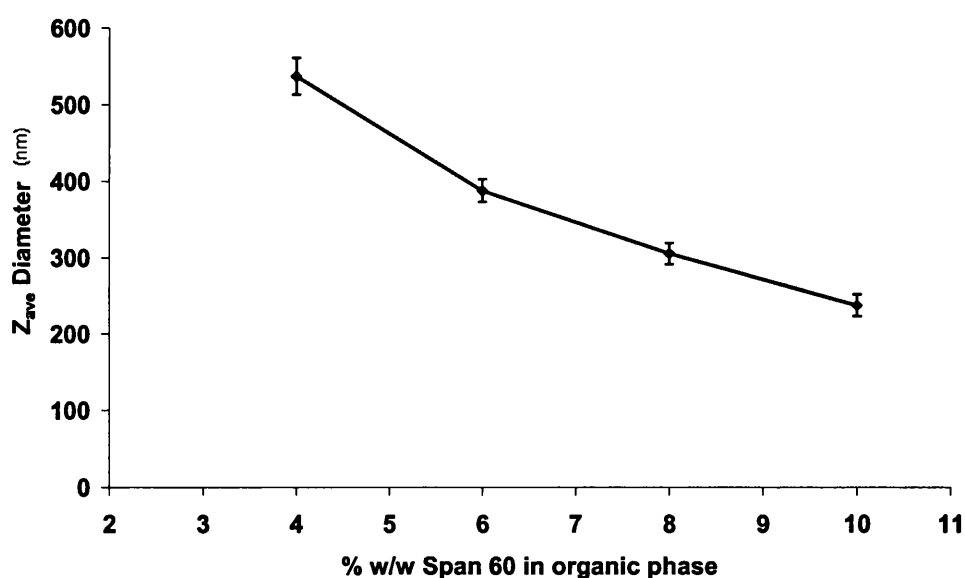


Figure 4.4.2.1: Effect of surfactant concentration on particle size of TS. Homogenisation speed = 24000 rpm, TS concentration = 10% w/w based on aqueous phase

Figure 4.4.2.2 confirmed that increasing the homogenisation speed, and therefore the energy (in the form of shear) applied to the emulsion, resulted in a significant reduction in particle size (greater shear causes droplets to break up more effectively (Gopal, 1968). Doubling the homogenisation speed from 11000 rpm to 22000 rpm caused a 41% reduction in size (t-Test, $p < 0.0001$). However, no significant difference in particle size was observed between 22000 rpm and 24000 rpm. This indicated that a maximum effect of homogenisation upon droplet size was achieved at these speeds.

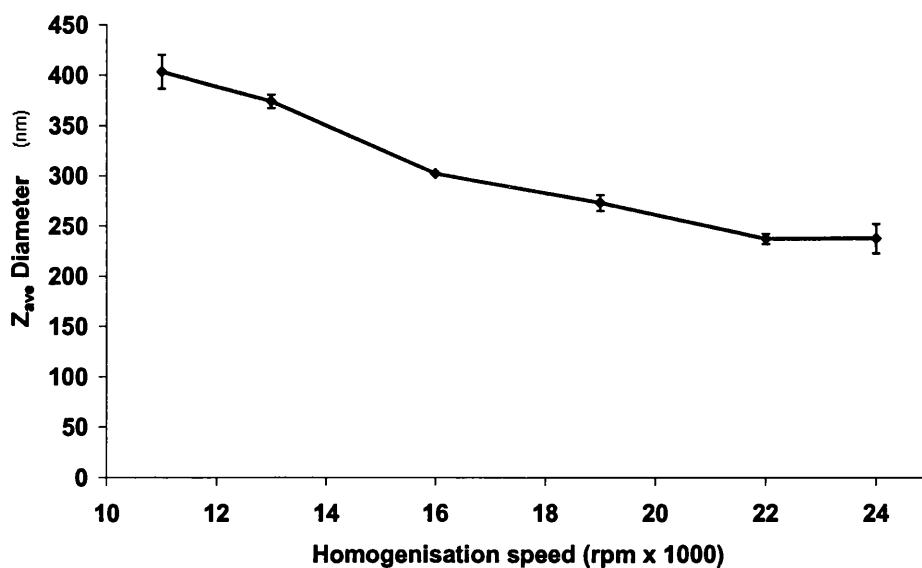


Figure 4.4.2.2: Effect of Homogenisation speed on particle size of TS. Span 60 concentration = 10% w/w based on organic phase, and TS concentration = 10% w/w based on aqueous phase.

Finally, Figure 4.4.2.3 showed that the TS nanoparticle size increased with increased amounts of TS in the aqueous phase. The data suggests that greater drug concentration in the aqueous phase destabilised the emulsion droplets, which resulted in a larger droplets and final nanoparticle size. The lowest particle size was achieved with 5% w/w aqueous TS solution (199 ± 2.5 nm).

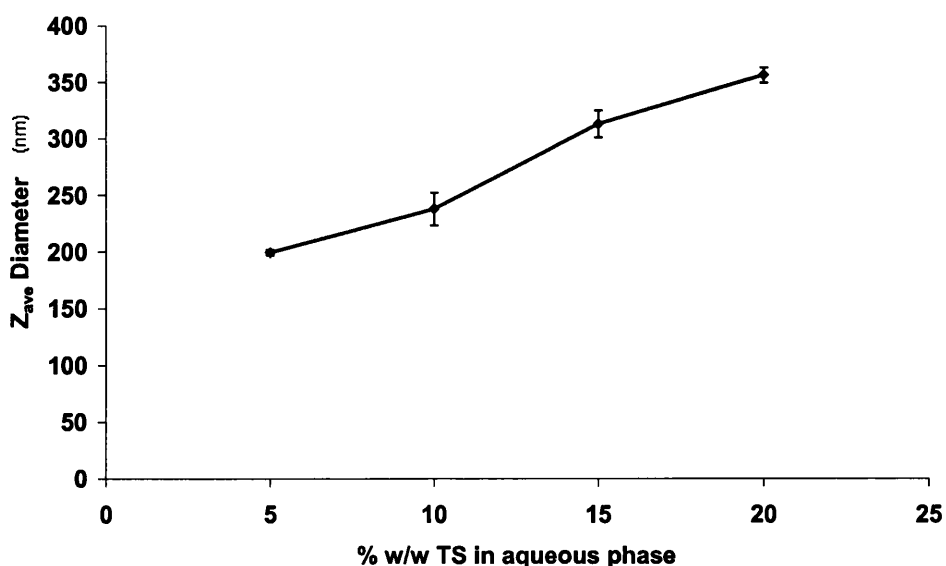


Figure 4.4.2.3: Effect of TS concentration in aqueous phase on final TS particle size. Homogenisation speed = 24000 rpm and Span 60 concentration = 10% w/w based on organic phase.

However, 10% w/w TS was used for all further nanoparticle production as particle size was acceptable and batch size was larger. A summary of formulation details and particle size range is presented in Table 4.4.2.2. A graphical display of the particle size distribution for this formulation is shown in Figure 4.4.2.4.

% w/w TS in aqueous phase	10 (100 mg to 1 g water)
% w/w Span 60 in organic phase	10 (500 mg to 5 g CFM)
Homogenisation Speed and Time	24000 rpm, 5 min
Lyophilisation	> 12 hr
Particle Size, Z_{ave}	238 ± 14 nm

Table 4.4.2.2: Parameters for TS nanoparticle preparation and size range (PCS). Homogenisation time was not varied as it is reported (Gopal, 1968) that under normal laboratory conditions, droplet size reaches its minimum size within 5 minutes. (Nanoparticles were also produced by using cineole, natural oil derived from eucalyptus, as an alternative to CFM in the organic phase. The same conditions yielded particles of 385 nm).

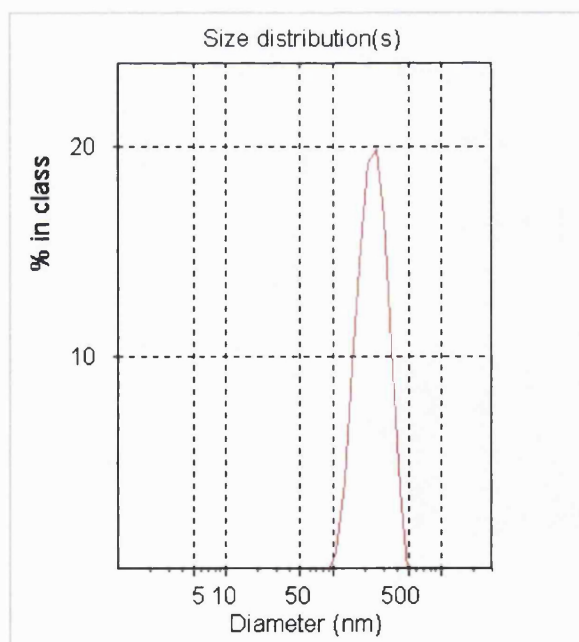


Figure 4.4.2.4: PCS particle size distribution generated for optimised nanoparticle formulation ($Z_{ave} = 232.8$ nm, polydispersity index = 0.168, indicating mid-range polydispersity).

4.4.3 Surfactant Removal from TS Nanoparticles

Washing of the particles by centrifugation was not possible in DCM or CFM at centrifugation speeds up to 21000 rpm. No sedimentation or creaming was observed which indicated that the TS particles were of approximately equal density to the halogenated solvents (DCM density = 1.325 g/mL, CFM = 1.492 g/mL). Acetone was therefore chosen as a solvent due to its lower density (0.791 g/mL) and good solvency for Span 60. The results for the number of washing cycles (15000 rpm) are displayed in Table 4.4.3.

Number of Centrifuge Cycles	Purity of Sample % w/w TS \pm SD
1	86.3 \pm 0.92
2	101 \pm 1.4

Table 4.4.3: Effect of number of washing cycles on TS nanoparticle purity.

One centrifugation cycle was insufficient to remove the surfactant covering from the nanoparticles (13.7% Span 60 remained). Two washes however removed the surfactant coat leaving high purity of the remaining TS nanoparticles. It is unlikely, however, that all surfactant is removed as a surface monolayer will remain.

Decanting the supernatant required care as the surface nanoparticle layer was easily disrupted by the movement of acetone. Overall yield from the centrifugation washing process was determined to be 94.3 \pm 3.0% following two wash cycles (based on amount recovered from the centrifuge tubes relative to amounts weighed into aqueous phase). These losses were primarily from the centrifugation process as losses to glassware during the emulsification steps accounted for just 2.2% of TS lost. Loss of TS during centrifugation was confirmed by evidence that washing the nanoparticles four times reduced the yield to 86.0 \pm 1.3%.

4.4.4 Morphological Characterisation of TS Nanoparticles

SEM photomicrographs of the TS nanoparticles provided the most valuable images. Figure 4.4.4.1 shows the lyophilisate structure in which the drug:surfactant ratio is 1:5. Span 60 appears to provide a continuous coating of the nanoparticles. Figure 4.4.4.2 shows the same batch, centrifuged twice in acetone. It is clear from the image that the Span 60 was removed effectively from TS nanoparticles (loss of smooth appearance of Span 60 and large particle size reduction).

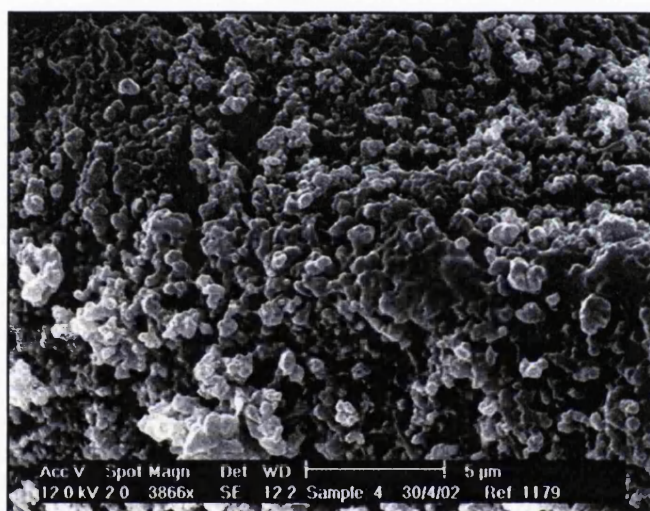


Figure 4.4.4.1: SEM image of freeze-dried w/o emulsion.

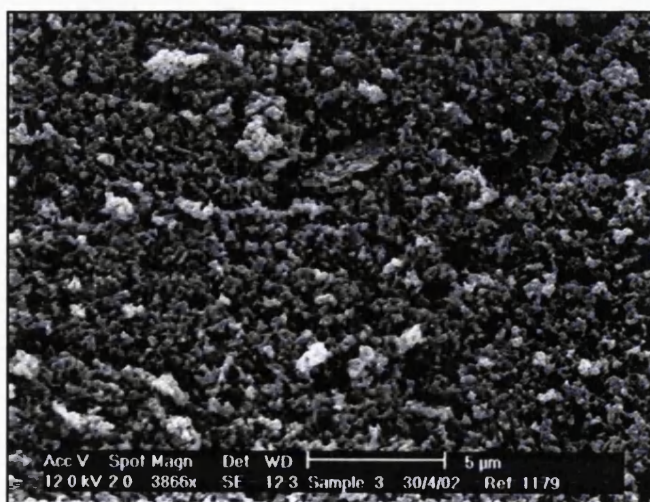


Figure 4.4.4.2: SEM image of washed TS nanoparticles. Image shows good correlation with PCS data.

TEM imaging was less than ideal due to poor resolution between the TS nanoparticles and the background (Figure 4.4.4.3). The TEM image does, however, show a number of particles in the expected size which are spherical in structure. Spherical morphology was expected since the particles were created from spherical emulsion droplets. Formulating the nanoparticles with a water-soluble heavy metal stain in the aqueous phase may be a way of improving contrast: however, this was not performed as SEM images were satisfactory.



Figure 4.4.4.3: TEM image of TS nanoparticles, evidence of spherical structure present.

4.4.5 Physicochemical Characterisation of TS Nanoparticles

Spray drying was used to prepare amorphous TS microparticles for use in XRPD. An SEM image showed a spherical and in most cases crenulated morphology with no visible indication of crystallinity (Figure 4.4.5.1).

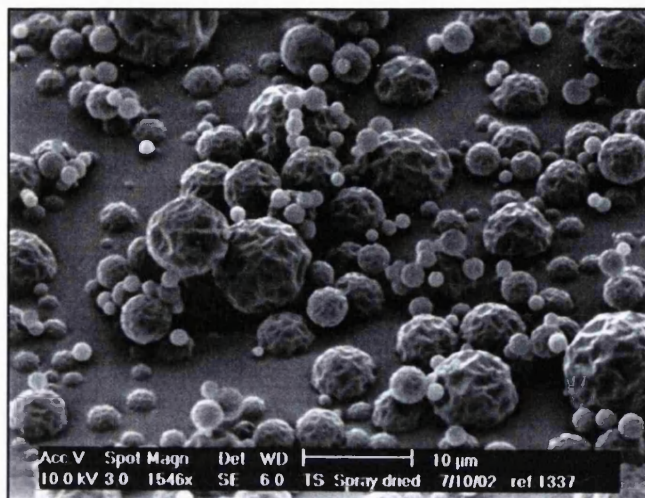


Figure 4.4.5.1: Spray dried pure TS from aqueous solution.

The amorphous form gave rise to a diffuse diffraction pattern with no sharp peaks as indicated in Figure 4.4.5.2. Several other authors have reported the diffuse diffraction pattern, characteristic for amorphicity: of sucrose (Briggner *et al.*, 1994), lactose (Elamin *et al.*, 1995), sucrose/lactose (Saleki-Gerhardt *et al.*, 1994), and in particular, salbutamol sulphate (Chawla *et al.*, 1994). The crystalline form has many narrow peaks indicative of a long-range order found in crystals, and this was seen for micronised crystalline TS (Figure 4.4.5.2).

The powder diffraction pattern for TS nanoparticles (Figure 4.4.5.3) was almost identical to that of the amorphous spray dried material. It should be noted, however, that XRPD does not provide conclusive proof for amorphous structure as the technique scans for long-range order, which may be deficient in material of small particle size (<1 μm). However, it is very unlikely that a hydrophilic active freeze-dried from water would display crystallinity unless the T_g of the active was low enough to permit rapid crystallization following freeze-drying.

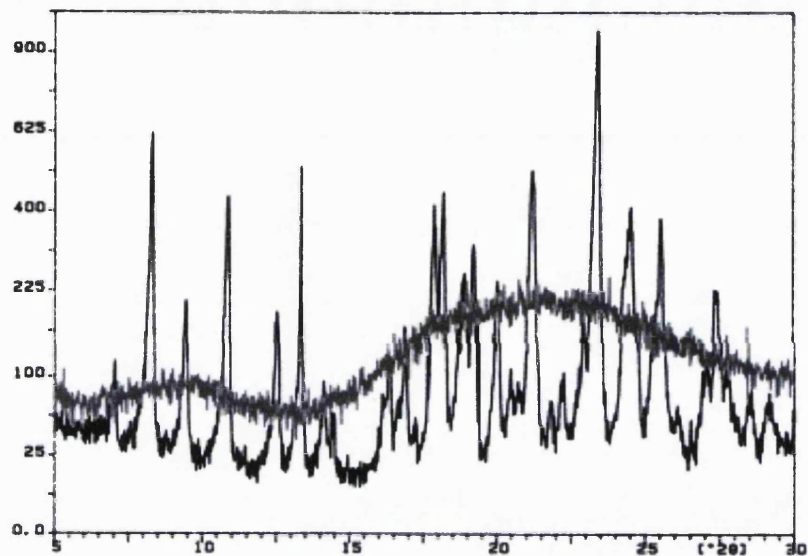


Figure 4.4.5.2: Powder X-ray diffractograms of crystalline TS (|) micronised, as received from AZ and amorphous TS (|) produced by spray drying the aqueous solution.

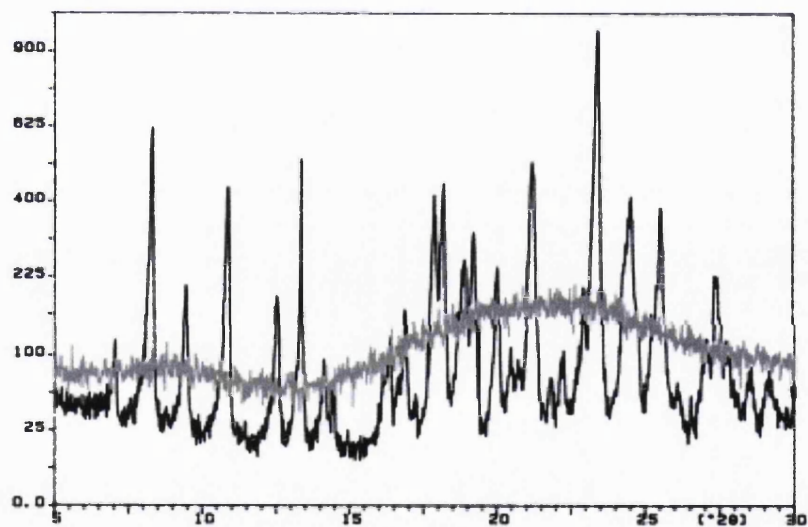


Figure 4.4.5.3: Powder X-ray diffractograms of crystalline TS (|) micronised, as received from AZ and nanoparticulate TS (|) produced through the emulsion-template process.

In order to provide supporting evidence for the amorphous state in the nanoparticles, DSC was performed at a fast scan rate (HyperDSC™) to accurately determine a T_g value for the nanoparticles. The scan results presented in Figure 4.4.5.4 show DSC thermal profiles for crystalline TS, as received from AstraZeneca, freshly prepared TS nanoparticles and TS nanoparticles that were conditioned at 80 °C for 12 hr. Crystalline TS

displayed no T_g as the molecules are already in a crystalline state. A clear T_g of 68.9 ± 0.4 °C was determined for freshly prepared TS nanoparticles ($n=3$). An increase in heat capacity is observed for glass transition (Clas *et al.*, 2002), thus more heat transfer was required to the sample pan – this is seen as a step in the thermal profile (Craig *et al.*, 1999). The change in heat capacity occurs over a range of temperatures, such that T_g is quoted as the midpoint temperature. Nanoparticles stored above the T_g for 12 hr (which permitted the amorphous to crystalline transition) displayed no glass transition, as expected. This evidence demonstrated strong verification of the XRPD data for the amorphous state.

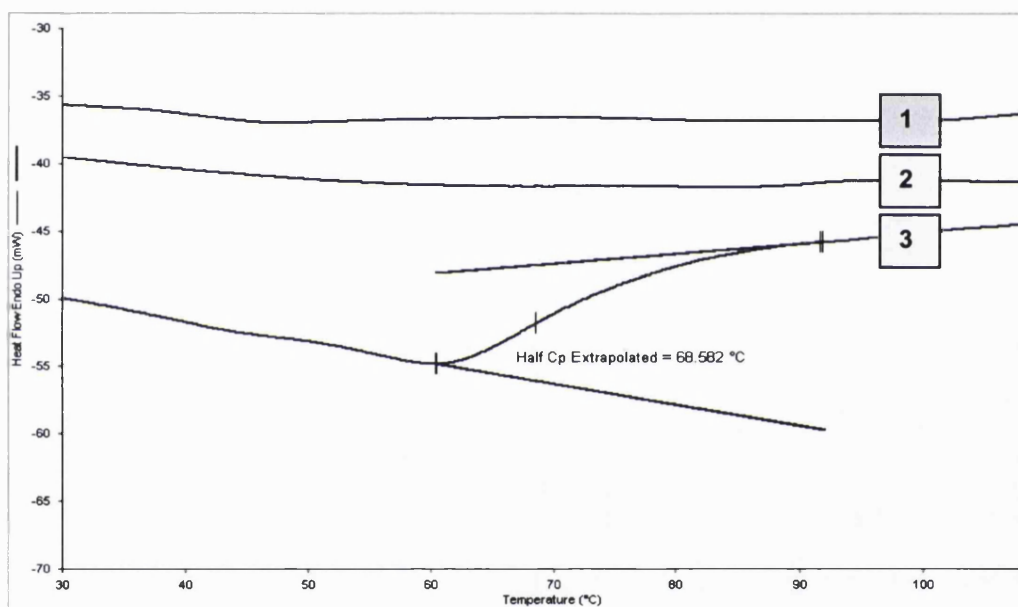


Figure 4.4.5.4: DSC traces of TS. Key: (1) Crystalline TS; (2) TS nanoparticles conditioned at 80 °C for 12 hr; (3) amorphous TS nanoparticles, with clear T_g .

4.5 Conclusion

Hydrophilic nanoparticles were successfully prepared from water-in-oil emulsions. The final particle size of the nanoparticles was found to depend strongly on the emulsification parameters (surfactant concentration, homogenisation speed and drug concentration). The nanoparticles selected for further work have a particle size of approximately 238 nm suitable for further coating without increasing the overall size beyond that suitable for inhalation.

Chapter 5: Hydrophobic SR Microparticles Containing TS Nanoparticles

5.1 Introduction

The purpose of this investigation was firstly to suspend TS nanoparticles in a feed solution containing dissolved hydrophobic SR excipient. Secondly, spray-drying this feed might produce a microparticle formulation, containing TS nanoparticles, suitable for pulmonary delivery and subsequent sustained release of TS. A continuous coat would provide a barrier to drug dissolution thereby achieving SR of the active (Ribeiro Dos Santos *et al.*, 2002). The thickness of the hydrophobic coat applied to hydrophilic drugs has been shown to be inversely proportional to drug release rate from microparticles (Pillai *et al.*, 1998).

Spray-drying has been used for some time in pharmaceutical processing (Newton, 1966) and can be used to encapsulate dissolved or dispersed drug substances (Porte and Couarraze, 1998). The technique is extremely useful for producing powders to predetermined specifications, since by altering and optimising process and formulation variables, considerable control can be exerted over the final product (Broadhead *et al.*, 1992). Spray-drying can be considered a one-step process that converts a liquid into dry particulate form (Sacchetti and van Oort, 1996). The spray-drying process consists of five stages (Masters, 2002) (1) atomisation of feed solution into a spray of droplets, (2) spray-air contact and droplet/particle flow, (3) evaporation of volatiles, particle formation and drying, (4) separation of particles from drying air, and (5) dried product handling.

Atomisation transforms the liquid feed entering the spray-drying nozzle into a droplet cloud that once contacted with hot drying air provides optimum conditions for solvent evaporation. There are a number of nozzle designs, however it is sufficient to discuss only pneumatic nozzle design within this introduction, as this type was used in the laboratory process detailed below. Liquid feed and atomising gas (typically compressed air or inert gas) are passed into the nozzle in co-current fashion. The high air velocity generated in the nozzle then breaks up the liquid into a spray of fine droplets, which can produce fine powders <20 µm in size.

Spray-air contact is frequently co-current and results in rapid evaporation with short drying times - ideal for heat sensitive products (Broadhead *et al.*, 1992). Heat transfer to the particle is by convection from air to the drying droplets and a saturated vapour film rapidly develops at the droplet surface where evaporation of volatiles (solvent) takes place. Solvent diffusion to the surface maintains saturated conditions at the surface, and evaporation takes place at a constant rate - termed primary drying (Figure 5.1). When the volatile content becomes too low to maintain surface saturation, the 'critical point' is reached and a dried layer of material forms at the surface. Further evaporation of solvent is now dependent upon diffusion through this surface layer (secondary drying), and the thickness of the layer increases with time until a solid particle is formed. During evaporation, the spray distribution undergoes a variety of size and shape changes, and the resultant particle distribution shows a degree of polydispersity (Masters, 2002).

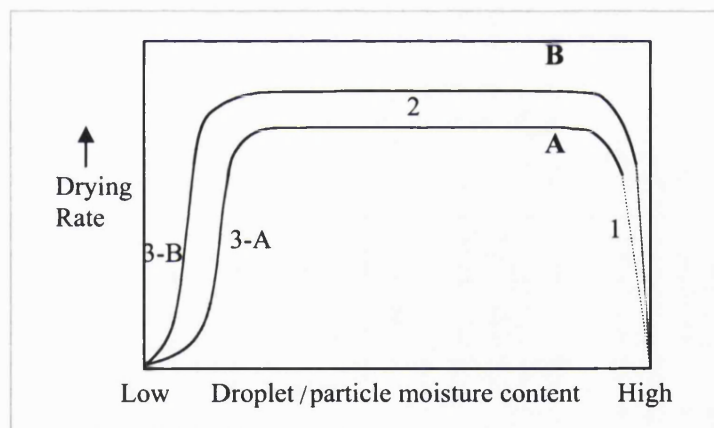


Figure 5.1: Droplet-Particle drying rate curve (adapted from Masters, 2002). A = Solution droplet drying; B = Suspension droplet drying. Primary drying phases are (1) heating up phase and (2) constant evaporation rate. The secondary drying stages are (3-A) falling rate (capillary/diffusion controlled) and (3-B) falling rate (vapour diffusion controlled).

Particles are typically separated from the drying air by means of cyclones and bag filters. These separations must be performed as efficiently as possible to maximise product yield and some authors have reported upwards of 90% product yield for inhalation powders (Batycky *et al.*, 2003).

The circulation of air within the cyclone produces a centrifugal force on the entrained spray-dried particles, which move radially outwards and downwards prior to impacting on the cyclone wall/collection vessel (Sacchetti and van Oort, 1996). The powder is physically removed from the collection vessel by agitation or by gentle scraping of the vessel wall. In the case of filter bags, application of positive pressure to the bags successfully removes particulates.

Alteration of the process variables is necessary to obtain a product with the desired characteristics (Conte *et al.*, 1994; Wendel and Celik, 1997). For instance, an increase in energy of atomisation will reduce atomised droplet size and final particle size; whereas increasing feed concentration or viscosity will produce particles of larger particle size. For pulmonary systems, the primary advantage of spray-drying is the ease in which process variables may be manipulated and controlled in order to obtain particulates of the correct size, shape and dispersibility (Broadhead *et al.*, 1992).

Spray-drying has been used previously to produce a variety of pure drug formulations in a size range suitable for pulmonary deposition, such as cromoglycate (Vidgren *et al.*, 1987) and salbutamol sulphate (Chawla *et al.*, 1994). A range of spray-dried formulations containing active drug and excipient molecules has also been developed for inhalation, such as salbutamol sulphate in albumin microspheres (Haghpanah *et al.*, 1994), estradiol within large porous particles containing phospholipids (Wang *et al.*, 1999) and sodium cromoglycate, salbutamol sulphate and formoterol fumerate in hollow porous particles (Dellamary *et al.*, 2000). Palmieri *et al.*, (1994) spray-dried a theophylline:Eudragit[®] coating polymer (from hydroalcoholic solution) and found that release of drug was immediate. They hypothesised that the ineffectiveness of SR was due to the high surface area of the particles (VMD < 10 µm) and high porosity. It was clear from this work, and from the results of Chapter 3, that a very effective barrier is essential in order to achieve the desired SR profile for TS.

Lipids, oils and waxes are relatively small biological molecules that have a strong tendency to associate through non-covalent forces. This phenomenon arises from the entropy-driven hydrophobic effect and also van der Waals interactions between the hydrocarbon regions of the molecules (Matthews and Van Holde, 1996). These apolar structures confer very low aqueous solubility (indeed, for waxes, the molecules act as a water repellent), which is an ideal property for SR coating/barrier formulation technology.

Hydrophobic excipients, such as lipids, typically display good solubility in a range of non-polar organic solvents (Rowe *et al.*, 2002). As a result they can be dissolved into an organic spray-drying feed solution. Whilst aqueous spray-drying is certainly more favourable in terms of residual solvent toxicity and the environment, this process is not compatible with TS nanoparticles as they would dissolve immediately. There are several organic spray-drying systems on the market, and a number of authors have reported organic based spray-drying processes. For instance, Bain *et al.*, (1999), spray-dried PLA microparticles from several solvents (ACT, DCM, CFM and halothane) and Wang and Wang, (2002), have shown that spray-drying PLGA from ethanol, ethyl acetate and DCM, can modify the release of a water-soluble drug from the polymer matrix.

The excipients should have a melting point of between 30 °C and 70 °C - if the melting point is too low, storage issues arise whereas if the melting point is too high, the material becomes difficult to process (Giannola and DeCaro, 1997). A practical lower limit of 40 °C however should be assumed as particle integrity would be compromised by excipients that melt at physiological temperature - lower melting point excipients are reserved for faster release applications such as suppositories.

5.2 Materials

5.2.1 Model Drugs

The hydrophilic drug, terbutaline sulphate (TS), was generously supplied in micronised form by Investigational Products at AstraZeneca R&D Charnwood (Loughborough, Leicestershire, UK, Lot 4104H). TS nanoparticles (~240 nm) were produced in accordance with Chapter 4, and used as required. In order to show applicability of the sustained release formulation to other hydrophilic drugs, salbutamol sulphate (SS) was purchased from Avocado Research Chemical Ltd. (Heysham, Lancashire, UK), and ipratropium bromide (IB) was a generous gift from Dr. Glyn Taylor at the Welsh School of Pharmacy, Cardiff, UK. Both SS and IB were formulated into nanoparticles under identical processing conditions as used for TS.

5.2.2 Hydrophobic Matrix Forming Excipients

Glyceryl dibehenate (Compritol ATO 888) was kindly donated by Gattefossé France (Saint-Priest, France). Tripalmitin was purchased from Fluka Chemicals Ltd. (Gillingham, Dorset, UK) and Tristearin was purchased from Acros Organics Ltd. (Loughborough, Leicestershire, UK). Cholesterol was obtained from Sigma-Aldrich Company Ltd. (Gillingham, Dorset, UK) and Paraffin wax from VWR International Ltd. (Poole, Dorset, UK). Hydrogenated palm oil (Dritex PST[®]) and Hydrogenated soybean oil (Dritex S[®]) flakes were donated by the ACH Food Company, Inc. (Memphis, TN, USA). Abbreviations used for the following work and melting points for the materials are shown in Table 5.2.2.

5.2.3 Phospholipids

Phospholipids, also used in spray-dried formulations were powdered lecithin (type P100), which was a gift from Degussa Bioactives GmbH (Freising, Germany) and used as received. Dipalmitoylphosphatidylcholine (DPPC) was purchased from Avanti Polar Lipids, Inc. (Alabaster, AL, USA).

Excipient	Abbreviation	Melting Range (°C)
Glyceryl dibehenate	GB	69-74
Tripalmitin	TP	58-64
Cholesterol	CST	147-150
Paraffin wax	PW	65-71
Hydrogenated Palm Oil	HPO	57-60
Hydrogenated Soybean Oil	HSO	66-71

Table 5.2.2: Abbreviations and melting points for excipients used as SR coatings.

5.2.4 Solvents

ACT, DCM and CFM were obtained from VWR International Ltd. Halothane (HAL) and water (HPLC grade) were purchased from Sigma-Aldrich Company Ltd. and Fisher Scientific Ltd. (Loughborough, Leicestershire, UK) respectively.

5.2.5 Release Media

Potassium dihydrogen orthophosphate, dipotassium hydrogen phosphate and orthophosphoric acid were used for buffer preparation and were purchased from Fisher Scientific Ltd. (Loughborough, Leicestershire, UK). For production of Simulated Lung Fluid (see section 5.3.4), magnesium chloride, sodium phosphate, sodium sulphate, sodium acetate and sodium bicarbonate were purchased from Sigma-Aldrich Company Ltd., and sodium chloride, potassium chloride, calcium chloride and sodium citrate were obtained from Fisher Scientific Ltd.

5.3 Methods

5.3.1 Spray-drying

The required amount of hydrophobic excipient, together with surface-active agent, were accurately weighed into a 50 mL volumetric flask. Surface-active agent was present to improve powder flow (Eldem *et al.*, 1991). A small amount of solvent (<5 mL) was then added to the flask, and the excipients were dissolved. TS nanoparticles were then added to the volumetric flask, and the resultant suspension was made up to volume with solvents that had no solvency for TS nanoparticles. The nanoparticle suspension was then sonicated for 5 minutes to ensure a homogeneous suspension was achieved.

In the spray-drying process, a Büchi B-191 Mini Spray-dryer was used (Büchi Laboratories, Flawil, Switzerland, Figure 5.3.1). Prior to suspension formulation, the spray-dryer was switched on for 30 min to ensure a stable operating temperature. Approximately 5 mL of blank feed solvent was pumped through the spray-dryer prior to use, as the presence of solvent reduced the outlet temperature. Once the selected outlet temperature was stable again, the TS nanoparticle suspension was spray-dried at an inlet temperature below the melting point of the hydrophobic excipients and above the boiling point of the solvent, as performed by Eldem *et al.*, (1991) for preparation of spray-dried lipid micropellets. The pneumatic nozzle used throughout investigations had a 0.5 mm orifice. The following parameters were all varied during investigations: pump rate (%), inlet temperature (°C), compressed air flow (L hr⁻¹) and aspiration (%).

Product was collected by gentle removal of the spray-dried material from the walls of the collecting vessel onto greaseproof paper using a plastic spatula. The material was then transferred to 7 mL glass vials and refrigerated at 4 °C, 0% RH.

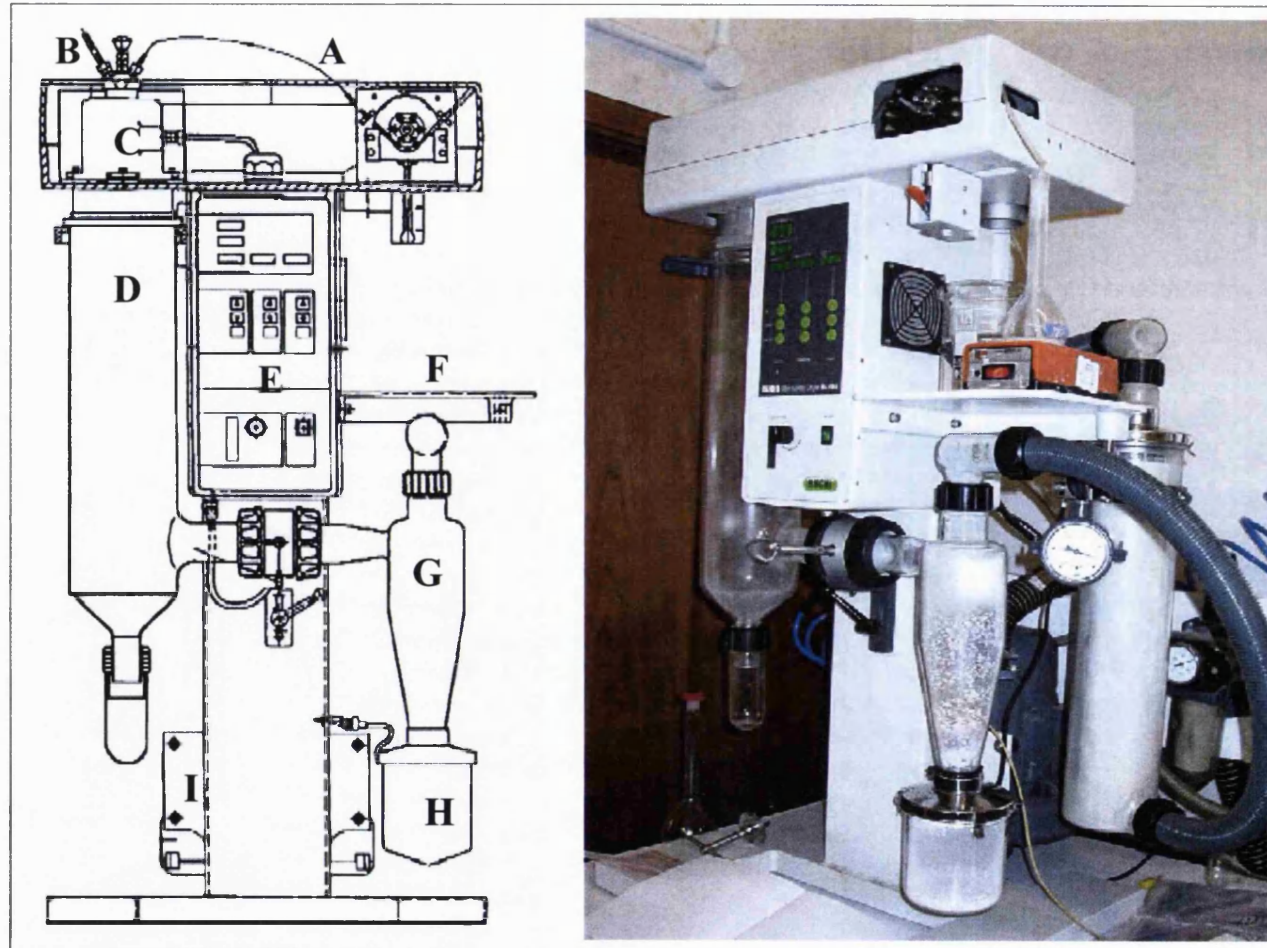


Figure 5.3.1: Outline of spray dryer (left) and photograph of spray drying in operation (right): A = Feed pump tubing, B = compressed air inlet, C = pneumatic nozzle, D = primary drying chamber, E = control panel, F = sample feed holder, G = spray drying cyclone, H = collection vessel, and I = aspirator.

5.3.2 Sustained Release Microparticle Characterisation

Microparticles were sized (n=3) by laser diffraction (Section 2.3.4). Microparticles, 10 mg, were dispersed in 5 mL 0.5% w/v Tween 80 aqueous solution by sonication for 30 seconds. The suspension was then dropped into the diffraction cell, which contained HPLC grade water (filtered), until an obscuration of 10-15% was achieved. Particle morphology was assessed with SEM.

5.3.3 Assessment of TS Release from Sustained Release Microparticles

The HPLC methodology for TS was used as described in Section 3.3.1. The HPLC method for TS was not adapted for salbutamol sulphate as the drug displayed similar chromatography, and the method used for ipratropium bromide is described in Appendix B2.2. Sustained release formulations were tested using a horizontal diffusion cell containing 0.05 M Phosphate buffer, pH 7.4, as detailed in Section 3.3.5.

5.3.4 Assessment of TS Release from Sustained Release Microparticles into Simulated Lung Media

0.05 M Phosphate buffer, pH 7.4 proved useful in the determination of terbutaline sulphate release for initial investigations. However, it was also necessary to consider alternative release media. For a solution to model the lung interstitial fluid, it must be as similar in composition as possible to the real solution (Moss, 1979). McConville *et al.*, (1999) used a modified twin stage impinger (TSI) with an attached reservoir containing deionised water in order to measure salbutamol base release from natural gums. The use of deionised water represents release media in its simplest form and was not appropriate for representing the *in vivo* state - especially as *in vitro* drug release rates may be slower in deionised water (Taylor *et al.*, 2002).

There were two types of simulated lung fluid reported in the literature - simulated interstitial lung fluid (SILF) and simulated surfactant lung fluid (SSLF). The majority of workers using SILF for dissolution studies are in the radiation protection field (Edison and Griffith, (1984); Fisher and Briant, (1994)). Recently, Davies and Feddah (2003), used SILF and SSLF to investigate *in vitro* dissolution of inhaled steroids.

Moss (1979) proposed a formula for SILF (Table 5.3.4), which, except for protein content, was identical to that of human interstitial lung fluid. The presence of protein caused excessive foaming of the fluid which made handling difficult. The protein was therefore replaced by an ionically equivalent amount of citrate. It should be noted, however, that specific proteins within the human lung fluid possess surface-active properties (Lee *et al.*, 1997) and may therefore play a role in enhanced wetting of sustained release particles. Dennis *et al.*, (1982) recommended the addition of 200 µg/mL DPPC to SILF to create SSLF, as DPPC is the primary surface-active component found in all mammalian lungs (Goerke, 1998).

Salt	Chemical formula	Moss formula (mg/L)
Magnesium Chloride	MgCl ₂ .6H ₂ O	203
Sodium Chloride	NaCl	6019
Potassium Chloride	KCl	298
Sodium Phosphate	Na ₂ HPO ₄ .7H ₂ O	268
Sodium Sulphate	Na ₂ SO ₄	71
Calcium Chloride	CaCl ₂ .2H ₂ O	368
Sodium Acetate	NaH ₃ C ₂ O ₂ .3H ₂ O	952
Sodium Bicarbonate	NaHCO ₃	2604
Sodium Citrate	Na ₃ H ₅ C ₆ O ₇ .2H ₂ O	97
DPPC*	C ₄₂ H ₈₄ O ₉ NP	200

Table 5.3.4: Formula for preparation of SILF. * = addition of DPPC for SSLF.

For SILF preparation, all salts were added to 950 mL deionised water under constant stirring, and once dissolved the solution was made up to final volume. Precipitation of salts was avoided by adding the salts in the order in

which they appear in Table 5.3.4. Once prepared, SILF was filtered through a 0.1 μm nylon membrane filter (Whatman International Ltd., Maidstone, Kent, UK). For SSLF, the required amount of DPPC was prepared as liposomes, in accordance with the manufacturer's guidelines (Avanti Polar Lipids Inc., Alabaster, AL, USA). DPPC, 100 mg, was accurately weighed into a 500 mL round bottom flask and dissolved in a 20 mL 50:50 chloroform:methanol mixture. The solvent was then removed by rotary evaporation (Rotorvap model R200, Büchi Laboratories, Flawil, Switzerland) until a thin film of lipid was formed. The dry lipid film was then rehydrated in the presence of SILF at 50 °C (above the phase transition temperature of DPPC, 42 °C) and spun on the rotary evaporation system without vacuum for 1 hr. The warm lipid suspension was then extruded through sequentially smaller pore size polycarbonate membranes (1 μm > 0.4 μm > 0.2 μm) at 50 °C under N_2 (g) overhead pressure of 8 bar. Particle size of the liposomes was checked following each extrusion with PCS (Section 4.3.4). The overall aim was to create a liposome particle size small enough to pass through the 0.45 μm nylon membrane filter used in the horizontal diffusion cell, therefore permitting interaction with the sustained release microparticles.

Once prepared, SILF and SSLF were stored at 4 °C in the refrigerator until required. Upon use, the pH was adjusted to 7.4 by bubbling through CO_2 gas (Moss, 1979).

5.3.5 Differential Scanning Calorimetry (DSC)

DSC (Section 4.3.8) was performed on drug-free and drug-loaded microparticles in order to assess the thermal characteristics of the microspheres (2 mg samples). At certain heating rates, whole transitions in lipid-based excipients can be obscured and the melting point can vary. It was therefore necessary to run samples at 2 °C/min in order to record the maximum number of transitions (Liversidge *et al.*, 1981). Samples were heated from 15 °C - 100 °C.

5.3.6 Dynamic Contact Angle (DCA) Measurement

DCA is a technique that measures wettability of substances (Pepin *et al.*, 1999). In this investigation the surface hydrophobicity of SR microparticles was examined. Powders can be formed into compact beams for analysis, however, Shanker *et al.*, (1994) developed a modified Wilhelmy plate method, where powder is adhered to a glass slide coated with glue, and demonstrated simplicity and reproducibility. The slide is then lowered into a liquid of known surface tension (usually water) and the contact angle determined from an immersion load measurement.

A glass slide was covered with spray PhotoMount[®] adhesive (3M UK PLC., Bracknell, Berkshire, UK), and powder (>100 mg) was pressed into the glue once dry to the touch. Excess powder was removed under a stream of air. The slide was then hung from a sensitive microbalance within the Model 312 DCA analyser (Cahn Instruments Inc., Cerritos, CA, USA) so the bottom face of the slide was within 5 mm above and perpendicular to, the water level. The slide was then automatically lowered at a speed of 10 mm/min into the water below (at 37 ± 0.5 °C). Contact angles (advancing and receding) were extrapolated from the force-displacement curve produced by the DCA analyser software.

5.3.7 Dynamic Vapour Sorption (DVS)

A concise study into vapour sorption characteristics of spray-dried powders was performed using DVS apparatus (Surface Measurement Systems Ltd., London, UK). The apparatus consisted of a Cahn microbalance housed inside a temperature-controlled cabinet. All experiments were performed at 90% Relative Humidity (RH) - the maximum RH that the machine could achieve with stability - and at 37 °C. These conditions closely mimic that of the lung (high saturation, physiological temperature). As the humid air passes over the sample, a zone of constant moisture concentration is established closely around the sample. This zone allows the rapid establishment of

equilibrium for water content between the humid air and particle surface, and any weight change arising from vapour sorption is recorded on an ultra-sensitive microbalance.

20.0 mg sample was accurately weighed into a glass weighing boat and placed on the Cahn microbalance. The DVS apparatus, held at 37 °C, was then closed to create a sealed atmosphere around the sample. Once the mass reading was stable a pre-programmed run was initiated. The system was held initially at 0% RH for 5 min. Nitrogen flow was then increased through the 'wet' air flow chamber, and system RH was quickly ramped up to 90% RH, and held at this humidity for 3 hr. Sample mass change versus time was recorded by the apparatus and samples were tested in triplicate.

5.3.8 Content Uniformity

Content uniformity was performed on the bulk spray-dried material to ensure that the distribution of the nanoparticles was equal within the hydrophobic microparticles. Test A of Appendix 264 of the British Pharmacopoeia (BP, 2003) for testing tablets, powders for parenteral use and suspensions for injection was performed. The TS content of ten, 10.0 mg, random samples from three batches of material spray-dried under identical conditions was quantified using HPLC. The preparation complied with the test if individual content was within 85% and 115% of the average content.

5.3.9 X-Ray Powder Diffraction (XRPD)

XRPD was performed as previously described (Section 4.3.8).

5.3.10 Visualisation of TS Nanoparticle Distribution Within Hydrophobic Microparticles

In order to assess the internal structure of the hydrophobic microparticles and distribution of the TS nanoparticles, the following techniques were utilised - focused ion beam sectioning and confocal laser scanning microscopy.

5.3.10.1 Focused Ion-Beam (FIB) sectioning

FIB sectioning is achieved by streaming positively charged gallium ions from a metal ion source, which sections the material under investigation (Phaneuf, 1999). Sectioning was performed on a Micrion 9100FIB instrument (FEI GmbH, Feldkirchen, Germany) by Mr. Alan Miller of FEI UK Ltd. (Almondsbury, Somerset, UK). Once the sample (5 mg, prepared as for SEM, Section 2.3.5.) was loaded into the machine, the microspheres were located and a tungsten strap was laid over the top of the area of interest (approximately $20 \times 2 \mu\text{m}$). A $5 \mu\text{m}$ channel was then milled through the tungsten and microparticles (Figure 5.3.10.1).

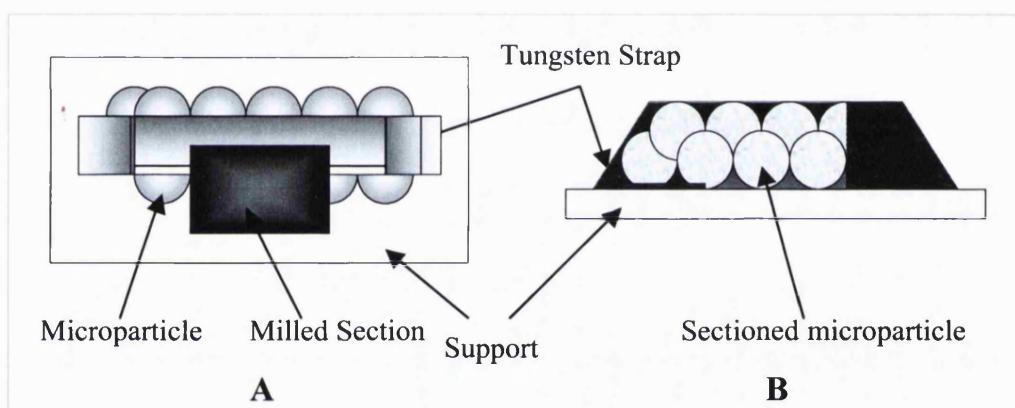


Figure 5.3.10.1: FIB process schematic. A = Microparticles were fixed to an adhesive support and then, a tungsten strap was deposited over the top, then, a channel was milled with gallium ions and then the section was finely 'polished' with low energy ion beam: B = Support was then rotated 45° away from the operator which permitted visualisation of cut section.

Once milled, the support was rotated away from the operator and the cross-section generated was visible. FIB is predominantly used in semiconductor repair and manufacture, materials science (Phaneuf, 1999) and microstructure fabrication (Vasile *et al.*, 1999). The technique is in its infancy in the biological arena (Mulders, 2003), such that this investigation was a test investigation of FIB applicability, in addition to morphology characterisation of the SR material.

5.3.10.2 Confocal Laser Scanning Microscopy (CLSM)

CLSM is a powerful technique due to its non-invasive nature and ability to visualise the internal structure of a variety of materials. The technique has shown significant use in a variety of pharmaceutical applications e.g. localisation of drug within SR pellets during release (Guo *et al.*, 2002), model protein (Bovine Serum Albumin) loading within polymer microspheres (Bouillot *et al.*, 1999), and macrophage uptake of nanoparticles (Langer *et al.*, 2003).

The emulsion-template method for production of TS nanoparticles was adapted by dissolving the hydrophilic fluorescent probe, 5,6-carboxyfluorescein (Acros Organics Ltd. (Loughborough, Leicestershire, UK) into the aqueous phase (0.1 mg/mL). Nanoparticle fluorescence was confirmed following nanoparticle manufacture using standard fluorescent microscopy (Microphot FXA Microscope, Nikon Inc, USA), equipped with a 510-550 nm module and digital image capture). Following processing of the fluorescent TS nanoparticles into the SR formulation by spray-drying, fluorescence was visualised at 63x magnification using a Zeiss LSM-510 confocal microscope (Carl Zeiss Ltd., Welwyn Garden City, Hertfordshire, UK). Laser excitation/emission was set to 488/543 nm. Dr. Nick Hartell and Dr. John O'Neil (Department of Pharmacology and Pharmaceutics, respectively, at the University of London School of Pharmacy) are gratefully acknowledged for their guidance with image capture.

5.4 Results and Discussion i: Lipid Excipients

5.4.1 Spray-drying TS Nanoparticles with GB as Hydrophobic Matrix Excipient

Initial spray-drying conditions that were used during method development were obtained from work by Eldem *et al.*, (1991) which had developed parameters for spray-drying lipids from organic solvents (Table 5.4.1).

[Solid Feed] (% w/v)	2
Excipient	GB
Surfactant	Lecithin, 3.5% w/w (based on GB content)
Inlet Temperature (°C)	59-60
Outlet Temperature (°C)	40-41
Solvent	50:50 DCM/CFM
Aspiration (%)	65
Air Flow (L hr ⁻¹)	800
Pump speed (%)	20

Table 5.4.1: Spray-drying conditions used for preliminary investigations (Eldem *et al.*, 1991).

LM of a spray-dried batch, which contained 66% w/w TS nanoparticle loading (Figure 5.4.1.1) showed that the product was within the particle size range required (<5 µm) and morphology appeared spherical. However, this particle size range was at the limits for LM and therefore little information was derived from the images. SEM images showed more detailed morphological information (Figure 5.4.1.2) and was therefore used as standard. Particles appeared polydisperse, with a proportion of particles in both the nanometre and micrometer range.

The release profile for this formulation showed a large degree of burst release ($t_{50} = 16.1$ minutes) followed by a period of SR (approximately 40% drug release from 15 minutes to 180 minutes). In light of the SEM image, it was possible that the burst release arose from uncoated/thinly coated sub-micron particles, whilst SR was achieved from the larger microparticle population.

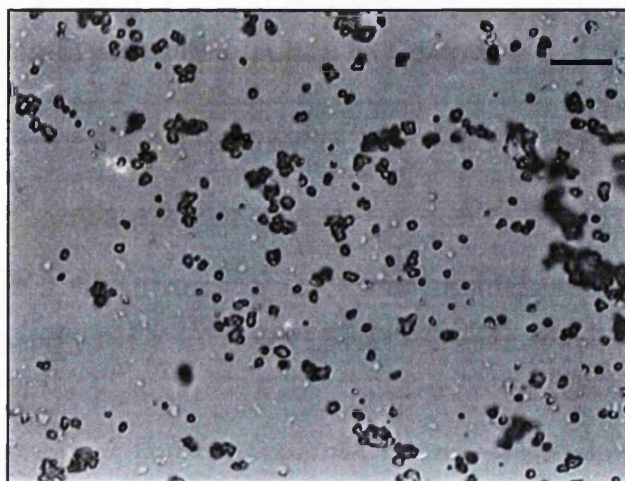


Figure 5.4.1.1: LM image of GB formulation (containing 66% w/w TS). 10 µm Scale bar

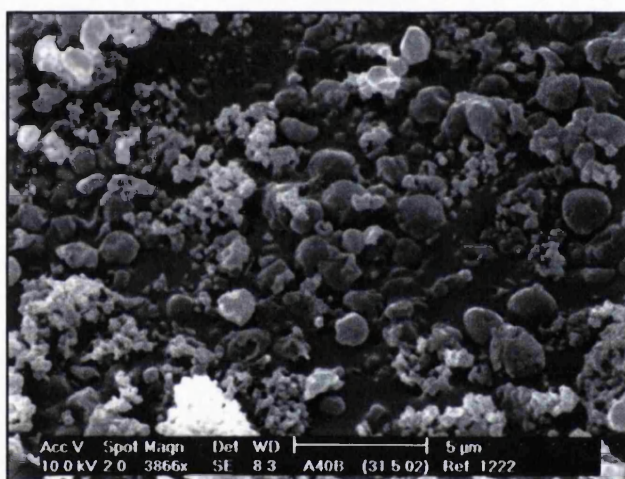


Figure 5.4.1.2: SEM image of GB spray-dried formulation. (containing 66% w/w TS). 5 µm Scale bar.

TS loading of the microparticles was reduced to approximately 14% w/w, however, spray-drying at 59-60 °C led to the formation of highly fused particles (VMD > 30 µm, measured by laser diffraction), as shown in Figure 5.4.1.3. This appeared to arise from incomplete solvent drying. A large reduction in particle size was shown for an elevation in inlet temperature e.g. at 69-70 °C, VMD = 5.53 µm. However, an inlet temperature of 74 °C was too high for the spray-drying process as build-up of molten lipid material occurred in the cyclone. This resulted in insufficient yield for particle size analysis.

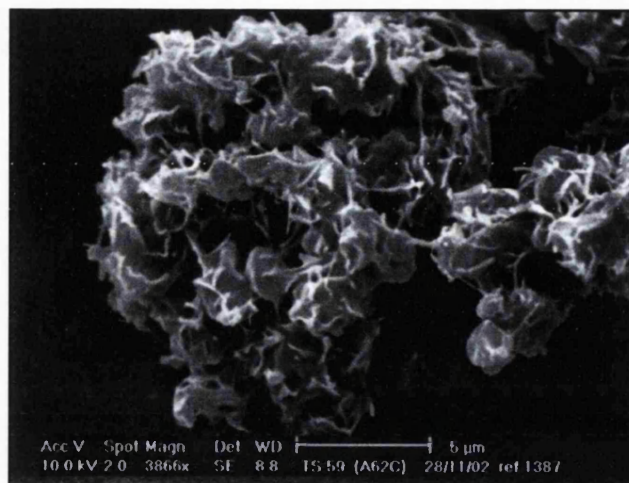


Figure 5.4.1.3: GB spray-dried formulation at 59 °C inlet temperature - heavy particle fusion observed.

TS release rate from GB microparticles (14.1% w/w TS content) displayed a large burst release (see Figure 5.4.2.1) similar to that for the TS loading of 66% w/w, despite a lack of evidence for uncoated TS nanoparticles (Figure 5.4.1.4). GB is a relatively hydrophilic lipid and therefore more susceptible to hydration (Janjikhel and Adeyeye, 1997), in particular due to its high content of free fatty acid molecules (Rowe *et al.*, 2002), which may explain the burst release. It was therefore decided to investigate the addition of TP into the SR matrix in an attempt to increase matrix hydrophobicity.

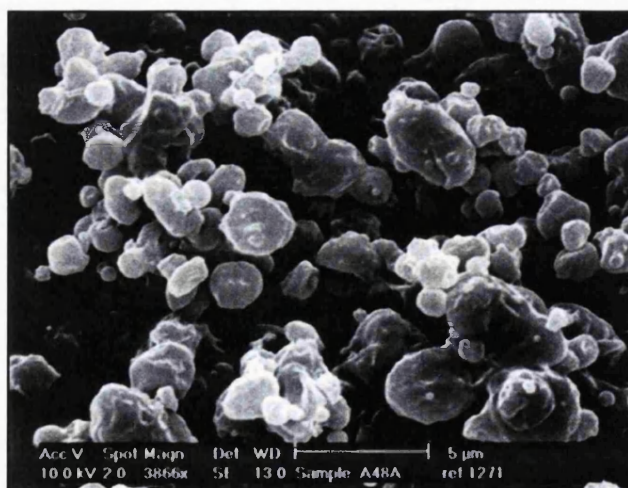


Figure 5.4.1.4: Spray-dried GB microparticles (14.1% w/w TS nanoparticle content). Nanoparticulate TS not visible (relative to Figure 5.4.1.2) suggesting effective encapsulation.

5.4.2 Spray-drying TS Nanoparticles with GB/TP as Hydrophobic Matrix Excipients

Increasing the proportion of TP in the spray-dried formulations served to retard the release of TS (Figure 5.4.2.1). Table 5.4.2 highlights the results of the investigation.

GB:TP ratio	VMD (μm)	TS Loading (% w/w)	% Release at 180 min \pm SD
100:0	5.53	14.1	95.6 \pm 2.8
75:25	5.31	14.1	90.9 \pm 1.7
65:35	5.11	14.0	29.4 \pm 5.9
55:45	5.15	14.5	29.3 \pm 3.2

Table 5.4.2: Effect of GB:TP ratio on particle size, drug loading and release at experimental endpoint (n=3).

The release rate for pure GB as SR excipient and 75:25 GB:TP were characterised by a large burst release of TS. However, the presence of higher proportions of TP in the matrix greatly retarded TS release. The data suggests that an increase in TP improves coating integrity, as incomplete coating gives rise to burst release (Obaidat and Obaidat, 2001).

The lower solubility of GB in the spray-drying feed (Eldem, 1991) resulted in rapid solidification of the matrix during drying, which led to poor matrix structure and therefore limited SR performance. Indeed, production conditions are crucial for GB spreadability and consistency, and therefore performance of the SR coating (Barthelemy *et al.*, 1999). As TP was more soluble in the solvent, it may dry more gradually and may lead to a more confluent coating (Bain *et al.*, 1999) of the nanoparticles.

Drug release from spherical lipophilic matrix systems, in which the drug is dispersed as solid particles, typically follows matrix-diffusion square root of time ($t^{1/2}$) kinetics (Higuchi, 1963). Several authors have reported $t^{1/2}$ -based

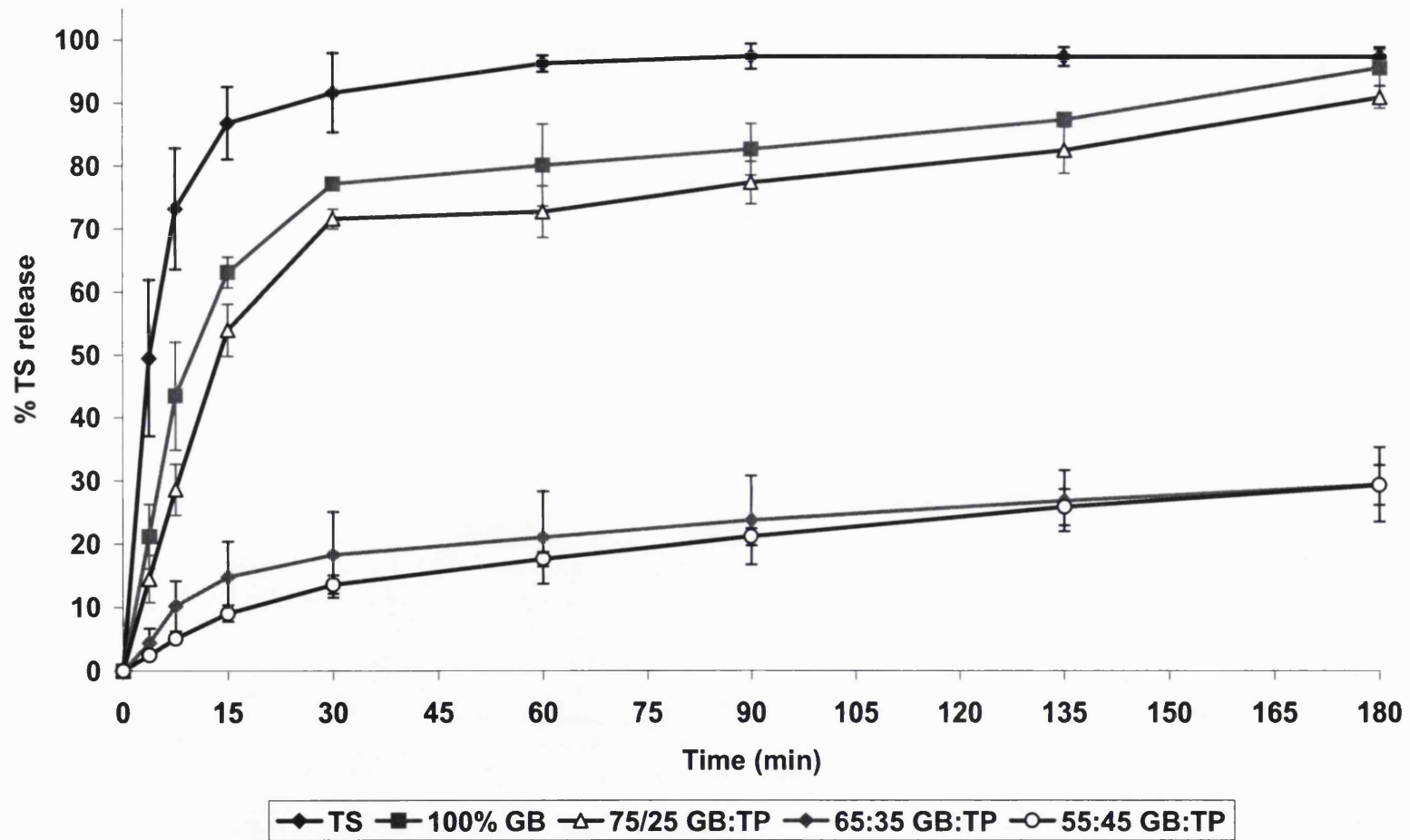


Figure 5.4.2.1: % TS release vs. time for pure micronised drug and the effect of GB:TP ratio upon drug release microparticles (n=3 ± SD, 20 °C). TS loading was 14.2 ± 0.2 % w/w for all batches.

kinetics for lipophilic matrices. Faham *et al.*, (2000) and Obaidat and Obaidat, (2001), showed the potential for hot-melt GB matrices in granular form to provide matrix release of theophylline and tramadol HCl, respectively. Ganthier and Aiache, (2003) also demonstrated matrix-diffusion kinetics for theophylline release from hydrogenated castor oil minispheres (1-2.8 mm diameter) generated from a rotary fluidised bed process. TS release from the 55:45 GB:TP ratio also adhered to a matrix diffusion $t^{1/2}$ relationship, a plot of drug release versus square root of time provided linearity ($r = 0.9924$).

5.4.3 Entrapment of SS and IB Nanoparticles in Hydrophobic Microparticles

Incorporation of SS and IB nanoparticles into lipid microparticles was successful, as indicated by VMD values of 2.61 ± 0.18 and 4.63 ± 0.32 μm respectively ($n=3$). Drug release from GB:TP 60:40, microparticles are shown in Figure 5.4.3 and indicate SR. The results showed that encapsulating other hydrophilic drugs within SR microparticles was possible i.e. the general applicability of the technology.

5.4.4 Effect of Feed Solvent on Hydrophobic Microparticle Size

In the previous examples, attaining particle sizes below 5 μm proved difficult. The effect of solvent choice was therefore investigated with the aim to reduce particle size. It should be noted that increased air-flow and reduced feed concentration were also alternative ways of reducing particle size for the spray-drying process. However, air-flow was already set to maximum in all previous experiments and 2% feed concentration was low relative to other authors, for instance Eldem *et al.*, (1991) used concentrations of 20-25% w/v lipid content.

Increasing the proportion of DCM in the CFM-based feed solvent from 50% to 100% significantly reduced VMD and $D(v, 0.9)$ ($n=3$, t-Test, $p<0.01$, Figure 5.4.4.1). The results showed that the choice of solvent was critical for microparticle preparation, in agreement with Bain *et al.*, (1999), who

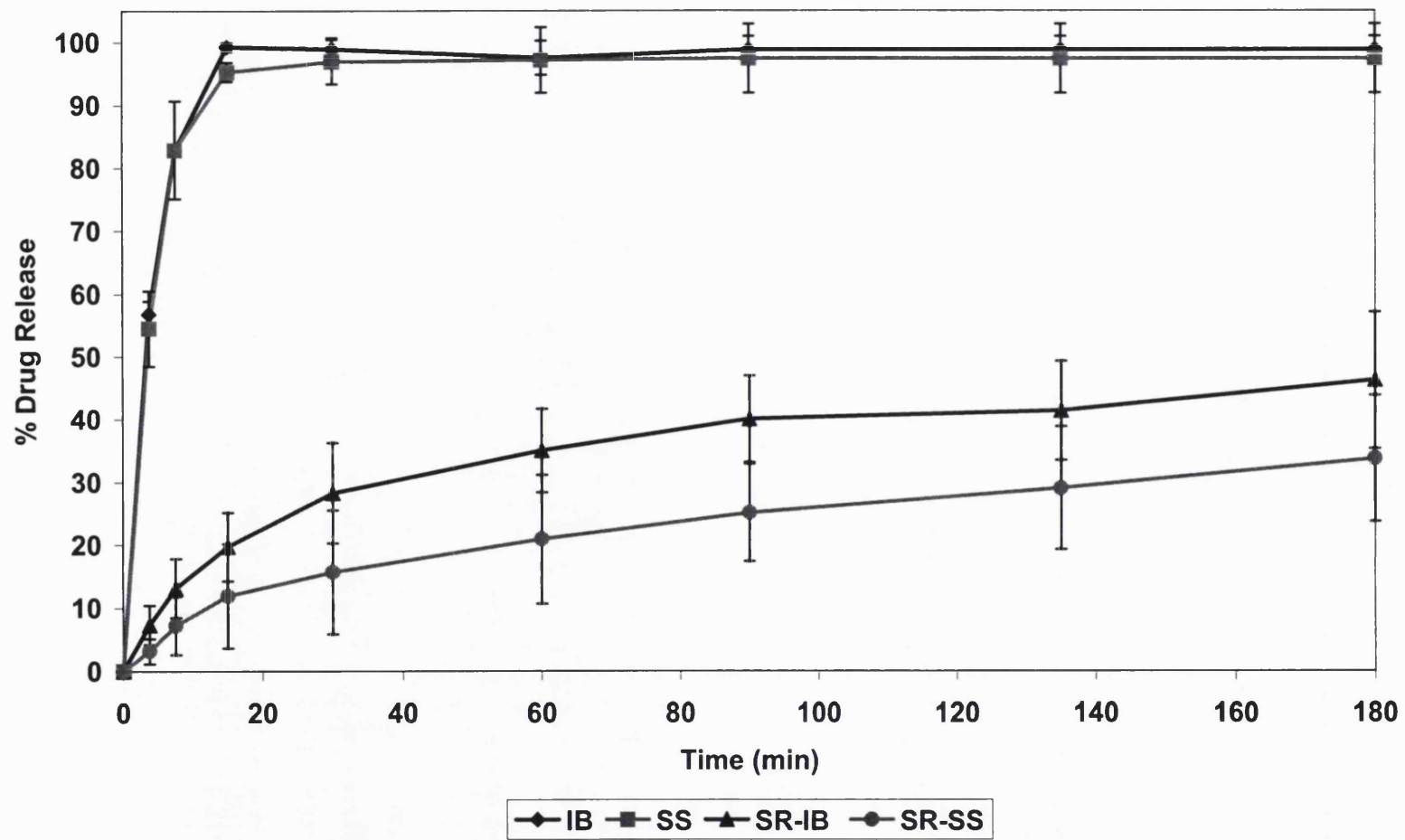


Figure 5.4.3: % Drug release vs. time for pure micronised drug (IB, SS) and the sustained release microparticles (SR-IB and SR-SS) (n=3 ± SD, 20 °C).

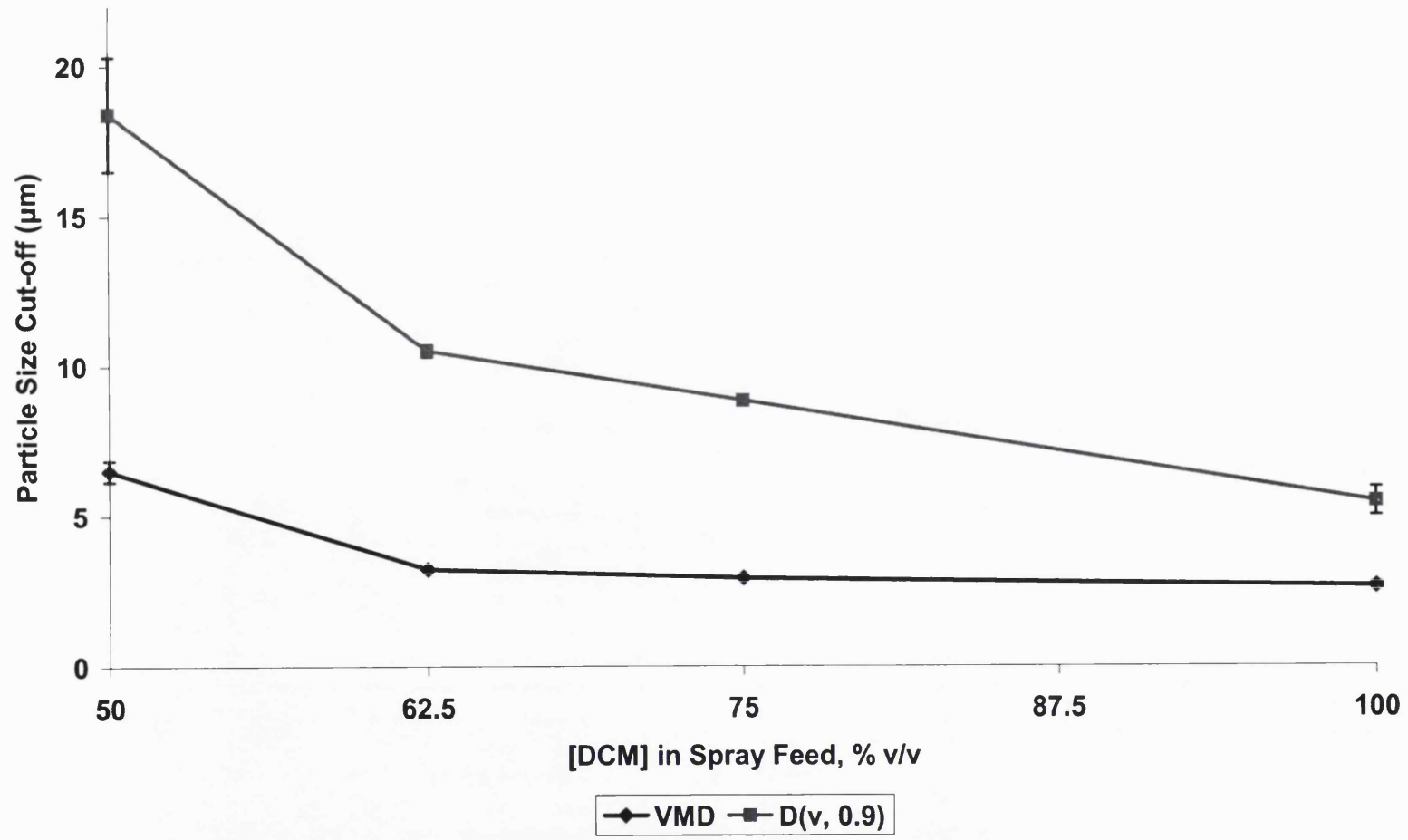


Figure 5.4.4.1: Effect of DCM content in spray-drying feed on particle size cut-off (n=3 ± SD).

concluded that solvent selection had remarkable influence over the morphology of, and drug release from, spray-dried poly(D,L-lactic acid) microspheres.

As the boiling point of a 50:50 DCM:CFM solvent mixture was higher than that of DCM (47 °C versus 40 °C), it was expected that rapid evaporation of 100% DCM presented particles to the cyclone in a 'dryer' state with less tendency to aggregate (Figure 5.4.4.2). Conversely for 50:50 DCM:CFM, particles that were still undergoing primary drying at entry to the cyclone had the tendency to fuse when they collided, thus particle diameter was increased (Figure 5.4.4.3).

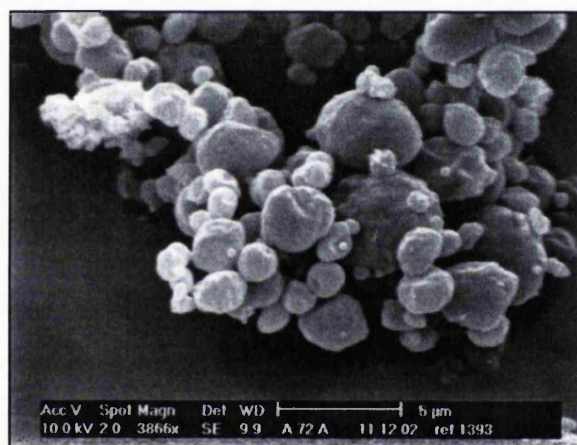


Figure 5.4.4.2: TS containing GB:TP 60:40 microparticles spray-dried from DCM.

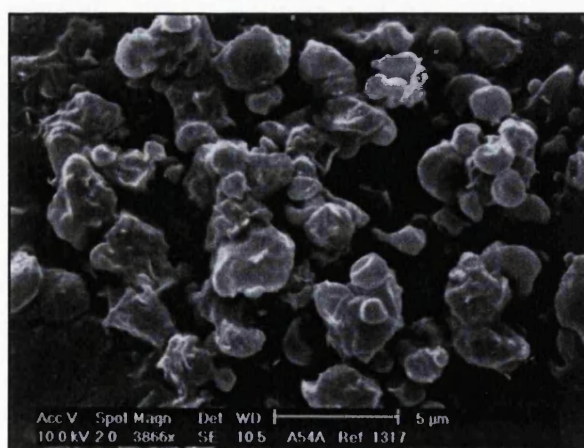


Figure 5.4.4.3: TS containing GB:TP 60:40 microparticles spray-dried from 50:50 CFM:DCM, note increased particle fusion relative to Figure 5.4.4.2. All other parameters were identical.

Drug release from different batches of microparticles, sprayed from DCM (under identical processing conditions), was not reproducible (Figure 5.4.4.4). The slowest TS release was observed from Batch 2, (time for 25% release, $t_{25} = 115 \pm 33$ min). For Batches 1 and 3, the t_{25} values were 25.6 ± 3.3 min and 45.0 ± 14.2 min, respectively. The variation was reasoned to arise from the matrix, as there was no variation in particle size distribution between batches. Also, drug loading was, in actual fact, elevated in Batch 2 relative to the other batches (15.2% w/w versus 13.3% w/w and 13.1% w/w), and therefore was expected to provide faster, not slower, TS release.

Microparticles spray-dried from DCM:HAL co-solvents generated smaller particles (VMD = 2.98 ± 0.22 μm , $n=3$) than those produced from 50:50 DCM:CFM system. The use of CFM as a feed solvent was not investigated further as a result. Release profiles from microparticles spray-dried from DCM:HAL co-solvents were studied as a function of time post-manufacture. Figure 5.4.4.5 and Table 5.4.4 shows that release rate immediately post-manufacture ('fresh' microparticles) was dramatically faster than the SR profiles for microparticles stored at 25 °C (SI60 Incubator, Fisher Scientific Ltd., Loughborough, Leicestershire, UK) for all periods. There was no significant difference in TS release at 7, 21 and 35 day post-manufacture ($n=3$, ANOVA $p>0.05$). This indicated that the effect of storage time upon reducing release rates was complete within 7 days, and the matrix was then stable. Application of the Higuchi model for release kinetics indicated that there were differences in the matrix for the 'fresh' microparticles and stored microparticles - matrix-diffusion kinetics were only strongly adhered to following storage (Table 5.4.4).

Time Point (days)	Regression coefficient for Higuchi Plot, r^2	% TS release at 180 min \pm SD
0 (fresh)	0.9320	79.1 \pm 3.8
7	0.9928	36.0 \pm 9.0
21	0.9869	36.2 \pm 3.3
35	0.9857	38.1 \pm 4.3

Table 5.4.4: TS release kinetics and profile for GB:TP 60:40 microparticles versus storage.

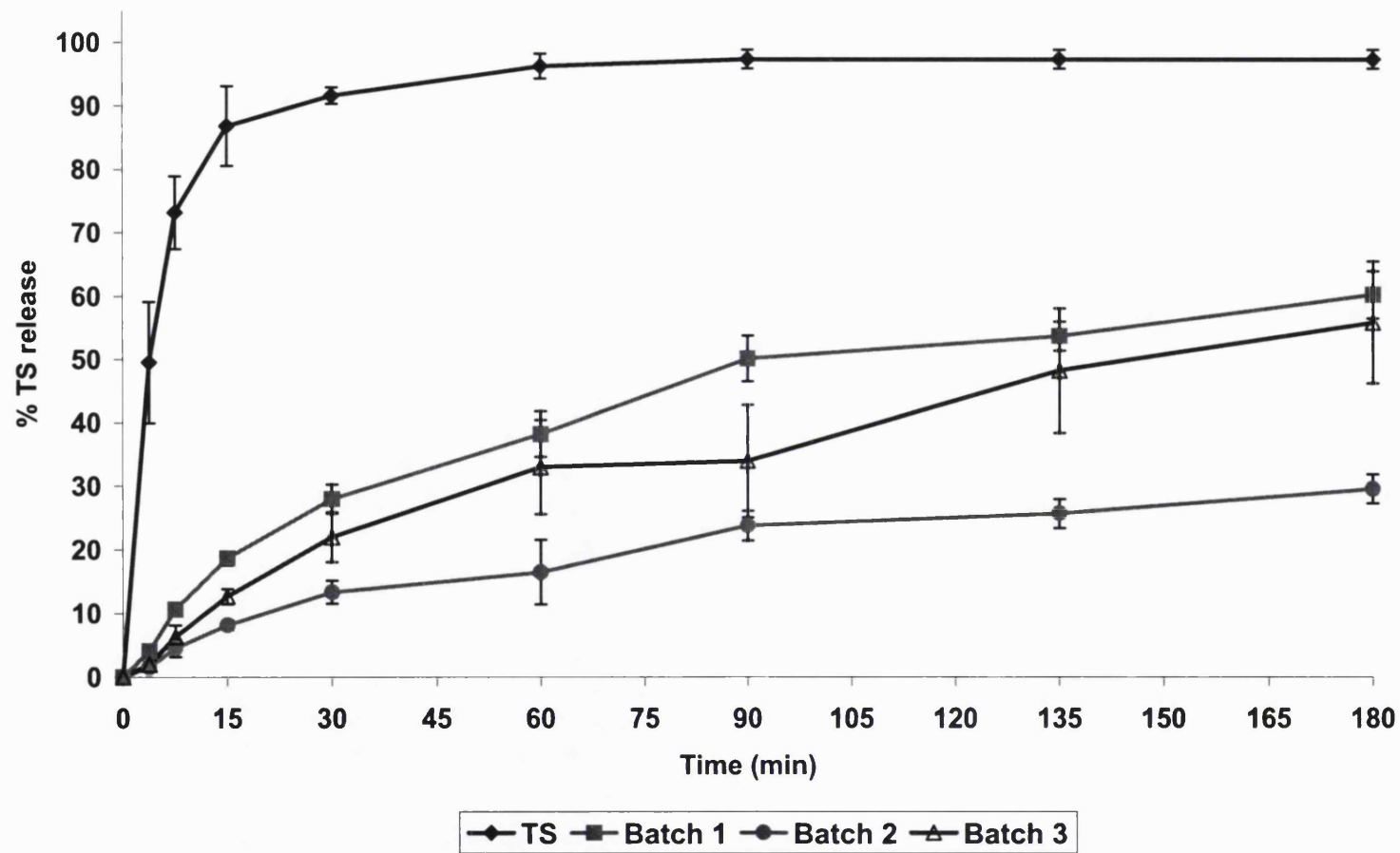


Figure 5.4.4.4: % TS release vs. time for pure TS and TS from three batches of GB:TP 60:40 microparticles: large inter-batch variation shown. (n=3 ± SD, 20 °C).

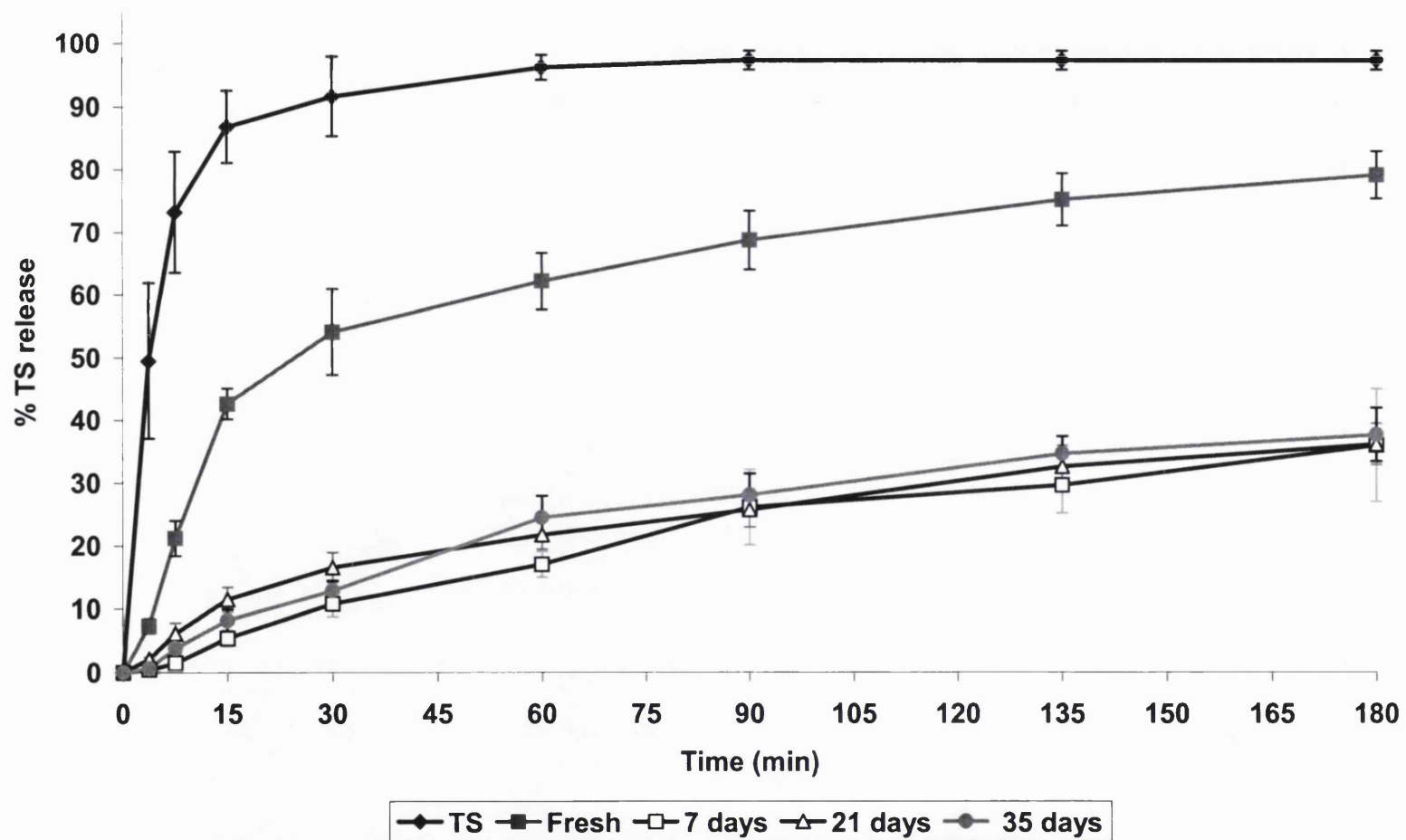


Figure 5.4.4.5: % TS release vs. time for pure TS and for TS from GB:TP 60:40 microparticles spray dried from 25:75 HAL:DCM (n=3 ± SD, 20 °C). Effect of product storage upon release is shown.

5.4.5 Physicochemical Characterisation of Lipid Microparticles

The storage effects outlined above indicated the requirement for a thermal analysis study to be undertaken in order to probe changes in the SR matrix. Changes to lipid-based pharmaceutical formulations due to polymorphic transitions have been recognised for a number of years. Lipid products are invariably chemically complex and exist in a variety of crystal forms, many of which are metastable (Sutananta *et al.*, 1994). Liversidge *et al.*, (1981), noted that upon storage, triglyceride-based suppositories gave rise to higher melting point ranges and reduced drug release rates. They also noted that at elevated storage temperatures, the time for the formulations to reach maximum melting points was substantially reduced. Freitas and Muller (1999), showed that the crystallinity of the lipid phase within solid lipid nanoparticles increased when the formulations were stored at increasing temperatures, and also upon exposure to light. These references support the findings reported in Table 5.4.4 and suggest that changes in the SR matrix were responsible for the effects observed.

A DSC thermal profile for freshly prepared microparticles is shown in Figure 5.4.5.1. The thermal profile revealed four distinct thermal events that consisted of three endothermic peaks and one exothermic peak. These peaks are classified (Table 5.4.5.1) according to Hagemann (1988).

Peak Number (Figure 5.4.5.1)	Temperature	Endothermic/ Exothermic	Classification
1	43-44	Endothermic	Melting of unstable α -crystalline form of TP
2	47-48	Exothermic	Recrystallization to stable β' form of TP
3	58-59	Endothermic	Melting of stable TP
4	66-67	Endothermic	Melting of stable GB

Table 5.4.5.1: Classification of peaks within DSC trace for lipid microspheres (derived from Hagemann, 1988).

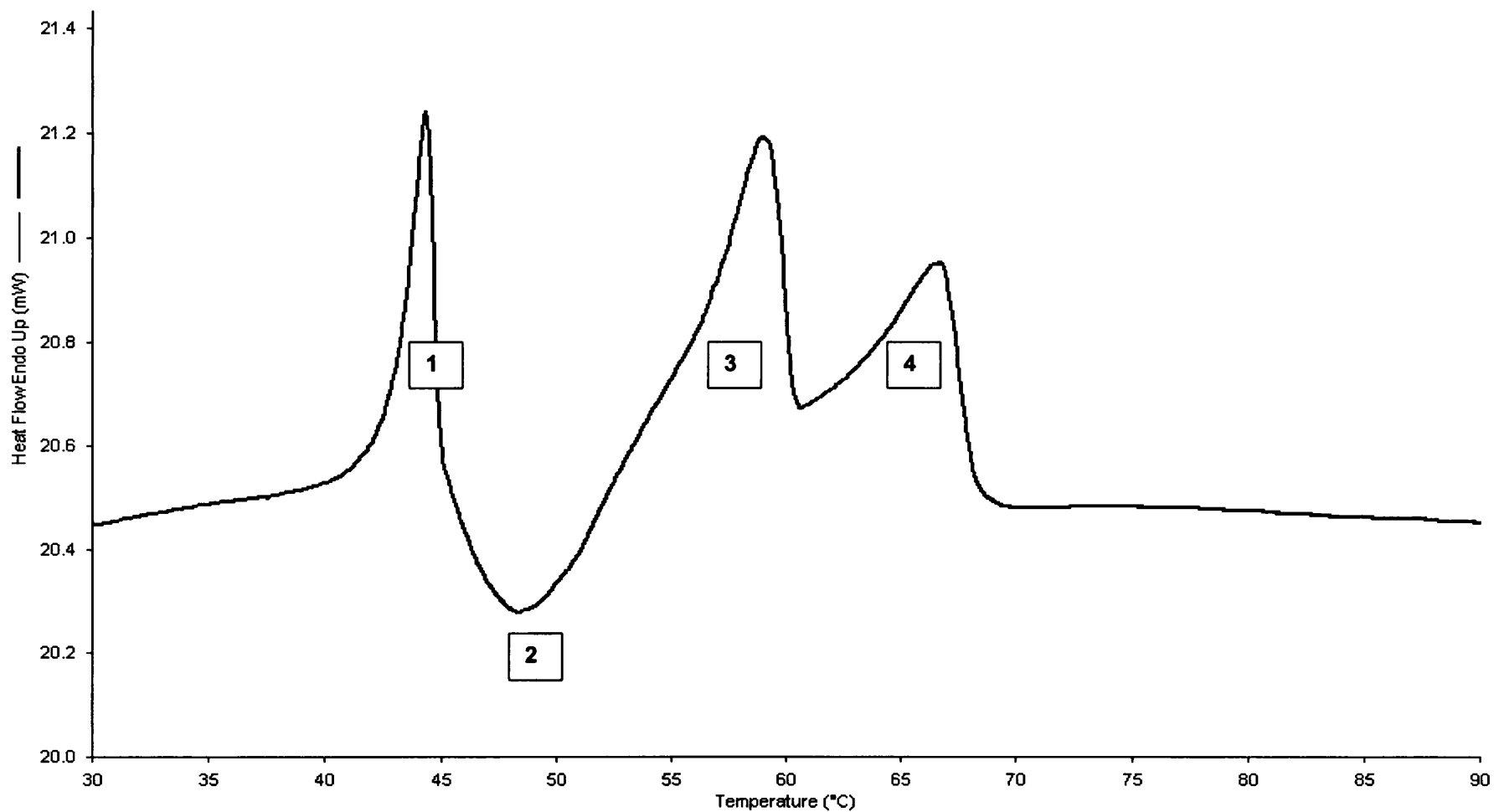


Figure 5.4.5.1: DSC thermal profiles for freshly prepared lipid microspheres showing four transitions: 1 = endothermic melting of α -form of TP, 2 = exothermic recrystallization of TP melt, 3 = endothermic melt of β' -form of TP, 4 = endothermic melt of β / β' -form of GB.

It should be noted that literature references discuss thermal changes for pure lipid samples. The microparticles discussed in this work are fabricated from a mixture of two products GB and TP, which may affect transition times. Also, TP was a technical grade product (purity 55%) thus displayed a wide melting range that diverged from reported literature values.

The least stable α -polymorphic form of triglycerides is typically created when lipids solidify rapidly, as was the case for spray-drying. The triglyceride molecules in the lipid matrix possess a hexagonally packed open structure (Hagemann, 1988) with freedom of molecular motion. Diglycerides, such as GB, do not possess an unstable polymorphic form and therefore no additional peak was observed for the GB. Indeed, when GB was spray-dried to create blank GB microparticles, the fresh sample displayed a single peak at 71.9 ± 0.38 °C.

The change from α to the β' form occurs when there is sufficient energy available to collapse the hydrocarbon chains into a tightly packed orthorhombic form. A complex transition to the most stable β form may occur upon further heating and is often associated with swelling or 'bloom' of the structure (Lutton and Fehl, 1970) and expulsion of molecularly dispersed drug during rearrangement of the crystal lattice (Mehnert and Mader, 2001). This transition can have severe consequences for formulation performance. However, the presence of additives such as surfactants can inhibit this transition (Aronhime *et al.*, 1990), e.g. Lecithin has been reported as an anti-bloom agent (Garti, 1988). In addition, diglycerides (e.g. GB) may also inhibit the β' - β transition of triglycerides by stabilising the β' crystal packing. In light of this evidence it was assumed TP in the lipid microparticles was stable in the β' polymorphic form.

Following spray-drying of lipid microparticles from DCM, samples were either stored at -10 ± 0.5 °C in the freezer or in an oven held at 35 ± 0.5 °C (Table 5.4.5.2). Freezer samples showed no change in peak melting temperatures for peak 1, 3 and 4 (terminology identical to Figure 5.4.5.1) and also peak area for peak 1. However, storage in the oven caused the Peak 1 area to reduce from 40 MJ to 0 MJ in the 48 hr time period (Figure 5.4.5.2).

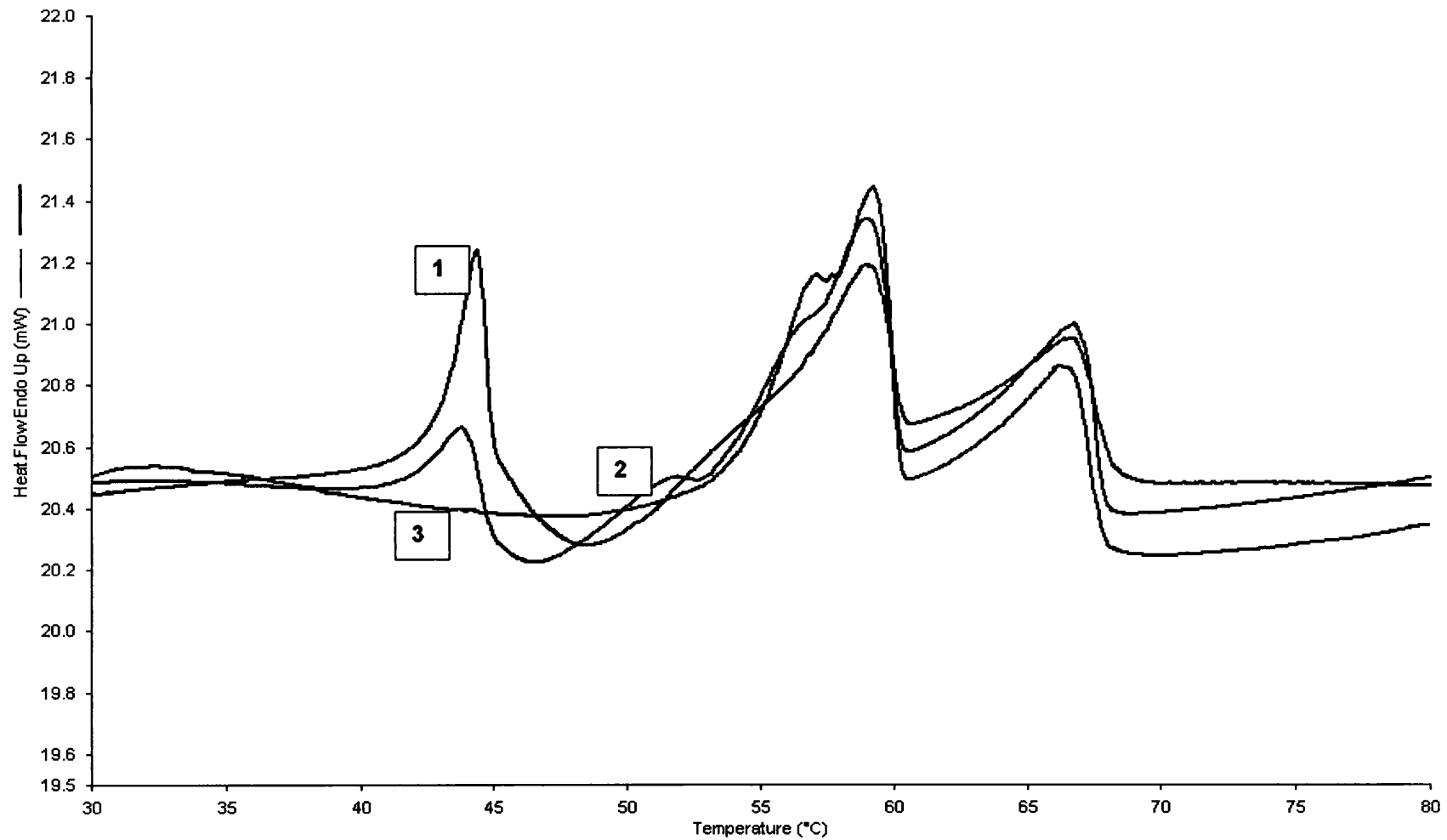


Figure 5.4.5.2: DSC thermal profiles of: 1 = fresh lipid microspheres, 2 = following storage at 35° C for 24 hr, 3 = following storage at 35° C for 48 hr. (Note reduction in 1st melting endotherm (Peak 1) to 0 over 48 hr storage period).

Time (days)	Storage (°C)	Peak 1 (°C) ± SD	Area Peak 1 (MJ) ± SD	Peak 2 (°C) ± SD	Peak 3 (°C) ± SD
0	-	44.0 ± 0.54	39.0 ± 4.1	59.1 ± 0.067	66.9 ± 0.12
1	-10	43.9 ± 0.030	38.5 ± 1.9	58.6 ± 0.087	66.3 ± 0.015
1	35	43.9 ± 0.18	15.0 ± 2.2	59.1 ± 0.33	66.9 ± 0.28
2	-10	44.1 ± 0.018	36.6 ± 0.92	58.9 ± 0.078	66.9 ± 0.032
2	35	44.1*	0.0543*	59.1 ± 0.30	67.4 ± 2.2

Table 5.4.5.2: Effect of storage on peak temperatures and peak area of unstable polymorph. (n=3). Melting points reported by Lutton and Fehl (1970), for pure TP are 44.7 (α) and 56.6 (β'). *small peak present in 1 batch only.

Storage at the elevated temperature conditioned the microparticles such that there was sufficient energy available to permit the polymorphic transition from the unstable α-form to the β' form. This transition exerted a large influence over drug release. The release of TS from the unconditioned 48 hour freezer samples was dramatically different to that of a sample taken from the same batch, stored at 35 °C for 48 hours (Table 5.4.5.3).

Storage conditions (°C and hr)	t ₂₅ (min)	t ₅₀ (min)	% TS release at 180 min
-10, 48	4.78	7.3	88.0
35, 48	92.3	> 180	40.3

Table 5.4.5.3: Effect of storage temperatures on release parameters.

Release from the unconditioned sample was rapid - burst release was exhibited for 75% of the drug load. The profile was therefore associated with release from a matrix structure that possessed the unstable α-form of TP. It was expected that the rapid release arose from the open structure of the α-form that provided an ineffective barrier to water ingress. Elimination of the α-form through storage at elevated temperature resulted in a matrix with effective SR properties that was associated with the higher packing density of the β' form. In a review of lipid formulation stability, Heurtault *et al.*, (2003) concluded that SR was also frequently related to the β' form. A repeat

experiment (conditioned microparticles) for the variation of GB:TP ratio confirmed the importance of TP in the formulation for SR properties as increased TP content provided greater SR (Appendix B3.1).

5.4.6 Effect of Storage upon Particle Size of Lipid Microparticles

Storage at elevated temperature for 48 hr increased the size of the GB:TP microparticles (Table 5.4.6). As shown, the microparticles increased by approximately 40% in size (VMD). A size change of this magnitude would have considerably negative consequences on aerosol performance.

Sample	VMD (μm) \pm SD	D(v, 0.9) (μm) \pm SD
Fresh	2.18 \pm 0.21	4.13 \pm 1.0
35 °C, 48 hr	3.07 \pm 0.62	6.54 \pm 1.1
% Increase	40.8%	58.4%

Table 5.4.6: Effect of storage at elevated temperature upon GB:TP microparticles.

Matrix = GB:TP 60:40 (n=5).

During conditioning at elevated temperature, melting and recrystallization of the α -form permitted adhesion of neighbouring particles and led to an increase in particle size. SEM evidence also showed a substantial change in morphology for the 35 °C stored particles (Figure 5.4.6.1, 5.4.6.2 and 5.4.6.3), that suggested a β' to β transition. During this transition, compressional forces (generated during spray-drying) within the microparticles were relaxed, which resulted in swelling (Hagemann, 1988). Low molecular weight constituents of the matrix also migrate to the surface and 'bloom' more readily at elevated temperatures (Urbanski, 1991) and grow as visible protrusions or 'whiskers' at the surface (as described by Okada, 1970). Whisker formation was observed in a number of batches, and was most severe with lecithin-free formulations stored at 35 °C for 48 hr (Figure 5.4.6.3) as no anti-bloom protection was exerted.

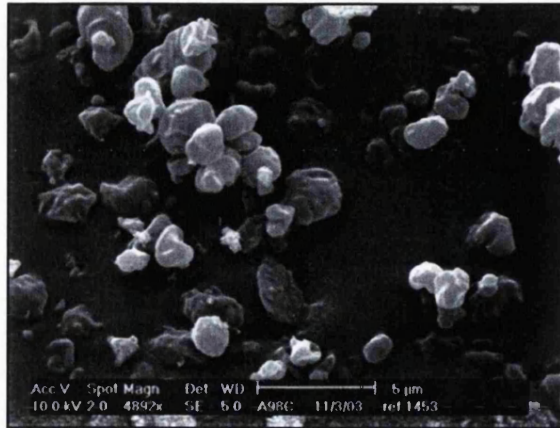


Figure 5.4.6.1: Freshly prepared GB:TP 60:40 microparticles (stored in freezer until SEM preparation).

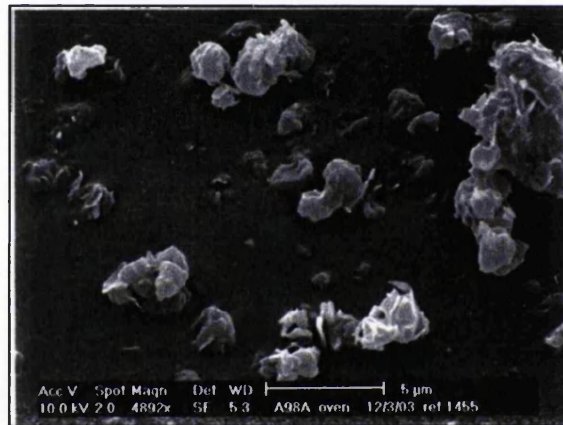


Figure 5.4.6.2: Oven-stored GB:TP 60:40 microparticles. Fusion of particles appears to have taken place.

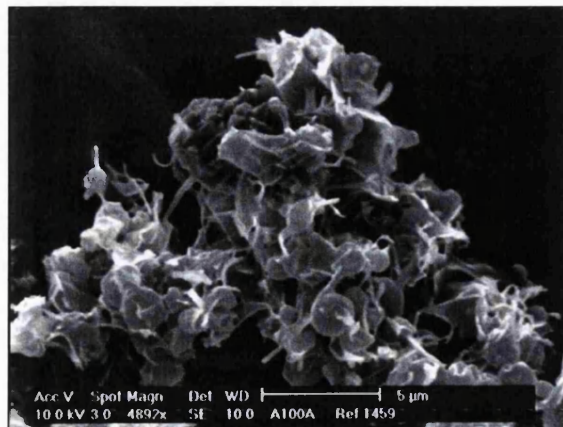


Figure 5.4.6.3: Oven-stored lecithin-free GB:TP 60:40 microparticles which displayed heavy 'whisker formation,' characteristic of the β' to β transition.

5.4.7 Effect of Release Media Temperature upon TS Release

The temperature of the release media was investigated in order to assess the performance of the SR profile at physiological temperature (37 ± 0.5 °C). Intermediate temperatures (25 and 31 ± 0.5 °C) were also investigated. Particles were conditioned prior to dissolution, at 35 °C for 48 hr. DSC analysis showed that the matrix had undergone the required polymorphic transition necessary to provide SR. Temperature is a key component of a diffusion-based release mechanism and an increase in temperature should elicit faster TS release rate from the matrix. Temperature of the diffusion cell was kept constant by means of a thermal water jacket attached to the diffusion cell in which water was circulated until the desired operating temperature was attained with stability. Table 5.4.7.1 and Figure 5.4.7.1 show the effect that temperature had on TS release rate from a matrix consisting GB:TP 60:40. Increasing temperature of the release media was observed to abolish SR profiles that were present for lower temperatures. Pillai *et al.*, (1998), also showed a major increase in disodium fluorescein release from wax condensation-coated microparticles when experiments were performed at elevated media temperatures (however, release from these microparticles was rapid; 100% release in 10 min at 37 °C and 22% in 10 min at 25 °C).

Temperature (°C)	Regression coefficient for Higuchi Plot, r^2	% TS release at 180 min \pm SD
19 (ambient)	0.9832	32.6 ± 5.8
25	0.8989	74.1 ± 0.23
31	0.8628	98.9 ± 3.1
37	0.8282	98.6 ± 3.9

Table 5.4.7.1: Effect of temperature on release kinetics and profile for GB:TP 60:40 microparticles.

The presence of lecithin was hypothesised to cause increased release rate at elevated temperature. To test this theory, lecithin-free microparticles were prepared and drug release was evaluated (Figure 5.4.7.2 and Table 5.4.7.2). Elevated temperature was still observed to have a profound effect

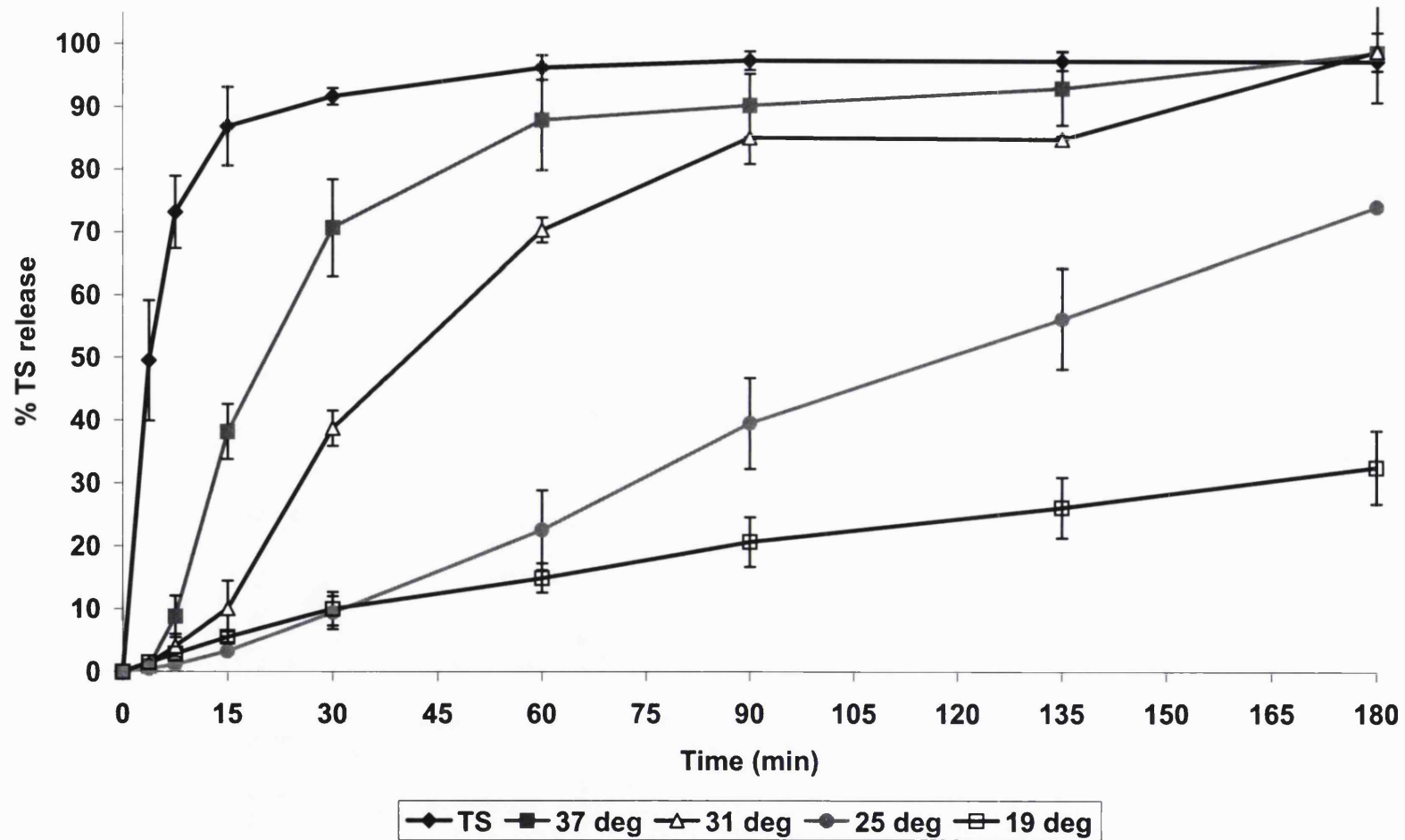


Figure 5.4.7.1: % TS release vs. time for pure TS and for TS from GB:TP 60:40 microparticles at temperatures indicated ($n=3 \pm SD$).

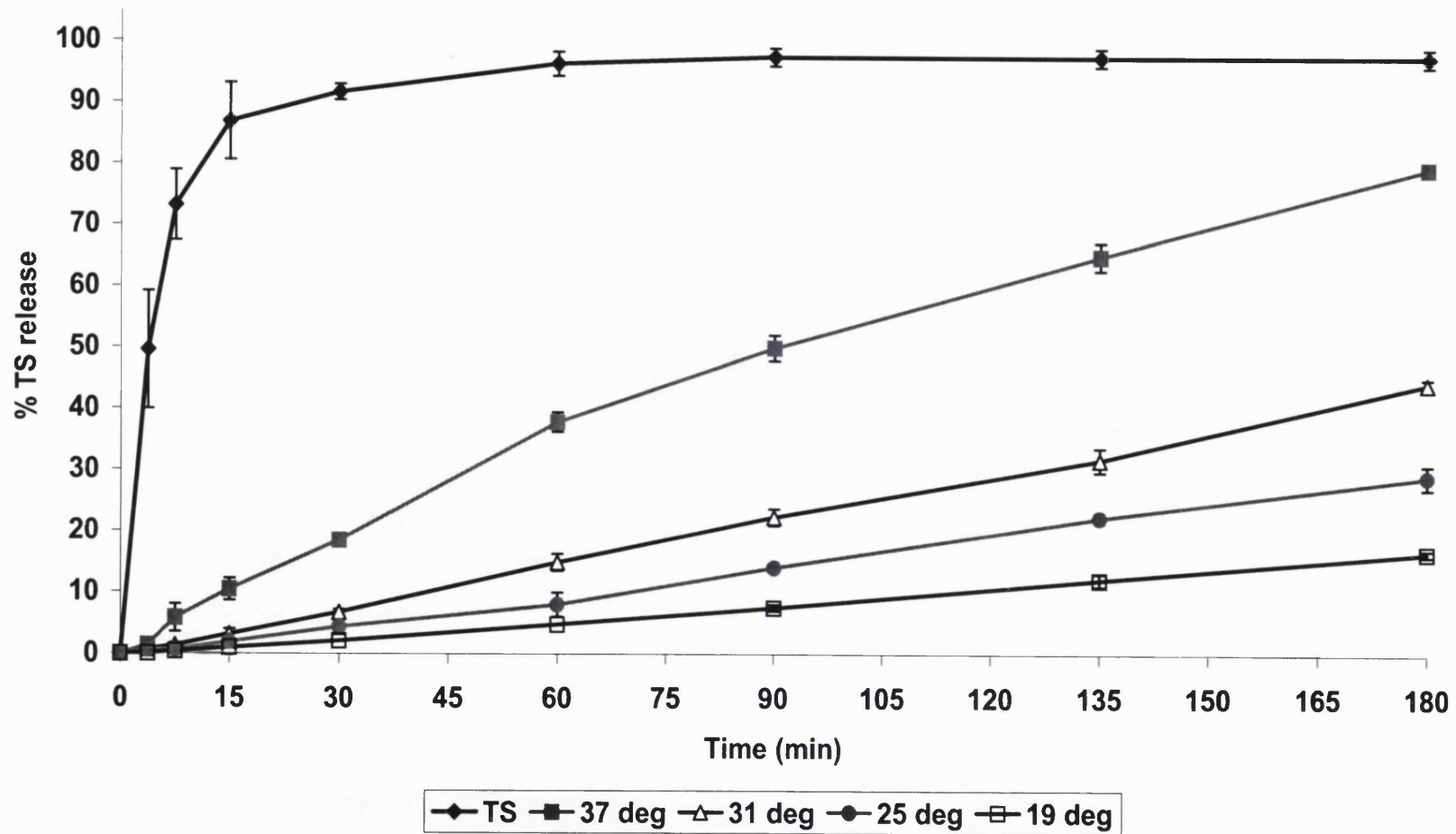


Figure 5.4.7.2: % TS release vs. time for pure TS and for TS from lecithin-free GB:TP 60:40 microparticles at temperatures indicated (n=3 ± SD).

on release rates, although not to the same extent that was observed for lecithin-containing systems. Drug release at 37 °C resulted in 79.2% drug release at 180 minutes for lecithin-free microparticles versus 98.6% drug release for lecithin-containing microspheres. The presence of 3.5% w/v lecithin in the matrix significantly increased TS release at 180 minutes for all temperatures levels (n=3, t-Test p <0.01).

Temperature (°C)	Regression Coefficient for Higuchi Plot, r ²	Regression Coefficient for Zero Order kinetics, r ²	% TS release at 180 min ± SD
19 (ambient)	0.9642	0.9699	16.4 ± 0.50
25	0.9289	0.9988	28.9 ± 1.9
31	0.9120	0.9958	44.1 ± 0.87
37	0.9081	0.9952	79.2 ± 0.37

Table 5.4.7.2: Effect of temperature of release kinetics and profile for lecithin-free GB:TP 60:40 microparticles.

As shown in Tables 5.4.7.1 and 5.4.7.2, release from the microparticles followed matrix diffusion kinetics at room temperature. Temperature elevation caused lecithin-containing and lecithin-free microparticles to increasingly deviate from matrix diffusion kinetics (reduction in regression coefficient). Further work would be required in order to elucidate the release mechanism at higher temperatures. Possible reasons (Higuchi, 1963) for deviation from matrix diffusion kinetics were (1) loss of matrix structure, (2) partial dissolution of matrix into receiver phase, (3) surface associated drug release (unlikely in this instance). At all temperatures, lecithin-free microparticles displayed linear release rates with relation to time over the study period (zero-order kinetics) - this observation suggested that the structure remained intact, otherwise dose-dumping or burst would have been observed.

The TS release rate from lecithin-free lipid based microparticles at 37 °C did not provide sufficient SR. Proof of concept for encapsulating hydrophilic nanoparticles in a hydrophobic matrix was shown at room temperature; however, a change in matrix composition was required to provide stable SR at physiological temperatures.

5.5 Results and Discussion II: Hydrogenated Oil Excipients

5.5.1 Assessment of TS Release from HPO Microparticles

Three hydrophobic excipients, CST, PW and HPO, were selected for initial study as new excipients to replace the GB:TP matrix. All investigations were performed at 37 °C. Spray-dried CST particles provided insufficient control over TS release ($t_{50} = 5.97 \pm 0.62$ min). PW microspheres showed promising SR at physiological temperature (20.4% TS release at 180 min); however, particle size was too large for progression (VMD = 12.5 μm).

Palm oil is a saturated (>99% w/w) natural oil obtained from the mesocarp of *Elaeis guineensis*, the palm tree (Johnson and Slaga, 2000). Hydrogenation is a process in which the majority of double bonds present in natural oils are reduced or 'saturated' with hydrogen. The absence of electron-dense double bonds allows the lipophilic chains to associate more closely through hydrophobic interactions, and this provides for a very effective barrier to water penetration. As hydrogenation is increased, the melting point of the material increases - the classic example of this is the transition from liquid sunflower oil to solid margarine upon hydrogenation. Commercial hydrogenation of oils is typically performed using a Ni catalyst, and depending on variation of process parameters, the same feed oil can be transformed into a final product with substantially different melting points (Karabulut *et al.*, 2003). For this reason, a variety of HPO sources were appraised and Dritex PST[®] was chosen as the melting point, 57-60 °C, was higher than body temperature.

Despite potential advantages for sustained release systems, hydrogenated oils have been used infrequently in the pharmaceutical industry. However, examples are theophylline encapsulation in HPO by means of SCF processing (Rodrigues *et al.*, 2003), although particle size suffered from high polydispersity and substantial burst release was present (> 75% drug release within 2 hr). Hydrogenated castor oil has been shown to provide excellent SR of sulfamethazine over 24 hr (Evrard and Delattre, 1996) in tablet form, and

ovalbumin sustained release has been achieved from HPO microparticles using a supercritical fluid based process (size > 10 µm, Perrut, 2003).

HPO was spray-dried at the conditions presented in Table 5.5.1.1, These conditions resulted in near spherical particles (Figure 5.5.1.1) with no evidence of unencapsulated TS nanoparticles. Employing HPO as SR coating material gave rise to favourable release profiles at all drug loadings investigated (Figure 5.5.1.2) with a very minor burst effect over the first 30 min. The ability of HPO to retard the release of a highly water-soluble drug such as TS at high drug loading and small particle size indicated impressive *in vitro* performance of the excipient in this SR application.

Formulation	200 mg TS nanoparticles + 800 mg HPO to 50 mL DCM
Spray-drying conditions	56 °C inlet, 46 °C outlet, 65% aspiration, 800 L hr ⁻¹ air flow, 20% pump
Final Drug loading	13.0 ± 0.17%

Table 5.5.1.1: Spray-drying conditions for HPO microparticles.

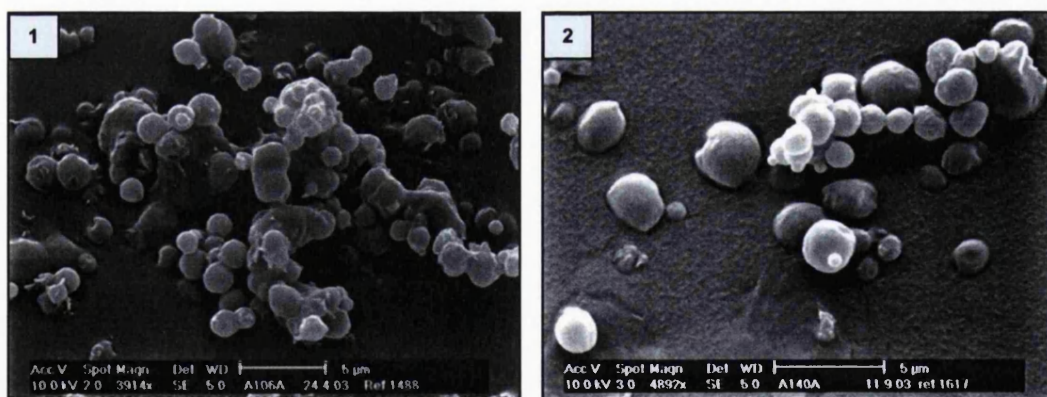


Figure 5.5.1.1: (1) SEM image for HPO microspheres, drug loading 13.0% w/w. Some particles appear fused, which may account for relatively large $D(v, 0.9)$ value of 15.4 µm. (2) SEM image for optimised HPO microsphere formulation, drug loading ~30% w/w (see section 5.5.3).

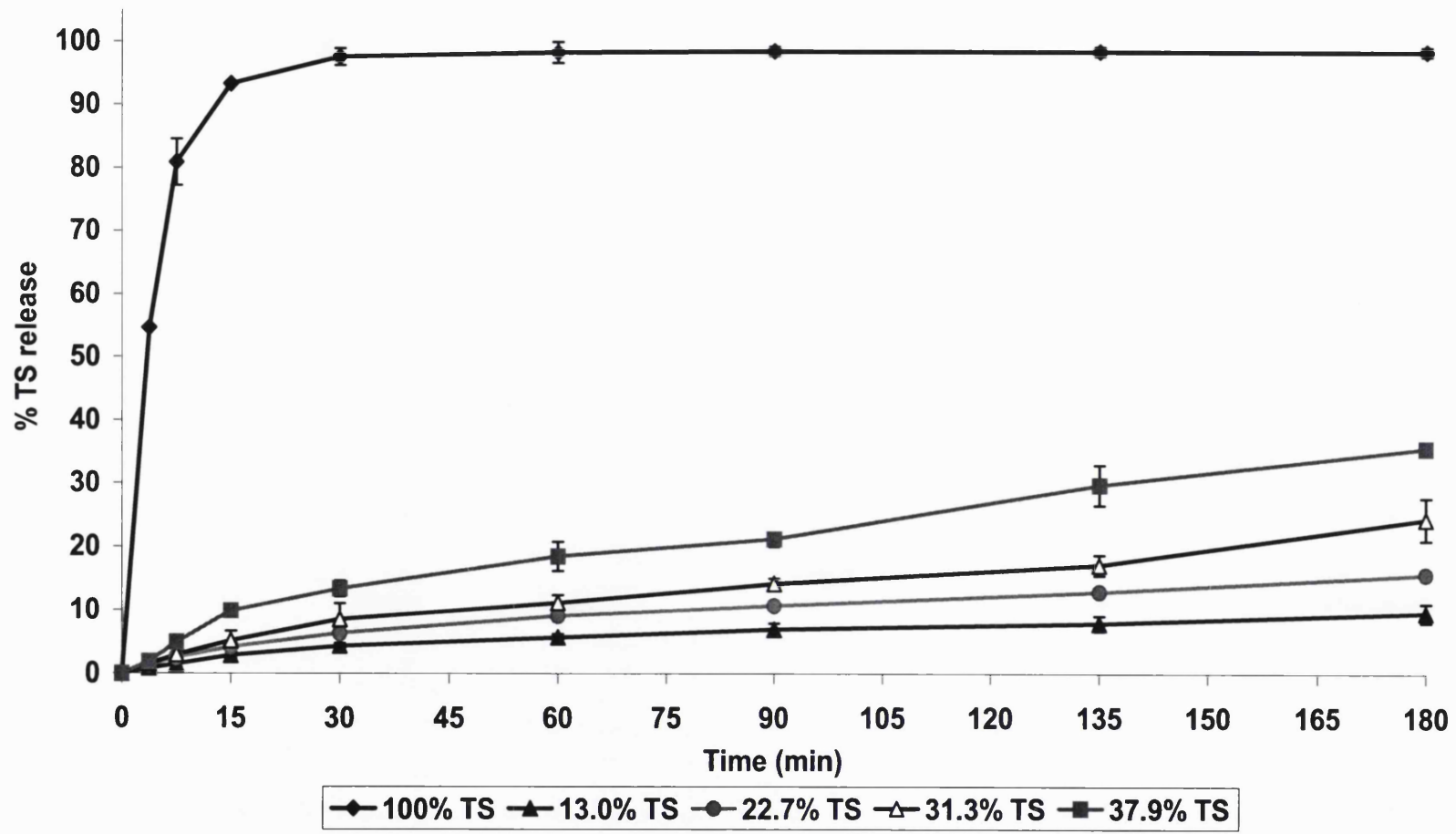


Figure 5.5.1.2: % TS release vs. time for pure micronised TS (100% TS) and different w/w TS nanoparticle loadings of HPO microparticles (n=3 ± SD, 37 °C).

TS loading (% w/w)	VMD (μm) \pm SD	D(v, 0.9) (μm) \pm SD	Regression coefficient for Higuchi Plot, r^2	% TS release at 180 min \pm SD
13.0	3.26 \pm 0.56	15.4 \pm 6.9	0.9904	9.59 \pm 1.5
27.7	3.52 \pm 0.051	17.2 \pm 4.9	0.9957	15.6 \pm 0.36
31.3	3.09 \pm 0.29	6.72 \pm 0.65	0.9755	24.3 \pm 3.4
37.9	2.96 \pm 0.59	11.78 \pm 6.14	0.9867	35.6 \pm 0.88

Table 5.5.1.2: Particle size and TS release characteristics at different TS drug loadings (n=3).

Release of TS from HPO matrix particles followed that of matrix diffusion as indicated by linearity in Higuchi plots (Table 5.5.1.2). The relationship between drug loading and TS release at 180 minutes was not linear, but was found to increase with higher TS content. VMD was within respirable range for all drug loadings. However, drug loadings of 13.0%, 22.7% and 37.9% w/w had large D(v, 0.9) values ($>10 \mu\text{m}$), which would have implications for pulmonary deposition in the throat/central airway. A drug loading of 31.3% w/w had the most favourable particle size distribution, and for this reason (together with the relatively high drug loading) was chosen for further investigations.

5.5.2 Effect of Release Media upon TS Release

Drug release was assessed in PB, SILF, and SSLF. The preparation method for SILF and SSLF was adjusted as bubbling CO_2 (g) through the fluid was ineffective as the pH was increased from 7.4 to 8.3 over 30 minutes. Therefore, pH was adjusted with 0.01 M HCl, in accordance with Thien *et al.*, (1982), which provided stability at pH 7.4. Particle size of the SSLF liposomal suspension was tracked using PCS during preparation, and the size (z_{ave}) prior to use was $168 \pm 4.2 \text{ nm}$ which was sufficiently small to penetrate the diffusion cell membrane and interact with the microparticles. Saturated solubility of TS was determined for all release media, and not found to be significantly different (n=3, ANOVA, $p>0.05$).

Davies and Feddah (2003), reported increased dissolution rates for steroids in SSLF (versus SILF) due to solubilisation. It was hypothesised that the presence of DPPC in SSLF might enhance solubility of the HPO matrix, and therefore increase TS release due to matrix disruption. However, release of TS from HPO microparticles was not affected by presence of DPPC. TS release into SILF appeared slower (Figure 5.5.2); however, there was no significant difference in percentage TS release at 180 min (n=6, t-Test, p>0.05). In light of these findings, further experimental work was performed with 0.05 M phosphate buffer, pH 7.4, owing to ease of preparation relative to both simulated lung fluids.

5.5.3 Factorial Design Experiment for Particle Size Optimisation

A factorial design optimisation was performed in order to improve the particle size distribution of the spray-dried SR product. Factorial design is a technique in which factors are evaluated simultaneously and their relative importance is assessed. The technique has found frequent use in spray-drying formulation (e.g. Billon *et al.*, 2000 for acetaminophen microparticles). The technique followed a conventional method described by Armstrong and James (1996) and the variables are displayed in Table 5.5.3.1.

Experiment code	Factor A Pump rate	Factor B Aspirator	Factor C Inlet Temp
1	-	-	-
a	+	-	-
b	-	+	-
ab	+	+	-
c	-	-	+
ac	+	-	+
bc	-	+	+
abc	+	+	+

Table 5.5.3.1: Factorial design matrix for optimising particle size and yield. Assignment of experiment code followed Armstrong and James (1996).

- = lower level of factor and + = higher level of factor:

For Factor A: - = 15% and + = 20% pump rate

For Factor B: - = 65% and + = 75% aspiration

For Factor C: - = 52-53 °C and + = 60-61 °C inlet temperature.

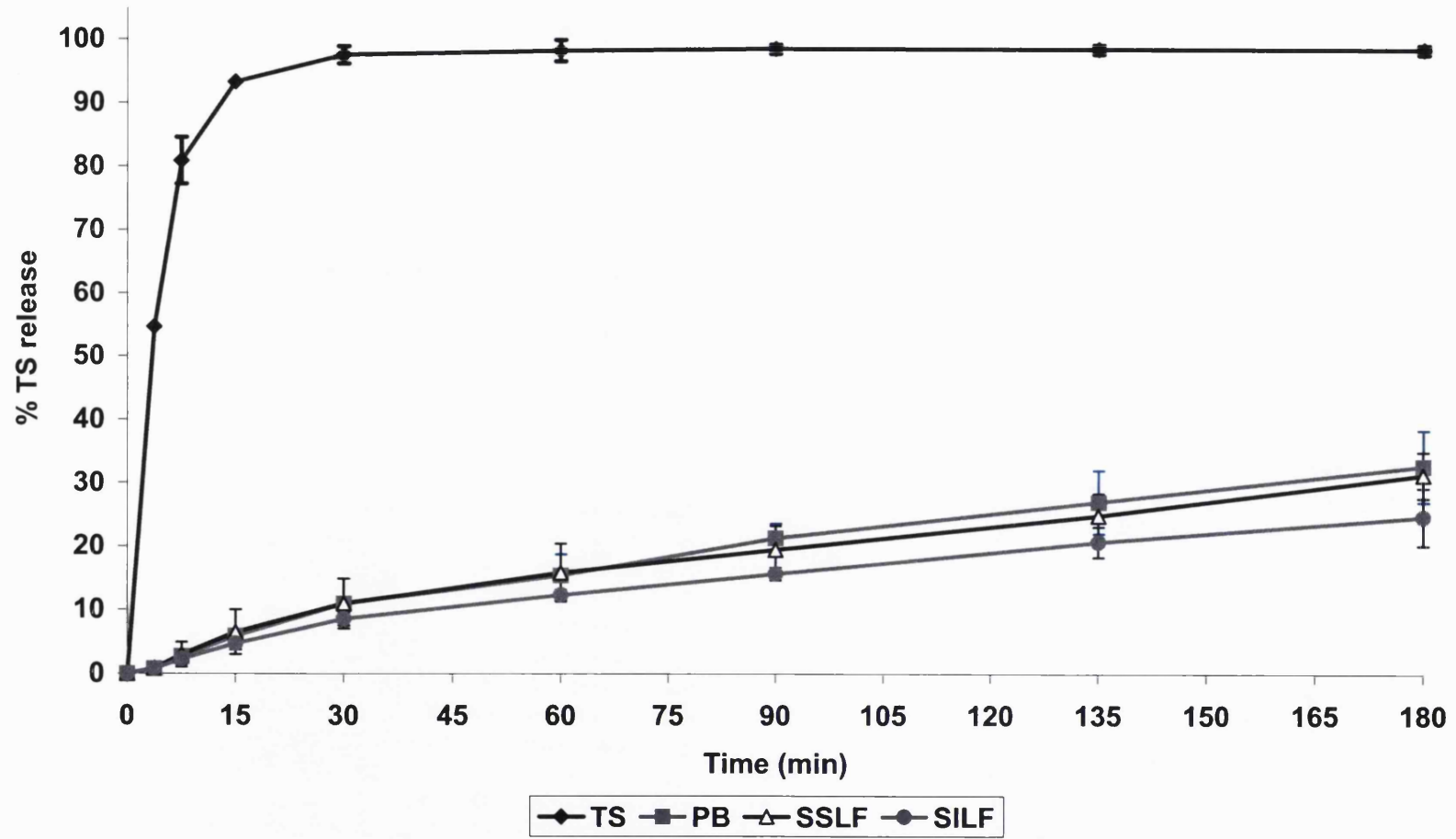


Figure 5.5.2: % TS release vs. time for pure micronised TS, and TS from HPO formulations into PB, SSLF and SILF (n=6 ± SD, 37 °C).

Two responses were considered, yield (%) and particle size (VMD and D(v, 0.9)). Selection of the higher inlet temperature exerted an overpowering effect on both yield and particle size (Table 5.5.3.2). The effect was large enough to render changes in pump rate and aspiration insignificant.

Response	60-61 °C Inlet	52-53 °C Inlet
Yield (%) ± SD	13.1 ± 5.1	28.7 ± 6.6
VMD (µm) ± SD	6.94 ± 2.4	3.18 ± 0.22
D(v, 0.9) (µm) ± SD	27.4 ± 7.1	7.90 ± 0.6

Table 5.5.3.2: Effect of varying inlet temperature on yield and particle size cut-off values (n=8).

At 60-61 °C inlet temperature, the yield was statistically lower (n=8, t-Test, p<0.0001) from yield at 52-53 °C inlet temperature. The lower yield arose from greater adhesion of molten lipid to the wall of the spray-dryer cyclone despite the outlet temperature prior to the cyclone being lower (48-49 °C) than that of the HPO melting point (57-60 °C). The adhesion of microparticles was also reflected in the particle size cut-off values as aggregation resulted in significantly larger sizes (n=8, t-Test, p<0.01 for VMD and p<0.0001 for D(v, 0.9)). Spray-drying at inlet temperatures above the melting point of HPO are therefore not possible. Batches (separate to experimental design, n=3) spray-dried at 48-49 °C inlet temperature had a larger particle size than particles from 52-53 °C inlet temperature. This increased particle size was thought to have arisen from incomplete drying of the microparticles. In conclusion, a narrow temperature range existed for successfully spray-drying HPO microparticles from DCM. Matrix excipients, e.g. HSO (Appendix B3.2) with higher melting points will provide greater flexibility in the range of temperatures employed for spray-drying (thereby increasing the range of solvents available for use).

The experiment was rerun with feed concentration (- = 1.5% and + = 2% w/v) as a replacement factor for inlet temperature. All experiments were performed at inlet temperatures of 52-53 °C. Analysis of the results to

observe the response of the product to the factors showed no significant differences in neither yield nor particle size (see Appendix B4). It was therefore concluded that spray-drying HPO microparticles from DCM was not sensitive to changes in pump rate, aspiration or feed concentration at the levels investigated.

Therefore, a combination of factors which produced small particles (VMD = 2.99 μm) with acceptable yield (26.8%) were selected for progression: Inlet temperature = 52-53 $^{\circ}\text{C}$, pump = 20%, aspiration = 75% and [feed] = 2% w/v.

5.5.4 Content Uniformity

An arbitrary sample of 10.0 mg was taken for content uniformity studies, as it was unknown what unit dose weight would be typically required for a clinical batch of SR material. TS/HPO microparticles were favourably inside BP (2003) limits (85%-115%) for content uniformity with each of three batches investigated having content within 96%-106% of the mean (Figure 5.5.4).

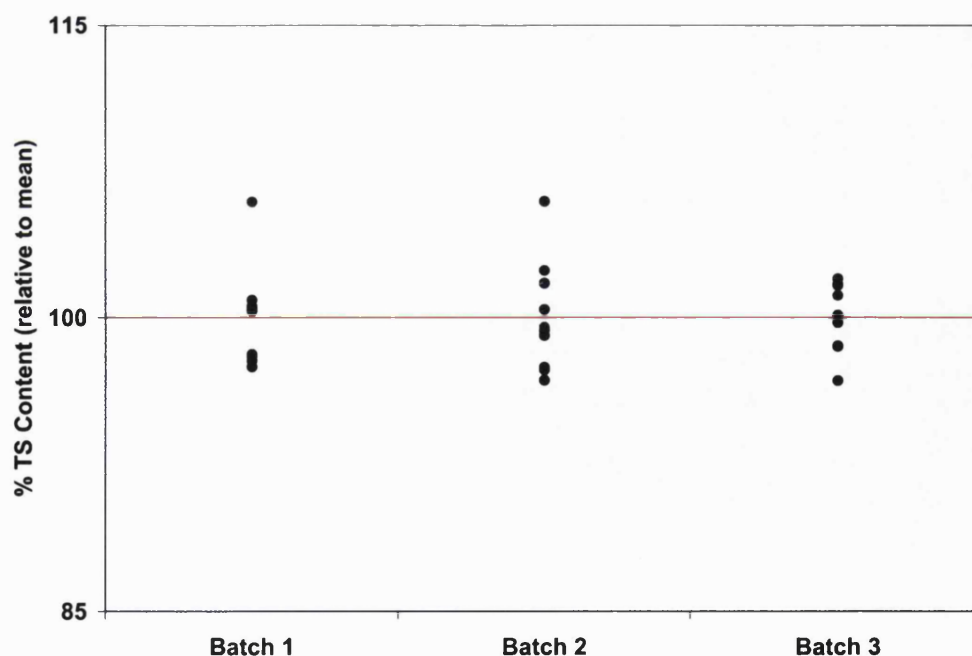


Figure 5.4.4: Content uniformity for three batches of HPO microparticles, containing ~30% w/w TS nanoparticle loading.

Inter-batch drug loading was significantly different (ANOVA, $p < 0.001$) - loadings for Batch 1, 2 and 3 were 29.8%, 31.2% and 34.3% respectively. Inter-batch variability is common in pharmaceutical processes and formulations, and was certainly expected from a multi-step formulation process such as preparing TS/HPO microparticles. However, specifications for drug loading would need to be established in scale-up investigations in order to decide at what level the formulations have insufficient or excessive drug content.

5.5.5 Comparison of HPO Formulation to GB:TP Formulation I: DCA Measurement

Contact angle is typically large for hydrophobic materials ($>90^\circ$), which provides good barrier properties to water (Buckton and Newton, 1985). It was expected that the DCA for GB:TP spray-dried microparticles (thermally conditioned) would be lower than that of HPO-based particles, as TS release was more rapid from the GB:TP microparticles. However, no significant difference (t-Test, $p > 0.05$) was observed in the advancing contact angle between the two different matrices (Table 5.5.5).

Formulation	Advancing Contact Angle \pm SD	Receding Contact Angle \pm SD
GB:TP	90.8 \pm 1.0 $^\circ$	60.1 \pm 2.4 $^\circ$
HPO	89.9 \pm 1.1 $^\circ$	88.2 \pm 1.0 $^\circ$

Table 5.5.5: Dynamic contact angle measurement (advancing and receding, $n=5$, 37 $^\circ\text{C}$). TS load was 13.4% and 13.2% for GB:TP and HPO microparticles, respectively.

There was significant difference ($n=5$, t-Test, $p < 0.05$) between the advancing and receding contact angles for both formulations ('contact angle hysteresis') that indicated wetting of the microparticle surface during the DCA testing process. The receding angles for GB:TP was significantly less ($n=5$, t-Test, $p < 0.0001$) than for the HPO-based microparticles. This indicated that the GB:TP microparticles were more susceptible to surface wetting (more hydrophilic surface). This effect was likely to arise from the presence of

lecithin on the surface of the GB:TP microparticles and provided evidence, in part, for faster TS release from the matrix. (A proportion of the difference between advancing and receding contact angle might have been due to entry of lecithin into the water bath from the microparticle, which then reduced surface tension).

For the GB:TP formulation, there was no significant difference (n=5, t-Test, p>0.05) for advancing and receding contact angle at 24 °C and 37 °C - this showed that the dramatic changes (Figure 5.4.7.1) in TS release from the GB-TP formulation as temperature increased were not due to changes in surface hydrophilicity.

5.5.6 Comparison of HPO Formulation to GB:TP Formulation II: DVS Investigation

Blank GB:TP microparticles displayed greater sorption of water vapour than HPO microspheres (Table 5.5.6). No vapour sorption was reported for the empty glass pan; therefore, all mass change recorded arose from the formulation tested. The results showed that the GB:TP microparticles had an increased tendency to interact and bind with water, relative to HPO, which was likely to facilitate TS release. Vapour sorption was also greater for unconditioned GB:TP microparticles relative to conditioned material, which suggested a change in hydrophilicity; however, the particle size increase during conditioning may be responsible for the reduced vapour sorption tendency (reduced particle surface area).

Formulation	Maximum % Mass Change ± SD
GB:TP 60:40 (unconditioned)	102.7 ± 0.30
GB:TP 60:40 (conditioned)	101.8 ± 0.054
HPO	100.3 ± 0.088

Table 5.5.6: Vapour sorption (presented as maximum % mass change) of GB:TP and HPO formulations (n=3) at 90% RH and 37 °C. Vapour sorption reached maximum for all formulations within 20 min.

5.5.7 Stability of HPO Microparticles

Stability of GB:TP microparticles was affected by a β' - β transition, which resulted in the development of surface protrusions and increased particle size. A study of the stability of HPO microparticles was therefore required. Three identical batches of microparticles were investigated immediately after preparation and following three months storage in the refrigerator (4 °C). Testing was performed on batches that contained a small percentage by weight (0.2%) of DPPC as the presence of this phospholipid has been shown to increase bioavailability/biocompatibility (Evora *et al.*, 1998 and Jones *et al.*, 2002) by reducing macrophage recognition, uptake and clearance.

No significant difference in particle size distribution was observed following storage (t-Test, $p > 0.05$ for $D(v, 0.1)$, VMD and $D(v, 0.9)$). Natural hydrophobic products, e.g. HPO, are rich in a variety of molecular structures. This variety promotes stability in the β' form (Millqvist-Fureby, 2003), such that 'bloom' of the microparticle structure was improbable, and particle size was retained. DSC thermal profiles for HPO as received, and spray-dried HPO/TS nanoparticles (fresh and after three months storage) are shown in Figure 5.5.7.1. The melting point of HPO was not changed with TS nanoparticle incorporation, which was a strong indication that there was no chemical interaction between drug and excipient. For freshly spray-dried HPO/TS, a small endothermic transition was observed at approximately 47 °C followed by an exothermic peak - characteristic of an unstable α -form melt and subsequent re-crystallization to the β' form. However, the presence of this α -form did not abolish SR release kinetics from HPO based microparticles as shown for GB:TP microparticles. Upon storage, the transitions associated with the α -form were diminished, however this did not affect the release profile (Appendix B3.3) as TS release at 180 min was not significantly different ($n=6$, t-Test, $p > 0.05$). Understanding of HPO crystallinity was complicated by a lack of XRPD evidence for crystallinity (Figures 5.5.7.2 and 5.5.7.3). However, this is common for natural lipids, which display less measurable crystallinity than pure lipid excipients due to the variety in structural composition (Westersen *et al.*, 1997).

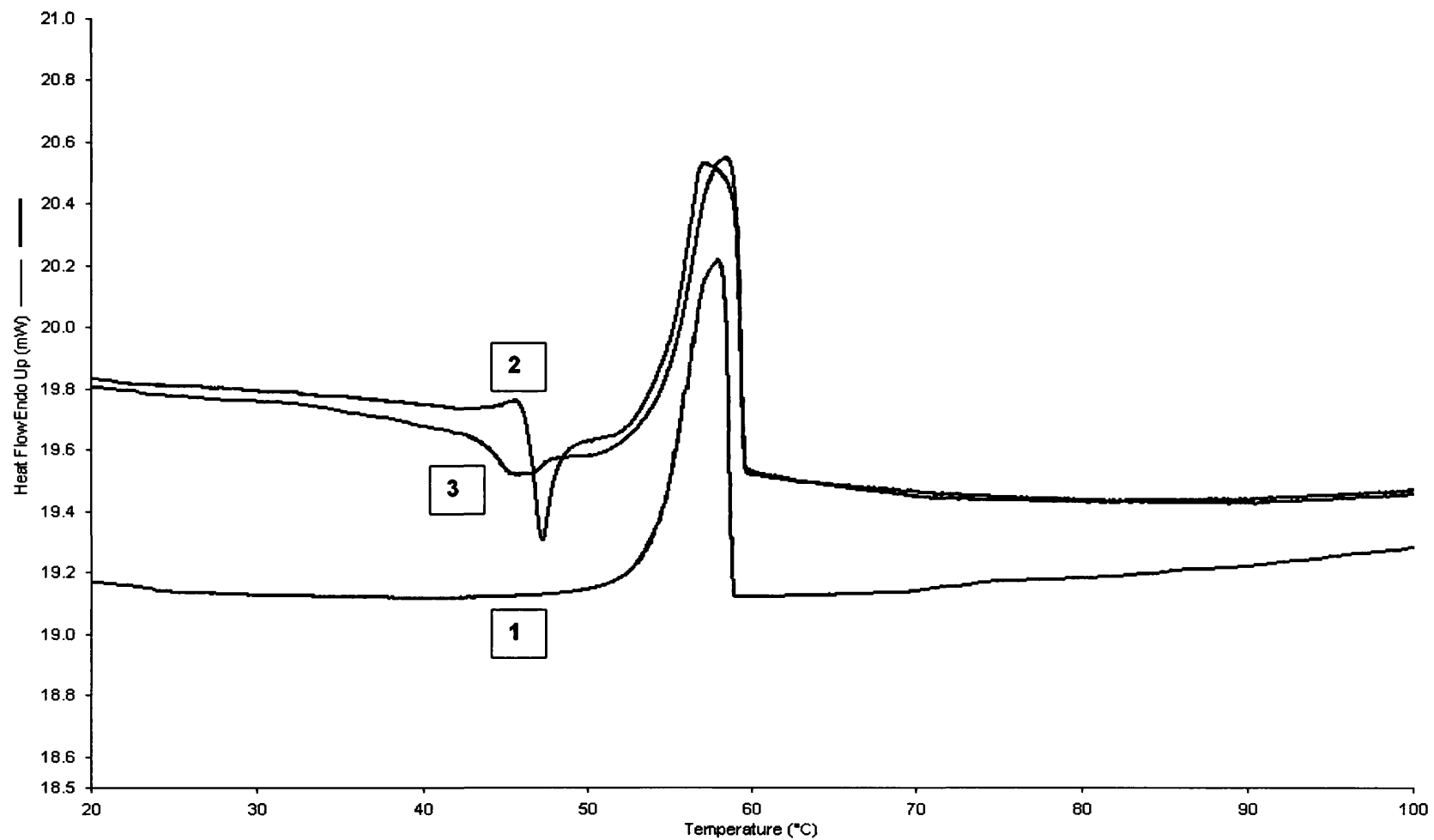


Figure 5.5.7.1: DSC thermal profiles of HPO-based formulations: 1 = HPO as received, 2 = freshly spray-dried SR-TS, 3 = spray-dried SR-TS following three months storage in the refrigerator (4 °C).

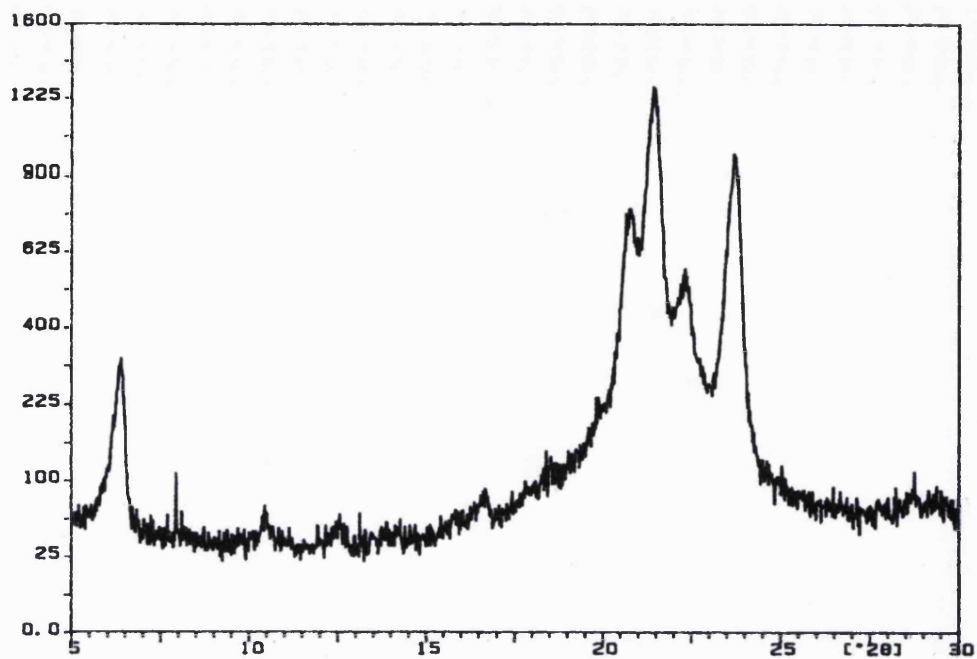


Figure 5.5.7.2: Powder X-ray diffractogram of HPO, as received (flakes were milled for 5 min total to reduce particle size for XRPD analysis, in 30 sec runs to avoid heating). Diffractogram showed evidence for crystallinity from 20-25 [$^{\circ}2\theta$].

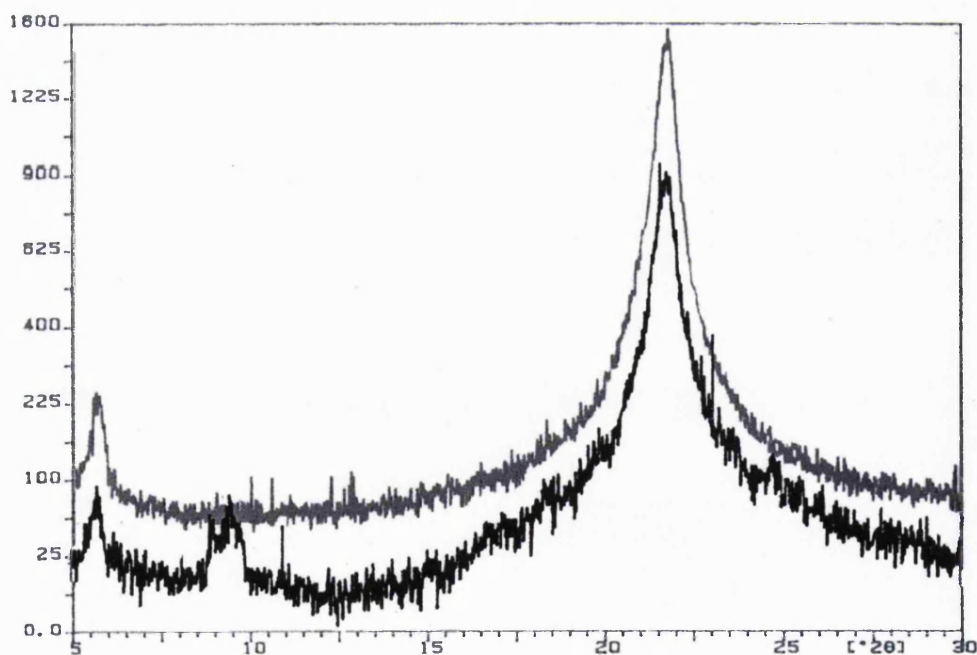


Figure 5.5.7.2: Powder X-ray diffractograms of spray-dried blank HPO (|) and HPO/TS microparticles (|) with 33.8% TS loading. Drug incorporation did not affect the XRPD pattern.

A stability study performed at 25 °C by Evrard and Delattre (1996), showed that a hydrogenated oil based tablet formulation was stable for one year with no changes in release for a water-soluble drug. However stability studies for a microparticulate SR formulation require further work as even slight changes in size or coating integrity will have drastic consequences for product performance. Such changes on the surface of a relatively large dosage form such as a tablet might not be noticeable. The results presented above show refrigerator stability for three months - this should only be interpreted as proof of minimum stability.

5.5.8 Visualisation of TS Nanoparticle Distribution Within Hydrophobic Microparticles

Content uniformity showed that TS was uniformly distributed within the bulk spray-dried SR material. However, it was not known how the nanoparticles were distributed within the microparticles - although the absence of TS burst release from HPO microparticles provided conclusive proof that the nanoparticles were not positioned at the surface.

A rough estimation to show the number of nanoparticles per microparticle was calculated from particle size information and drug loading data. Assuming a microparticle diameter of 2.75 μm , the microparticle volume was 10.9 μm^3 . For 30.0% w/w drug loading, 3.27 μm^3 (30% of the microparticle volume) was the volume that the TS nanoparticles occupied. This volume corresponded to 450 TS nanoparticles/microparticle, based on a TS nanoparticle z_{ave} of 240 nm and volume of 0.00724 μm^3 . This approximate calculation suggested that each microparticle contained large numbers of nanoparticles. However, the number of nanoparticles per microparticle, vastly changed with both nanoparticle and microparticle size (Appendix B5).

The traditional method for assessment of internal morphology of formulations is TEM. However, all attempts to prepare HPO microparticle sections resulted in failure as (1) HPO displayed solubility in the TEM sectioning resins and microparticle structure was lost or (2) when HPO was not soluble

in the sectioning resin, the resin was too soft for sectioning and microparticles were pushed from the microtome instead of being cut. Alternative imaging methods were therefore investigated (FIB and CLSM).

Microparticles were easily located using FIB microscopy, and suitable clusters of microparticles were selected for sectioning with the ion beam. However, heat generated by the FIB during sectioning caused the microparticle cross-sectional surface to melt, which concealed any morphology associated with the nanoparticles (Figure 5.5.8.1). FIB microscopy was therefore not appropriate for visualising the internal morphology of the microparticles. With access to a cryo-stage (Mulders, 2003), the heating effect of the ion beam during sectioning would be diminished and visualisation of nanoparticles might be achieved.

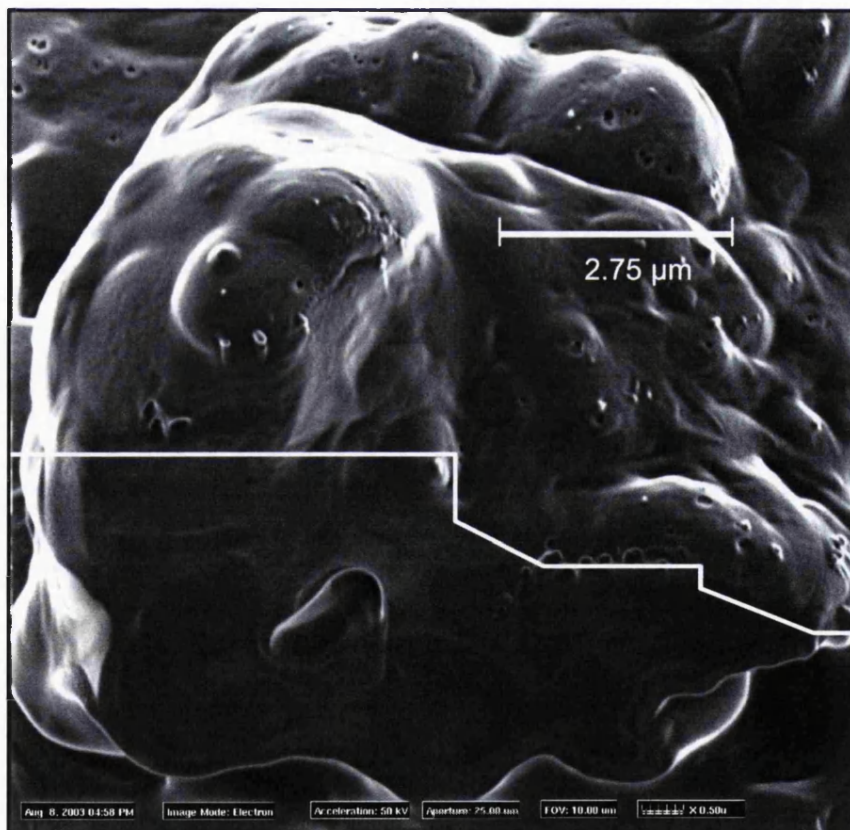


Figure 5.5.8.1: FIB sectioned cluster of TS/HPO microparticles. White jagged line running horizontally represents the top leading edge of the section, with sectioned microparticles beneath this line. The morphology appears melted with no evidence for TS nanoparticles.

Nanoparticle location, instead, was successfully imaged with CLSM. TS nanoparticles containing 5,6-carboxyfluorescein were prepared and displayed intense green fluorescence under standard fluorescent microscopy prior to incorporation into HPO microparticles. Microparticles were visualised using Differential Interference Contrast (DIC) microscopy, and then the image generated from laser raster was placed on top of the DIC image in order to show nanoparticle location (Figure 5.5.8.2). However, owing to the small size of the microparticles and the limited magnification (63x) of the microscope, resolution was limited (as apparent in Figure 5.5.8.3).

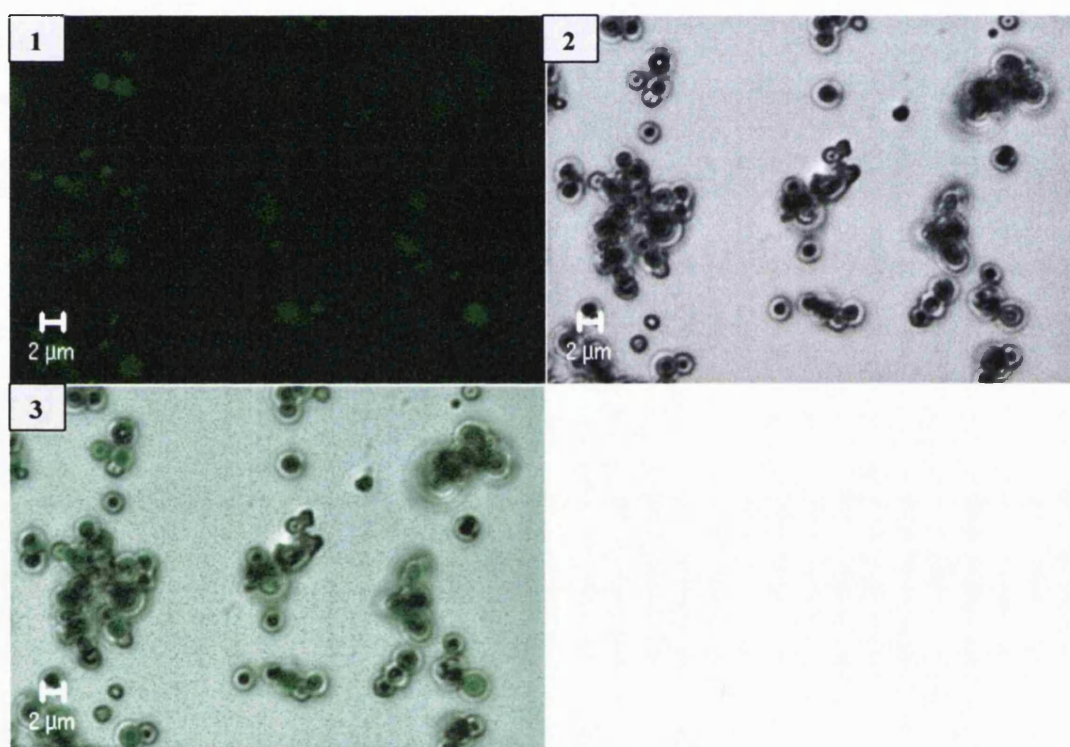


Figure 5.5.8.2: Visualisation of nanoparticle encapsulation within HPO microparticles: 1 = mapping of 5,6-carboxyfluorescein (representing TS nanoparticles), 2 = DIC image of microparticles, 3 = Combined image, showing nanoparticle location within microparticles.

CLSM was also used to 'section' through the microparticles by scanning at different depths (200 nm sections were generated). All images from the different depths of section contained different patterns of green fluorescence when played-back on the monitor - this showed that the nanoparticles were uniformly distributed as opposed, for instance, to all being clustered at the core of the microparticle. Some microparticles appeared to display minimal

fluorescence, which suggested a variation in loading; however, this effect may have simply arisen from the microparticles being at a depth not scanned by the laser (i.e. microparticles were 'out of focus').

Variation of the intensity of fluorescence was also mapped across individual microparticles (Figure 5.5.8.3). From the surface of the microparticle to a depth of approximately 200-400 nm, there was low fluorescence, which indicated absence of nanoparticles, and therefore presence of excipient. This finding was consistent with absence of burst release. Fluorescence was then observed to be present in steps, the size of which approximately corresponded to the size of TS nanoparticles.

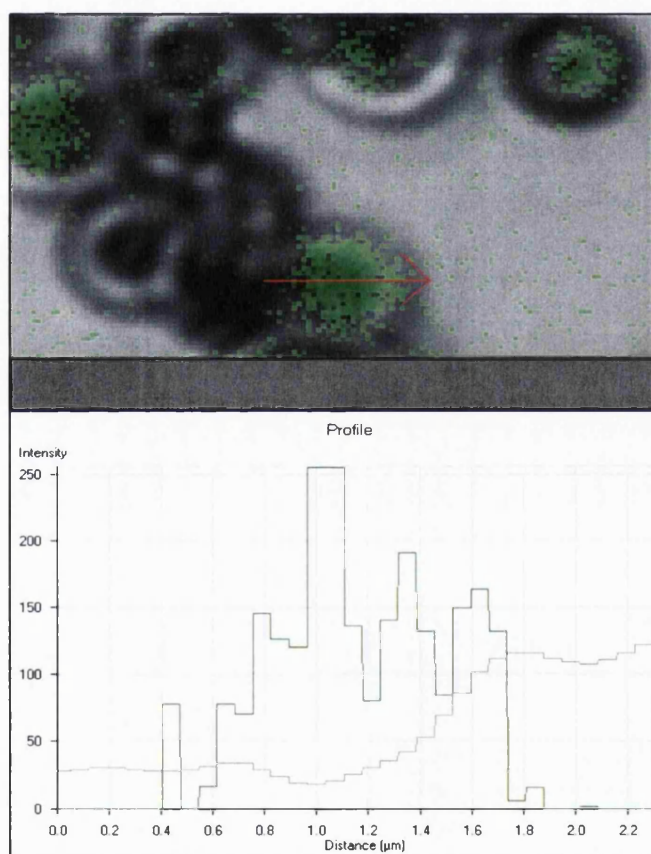


Figure 5.5.8.3: Fluorescence scan through individual microparticles. Red arrow in combined DIC/fluorescence image corresponds to 2.3 μm , the length displayed as the x-axis in the intensity vs. distance graph beneath the image.

5.6 Conclusion

Proof of concept for the encapsulation of nanoparticles into hydrophobic microparticles was achieved in this investigation, and *in vitro* SR profiles were promising for HPO-based microparticles.

TS release from GB:TP microparticles was sustained at ambient temperature, following thermal conditioning of the matrix. This step was necessary to convert the unstable α polymorph (which permitted fast TS release) into the β' polymorph. However, this conditioning led to an unacceptable increase in particle size. Also, TS release from GB:TP-based microparticles showed poor SR at physiological versus ambient temperature, which in part was due to the presence of lecithin.

HPO-based microparticles provided suitable SR of TS at all drug loadings investigated. No burst release of drug was observed, and 25% of the drug (for particle loading = 30% w/w) had been released at the 3 hr time point. Absence of burst indicated that the TS nanoparticles were not surface associated, and therefore matrix integrity at the surface was high. TS release profiles were observed to be stable in all release media investigated, (phosphate buffer, SILF and SSLF) and also following three months storage in the refrigerator. A TS nanoparticle loading of ~30% w/w and 0.2 % w/w DPPC was chosen for further aerosol characterisation (Chapter 6).

DCA and DVS data showed small differences between the GB:TP and HPO-based formulations, but differences were not large enough to explain the vastly different release profiles between the two formulations at physiological temperatures.

Finally, TS nanoparticle loading met pharmacopoeial content uniformity testing, and nanoparticles were shown to be well dispersed throughout the HPO matrix (except at surface) in preliminary CLSM studies.

Owing to the novelty of the microparticle generation method, the process technology described in Chapters 4 and 5 of this thesis are the subject of a UK patent application, GB0323003.4.

Chapter 6: Aerosol Development for HPO Microparticles

6.1 Introduction

Chapter 5 reported that it was possible to prepare SR microparticles, containing TS nanoparticles in a geometric size range deemed suitable for inhalation. However, particles for inhalation typically cannot be manufactured without a degree of aggregation which may affect aerosol performance (Hickey *et al.*, 1994) for a number of reasons; for instance (1) association forces (van der Waals, capillary, electrostatic, mechanical interlocking) (2) soft particles with low melting points may deform or adhere during manufacture. Spray-dried material has shown enhanced dispersibility relative to micronised drug (Vidgren, *et al.*, 1987), and the main purpose of this investigation was to assess HPO-based microparticle dispersion versus pure micronised drug. The clinical effectiveness of SR microparticles is determined by the amount of drug deposited in regions where the particles are not subject to mucocilliary clearance (Section 1.6.2); therefore, a small MMAD (<5 μm) and high FPF was required.

It is generally believed that the lung deposition of inhaled particles depends on the aerodynamic size. This can be measured *in vitro* by inertial separation devices. Their use in formulation development is attractive owing to simplicity of use, high power to detect differences and low variability compared with *in vivo* experiments (Weda *et al.*, 2002). Inertial separation devices typically encountered in pharmaceutical inhalation testing (BP, 2003; USP, 2000) are the Twin Stage Impinger, Metal Impinger, Multi-Stage Liquid Impinger, Andersen Cascade Impactor (ACI), and lastly, the Next Generation Impactor. The devices differ principally in the number of stages used, which act as particle size cut-offs.

In this investigation, the ACI was used. The ACI has 8 stages, together with an induction port (which mimics the throat) and a filter to collect submicron fine particles. This device provides a method in which the particles are fractionated into 10 particle size subsets, which provides a useful way of characterising and comparing aerosol particle size distributions.

6.2 Materials

6.2.1 Candidate SR Formulation

HPO microparticles containing TS nanoparticles and DPPC were prepared in accordance with Chapter 5. Unless otherwise stated, the spray dried feed contained ~2% w/v volume solids, consisting of 1.2% w/v HPO, 0.8% w/v TS nanoparticles and 0.004% w/w DPPC (0.2% w/w based upon HPO/TS content). Conditions used were 52-53 °C inlet temperature, 41-42 °C outlet temperature, 75% aspiration, 20% pump speed and 800 L hr⁻¹ airflow. Batches prepared under these conditions were classed as the 'candidate formulation' and referred to in the text as **SR-TS**. Pure, micronised TS was used as received, and referred to as **IR-TS**.

6.2.2 HFA propellants

HFA-134a and HFA-227 were purchased from Solvay Fluor and Derivate GmbH (Hanover, Germany).

6.2.3 Additional Chemicals

A range of surface-active agents were utilised for pMDI formulation: Brij[®] 30, polyethylene glycol 1000MW (PEG-1000), Poly(vinylpyrrolidone) 10000MW Triton[®] X-100, Tween[®] 20 and tyloxapol were all purchased from Sigma-Aldrich Co. Ltd. (Gillingham, Dorset, UK). Pluronic[®] L31 and L43 were donated by BASF (Mount Olive, NJ, USA), and Eudragit[®] RS-PO and E100 polymers were a gift from Rohm Pharma Polymere GmbH (Darmstadt, Germany).

Additional phospholipids required for investigation were distearoyl-phosphatidylcholine (DSPC) and dipalmitoylphosphatidylethanolamine (DPPE), which were purchased from Sigma-Aldrich Company Ltd. For ACI plate coating, Brij[®] 35 and glycerol were obtained from Sigma-Aldrich Company Ltd. and VWR International Ltd. (Poole, Dorset, UK), respectively.

For ACI plate washing, 0.05 M phosphate buffer was prepared as before (Section 3.3.1.2). Acetone (ACT), methanol and absolute ethanol were purchased from VWR International Ltd., and deionised water was dispensed from an Option 4 Purifier (Elga Ltd., High Wycombe, Buckinghamshire, UK).

6.3 Methods

Sections 6.3.1 and 6.3.2 are associated with formulation of the SR-TS microparticles into a pMDI.

6.3.1 Procedure for Filling PET Bottles with HFA Propellant

SR-TS (10.0 mg), and surface-active agent (various weights), were accurately weighed into transparent poly(ethylene terephthalate) (PET) bottles. A manual crimper (Aerotech Laboratory Equipment Co. Inc., Maryland, NY) was then used to crimp a continuous pMDI valve onto the PET bottleneck - the bottle was then tared on a 5-place balance. An HFA cylinder was then attached to a pressure burette (Aerotech Laboratory Equipment Co. Inc.) and liquid HFA entered the burette. A N₂ headspace pressure (6 bar) was created above the liquid HFA within the burette (necessary to create the downward pressure required for filling the PET bottle). The PET bottle was then connected to the base of the burette, and filled with liquid HFA through the continuous valve. The process was repeated until the desired fill weight (10.0 g HFA) was achieved.

6.3.2 Determination of HPO Solubility in HFA Propellants

HFA propellant (HFA-134a and HFA-227) was added to test PET bottles (n=3 for each propellant) containing an excess of spray-dried blank HPO microparticles. The bottles were then placed horizontally onto a magnetic stirrer (RT10 power stirrer, IKA-Werke GmbH, Staufen, Germany) and stirred for 72 hours. Excipient solubility was then determined in a method similar to that developed by Verveat *et al.*, (1999), using an AstraZeneca R&D Charnwood (Loughborough, Leicestershire, UK) custom-built pressure filter

device containing a 0.22 µm Durapore® 25 mm filter discs (Millipore Ltd., Camigtavanill, Co. Cork, Ireland). Briefly, the filled bottle was attached to a leak proof coupling whilst being held in a vertical position. An accurately weighed (6-figure balance) empty receiver bottle was attached to the base of the filter unit through a second leak proof coupling. The continuous valves of the bottles were simultaneously depressed in order to engage the valves. The contents of the test bottle were thus pressure-filtered into the receiver bottle. Following weighing to determine the amount of propellant present, the propellant was evacuated through the valve and completely removed by piercing the valve and allowing the bottle to equilibrate with air for 6 hours. The amount of HPO dissolved in the saturated propellant was determined by mass difference between the accurately weighed (6-place balance) empty receiver bottle and the weight following HFA removal. HPO solubility was then calculated as percentage w/w (HPO/HFA).

6.3.3 Assessment of Aerodynamic Particle Size

An aerodynamic particle sizer (APS, Model 3300, TSI Instruments Inc., St. Paul, MN, USA) was used to determine the particle size distribution of particles from 0.5 to 30 µm in diameter. The instrument sized particles aerodynamically by detecting the time for each particle to pass between a pair of two overlapping laser beams (time of flight). This time was then converted to aerodynamic size using a pre-programmed calibration. Mass median aerodynamic diameter (MMAD) and geometric standard deviation (GSD) of spray-dried formulations were calculated using Aim® software (TSI Instruments Inc.). The APS was run at 5 L min⁻¹ compressed airflow and was equipped with two 3302 aerosol diluters in sequence.

The machine was switched on for 30 minutes prior to adjusting flowmeters to manufacturer-calibrated airflow values, which allowed stable operation. Passing monodisperse latex spheres of known MMAD through the machine checked performance of the APS. Then, samples of powder (>100 mg, either IR-TS or SR-TS) were pulled into the machine by suction from overhead

airflow and sampled for 5 seconds, 15 times. This sampling procedure was repeated in triplicate for each batch to ensure reproducibility.

6.3.4 Filling, Operation and Validation of Penn-Century DP-4 Insufflator

A Penn-Century DP-4 dry powder insufflator device (Figure 6.3.4, Penn-Century Inc., Philadelphia, PA, USA) was used as a DPI device for aerosolisation studies. The device was chosen as it can deliver small amounts of powder (<5 mg) and did not require the drug powder to be blended with carrier particles.

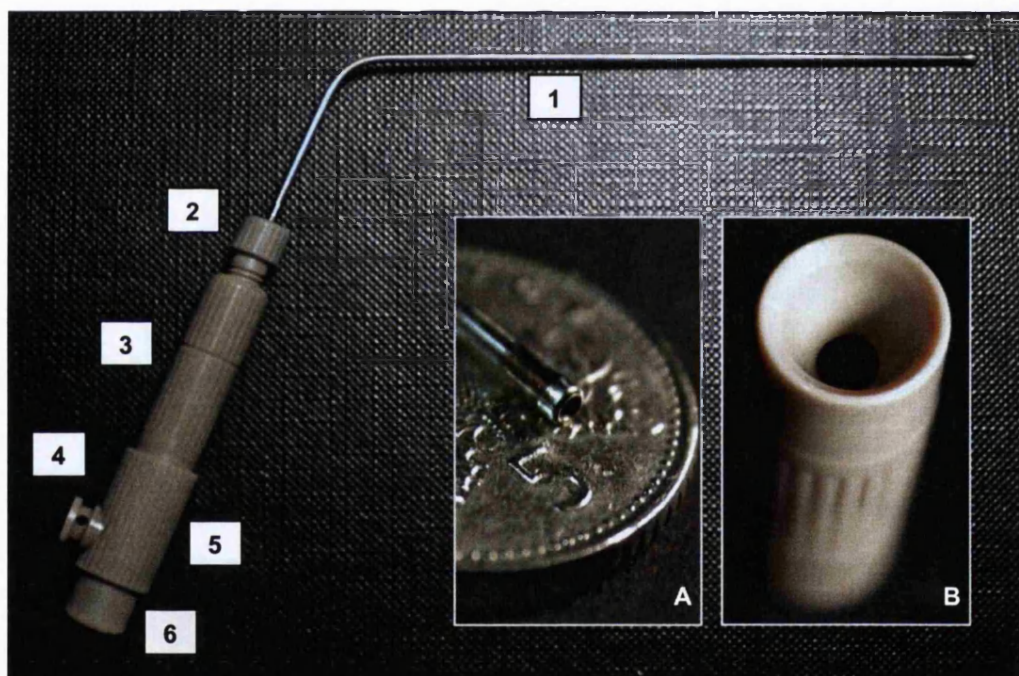


Figure 6.3.4: Penn-Century model DP-4 dry powder insufflator. 1 = Stainless Steel delivery tube: 2 = Rheodyne fitting: 3 = Sample chamber/aerosol dispersion chamber: 4 = Air Inlet valve: 5 = Air chamber + one-way silicone valve: 6 = Luer-lock connection for syringe. Inset A = Close-up of delivery tube at exit orifice (tube widened at exit). Inset B = Sample chamber close-up (sample placed in central well).

The Penn-Century insufflator is a relatively new device, which has been successfully used to deliver dry powders by intratracheal administration to a variety of small animals. For instance, Sprague-Dawley rats were vaccinated with lipophilic hollow-porous particles containing influenza virus antigen (Bot,

et al., 2001) and Wistar rats were dosed with parathyroid hormone (PTH) particles (Codrons *et al.*, 2003).

6.3.4.1 Filling and Assembly

Dry powder formulations were accurately weighed into aluminium DSC pans (Kit No. 0219-0041, Perkin Elmer Inc., Shelton, CT, USA) and transferred to the sample chamber of the DP-4 insufflator. The empty DSC pan was then reweighed to determine the amount of formulation transferred. The delivery tube was attached to the sample holder through a rheodyne fitting ensuring a tight connection. The air chamber was attached and the device was weighed. Finally, an empty 5 mL syringe was attached to the air chamber prior to use.

6.3.4.2 Determination of Emitted Dose (ED) from DP-4 Insufflator

The device was weighed pre-delivery and post-delivery. The difference in these weights was used to calculate ED, which was expressed as a percentage relative to the drug load. ED was calculated five times for each formulation tested. The effect of drug load (mg) and air bolus force through the device (evacuation of syringe with plunger) was investigated.

6.3.5 High Speed Photography

Digital photographs of powder exit from the DP-4 insufflator were captured using a Model 4500 camera (Nikon Corp., Tokyo, Japan) at a shutter rate of 70 frames per 3 sec time interval.

6.3.6 Assessment of Particle Deposition using Andersen Cascade Impaction (ACI)

For this investigation, it was decided to characterise the aerosol cloud generated directly from the DP-4 insufflator device. The ACI classifies aerosol particles (and droplets) on the basis of their aerodynamic diameters. Particle size distributions for all formulations were determined in triplicate

using an aluminium ACI (Copley Scientific Ltd. Nottingham, UK) operating at 28.3 L min^{-1} . The method for ACI operation, specifically for TS, was developed at AstraZeneca R&D Charnwood (Hargreaves, 1996). A schematic (adapted from BP, 2003) is presented in Figure 6.3.6, and the effective cut-off diameters (ECD) for each stage of the impactor are displayed in Table 6.3.6. For testing of dry powders for inhalation, pharmacopoeial methods required testing at 60 L min^{-1} in order to overcome the high resistance within DPI devices. However, as the dry powder formulation was actively propelled from the DP-4 insufflator device, a flow of 28.3 L min^{-1} was used.

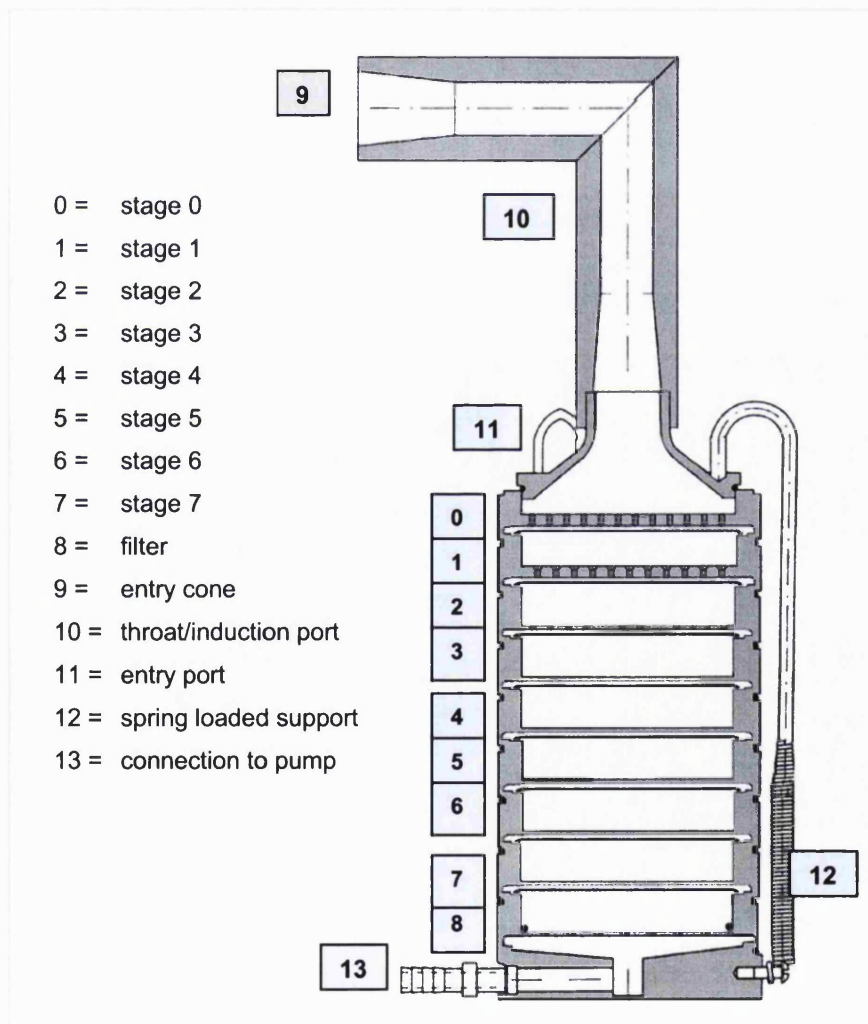


Figure 6.3.6: ACI schematic. (An impaction plate was beneath each of stages 0 through 7).

Stage	ECD (μm)
Throat	> 9.0
0	9.0
1	5.8
2	4.7
3	3.3
4	2.1
5	1.1
6	0.7
7	0.4
F	< 0.4

Table 6.3.6: ECD values for each stage when operating at 28.3 L min^{-1} .

6.3.6.1 ACI Operation Procedure

A glass fibre filter (Schiecher & Schuell GmbH, Dassel, Germany) was cut to size and sealed in place with an o-ring inside the filter stage. Glass fibre filters were chosen as they permit adequate airflow through the impactor. To ensure efficient particle capture by minimising 'bounce' (BP 2003; Miller *et al.*, 1998), coating solution (1 mL 0.15% w/v Brij 35 (aq) mixed with 5 mL glycerol) was applied thinly to each Andersen plate with a small sponge. The stages, together with the throat and entry port, were assembled and held in place using the spring-loaded support. The base was then connected to a Model 1531-176A-G445X vacuum pump (Schaefer Techniques S.a.r.l, Nozay, France), and immediately after the pump was started, airflow ($28.3 \pm 0.5 \text{ L min}^{-1}$) was measured using a model DFM2 digital flowmeter (Copley Scientific Ltd. Nottingham, UK).

With the vacuum pump running, the DP-4 insufflator was positioned with the delivery tube centrally located 1 cm inside the throat. The device was then 'fired' into the ACI by evacuating a known quantity of air from the syringe. Several air boli were then fired to ensure efficient dose delivery from the device. The pump was switched off 10 seconds following the last air bolus. The ACI assembly was then carefully dismantled. Firstly the throat and entry port were rinsed with rapid streams of 0.05 M phosphate buffer, pH 2.5, from a wash bottle. Each stage was rinsed together with the impaction plate below the stage and collected through a 20 cm diameter glass funnel into

appropriately sized volumetric flasks (100 mL for throat and stages 0-5, 50 mL for stages 6-7). The filter was then removed and placed in a vial containing 20 mL phosphate buffer. Following intermittent stirring over 5 minutes, the filter was drained and the buffer was transferred to a 25 mL volumetric flask. For IR-TS, the contents of the volumetric flasks were thoroughly mixed. A sample from each flask was taken and diluted to within the calibration range of the HPLC (Section 3.3.1) and each sample assayed for TS content in duplicate. For SR-TS, each volumetric flask was stored on a heated magnetic stirrer (40 ± 0.5 °C) for a minimum of 24 hours to permit TS release. Samples from the flasks (10 mL) were then filtered through 0.22 μm syringe filters (Millipore Ltd.) and aliquots of the filtrate were taken and then assayed as described for IR-TS. The mass of TS on each stage, throat and filter was summed and compared to the amount of TS delivered to the ACI, to ensure sufficient TS recovery (mass balance).

6.3.6.2 Calculations of FPF, MMAD and GSD (USP, 2000)

The total mass of drug (ΣA) delivered from the PennCentury device was calculated. The mass of drug deposited as a respirable dose, R (Stage 3 and below, ECD = <4.7 μm) was also calculated. The percentage of drug deposited as R, relative to ΣA was taken as the FPF.

Only drug recovered on stages 0 and below was used to calculate the MMAD and GSD. The aerosol MMAD and GSD were determined by plotting the cumulative percentage of drug less than the ECD of each plate versus the ECD, on log probability paper. MMAD was determined at the cumulative 50% value, and GSD was calculated using equation 6.3.6.2.

$$\text{GSD} = \sqrt{\frac{\text{particle size at cumulative 84.13\% value}}{\text{particle size at cumulative 15.87\% value}}}$$

Equation 6.3.6.2: Calculation of GSD. (A GSD of <1.22 refers to a monodisperse aerosol, and >1.22 , a polydisperse aerosol (Fuchs and Sutugin, 1966)).

6.4 Results and Discussion

6.4.1 Formulation of HPO Microparticles into HFA Propellants

After propellant filling, PET bottles that contained SR-TS were observed to have ideal suspension characteristics. However, within one hour the microspheres became heavily flocculated. Investigations to reduce the extent of flocculation with a range of surfactants or polymeric stabilisers at a variety of concentrations had no effect on the apparent flocculation (Figure 6.4.1.1), in both HFA propellants. Creaming of the formulation indicated that HPO microparticles had a lower density than that of the propellants.



Figure 6.4.1.1: Flocculation in HFA formulations of SR-TS microparticles (10.0 mg): 1 = surfactant free, 2 = 0.1% w/v Tween 20, 3 = 0.05% w/v Tween 20, 4 = 0.025% w/v Tween 20. Photograph taken 10 sec following vigorous shaking (10 sec). Other surfactants displayed identical behaviour.

The setback of flocculation was not overcome with surfactant addition. Therefore, attention focused on excipient solubility within the propellants. Initially, HPO samples were collected from PET bottles after 1 hr, 48 hr and 14-day exposure to the propellant (HFA-134a). SEM was used to look for morphological differences in the formulation at these time points (Figure 6.4.1.2).

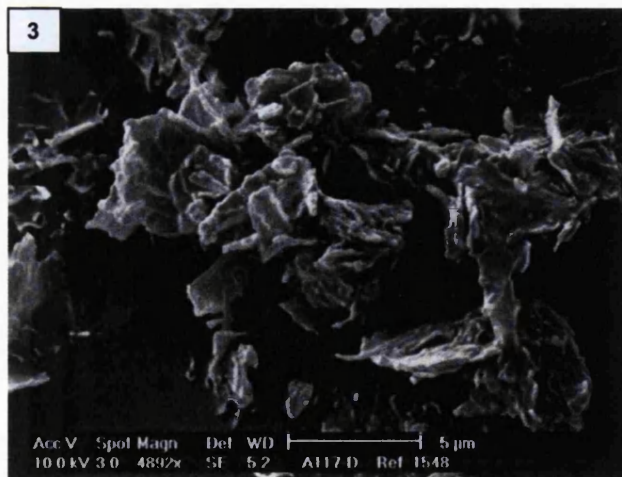
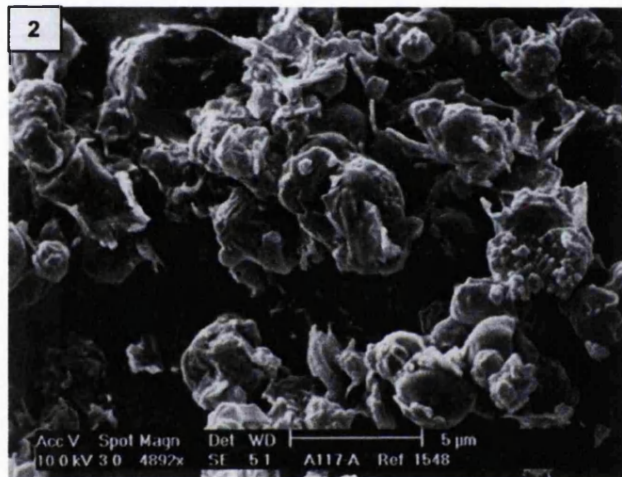
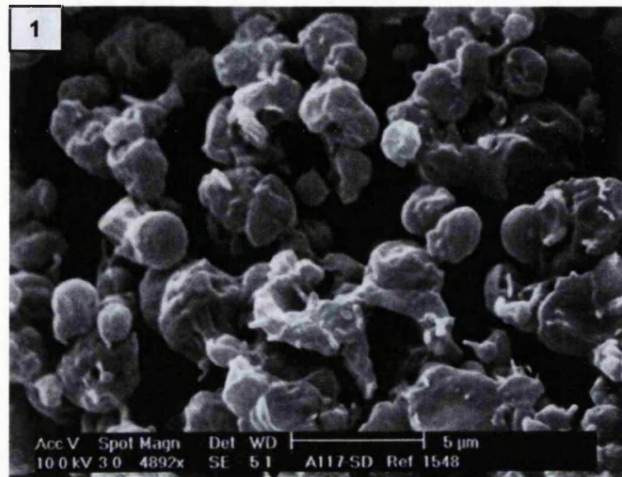


Figure 6.4.1.2: Photomicrographs of spray-dried HPO following exposure to HFA-134a for different time points: 1 = 1 hr post-filling; 2 = 48 hr post-filling; 3 = 14-day post-filling. Complete loss of structural integrity was observed after 14-day exposure length to HFA-134a.

Changes were observed in the HPO microparticle formulations that were detrimental to structure, the integrity of which was a key requirement for the maintenance of sustained release (Batycky *et al.*, 2003). It was hypothesised that partial solubility of the HPO was responsible for the changes, which permitted rearrangement of structure and particle growth (Otswald Ripening).

6.4.2 Determination of HPO Solubility in HFA Propellants

An investigation of HPO solubility in HFA-134a and HFA-227 confirmed that partial solubility of the excipient was responsible for the morphological changes (Table 6.4.2).

Propellant	HPO Solubility (% w/w) \pm SD
HFA-134a	0.034 \pm 0.011
HFA-227	0.015 \pm 0.0056

Table 6.4.2: Solubility of spray-dried HPO microparticles in HFA propellants (n=3).

Partial solubility of the hydrophobic excipient was unexpected and, despite the values for solubility appearing low, calculations highlighted the incompatibility of HPO microparticles in the HFA propellant environment e.g. for an inhaler that contained 20 mg SR-TS dispersed in 10 g HFA, 3.4 mg and 1.5 mg of the HPO content would be solubilised into HFA-134a and HFA-227 respectively.

These findings showed that HPO-based formulations were not compatible with both HFA propellants investigated, and no further work was performed for pMDI development.

6.4.3 Assessment of Aerodynamic Particle Size

The results of APS testing showed that MMAD of SR-TS was significantly smaller than IR-TS (t-Test, $p < 0.001$, Table 6.4.3). Monodisperse calibration microspheres were also tested, and the MMAD determined by the APS was identical to that recorded at the original APS installation and validation.

Formulation	MMAD (μm) \pm SD	GSD \pm SD	VMD (μm) \pm SD
IR-TS	7.56 \pm 0.42	2.32 \pm 0.038	2.96 \pm 0.067
SR-TS	3.71 \pm 0.19	2.03 \pm 0.031	2.74 \pm 0.089

Table 6.4.3: APS Aerosol characterisation of IR-TS and SR-TS formulations (n=5).

The relatively large MMAD for IR-TS was unexpected and suggested a strong tendency for cohesion. Both formulations had larger MMAD values than their respective geometric VMD values. This phenomenon was either due to insufficient particle dispersion or particle coincidence, a common error caused by two particles crossing the beam at once (Armendariz and Leith, 2002).

A recently published article (Biddiscombe *et al.*, 2003) has shown good correlation between MMAD values obtained by APS measurement and ACI for salbutamol aerosols. In light of this, an MMAD of 3.71 μm for SR-TS indicated that the microparticles were within the correct aerodynamic particle size range for pulmonary deposition, and ACI characterisation was initiated. For SR-TS, a GSD value of 2.03 is typical of a therapeutic aerosol (Schulz, 1998).

6.4.4 Validation of Penn-Century DP-4 Insufflator

Figure 6.4.4 shows that ED (loading was 0.5 mg IR-TS) increased with faster firing speed (the rate of syringe evacuation was either immediate or controlled). The results showed that rapid evacuation of the syringe was

required to ensure sufficient delivery of powder from the device (1 shot, followed by three repeats for each speed was performed).

Further shots from the device (up to 9 times after the initial firing) did not increase the ED. However, even with rapid evacuation of the syringe, only $66.1 \pm 11\%$ of IR-TS was emitted from the device - which resulted from inadequate particle dispersal from the device.

ED was significantly greater ($89.0 \pm 5.3\%$: $n=5$, t-Test, $p>0.001$) for delivery of SR-TS from the device than IR-TS (Figure 6.4.4). ED was in fact higher for the SR-TS formulation than IR-TS at all dose loadings investigated (0.5, 1, 2, 3 mg, data not shown).

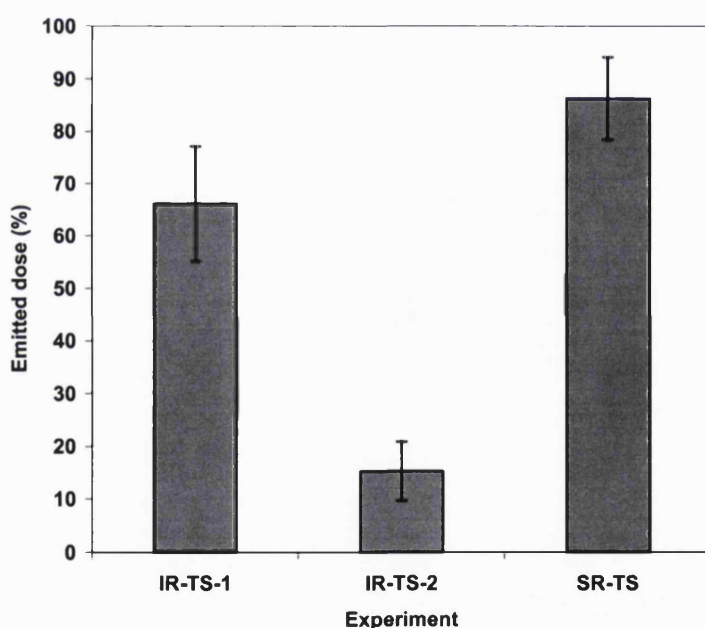


Figure 6.4.4: Delivery efficiency from DP-4 insufflator for different formulations ($n=5$): IR-TS-1 = rapid delivery of IR-TS; IR-TS-2 = controlled (slower) delivery of IR-TS; SR-TS = rapid delivery of SR-TS.

6.4.5 Assessment of Particle Deposition using Andersen Cascade Impaction (ACI)

A preliminary investigation into characterising IR-TS and SR-TS delivery from the DP-4 Insufflator showed that it was possible to overload the device as shown by greater throat deposition at the higher loadings (Table 6.4.5, Figures in Appendix B6.1 and B6.2).

Formulation	Device Loading (mg)	Throat deposition (%) \pm SD	FPF (%) \pm SD	MMAD (μ m) \pm SD	GSD \pm SD
IR-TS	0.5	4.24 \pm 0.70	71.2 \pm 5.3	3.23 \pm 0.15	1.93 \pm 0.058
IR-TS	2	25.7 \pm 5.0	40.6 \pm 7.7	4.67 \pm 0.99	2.30 \pm 0.20
SR-TS	0.5	23.3 \pm 2.2	29.7 \pm 1.8	6.63 \pm 0.67	2.53 \pm 0.42
SR-TS	2	35.8 \pm 5.4	24.6 \pm 4.6	6.3 \pm 0.96	2.00 \pm 0.00

Table 6.4.5: Throat deposition and ACI characterisation of IR-TS and SR-TS formulations from DP-4 Insufflator at two different loadings (n=3). Mass balance for all ACI investigations was within 90-112% of delivered dose which complied to set limits (Appendix 6.3, USP 2000 limits 75-125% recovery required)

Delivery of 0.5 mg IR-TS from the DP-4 Insufflator showed an ideal cascade profile. Throat deposition was minimal (<5%), FPF was remarkably high, and MMAD was suitable for pulmonary deposition. This result conflicted with the MMAD obtained from previous APS measurement for IR-TS - this suggested that the device provided more efficient aerosolisation than the APS apparatus. This was expected to result from higher airflow through the ACI relative to the APS (28.3 versus 5 L min⁻¹). Increased IR-TS loading (2 mg) greatly enhanced throat deposition (6-fold increase), which had negative effects on the FPF and MMAD. It was expected that the device was overloaded, and there was not sufficient flow to aerosolise the greater quantity of powder effectively. This was confirmed by high-speed photography that showed aggregates leaving the device when higher drug loadings were used (Figure 6.4.5). In addition, no significant difference was shown between FPF and MMAD for delivery of 0.5 mg IR-TS and 0.5 mg TS extracted from a commercial inhaler (Bricanyl[®] Turbohaler[®], Appendix B6.4).

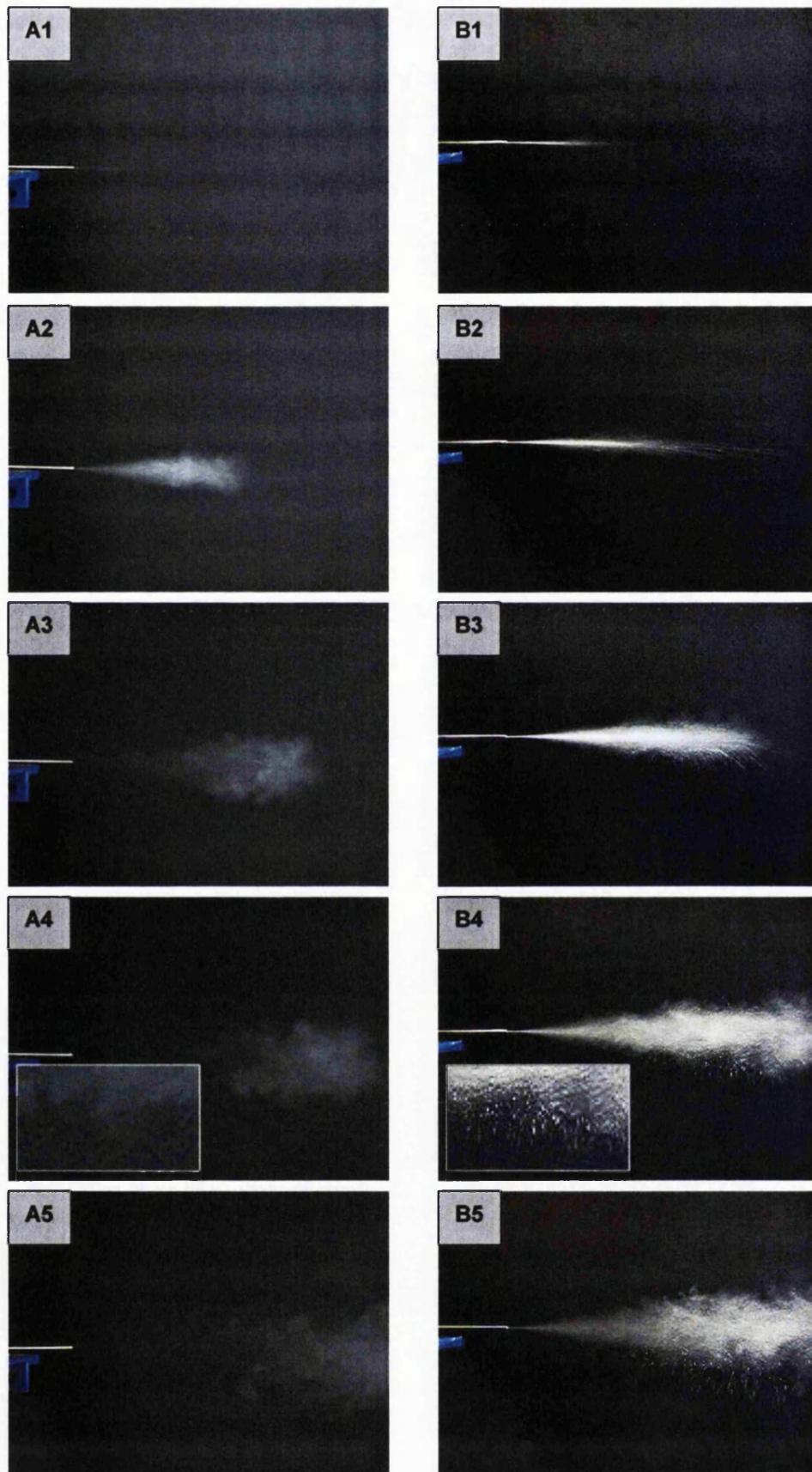


Figure 6.4.5: Delivery of SR-TS from DP-4 Insufflator: A1-A5 = 0.5mg dose load: B1-B5 = 2 mg dose load. (time/frame = 0.042 sec). Insets in A4 and B4 showed absence of aggregates for 0.5 mg but presence for 2 mg loading, which were expected to impact in the throat.

For SR-TS, aerosol performance was not as favourable as IR-TS due to low FPF and high MMAD (Table 6.4.5) Throat deposition was also increased at higher loading; however, there was no significant difference in MMAD (n=3, t-Test, p<0.05) between the these loadings. SR-TS, also, did not show correlation with MMAD measurements from the APS. The relatively large MMAD and low FPF for SR-TS required further investigations (to decrease MMAD and increase FPF) in order to reduce detrimental throat/central airway deposition (Taylor and Gumbleton, 2002).

6.4.6 Improvement of Aerosol Performance for SR-TS formulation

For *in vivo* SR-TS performance, a FPF of 25-30% would be insufficient. Therefore, the following experiments were aimed at improving the dispersibility of the powder. As firing 0.5 mg of the SR-TS formulation represented a low TS dose, it was decided to work on 1 mg as a standard dose load for SR-TS.

Immediate improvement in FPF was achieved by increasing the syringe volume (5 mL versus 3 mL) that provided the air bolus (Figure 6.4.6.1). Despite elevation of drug loading from 0.5 mg to 1 mg, FPF was significantly increased from 29.7% to 36.0% (n=3, t-Test, p<0.01) with the larger syringe volume. As the syringe was plunged immediately in each case, airflow velocity through the device was faster for the 5 mL syringe, thereby providing greater shear at the device tube exit, which deaggregated the powder more effectively. MMAD was accordingly reduced from 6.63 ± 0.67 to 5.03 ± 0.23 μm (n=3, t-Test, p<0.05). An HSO-based formulation was also evaluated (Appendix B6.5), and despite a decreased MMAD relative to the candidate formulation (4.5 ± 0.2 versus 5.03 ± 0.23 μm) and slightly higher FPF ($39.0 \pm 1.5\%$ versus $36.0 \pm 1.5\%$), the magnitude of improvement did not justify a change of excipient from HPO to HSO.

Reduction of the device exit tube diameter by approximately 50% (10 μL pipette tip attached over the device, to provide greater exit shear) was expected to improve FPF and MMAD. In fact, the reverse was true as high throat deposition ($40.0 \pm 2.8\%$) resulted in a low FPF ($26.4 \pm 2.0\%$) (Appendix B6.6)

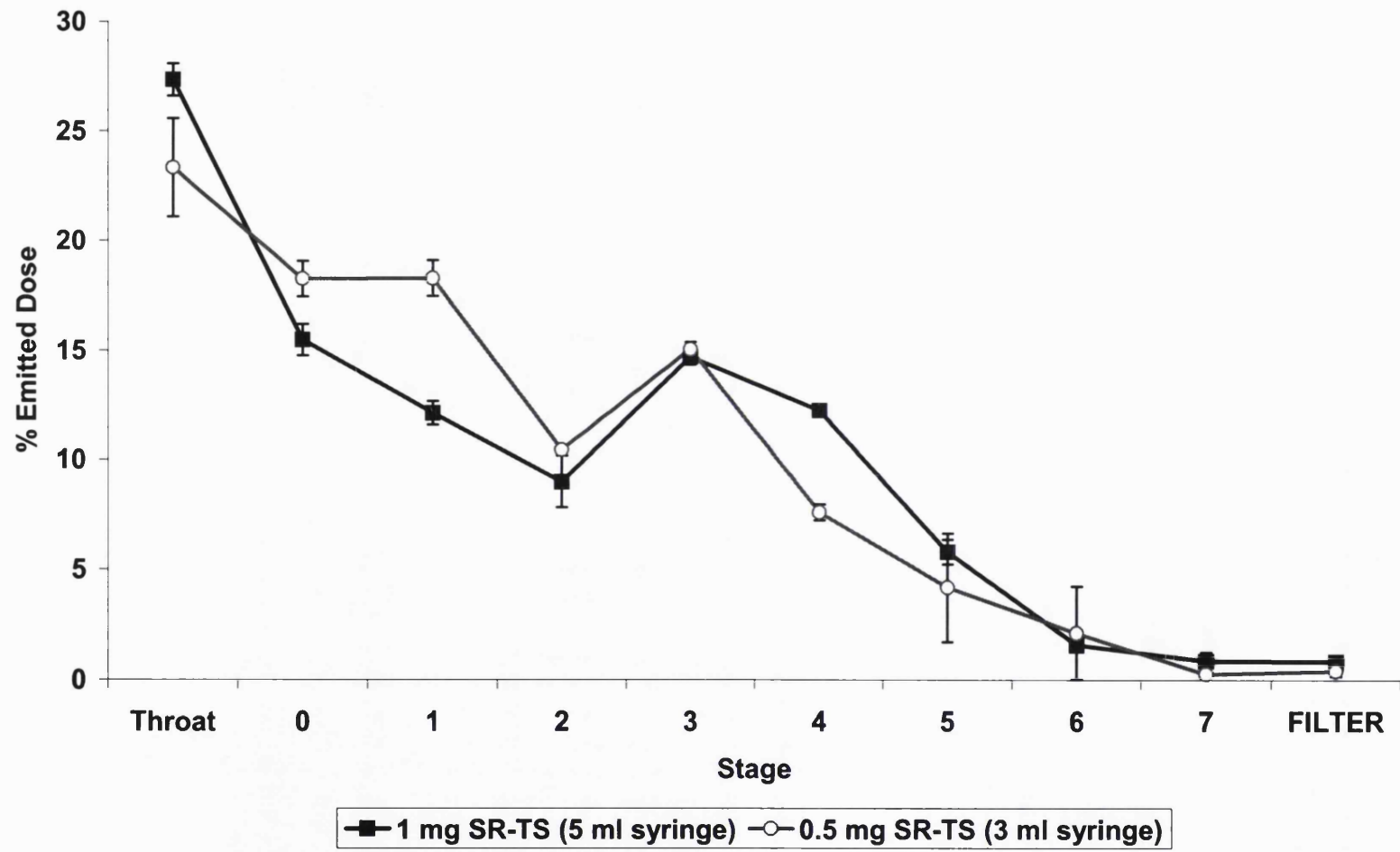


Figure 6.4.6.1: ACI profile for SR-TS delivered from DP-4 insufflator with 5 mL and 3 mL air bolus volume (n=3 ± SD).

Increased DPPC content in the formulations had substantial effects on improving aerosolisation, in terms of MMAD and FPF (Table 6.4.6.1). However, only particles that contained 2% and 3% w/w DPPC showed significant increases in FPF and reduction in MMAD. Figure 6.4.6.2 shows the changes in the ACI profile. For 3% w/w DPPC content, throat deposition was minimised ($9.95 \pm 0.82\%$) and deposition on stages 3 and above was maximised. The presence of surfactant on the surface of particles has been shown to improve dispersibility of powders (Basu *et al.*, 2001); however, another key factor was geometric microparticle size, which reduced significantly as DPPC content increased, e.g. VMD = $2.13 \pm 0.20 \mu\text{m}$ for 3% w/w DPPC microparticles versus $2.74 \pm 0.089 \mu\text{m}$ for 0.2% w/w DPPC ($n=5$, t-Test, $p<0.001$).

% w/w DPPC in Formulation	FPF (%) \pm SD	MMAD (μm) \pm SD	GSD \pm SD
0.2	36.0 ± 1.5	5.03 ± 0.23	2.33 ± 0.058
0.4	35.3 ± 1.3	4.66 ± 0.37	2.06 ± 0.058
1	40.4 ± 7.1	4.5 ± 0.44	2.06 ± 0.11
2	$57.9 \pm 1.9^\dagger$	$3.8 \pm 0.20^\dagger$	2.10 ± 0.11
3	$71.9 \pm 3.3^\ddagger$	$3.06 \pm 0.21^\ddagger$	1.73 ± 0.058

Table 6.4.6.1: ACI characterisation of SR formulations containing different amounts of DPPC ($n=3$). As DPPC content increased, FPF increased and MMAD decreased. Key for additional t-Tests: $^\dagger = p<0.01$, $^\ddagger = p<0.001$, relative to 0.2% w/w DPPC content.

No significant difference ($n=3$, $p>0.05$, t-Test) was shown between FPF and MMAD for delivery of 1 mg SR formulation containing 3% w/w DPPC and 0.5 mg IR-TS. This formulation therefore represented comparative performance IR-TS. Unfortunately, the presence of DPPC in the formulation severely compromised SR of TS (Figure 6.4.6.3). TS release from HPO microparticles containing 3% w/w DPPC displayed a large burst release of approximately 70% over 30 min. Release rate from HPO microparticles containing 1% w/w DPPC showed less burst (47% over 30 min); however, the SR profile was not one suitable for progression as *in vitro* TS release would be complete within 4 hr (by extrapolation). Therefore, despite the beneficial effect that DPPC

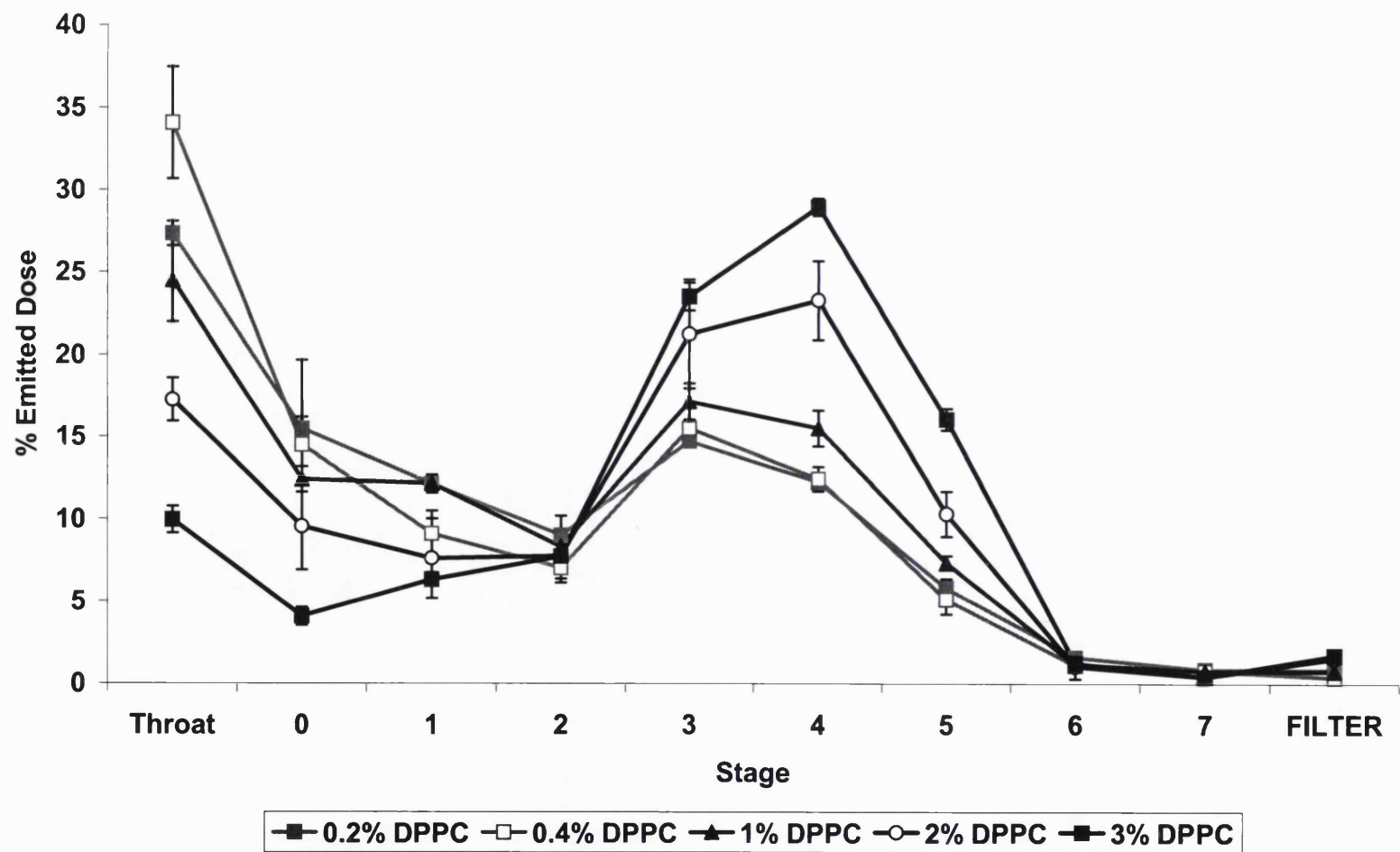


Figure 6.4.6.2: ACI profile for SR-TS formulations with increasing w/w DPPC content, as indicated ($n=3 \pm SD$). Improvement in aerosol performance was proportional to DPPC content of the particle.

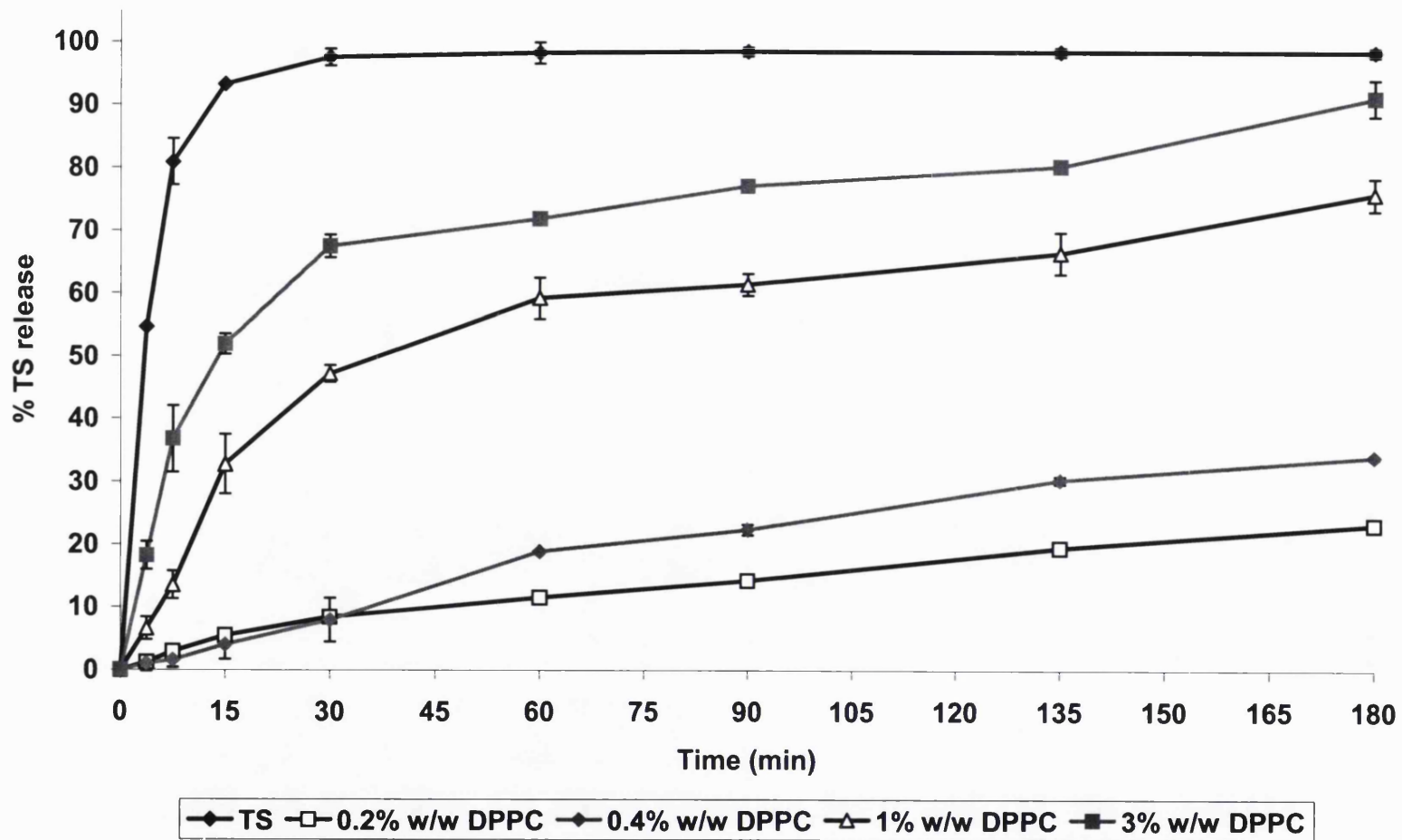


Figure 6.4.6.3: Release profile of pure TS and TS from SR-TS formulations containing increasing DPPC content ($n=3 \pm SD$, 37 °C). Burst release was evident for formulations containing 1% w/w DPPC or more.

conferred to aerosol performance, the effects were not exploited as the microparticles displayed poor SR - even at DPPC contents which offered no advantage to FPF or MMAD (e.g. 1% w/w and less). Substitution of 3% w/w DPPC with DSPC or DPPE was investigated as the higher phase transition temperatures of these phospholipids relative to DPPC have been reported to impart enhanced SR properties to pulmonary formulations (Basu *et al.*, 2001). However, for HPO-based formulations, the presence of DPPE and DSPC led to similar burst release (Appendix B7.1) as for those that contained DPPC (i.e. $t_{50} < 20$ min).

SR-TS particles were also tumbled in the presence of 5% w/w DPPC (DPPC was lyophilised in order to make the structure more friable) in order to coat the particle surface with phospholipid, but avoid the disadvantages of DPPC incorporation. FPF was significantly increased to $41.9 \pm 2.2\%$ (t-Test, $p < 0.05$) and MMAD was reduced to $4.03 \pm 0.14 \mu\text{m}$ (See Appendix B6.7). However, when the device (containing rolled particles) was fired to waste in front of a black background, it was evident that large flakes of DPPC also left the device. This effect was also observed during cascade impaction, as DPPC flakes were visible in the throat and on Stage 0. As a result, content uniformity was likely to be poor and therefore this formulation was not investigated further.

Lastly, the effect of 5% v/v acetone (ACT) in the DCM spray-drying feed was investigated. Acetone was reported to increase porosity of spray-dried microparticles (Bain *et al.*, 1999), which might improve aerosolisation performance; however, no porosity was observed in SEM images. An increase in porosity would also have been expected to increase release rate; however, there was no significant difference ($n=3$, t-Test, $p > 0.05$) between the amount of TS released at all time points for particles spray-dried from 100% DCM and those from 5% v/v acetone in DCM (Appendix B7.2). This result confirmed the absence of porosity. However, geometric particle size was reduced when acetone was present. This reduction also resulted in a reduction in MMAD and elevation in FPF, as shown in Table 6.4.6.2. The ACI profile is shown for the two formulations in Figure 6.4.6.4.

Feed (ACT:DCM)	VMD (μm) \pm SD	Throat deposition (%) \pm SD	FPF (%) \pm SD	MMAD (μm) \pm SD	GSD \pm SD
0:100	2.74 \pm 0.089	27.3 \pm 0.74	36.0 \pm 1.5	5.03 \pm 0.23	2.33 \pm 0.058
5:95	2.20 \pm 0.19	23.9 \pm 0.34	46.5 \pm 1.8	3.93 \pm 0.12	2.00 \pm 0.10

Table 6.4.6.2: Effect of 5% v/v ACT in DCM feed upon geometric particle size and aerosol performance (n=5 for VMD and n=3 for Throat deposition, FPF, MMAD and GSD).

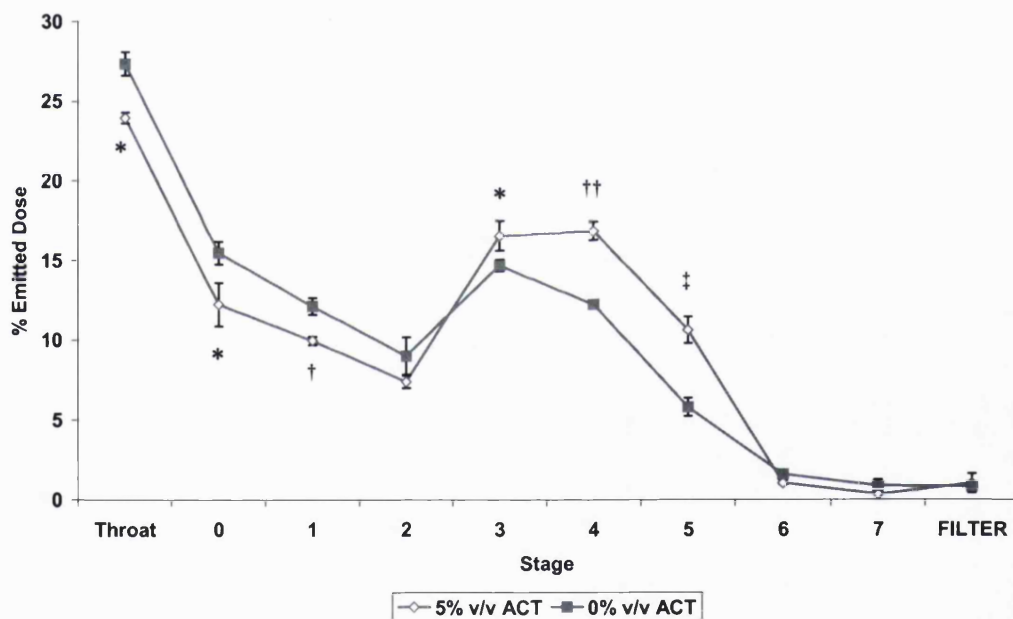


Figure 6.4.6.4: Effect of 5% v/v ACT in DCM feed, upon ACI deposition profile (n=3 \pm SD).

t-Test Key: * = p < 0.05, † = p < 0.01, ‡ = p < 0.001, †† = p < 0.0001.

6.5 Conclusion

Formulation of SR-TS microparticles into a pMDI was not successful as HPO displayed partial solubility in both HFA-134a and HFA-227 propellants, and was therefore incompatible. The solubility of the excipients was sufficient that microparticle structure was affected significantly after 48 hr and completely lost after 14 days.

Aerosol behaviour of the SR-TS formulation at first was poor (24.6% FPF), compared with excellent dispersibility shown by the IR-TS formulation (71.2% FPF). It was observed that the Penn-Century dry powder insufflator could be overloaded, which was responsible for high throat deposition when powder quantities of 2 mg powder or more were used. However, despite reducing the load into the device, no significant benefits in dispersibility were achieved for SR-TS, so the formulation was changed.

The most significant improvement in powder dispersibility was achieved by elevating the DPPC content of the SR-TS formulation, which resulted in comparable ACI profiles to that of IR-TS. However, the greater quantity of DPPC in the matrix facilitated TS release such that the SR profile was lost.

A small change in spray-drying feed solvent from 100% DCM to 5:95 ACT:DCM produced a SR-TS formulation with greater dispersibility (46.5% FPF). This FPF represents feasible aerosol performance for further characterization work e.g. *in vivo* testing. SR profiles were not affected by the change in spray-drying feed solvent.

It was difficult to compare the SR-TS formulation to other examples of modified release preparations in the literature, in particular due to the nature of dissolution testing. Aerosol performance of this system was also difficult to compare to the literature owing to the array of formulations, devices and airflows, which may be selected. However, several literature examples warrant comparison and are displayed in Table 6.5. These examples suggest that the SR-TS aerosol performance is of use in pulmonary formulation development.

Formulation	MMAD	FPF (% < 4.7 µm)	Authors
Hollow porous particles ^{S,D} 50% w/w albuterol sulphate 46% w/w DPPC 4% w/w calcium chloride	3.4 ± 0.1	66.9 ± 0.6 (% < 5.8 µm)	Dellamary <i>et al.</i> , (2000)
Large Porous particles ^{S,M} 4% albuterol sulphate 18% human serum albumin 18% lactose, 60% DPPC	10.0 ± 4.0	48.5 ± 3.7	Ben-Jebria <i>et al.</i> , (1999)
SR-TS, optimised ^{S,D} 29.5% terbutaline sulphate	3.93 ± 0.12	46.5 ± 1.8	Kellaway and Cook (2003) (Appendix C)
1% parathyroid hormone ^{S,D} 30% human serum albumin 10% lactose, 60% DPPC	4.7	46.4	Codrons <i>et al.</i> , (2003)
5.4% nedocromil sodium ^{E,D} 94.6% Poly(L-lactic acid)	2.65 ± 0.01	26.4 ± 0.66	El-Baseir and Kellaway (1998)
Poly(PEG:sebacic acid) ^{E,D} Porous microparticles with rhodamine B marker	2.9	17.4	Fiegel and Hanes (2003)

Table 6.5: Comparison of SR-TS to a selection of formulations that have been delivered into an ACI at 28.3 L min⁻¹. Key to superscript in formulation column: S = spray-dried formulation, E = particles produced from emulsification, D = DPI, M = pMDI

Chapter 7 General Discussion and Future Directions

7.1 General Discussion

Formulation of a highly water-soluble drug into microparticles for sustained release drug delivery to the lung was a clear challenge. As TS was too hydrophilic for direct incorporation into a lipophilic matrix, initial research centred on generating TS microparticles suitable for coating.

Controlled crystallization of TS (Chapter 2) led to significant reductions in particle size relative to crystals that were produced without growth retardants. Crystals prepared from PVP-ethanol systems yielded very small crystals, in some cases submicron in size. However, these crystals were in an irreversible, highly aggregated state that precluded additional processing. Poloxamer surfactants exerted less control over particle size but aggregation was absent. The particle size obtained, 3.6 μm , was not suitable for coating as the final coated particle size would be beyond that suitable for pulmonary delivery.

In a shift away from the research focus of coating pure TS particles, TS was molecularly dispersed into polysaccharide microparticles, to see whether SR could be achieved from such a system (Chapter 3). Modification of the release profile was achieved with negatively charged sulphated polysaccharides, but not with positively charged polysaccharides e.g. chitosan. This finding highlighted an electrostatic interaction between TS and the excipient, which was the expected mechanism for SR (Ranga Rao *et al.*, 1990; Bonferoni *et al.*, 1993). SR of TS from polysaccharide microparticles, however, was not sufficient as release rates from more biocompatible (lower molecular weight) polysaccharides were too fast, especially with spray-dried microparticles in a size range suitable for inhalation. Moreover, release studies were performed at ambient temperature - an increase to physiological temperature would increase the TS release kinetics and reduce SR. It was concluded that a significantly more hydrophobic matrix was required to generate SR microparticles containing TS.

The application of granule coating with hydrophobic excipients for oral formulation is established (reviewed by Achanta *et al.*, 1997) and provides favourable SR profiles. However, SR dosage forms for oral delivery are typically 4000 times larger than the particle size required for pulmonary delivery (~1 cm versus 2.5 μm). In order to develop a SR microparticle formulation for pulmonary delivery, the drug 'granules' would have to be in the nanometre size range. Investigations therefore centred on the generation of high purity TS nanoparticles.

The preparation of TS nanoparticles using an emulsion-template method was investigated (Chapter 4). Initial research generated TS particles >1 μm in size. Process variables during emulsification (homogenisation speed, surfactant concentration and drug concentration) were therefore studied to optimise the method for generating smaller nanoparticles. The final optimised particle size achieved was 238 ± 14 nm; which, at ten times smaller in size than the expected SR microparticles, was an ideal size for progression. Purity of the nanoparticles was increased from $86.3 \pm 0.92\%$ to $101 \pm 1.4\%$ by repeating a centrifuge washing cycle in acetone to remove residual Span 60 from the emulsion process. The TS nanoparticles were shown to be amorphous using XRPD although this finding was not conclusive due to the small particle size; however, a clear glass transition observed for the TS nanoparticles (DSC) at 68.9 ± 0.4 °C confirmed the amorphous state.

The nanoparticles were dispersible in organic spray-drying feed solvents. No sedimentation occurred post-dispersion as the nanoparticles had a similar density to the feed solvent chosen. GB as a coating excipient has provided sustained release in hot-melt coating and solid lipid nanoparticle technology, and was therefore chosen as a spray-drying SR excipient. However, TS release from the spray-dried microparticles suffered from large burst effects. Subsequent addition of TP to the GB formulation improved the SR release profiles. Storage time had a strong effect on release rate since fresh microparticles exhibited burst release whereas microparticles that had been stored at 25 °C for 7 days and longer showed no burst. DSC scans of the microparticles showed that the microparticles contained an unstable

polymorphic form, which permitted burst release. A literature review of fat and oil polymorphism revealed that the unstable polymorph was the α -form open-crystal structure of TP (Hagemann, 1988). Thermal conditioning of the microparticles at 35 ± 0.5 °C for 48 hours permitted recrystallization of the unstable α -form to the more stable β' form, the structure of which provided SR barrier properties. Unexpectedly, release at physiological temperature (versus ambient temperature), drastically reduced SR performance of the matrix as TS was released very rapidly in the first 15 minutes. Microparticles that were spray-dried without lecithin did not suffer from the same burst release effects at physiological temperature; however, SR performance was still compromised.

HPO was selected as a more hydrophobic excipient, and favourable SR was achieved at physiological temperatures. In fact, HPO-based microparticles released TS at a slower rate than GB:TP microparticles, despite a three-fold increase in drug loading. Release of TS from the HPO microparticles was proportional to drug loading, displayed an absence of burst release, and adhered to diffusion-based matrix release kinetics, as described by Higuchi (1963). Absence of burst release inferred that coating was integral and provided an effective barrier to the aqueous environment. Preliminary CLSM studies with HPO microparticles (containing fluorescent labelled TS nanoparticles) showed an absence of nanoparticles in the first 400 nm depth of the HPO matrix, which confirmed coating performance. The nanoparticles beyond the first 400 nm were well dispersed through the remaining microparticle. However, CLSM data should be used with caution as the machine was operating at the limit of resolution owing to the size of the nanoparticles.

TS release profiles were not affected by release media that were more representative of the lung environment (SILF and SSLF). SR would therefore be anticipated *in vivo*. However, it cannot be assumed that the *in vitro* horizontal diffusion cell results would mimic *in vivo* data. When administered in aerosol form during *in vivo* experiments, the formulation would be effectively dispersed across the large epithelial surface area of the lung, and

one might expect faster release profiles. If release profiles were too fast, the drug loading would be reduced to provide greater SR, as indicated in Figure 5.5.1.2. On the other hand, the diffusion cell was a stirred system and the depth of release media on top of the membrane was expected to be greater than the epithelial lining fluid depth, such that release could be faster *in vitro*. If subsequent release was too slow *in vivo*, the release rate could be increased by increasing the drug:excipient ratio, or by increasing the phospholipid content as shown in Figure 6.4.6.3. In either case, it must be considered that the model drug used, TS, being ionized, hydrophilic and of low molecular weight represents the most challenging of molecules to incorporate into a pulmonary SR formulation. This implies that release rates for less hydrophilic, non-ionized and high molecular weight drugs would be slower.

Content uniformity of TS within the HPO microparticles was well within pharmacopoeial limits. Optimisation of particle size by varying spray-drying parameters showed that temperature had a significant effect. A restrictive 'window' for the spray-drying inlet temperature existed at 52-53 °C as spray-drying at 48-49 °C produced larger particles, and 60-61 °C yielded highly fused particles due to melting of the excipient. Any significant effect on particle size from the variation of aspiration, feed concentration and pump rate was hidden by the variable nature of the spray drying process, which produced particle VMD values between 2.99 and 3.45 µm (Appendix B4.1). Incorporation of 0.2% w/w DPPC (based on solid content of feed solvent) slightly reduced particle size further and improved variability between batches (VMD = 2.74 ± 0.089 µm, n=5).

As discussed, HPO offered SR at physiological temperature, but the GB:TP matrix performed poorly. DCA measurements showed that lecithin containing GB:TP microparticles were more susceptible to wetting which, in part, explained faster TS release. An investigation with lecithin-free GB:TP microparticles using DVS at pseudo-pulmonary conditions showed that the GB:TP microparticles adsorbed more vapour than the HPO microparticles (% mass change = 102.7 ± 0.30 versus 100.3 ± 0.088, respectively). Both the

DCA and DVS experiments only provided hints towards why SR performance was improved with HPO-based microparticles. An in-depth investigation using both techniques is required to generate more data on differences between the excipients.

A TS loading of 30% w/w in the HPO microparticles did not change the melting point (and range) of HPO, which showed an absence of interaction between drug and excipient. However, a DSC thermal profile of freshly prepared HPO microparticles showed a very small process-induced endothermic melting point followed by an exothermic recrystallization (Figure 5.4.5.1). Upon storage the transitions were minimised without apparent effects on TS release profile or particle size; however, controlling the transitions or removing them entirely would enhance process reproducibility. For instance, Chickering III *et al.*, (2001), describes a spray-drying process in which a secondary heated drying chamber is used in the spray drying process to extend drying particle residence time - this additional time might be sufficient to allow recrystallization of the excipient.

Development of a DPI formulation was initiated after it was clearly shown in pMDI development that HPO had partial solubility in both HFA propellants, and was therefore incompatible due to the severe changes in particle structure. Aerosol performance was assessed from an insufflator (Chapter 6), which yielded results designed to assess *in vivo* performance and acted as a simulation for aerosol delivery (Hickey and Garcia-Contreras, 2001).

MMAD was determined for pure drug, and the SR formulation, with APS apparatus. The results were favourable for the SR formulation, which had a smaller MMAD than the pure, micronised drug ($3.71 \pm 0.19 \mu\text{m}$ versus $7.56 \pm 0.42 \mu\text{m}$, respectively). However, the reverse was true for early ACI investigations - despite a low ED for the pure drug, MMAD and FPF were excellent ($3.23 \pm 0.15 \mu\text{m}$ and $71.3 \pm 5.3\%$, respectively). The SR formulation, despite having a high ED, had a large MMAD and low FPF ($6.63 \pm 0.15 \mu\text{m}$ and $29.7 \pm 1.8\%$). The results were surprising given the APS data, and suggested that the insufflator did not overcome adhesive forces

between the SR microparticles. Such high throat deposition and central airway deposition would be unacceptable for *in vivo* SR performance given that the majority of the microparticles would be subject to rapid mucociliary clearance. Increasing the air bolus through the insufflator from 3 ml to 5 ml, and adjusting the spray-drying feed solvent to contain 5% v/v acetone improved aerosol performance, which yielded an encouraging MMAD and FPF of $3.93 \pm 0.12 \mu\text{m}$ and $46.5 \pm 1.8\%$, respectively. These figures imply that a favourable amount of SR formulation would reach the bronchiolar and alveolar non-ciliated regions where extended residence would be expected to occur (Byron, 1986).

In conclusion, the present study has proven the concept of encapsulating hydrophilic drug nanoparticles into a hydrophobic microparticle to achieve SR. The technology therefore represents an addition to pulmonary formulation strategies.

7.2 Future Directions

A. Controlled crystallization remains a viable alternative to crystallization/micronisation, as the addition of growth retardant during crystallization limits particle size to that suitable for inhalation. Crystals may be readily dispersible in HFA propellants with or without additional surfactant, and further work is warranted.

B. For nanoparticle development, the fact that the nanoparticles are produced in an amorphous state may pose long-term stability issues. Alternatively, (1) the emulsion-template method could be slightly adapted to a solvent-diffusion method where a bridging solvent, e.g. acetone, could precipitate TS nanocrystals from the aqueous emulsion droplets, or (2) nanoparticles of TS could be produced from SCF technology. Nanoparticles might also be directly dispersed into HFA inhalers, providing suitable surfactants were chosen. The process could also be adapted to produce peptide/polypeptide/protein nanoparticles.

C The only excipient for pulmonary drug delivery approved by regulatory bodies is lactose, an excipient that will not provide sustained release. It would therefore be necessary to evaluate the toxicology of the SR excipient, in this case, HPO. Such evaluations would necessitate great investment of resources by the pharmaceutical industry to obtain regulatory approval (Hickey, 2003). Palm oil is the second largest consumed vegetable oil in the world (Edem *et al.*, 2002) and has an oral LD50 in rats of >5 g/Kg (Johnson and Slaga, 2000) which highlights promising low toxicity. Also, HPO holds 'generally regarded as safe' (GRAS) status for use in oral and rectal pharmaceutical dosage forms (FDA, 1996). However, because toxic effects on the respiratory tract are of concern following inhalation, a multitude of tests should be employed to ensure safety (Hickey and Garcia-Contreras, 2001). These include specialised animal testing for hypersensitivity, reprotoxicity, genotoxicity and carcinogenicity (Rosario and Otulana, 2003). Guidelines for testing excipients for inhalation are reviewed by Tamulinas and Leach (2000). More simple preliminary checks for excipient acceptability may be achieved by testing the effect of formulations on histology and bronchoalveolar lavage fluids from *in vivo* experimentation (Hickey and Garcia-Contreras, 2001) or effects upon cell lines relevant to the respiratory tract (Forbes *et al.*, 2000).

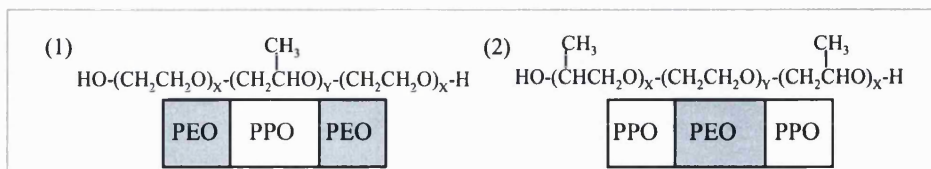
D It is necessary to investigate the extent to which phagocytosis of the SR formulation occurs in the alveolar compartment, as high levels of phagocytosis will impair SR performance. The optimised formulation contains 0.2% w/w DPPC, but it is unknown at this stage how much of the phospholipid is present at the surface. Further testing is required which could use methods described in work by Evora *et al.*, (1998), and Jones *et al.*, (2002).

E Residual solvent in the HPO/TS microparticles may arise from two sources: (1) contamination with chloroform from nanoparticle production - although this is expected to be insignificant and (2) the spray-drying process using dichloromethane. DCM is classed in the British Pharmacopoeia (BP, 2003) 'solvents to be limited' list with a permitted daily exposure (PDE) of 6.0

mg/day. Although residual DCM was not quantified for the HPO/TS particles, exposure of this magnitude is clearly not possible with the formulation described, as only 6.67 mg of the SR formulation (assuming 30% w/w loading) would be required to provide a daily TS dose equivalent to the maximum inhaled daily dose of the free drug (500 mcg, four times daily). The preferred method of residual solvent testing is headspace analysis by gas chromatography (reviewed by B'Hymer, 2003). If residual DCM levels were high, the following steps could be taken: (1) spray-drying could be carried out at an elevated temperature as this would be expected to reduce residual solvent content; although, as evident in the results, higher temperatures would require a change in excipient, e.g. to HSO, (2) the spray-drying solvent could be substituted with less toxic halothane or if a nitrogen based spray-drying system was used, greater proportions of acetone could be used.

Appendix A Poloxamer Terminology and Structure

Poloxamers are non-ionic polymeric surfactants, which are triblock copolymers of poly(ethylene oxide) (PEO, hydrophilic) and poly(propylene oxide) (PPO, hydrophobic). The structures are shown in Figure A1.



A1: (1) Structure of poloxamer surfactant. (2) Structure of reverse-poloxamer surfactant. Key: PEO = poly(ethylene oxide), PPO = poly(propylene oxide).

Nomenclature (BASF system for Pluronic® poloxamers):

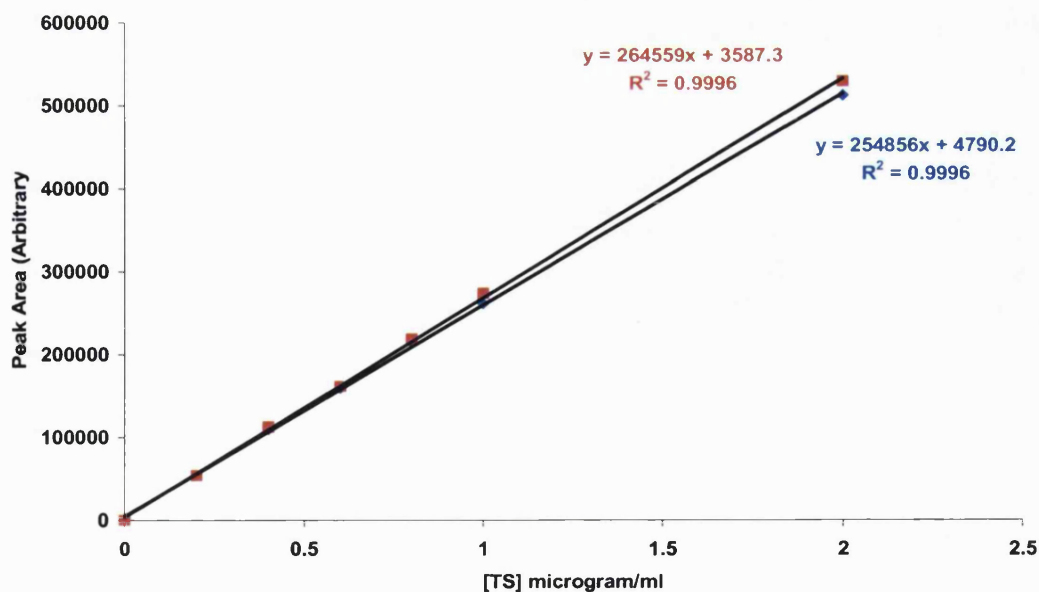
Poloxamers: e.g. L44, L64, L101, P104, F68, F128.

L, P and F, refer to the physical forms liquid, paste and solid respectively. The first (or 2 in a three digit number), multiplied by 300 gives the approximate molecular weight of the PPO chain, and the final digit when multiplied by 10 gives the PEO content (%).

Reverse poloxamers: e.g. 10R5, 17R2, 25R4.

First 2 digits when multiplied by 100 yields the approximate molecular weight of the PPO chain. The R refers to the reverse structure compared to poloxamers, and the final digit when multiplied by 10 gives the PEO content (%).

Appendix B1 HPLC calibration curve for TS



B1: Peak area versus TS concentration for HPLC assay. Working standards were selected at 1 µg/mL, and samples were typically diluted to <1.5 µg/mL.

Appendix B2 HPLC Notes

B2.1: Washing Procedure for Silica-Based Reversed Phase Column

The column was disconnected, connected to the pump in reverse flow with the other end of the column running to waste (detector bypassed). Flow was set at 1.5 mL/min.

- 1) 10 mL water
- 2) 30 mL methanol
- 3) 30 mL acetonitrile
- 4) 30 mL propan-2-ol
- 5) 30 mL dichloromethane
- 6) 30 mL methanol
- 7) 10 mL water
- 8) mobile phase

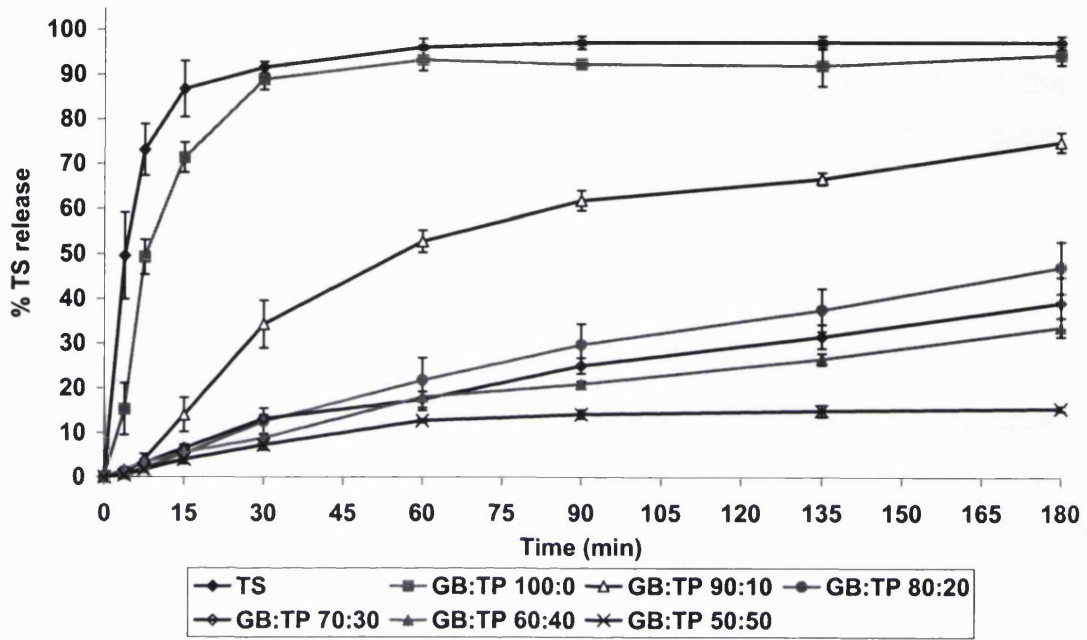
B2.2: HPLC Assay Details for Ipratropium Bromide (IB)

HPLC analysis was carried out using a reverse phase Supelco Kromasil C18 column, with UV detection at 220 nm. The flow rate used was 1 mL/min with an injection volume of 0.2 mL.

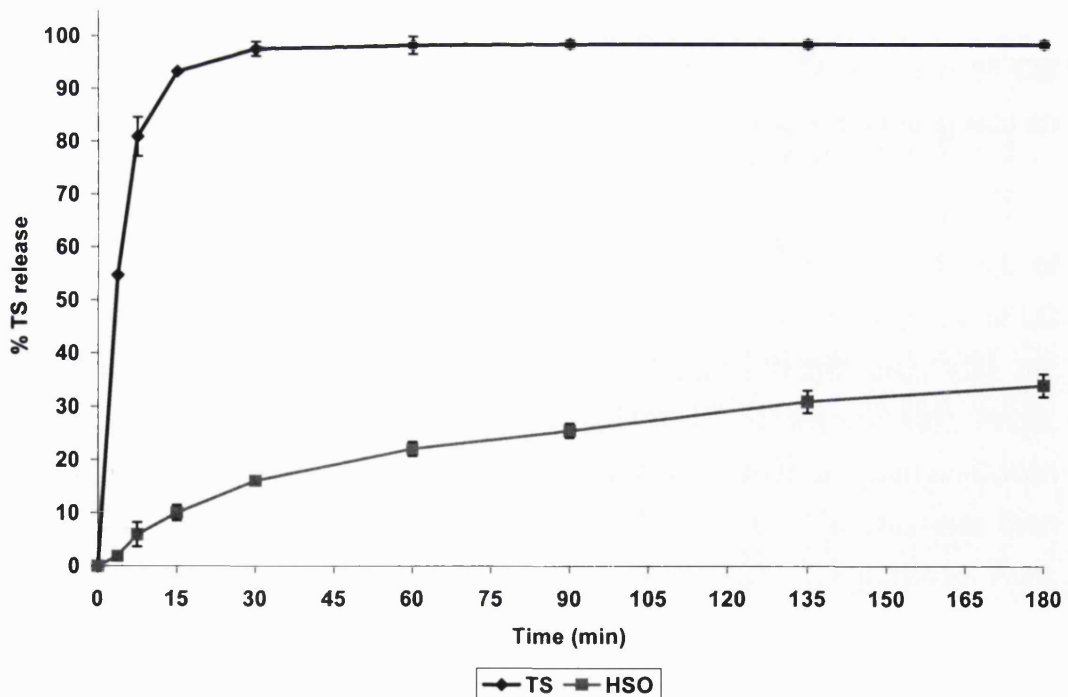
Mobile phase consisted methanol/acetonitrile 32:20. Therefore, 1000 mL of mobile phase contained 320 mL methanol, 200 mL acetonitrile (both HPLC Grade, Fisher Scientific Ltd., Loughborough, Leicestershire, UK), 3.34 mL triethylamine and 1.38 mL acetic acid (both VWR International Ltd., Poole, Dorset, UK) made up to 1000 mL with distilled water, dispensed from an Option 4 purifier (Elga Ltd., High Wycombe, Buckinghamshire, UK). This was then filtered using a 0.2 µm nylon membrane filter (Whatman Ltd., Maidstone, Kent, UK) and then stored at 5 °C until needed.

Sample quantification was achieved by reference to a standard solution containing 3.2 µg/mL ipratropium bromide. The standards were made up to volume with distilled water (Retention time = 4.9 min).

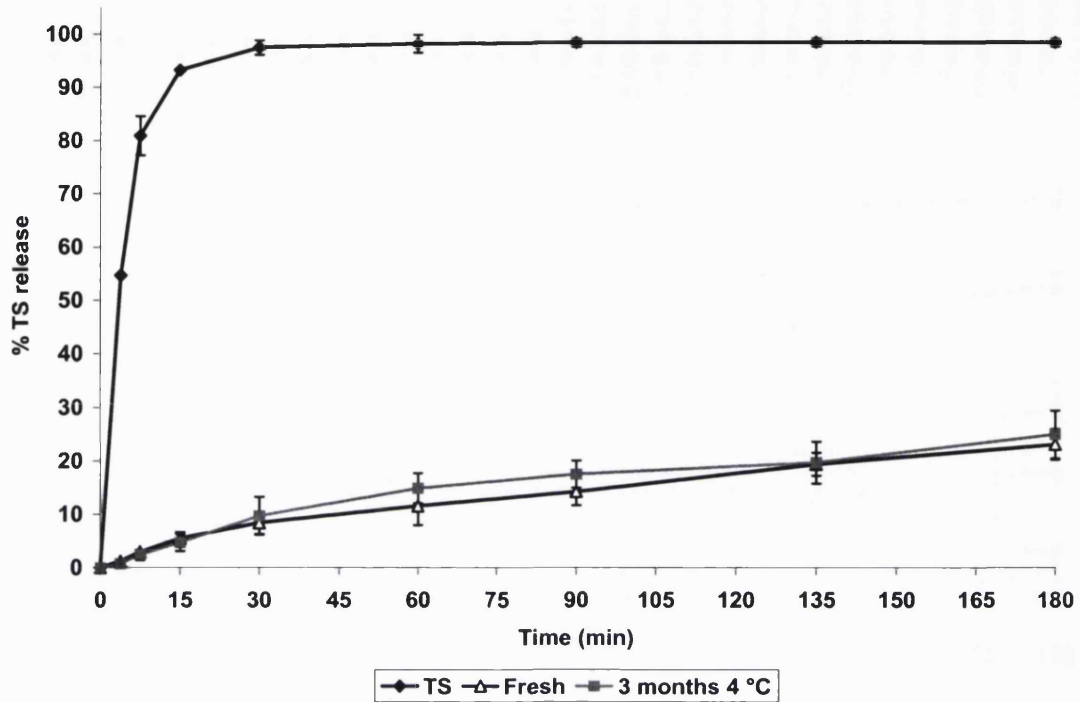
Appendix B3 Additional TS release profiles for Chapter 5



B3.1: % Release of pure TS and TS from GB:TP microparticles) following storage. (n=3 ± SD, ambient). Data showed that GB did not exert control over TS release.

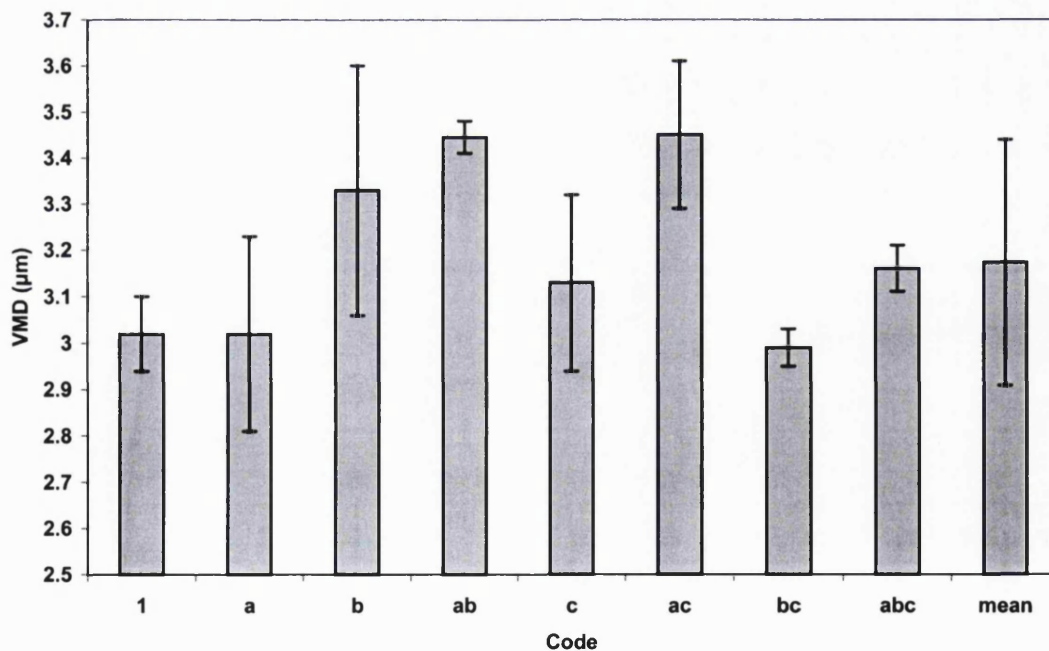


B3.2: Release of TS from HSO microparticles. (n=4 ± SD, 37 °C). HSO may be spray-dried at higher temperatures due to its higher melting point than HPO.

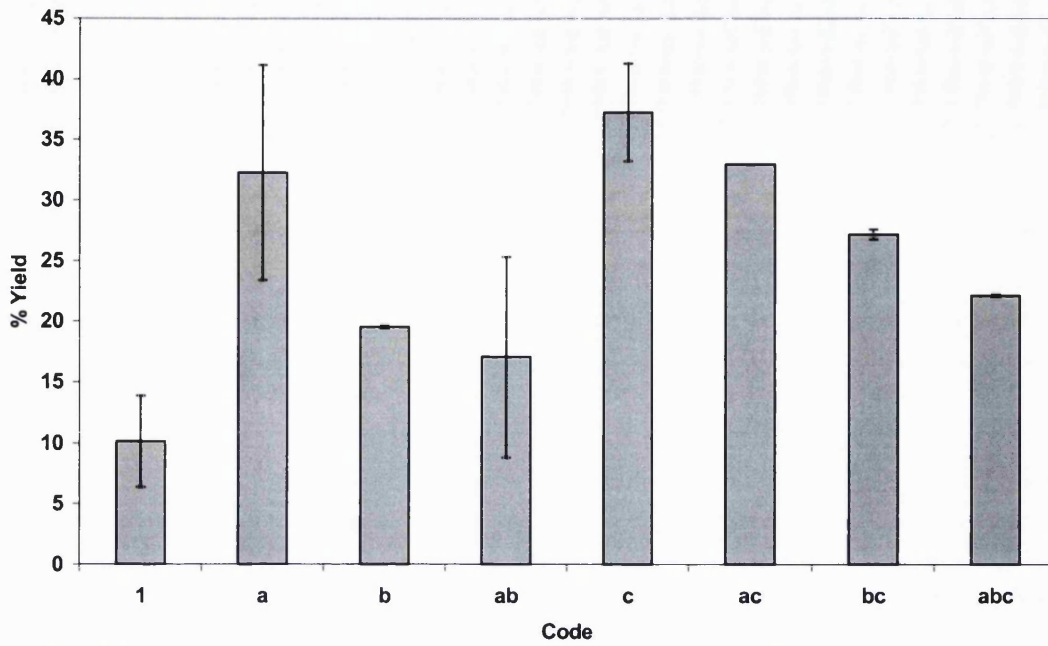


B3.3: Release of TS from HPO microparticles. (n=6 ± SD, 37 °C). No changes in release profile were observed after storage at 4 °C for three months.

Appendix B4 Factorial Design Experimental Results

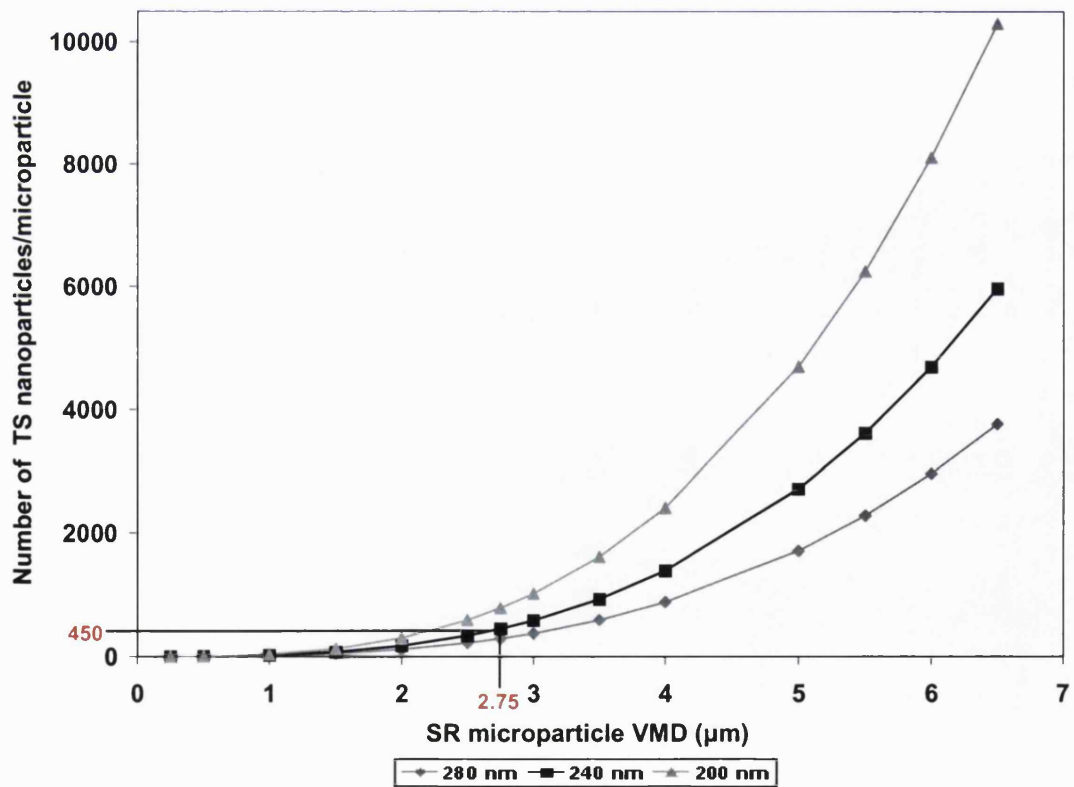


B4.1: Effect of experimental variables (for abbreviations, see Table 5.5.3.1) on VMD. Intra-batch variation was large as indicated by error bars.



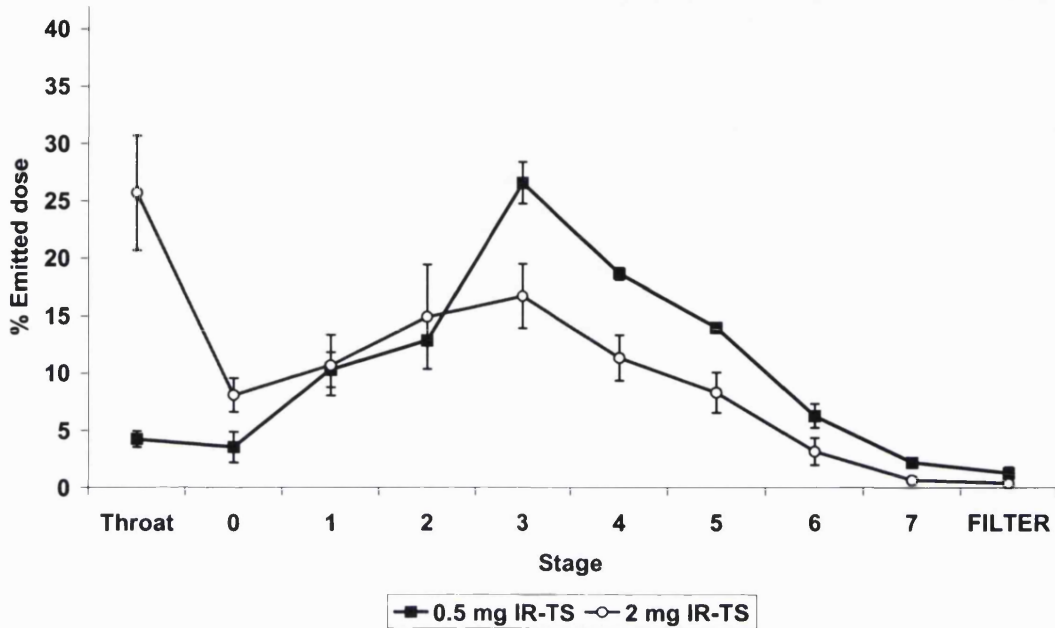
B4.2: Effect of experimental variables (for abbreviations, see Table 5.5.3.1) on yield.

Appendix B5 TS nanoparticle loading (Section 5.5.8)



B5: Estimation of number of nanoparticles (different sizes) versus microparticle size for 30% w/w drug loading.

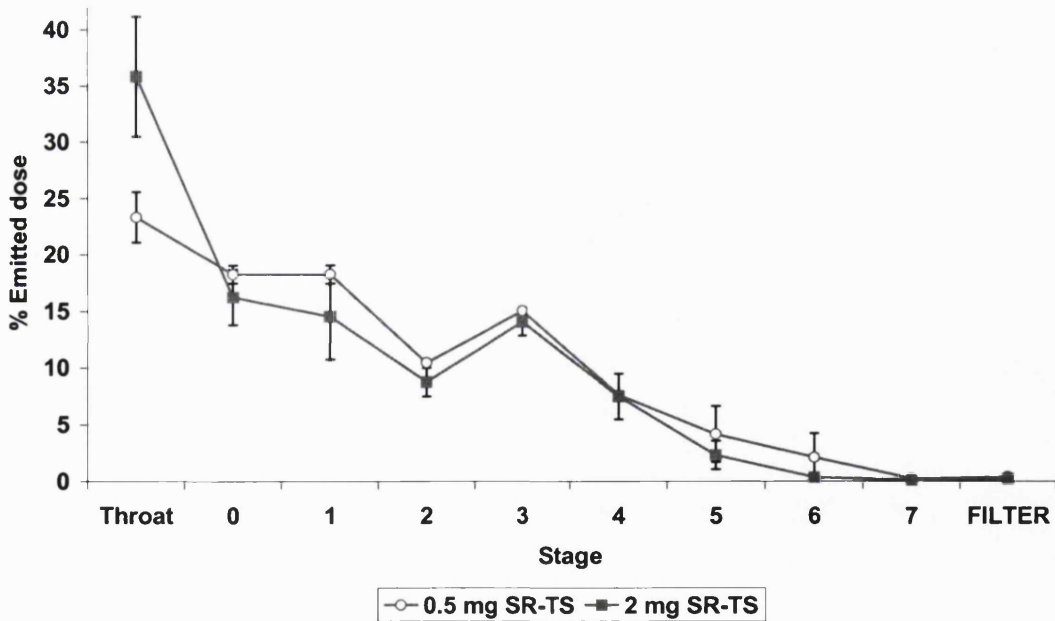
Appendix B6 Additional ACI data from Chapter 6.



B6.1: ACI Deposition profile of IR-TS at two different device loadings ($n=3 \pm SD$). 2 mg IR-TS displayed significantly greater throat deposition ($n=3$, t-Test, $p<0.001$).

0.5 mg IR-TS: FPF = 71.2 ± 5.3 , MMAD = 3.23 ± 0.15 , GSD = 1.93 ± 0.058

2 mg IR-TS: FPF = 40.6 ± 7.7 , MMAD = 4.67 ± 0.99 , GSD = 2.30 ± 0.20



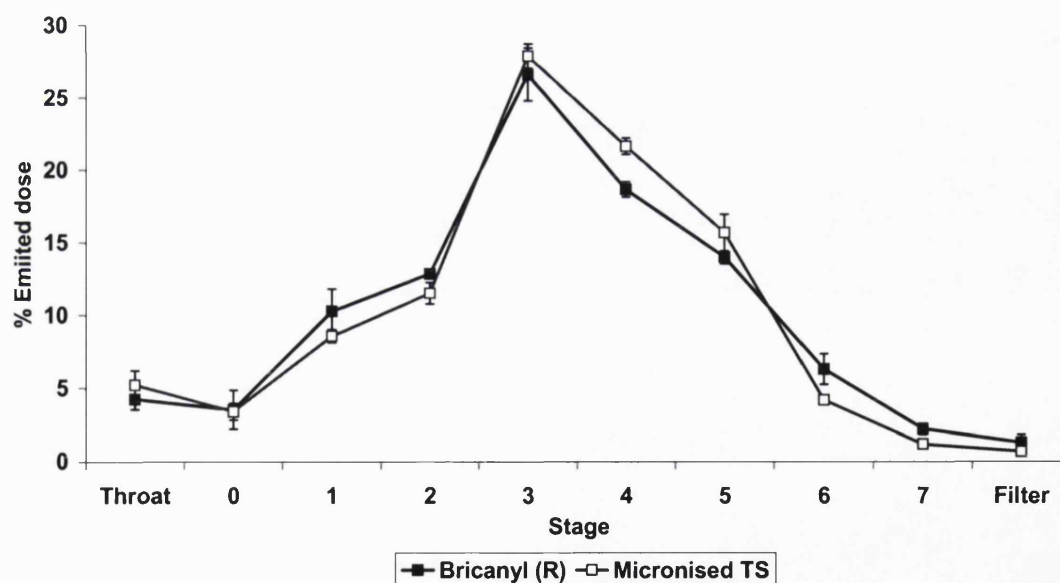
B6.2: ACI Deposition profile of SR-TS at two different device loadings ($n=3 \pm SD$). 2 mg SR-TS displayed significantly greater throat deposition ($n=3$, t-Test, $p<0.05$). MMAD for both formulations however, was not significantly different ($n=3$, t-Test, $p>0.05$).

0.5 mg SR-TS: FPF = 29.7 ± 1.8 , MMAD = 6.63 ± 0.67 , GSD = 2.53 ± 0.42

2 mg SR-TS: FPF = 24.6 ± 4.6 , MMAD = 6.30 ± 0.96 , GSD = 2.00 ± 0.00

Formulation	Amount (mg)	Run	Run	Run	ED (%) ± SD	TS Recovery (%) ± SD
		1	2	3		
IR-TS	TS loaded	0.62	0.61	0.63		
	TS emitted	0.33	0.34	0.38	56.5 ± 3.6	91.0 ± 6.2
	TS collected	0.316	0.319	0.32		
SR-TS 5:95 ACT:DCM feed	Dose loaded	0.99	1.03	1.01		
	Dose emitted	0.95	0.87	0.88	89.1 ± 6.0	93.3 ± 3.5
	TS emitted	0.28	0.26	0.26		
	TS collected	0.250	0.247	0.249		
SR-TS, containing 3% w/w DPPC	Dose loaded	1.00	1.04	1.02		
	Dose emitted	0.89	0.85	0.91	86.6 ± 4.3	97.2 ± 8.5
	TS emitted	0.27	0.25	0.27		
	TS collected	0.252	0.268	0.248		

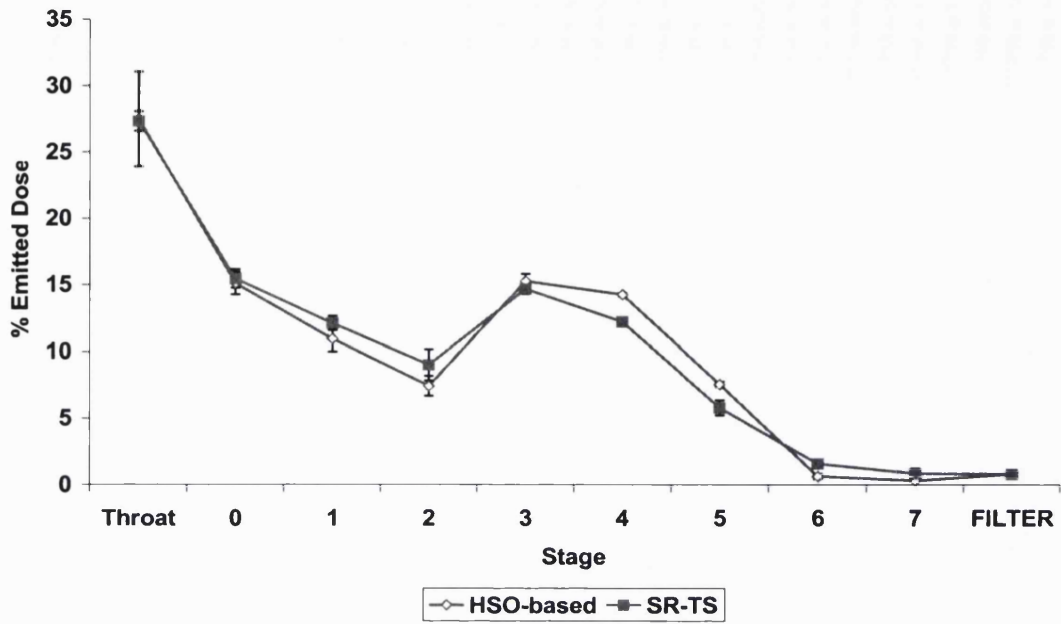
B6.3: Representative mass balance data from ACI investigations.



B6.4: ACI Deposition profile of 0.5 mg IR-TS and 0.5 mg TS extracted from a commercial inhaler (Bricanyl® Turbohaler®, AstraZeneca Ltd., Luton, Bedfordshire, UK) (n=3 ± SD).

IR-TS: FPF = 71.2 ± 5.3, MMAD = 3.23 ± 0.15, GSD = 1.93 ± 0.058

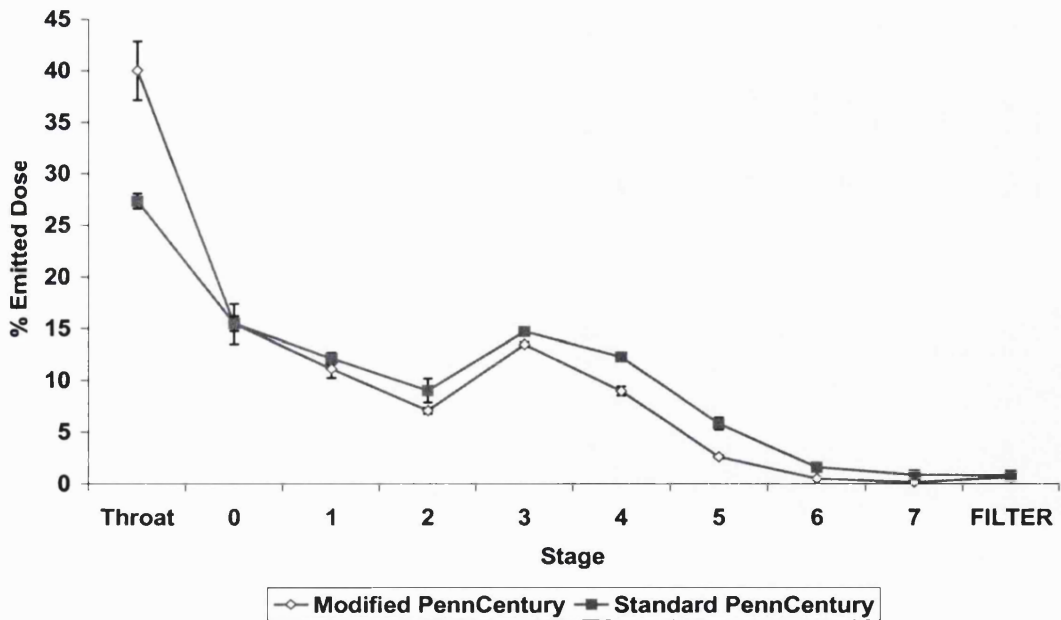
Bricanyl: FPF = 69.1 ± 2.9, MMAD = 3.27 ± 0.15, GSD = 2.13 ± 0.058



B6.5: ACI Deposition profile for HSO-based formulation and SR-TS (HPO) (n=3 ± SD)

SR-TS: FPF = 36.0 ± 1.5, MMAD = 5.03 ± 0.23, GSD = 2.33 ± 0.058

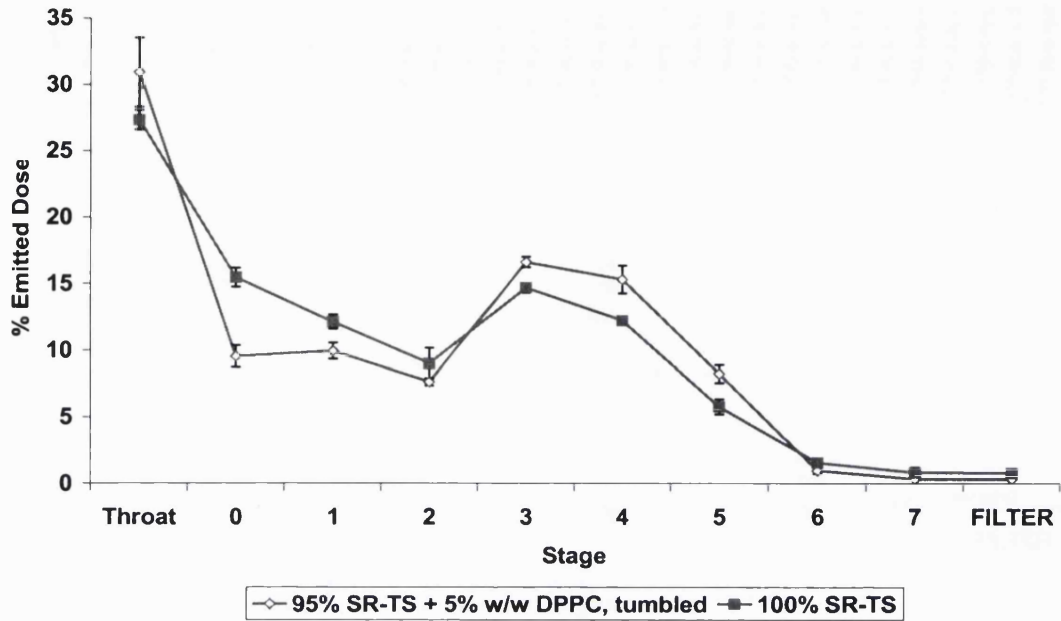
HSO-based: FPF = 39.0 ± 1.5, MMAD = 4.50 ± 0.20, GSD = 2.03 ± 0.12



B6.6: ACI Deposition profile of SR-TS from standard (unmodified PennCentury device) and from PennCentury device modified with 10 µL pipette tip. (n=3 ± SD).

SR-TS: FPF = 36.0 ± 1.5, MMAD = 5.03 ± 0.23, GSD = 2.33 ± 0.058

SR-TS modified device: FPF = 26.4 ± 2.0, MMAD = 5.70 ± 0.36, GSD = 2.13 ± 0.058



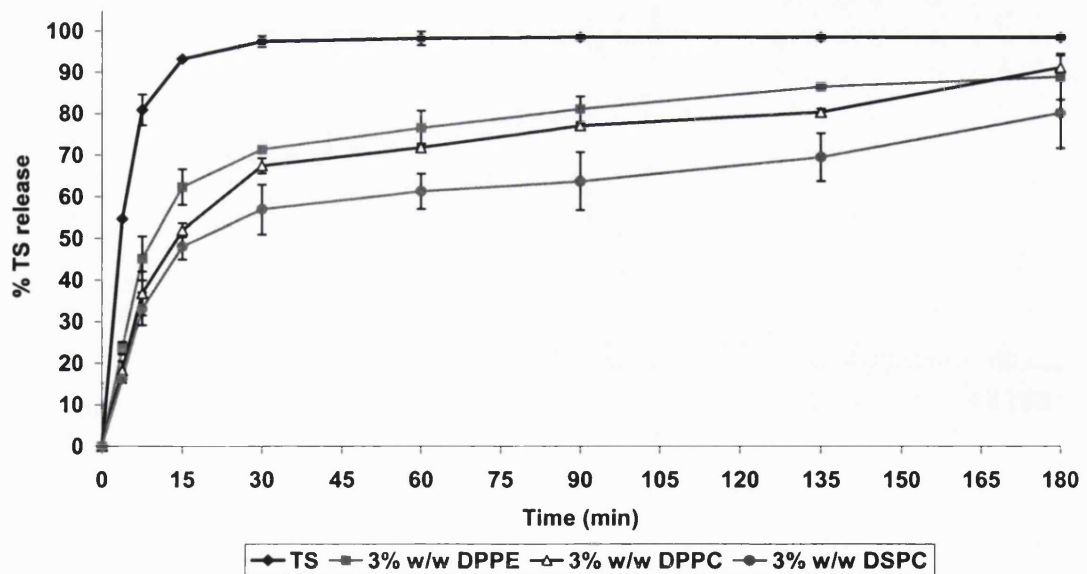
B6.7: Effect of rolling SR-TS in the presence of 5% w/w DPPC on ACI profile ($n=3 \pm SD$).

SR-TS: FPF = 36.0 ± 1.5 , MMAD = 5.03 ± 0.23 , GSD = 2.33 ± 0.058

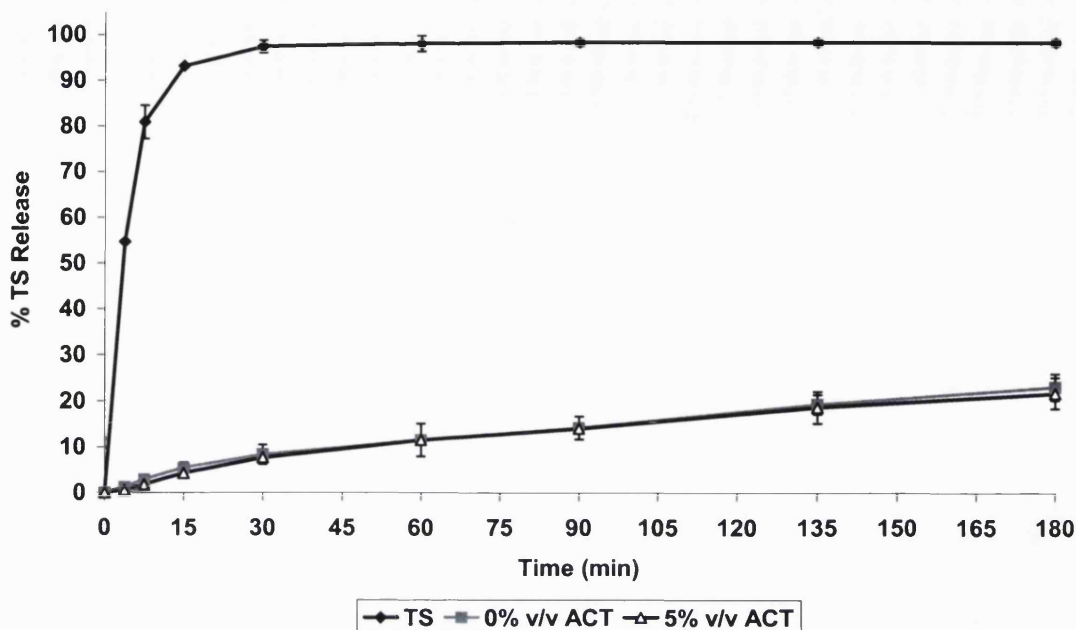
95% SR-TS + : FPF = 41.9 ± 2.2 , MMAD = 4.03 ± 0.15 , GSD = 1.90

5% w/w DPPC

Appendix B7 Additional TS Release profiles for Chapter 6



B7.1: Release profile of pure TS and TS from SR-TS formulations containing alternative phospholipids ($n=3 \pm SD$, 37 °C).



B7.2: Release profiles of pure TS and TS from SR-TS formulations, spray-dried with or without 5% v/v ACT in DCM feed (n=3 ± SD, 37 °C).

Appendix C Patent Application: Publication Number GB0323003.4

A patent application covering the process technology detailed in Chapter 4 and Chapter 5 was lodged with the UK Patent Office on 01/10/2003.

School of Pharmacy: Process for formulating water-soluble compounds:

Abstract

Process for Formulating Water-soluble Compounds

Sustained release compositions for release of biologically active compounds into the surrounding environment comprise nanoparticles of active compounds surrounded by a matrix of hydrophobic material. The microparticles are formed by a process in which nanoparticles of the biologically active compound are coating by and agglomerated with a hydrophobic material in the form of a liquid which is then solidified. Suitably the nanoparticles are formed by freeze-drying a water-in-oil emulsion comprising the active dissolved in the aqueous phase, to form nanoparticles, followed by suspension of nanoparticles in an organic non-solvent for drug, containing dissolved hydrophobic substance, and spray drying the suspension. The active is water soluble and is generally a medicament. The hydrophobic substance has a melting point above body temperature, preferably above the boiling point of the solvent used in the spray drying process. Examples of hydrophobic substance are hydrogenated palm oil, glyceryl behenate and tripalmitin. The active is for instance selected from terbutaline, salbutamol, ipratropine, oxitropine and nedocromil. The microparticulate product is preferably inhalable, as a dried powder.

References

- Achanta, A.S., Adusumilli, P.S., James, K.W., Rhodes, C.T., 1997. Development of hot-melt coating methods. *Drug. Dev. Ind. Pharm.*, 23, 441-449.
- Adjei, A.L., 2003. The pressurised metered dose inhaler. In: Rathbone, M.J., Hadgraft, J., Roberts, M.S., (Eds.), *Modified-release drug delivery technology*, 1st Ed., Marcel Dekker, New York.
- Adjei, A.L., Gupta, P.K., 1997, (Eds.), *Inhalation delivery of therapeutic peptides and proteins*, 1st Ed., Marcel Dekker, New York.
- Alcock, R., Blair, J.A., O'Mahony, D.J., Raouf, A., Kirk, A.V., 2002. Modifying the release from spray dried OED microparticles. *J. Controlled Release*, 82, 429-440.
- Alexandridis, P., Holzwarth, J.F., Hatton, T.A., 1994. Micellization of poly(ethylene oxide) - poly(propylene oxide) - poly(ethylene oxide) triblock copolymers in aqueous solutions: Thermodynamics of copolymer association. *Macromolecules*, 27, 2414-2425.
- Al-hadithi, D., Buckton, G., Brocchini, S., Lowther, N., Singh, D., 2002. Partially amorphous carriers in dry powder inhalation. In: Byron, P.R., Dalby, R.N., Preat, V., (Eds.) *Respiratory Drug Delivery VIII*, Vol 2, 679-681.
- Altieri, R.J., Thompson, D.C., 1996. Physiology and Pharmacology of the airways. In: Hickey, A.J., (Ed.), *Inhalation Aerosols: Physical and Biological basis for therapy*, 1st Ed., Marcel-Dekker, New York.
- Armendariz, A.J., Leith, D., 2002. Concentration measurement and counting efficiency for the aerodynamic particle sizer 3320. *Aerosol. Sci.*, 33, 133-148.
- Armstrong, D.J., Elliott, P.N.C., Ford, J.L., Gadson, D., McCarthy, G.P., Rostron, C., Worsley, M.D., 1996. Poly-(D,L-lactic acid microspheres incorporating histological dyes for intra-pulmonary histopathological investigations. *J. Pharm. Pharmacol.*, 48, 258-262.
- Armstrong, N.A., James, K.C., 1996. *Pharmaceutical Experimental Design and Interpretation*, 1st Ed., Taylor and Francis, London.
- Aronhime, J., Sarig, S., Garti, N., 1990. Emulsifiers as additives in fats: effect on polymorphic transformation and crystal properties of fatty acids and triglycerides. *Food Structure*, 9, 337-352.
- Arppe, J., Vidgren, M., Waldrep, J.C., 1998. Pulmonary pharmacokinetics of cyclosporin A liposomes. *Int. J. Pharm.*, 161, 205-214.

Ashurst, I., Malton, A., 2003. Passive dry powder inhalation technology. In: Rathbone, M.J., Hadgraft, J., Roberts, M.S., (Eds.), Modified-release drug delivery technology 1st Ed., Marcel Dekker, New York.

Bain, D.F., Munday, D.L., Smith, A., 1999. Solvent Influence on spray-dried biodegradable microspheres. *J. Microencapsulation*, 16, 453-474.

Baker, R.W., Lonsdale, H.K., 1974. Controlled release: mechanisms and rates. In: Tanquary, A.C., Lacey, R.E. (Eds.), Controlled release of biologically active agents, 1st Ed., Plenum Press, London.

Barker, S.A., Taylor, K.M.G., Short, M.D., 1994. The deposition and clearance of liposome entrapped ^{99m}Tc-DTPA in the human respiratory tract. *Int. J. Pharm.*, 102, 159-165.

Barnes, P., 2003. Therapy of chronic obstructive pulmonary disease. *Pharmacol. Ther.*, 97, 87-94.

Barta, S.K., Crawford, A., Roberts, C.M., 2002. Survey of patient's views of domiciliary nebuliser treatment for chronic lung disease. *Respiratory Medicine*, 96, 375-381.

Barthelemy, P., Laforet, J.P., Farah, N., Joachim, J., 1999. Compritol™ 888 ATO: An innovative hot-melt coating agent for prolonged release formulations. *Eur. J. Pharm Biopharm.*, 47, 87-90.

Basu, S.K., Li, W-I., Lipp, M.M., Giovanni, C., Elbert, K., Hrkach, J.S., 2001. Modulation of release from dry powder formulations. World Patent WO0113891.

Batycky, R., Deaver, D., Dwivedi, S., Hrkach, J., Johnston, L., Olsen, T., Wright, J.E., 2003. The development of large porous particles for inhalation drug delivery. In: Rathbone, M.J., Hadgraft, J., Roberts, M.S. (Eds.), Modified-release drug delivery technology, 1st Ed., Marcel Dekker, New York.

Bell, J.H., Hartley, P.S., Cox, J.S.G., 1971. Dry powder aerosols. I. A new powder inhalation device. *J. Pharm. Sci.*, 60, 1559-1564.

Ben-Jebria, A, Chen, D., Eskew, M, Vanbever, R., Langer, R., Edwards, D.A., 1999. Large porous particles for sustained protection from carbochol-induced bronchoconstriction in guinea-pigs. *Pharm. Res.*, 16, 555-561.

Berthold, A., Cremer, K., Keuter, J., 1996. Preparation and characterisation of chitosan microspheres as drug carrier for prednisolone sodium phosphate as a model for anti-inflammatory drugs. *J. Controlled Release*, 39, 17-25.

Bhardwaj, T.R., Kenwar, M., Lal, R., Gupta, A., 2000. Natural gums and modified natural gums as sustained-release carriers. *Drug Dev. Ind. Pharm.*, 26, 1025-1038.

B'Hymer, C., 2003. Residual solvent testing: a review of gas-chromatographic and alternative techniques. *Pharm. Res.*, 20, 337-344.

Biddiscombe, M.F., Usmani, O.S., Barnes, P.J., 2003. A system for the production of monodisperse salbutamol aerosols to the lung. *Int. J. Pharm.*, 254, 243-253.

Billon, A., Bataille, B., Cassanas, G., Jacob, M., 2000. Development of spray-dried acetaminophen microparticles using experimental design. *Int. J. Pharm.*, 203, 159-168.

BNF, British National Formulary, 2003., 46th Ed., British Medical Association and Royal Pharmaceutical Society of Great Britain, London.

Bodmeier, R., Paeratakul, O., 1989. Spherical agglomerates of water-insoluble drugs. *J. Pharm. Sci.*, 78, 964-967.

Bonferoni, M.C., Rossi, S., Tamayo, M, Pedraz, J.L., Dominguez-Gil, A., Caramela, C., 1993. A lambda carrageenan hydrophilic matrix for constant release of salbutamol sulphate. *Proceed. Intern. Symp. Control. Rel. Bioact. Mater.*, 20, 340.

Borgstrom, L., O'Callaghan, C., Bisgaard, H., Pedersen, S., 2002. Dry powder inhalers. In: O'Callaghan, C., Smaldone, G.C., (Eds.), *Drug delivery to the lung*, 1st Ed., Marcel Dekker, New York.

Bot, A.I., Smith, D.J., Bot, S., Dellamary, L., Tarara, T.E., Harders, S., Phillips, W., Weers, J.G., Woods, C.M., 2001. Receptor-mediated targeting of spray-dried lipid particles coformulated with immunoglobulin and loaded with a prototype vaccine. *Pharm. Res.*, 18, 971-979.

Bouillot, P., Ubrich, N., Sommer, F., Duc, T.M., Loeffler, J-P., Dellachrie, E., 1999. Protein encapsulation in biodegradable amphiphilic microspheres. *Int. J. Pharm.*, 181, 159-172.

BP, British Pharmacopoeia, 2003. Volume VI, The Stationary Office, London.

Briggner, L.E., Buckton, G., Bystrom, K., Darcy, P., 1994. The use of isothermal microcalorimetry in the study of changes in crystallinity induced during the processing of powders. *Int. J. Pharm.*, 105, 125-135.

Brigham, K.L., 1997., (Ed.), *Gene therapy for diseases of the lung*, 1st Ed., Marcel Dekker, New York.

British Thoracic Society., 1997. BTS guidelines for the management of chronic obstructive pulmonary disease. *Thorax*, 52, S1-S28.

British Thoracic Society, National Asthma Campaign, Royal College of Physicians in London in association with the General Practitioners in Asthma Group, British Association of Accident and Emergency Medicine, British Paediatric Society, and Royal College of Paediatrics and Child Health, 1997. The British guidelines on asthma management: review and position statement. *Thorax*, 52, S1-S21.

Broadhead, J., Edmond-Rouan, S.K., Rhodes, C.T., 1992. The spray drying of pharmaceuticals. *Drug Dev. Ind. Pharm.*, 18, 1169-1206.

Brown, B., 2002. 5 myths about MDIs. *Drug Deliv. Tech.*, 2, 52-59.

Brown, B., Thatcher, M.L., Smith, K.L., Johnson, P.R., Podgorski, J.J., 2002. The stability of a particle size reduced therapeutic protein in an HFA metered dose inhaler formulation. In: Byron, P.R., Dalby, R.N., Preat, V., (Eds.) *Respiratory Drug Delivery VIII*, Vol 2, 311-313.

Bubnis, W.A., 1998. Carrageenan. In: *FMC Problem Solver and Reference Manual*, 2nd Ed., FMC Corporation, Philadelphia.

Buckton, G., Newton, J.M., 1985. Assessment of the wettability and surface energy of a pharmaceutical powder by liquid penetration. *J. Pharm. Pharmacol.*, 37, 605-609.

Buhl, R., 2003. Omatizumab (Xolair[®]) improves quality of life in adult patients with allergic asthma. *Resp. Med.*, 97, 123-129.

Byron, P., 1986. Prediction of drug residence times in regions of the human respiratory tract following aerosol inhalation. *J. Pharm. Sci.*, 75, 433-438.

Canselier, J.P., 1993. The effects of surfactants on crystallization phenomena. *J. Dispersion Sci. Tech.*, 14, 625-644.

Caramori, G., Adcock, I., 2003. Pharmacology of airway inflammation in asthma and COPD. *Pulm. Pharm. Ther.*, 16, 247-277.

Chawla, A. Taylor, K.M.G. Newton, J.M. Johnson, M.C.R., 1994. Production of spray dried salbutamol sulphate for use in dry powder aerosol formulation. *Int. J. Pharm.*, 108, 233-240.

Chmelik, F., Doughty, A., 1994. Objective measurements of compliance in asthma treatment. *Ann. Allergy*, 73, 527-532.

Chen, X., Young, T.J., Sarkari, M., Williams III, R.O., Johnston, K.P., 2002. Preparation of cyclosporine A nanoparticles by evaporative precipitation into aqueous solution. *Int. J. Pharm.*, 242, 2-14.

Chickering III, D.E., Howard, B., Keegan, M., Randall, G., Straub, J., 2001 Spray-drying apparatus and methods of use. US Patent, US6223455.

Clark, A.R., 2003. Dry powder inhalation systems from Inhale Therapeutic Systems. In: Rathbone, M.J., Hadgraft, J., Roberts, M.S., (Eds.), *Modified-release drug delivery technology*, 1st Ed., Marcel Dekker, New York.

Clas, S-D., Dalton, C.R., Hancock, B.C., 1999. Differential Scanning Calorimetry: applications in drug development. *Pharm. Sci. Technol. Today*, 8, 311-341.

Clas, S-D., Dalton, C.R., Hancock, B.C., 2002. Calorimetry in Pharmaceutical Research and Development. In: Sharbrick, J., Boylan, J.C. (Eds.), *Encyclopedia of Pharmaceutical Technology*, Vol 1, 2nd Ed., Marcel Dekker, New York.

Clark, A.R., 1992. The physics of aerosol formulation by MDIs - limitations of the current approach. *J. Biopharm. Sci.*, 3, 69-76.

Codrons, V., Vanderbist, F., Verbeeck, R.K., Arras, M., Lison, D., Preat, V., Venbever, R., 2003. Systemic delivery of parathyroid hormone (1-34) using inhalation dry powders in rats. *J. Pharm. Sci.*, 92, 938-950.

Colthorpe, P., 2003. Industry experiences of the HFA transition. *Drug Deliv. Sys. Sci.*, 3, 41-43.

Columbano, A., Buckton, G., Wikeley, P., 2002. A study of the crystallization of amorphous salbutamol sulphate using water vapour sorption and near infrared spectroscopy. *Int. J. Pharm.*, 237, 171-178.

Conte, U., Conti, B., Giunchedi, P., Maggi, L., 1994. Spray-dried polylactide microsphere preparation: influence of the technological parameters. *Drug Dev. Ind. Pharm.*, 20, 253-258.

Corn, M., 1966. Adhesion of particles. In: Davies, C.N., (Ed.), *Aerosol Science*, 1st Ed., Academic Press, London.

Courier, H.M., Butz, N., Vandamme, T.F., 2002. Pulmonary drug delivery systems: Recent developments and prospects. *Crit. Rev. Ther. Drug Carrier Systems*, 19, 425-498.

Couvreur, P., Dubernet, C., Puisieux, F., 1995. Controlled drug delivery with Nanoparticles: current possibilities and future trends. *Eur. J. Pharm. Biopharm.*, 41, 2-13.

Craig, D.Q.M., Royall, P.G., Kett, V.L., Hopton, M.L., 1999. The relevance of the amorphous state to pharmaceutical dosage forms: glassy drugs and freeze-dried systems. *Int. J. Pharm.*, 179, 179-207.

Dalby, R.N., Suman, J., 2003. Inhalation therapy: technological milestones in asthma treatment. *Adv. Drug Delivery. Rev.*, 55, 779-791.

Dalby, R.N., Tiano, S.L., Hickey, A.J., 1996. Medical devices for the delivery of therapeutic aerosols to the lung. In: Hickey, A.J., (Ed.), *Inhalation Aerosols: Physical and Biological basis for therapy*, 1st Ed., Marcel Dekker, New York.

D'Alonzo, G.E., Crocetti, J.G., Smolensky, M.H., 1999. Circadian rhythms in pharmacokinetics and clinical effects of β -agonists, theophylline and anticholinergic medications in the treatment of nocturnal asthma. *Chronobiol. Int.*, 16, 663-682.

Darwis, Y., Kellaway, I.W., 2001. Nebulisation of rehydrated freeze-dried beclomethasone dipropionate liposomes. *Int. J. Pharm.*, 215, 113-121.

David, R., Giron, D., 1998. Crystallization. In: Chulia, D., Deleuil, M., Pourcelot, Y. (Eds.), *Powder technology and pharmaceutical processes*, 2nd Ed., Elsevier Science, Amsterdam.

Davies, C.N., 1966. Deposition from moving aerosols. In: Davies, C.N., (Ed.), *Aerosol Science* 1st Ed., Academic Press, London.

Davies, N.M., Feddah, M.R., 2003. A novel method for assessing dissolution of aerosol inhaler products. *Int. J. Pharm.*, 255, 175-187.

Dellamary, L.A., Tarara, T.E., Smith, D.J., Woelk, C.H., Adractas, A., Costello. M.L., Gill, H., Weers, J.G., 2000. Hollow porous particles in metered dose inhalers. *Pharm Res.*, 17, 168-174.

Dennis, N.A., Blauer, H.M., Kent, J.E., 1982. Dissolution fractions and half-times of single source yellow cake in simulated lung fluids. *Health Phys.*, 42, 469-477.

Derom, E., Thorsson, L., 2002. Factors affecting the clinical outcome of aerosol therapy. In: O'Callaghan, C., Saldone, G.C., (Eds.), *Drug delivery to the lung*, 1st Ed., Marcel Dekker, New York.

Dickinson, P.A., Howells, S.W., Kellaway, I.W., 2001. Novel nanoparticles for pulmonary drug administration. *J. Drug Targeting.*, 9, 295-302.

Dolovich, M.A., 2000. Influence of respiratory flow rate, particle size and airway calibre on aerosolised drug delivery to the lung. *Resp. Care*, 45, 597-608.

Dunne, M., Corrigan, O.I., Ramtoola, Z., 2000. Influence of particle size and dissolution conditions on the degradation properties of polylactide-co-glycolide particles. *Biomaterials*, 21, 1659-1668.

Eccleston, G.M., 2002. Emulsions and Microemulsions. In: Sharbrick, J., Boylan, J.C. (Eds.), *Encyclopedia of Pharmaceutical Technology*, Vol 2, 2nd Ed., Marcel Dekker, New York.

Edem, D.O., 2002. Palm oil: biochemical, physiological, nutritional, haematological, and toxicological aspects: a review. *Plant Foods for Human Nutrition*. 57, 319-341.

Edison, A.F., Griffith, W.C., 1984. Techniques for yellowcake dissolution studies in vitro and their use in bioassay interpretation. *Health Phys.*, 46, 151-163.

Edwards, D.A, Hanes, J., Caponetti, G., Hrkach, J., Ben-Jebria, A., Eskew, M-L., Mintzes, J., Deaver, D., Lotan, N., Langer, R., 1997. Large porous particles for pulmonary delivery. *Science*, 276, 1868-1871.

Elamin, A.A., Sebhatu, T., Ahlneck, C., 1995. The use of amorphous substances to study mechanically activated materials in the solid state. *Int. J. Pharm.*, 119, 25-36.

El-Bary, A.A., Kassem, M.A.A, Foad, N., Tayel, S., Badawi, S.S., 1990. Controlled crystallization of chlorpropamide from surfactant and polymer solutions. *Drug Dev. Ind. Pharm.*, 16, 1649-1660.

El-Baseir, M.M., Kellaway, I.W., 1998. Poly(L-lactic acid) microspheres for pulmonary drug delivery: release kinetics and aerosolisation studies. *Int. J. Pharm.*, 175, 135-145.

Eldem, T., Speiser, P., Hincal, A., 1991. Optimization of spray-dried and -congealed lipid micropellets and characterization of their surface morphology by scanning electron microscopy. *Pharm Res.*, 8, 47-54.

Evora, C., Soriano, I., Rogers, R.A., Shakesheff, K.M., Hanes, J., Langer, R., 1998. Relating the phagocytosis of microparticles by alveolar macrophages to surface chemistry: the effect of 1,2-dipalmitoyl phosphatidylcholine. *J. Controlled Release.*, 51, 43-152.

Evrard, B., Delattre, L., 1996. In vitro evaluation of lipid matrices for the development of a sustained release sulfamethazine bolus for lambs. *Drug Dev. Ind. Pharm.*, 22, 111-118.

Faham, A., Prinderre, P., Piccerelle, P., Farah, N., Joachim, J., 2000. Hot melt coating technology. Influence of Compritol™ 888 ATO and granule size on chloroquine release. *Pharmazie.*, 55, 444-448.

FDA, 1996. Inactive ingredient guide. (from www.fda.gov)

FDA, 1998 Metered dose inhaler (MDI) and dry powder inhaler (DPI) drug products. Draft guidance for industry. (from www.fda.gov)

Fiegel, J., Hanes, J., 2003. Effect of surface properties on aerosolisation of PEGylated poly(ether-anhydride) microspheres. *Proceed. Intern. Symp. Control. Rel. Bioact. Mater.*, 30, 719.

Fielding, R.M., Abra, R.M., 1991. Factors affecting the release rate of terbutaline from liposome formulations after intratracheal instillation in the guinea pig. *Pharm. Res.*, 9, 220-223.

Fisher, D.R., Briant, J.K., 1994. Assessment of accidental intakes of uranyl acetylacetonone (UAA). *Radiation Protection Dosimetry.*, 53, 263-267.

Florence, A.T., Attwood, D., 1988. *Physicochemical principles of pharmacy*, 2nd Ed., Macmillan Press, London.

Forbes, B., Hashmi, N., Martin, G.P., Lansley, A.B., 2000. Formulation of inhaled medicines: effect of delivery vehicle on immortalised epithelial cells. *J. Aerosol. Med. Deposition Clearance and Effects in the Lung*, 13, 281-288.

Franks, F., 1998. Freeze-drying of bioproducts: putting principles into practice. *Eur. J. Pharm. Biopharm.*, 45, 221-229.

Freitas, C., Muller, R.H., 1999. Correlation between long-term stability of solid lipid nanoparticles (SLN™) and crystallinity of the lipid phase. *Eur. J. Pharm. and Biopharm.*, 47, 125-132.

Fuchs, N.A., Sutugin, H.G., 1996. Generation and use of monodisperse aerosols. In: Davies, C.N., (Ed.), *Aerosol Science*, 1st Ed., Academic Press, London.

Gabrio, B.J., Stein, S.W., Velasquez, D.J., 1999. A new method to evaluate plume characteristics of hydrofluoroalkane and chlorofluorocarbon metered dose inhalers. *Int. J. Pharm.*, 186, 3-12.

Ganthier, P., Aiache, J-M., 2003. Manufacture and dissolution studies of lipid spheres: Part 1. *Pharm. Tech. Eur.*, 15, 55-66.

Ganza-Gonzalez, A., Anguiano-Igea, S., Otero-Espinar, F.J., Blanco Mendez, J., 1999. Chitosan and chondroitin microspheres for oral-administration controlled release of metoclopramide. *Eur. J Pharm Biopharm.*, 48, 149-155.

Garekani, H.A., Ford, J.L, Rubinstein, M.H., Rajabi-Siahboomi, A.R., 2000. Highly compressible paracetamol: I: crystallization and characterization. *Int. J. Pharm.*, 208, 87-99.

Garti, N., 1988. Effects of surfactants on crystallization and polymorphic transformation of fats and fatty acids. In: Garti, N., Sato, K., (Eds.), *Crystallization and polymorphism of fats and fatty acids*, 1st Ed., Marcel Dekker, New York.

Giannola, L.I., DeCaro, V., 1997. Entrapment of phenytoin into microspheres of oleaginous materials: process development and in vitro evaluation of drug release. *Drug Dev. Ind. Pharm.*, 23, 1145-1152.

Gilbert, B.E., 1996. Aerosolized amBisome treatment of pulmonary *Cryptococcus neoformans* infection in mice. *J. Aerosol. Med.*, 9, 263-276.

Goerke, J., 1998. Pulmonary surfactant: functions and molecular composition. *Biochem. Biophys. Acta*, 1408, 79-89.

Gonda, I., 1981. A semi-empirical model of aerosol deposition in the human respiratory tract for mouth inhalation. *J. Pharm. Pharmacol.*, 33, 692-696.

Gonda, I., 1985. Development of a systematic theory of suspension inhalation aerosols. I. A framework to study the effects of aggregation on the aerodynamic behaviour of drug particles. *Int. J. Pharm.*, 27, 99-116.

Gonda, I., 1992. Targeting by deposition. In: Hickey, A.J., (Ed.), *Pharmaceutical Inhalation aerosol technology*, 1st Ed., Marcel Dekker, New York.

Gonda, I., 2000. The ascent of pulmonary drug delivery. *J. Pharm Sci.*, 89, 940-945.

Gonda, I., Byron, P.A., 1978. Perspectives on the biopharmacy of inhalation aerosols. *Drug Dev. Ind. Pharm.*, 4, 243.

Gopal, E.S.R., 1968. Principles of Emulsion Formation. In: Sherman, P. (Ed.), *Emulsion Science*, 1st Ed., Academic Press, London.

Gou, H.X., Heinamaki, J., Yliruusi, J., 2002. Amylopectin as a subcoating material improves the acidic resistance of enteric-coated pellets containing a freely soluble drug. *Int. J. Pharm.*, 235, 79-86.

Green, R.J., Harris, N.D., 1998. *Pathology and therapeutics for pharmacists*, 1st Ed., Pharmaceutical Press, London.

Grossman, J., 1994. The evolution of inhaler technology. *J. Asthma*, 31, 55-64.

Hagemann, J.W., 1988. Thermal behaviour and polymorphism of acylglycerides. In: Garti, N., Sato, K., (Eds.), *Crystallization and polymorphism of fats and fatty acids*, 1st Ed., Marcel Dekker, New York.

Hampson, N.B., Mueller, M.P., 1994. Reduction in patient timing errors using a breath-activated metered dose inhaler. *Chest*, 106, 462-465.

Han, R., Papadopoulos, G., Greenspan, B.J., 2002. Investigation of powder dispersion inside a Spiros[®] dry powder inhaler using particle image velocimetry. *Powder. Tech.*, 125, 266-278.

Hardy, J.G., Chadwick, T.S., 2000. Sustained release drug delivery to the lungs. *Clin. Pharmacokinet.*, 39, 1-4.

Hargreaves, J., 1996. Determination of the particle size distribution of Terbutaline sulphate in the spray of pressurized metered dose inhalers, using an Andersen particle sizing sampler by high performance liquid chromatography. AstraZeneca Test Method: AS165.002.

He, P., Davis, S.S., Illum, L., 1999. Chitosan microspheres prepared by spray drying. *Int. J. Pharm.*, 187, 53-65.

Heurtault, B., Saulnier, P., Pech, B., Proust, J-E., Benoit, J-P., 2003. Physico-chemical stability of colloidal lipid particles. *Biomaterials*, 24, 4283-4300.

Hickey, A.J., 2003. Formulation challenges of powders for the delivery of small-molecular-weight molecules as aerosols. In: Rathbone, M.J., Hadgraft, J., Roberts, M.S., (Eds.), *Modified-release drug delivery technology*, 1st Ed., Marcel Dekker, New York.

Hickey, A.J., Byron, P.R., 1986. Preparation, characterization, and controlled release from coprecipitates of fluorescein and magnesium hydroxide. *J. Pharm. Sci.*, 75, 756-759.

Hickey, A.J., Concessio, N.M., van Oort, M.M., Platz, R.M., 1994. Factors influencing the dispersion of dry powders as aerosols. *Pharm Tech.*, 18, 58-64, 82.

Hickey, A.J., Garcia-Contreras, L., 2001. Immunological and toxicological implications of short-term studies in animals of pharmaceutical aerosol delivery to the lungs: relevance to humans. *Crit. Rev. Ther. Drug Carrier Systems*, 18, 387-341.

Higuchi, T., 1963. Mechanism of sustained action medication: Theoretical analysis of rate of release of solid drug dispersed in solid matrices. *J. Pharm. Sci.*, 52, 1145-1149.

Hinds, W.C., 1998. *Aerosol technology. Properties, Behavior, and measurement of airborne particles*, 2nd Ed., John Wiley and Sons, New York.

Hope, R.A., Longmore, J.M., McManus, S.K., Wood-Allum, C.A., 1999. *Oxford handbook of clinical medicine*, 4th Ed., Oxford University Press, Oxford.

Hormes, R., Swift, R.W. Transparent containers for pressurized aerosol formulations. In: Byron, P.R., Dalby, R.N., Preat, V., (Eds.) *Respiratory Drug Delivery VIII*, Vol 2, 585-587.

Howlett, D., Colwell, J., Goldsmith, S., McCallion, O., 2002. Correlation of extractables and leachables from marketed pMDIs. In: Byron, P.R., Dalby, R.N., Preat, V., (Eds.) *Respiratory Drug Delivery VIII*, Vol 1, 129-136.

Hurd, S.S., Pauwels, R., 2002. Global initiative for chronic obstructive pulmonary diseases (GOLD). *Pulmonary Pharmacol. Ther.*, 15, 353-255.

Imai, T., Shiraishi, S., Saito, H., Otagin, M., 1991. Interaction of indomethacin with low molecular weight chitosan and improvements of some pharmaceutical properties of indomethacin by low molecular weight chitosans. *Int. J. Pharm.*, 67, 11-20.

Im-Emsap, W., Siepmann, J., Paeratakul, O., 2002. Disperse systems. In: Banker, G.S., Rhodes, C.T., (Eds.), *Modern Pharmaceutics*, 1st Ed., Marcel Dekker, New York.

Ivanova, R., Alexandridis, P., Lindman, B., 2001. Interaction of poloxamer block copolymers with cosolvents and surfactants. *Colloids and Surfaces A. Physicochemical and engineering aspects*, 183, 41-53.

Jacobs, C., Muller, R.H., 2002. Production and characterization of a budesonide nanosuspension for pulmonary administration. *Pharm. Res.*, 19, 189-194.

Janjikhel, R.K., Adeyeye, C.M., 1997. Stereospecific formulation and characterization of sustained release ibuprofen microspheres. *J. Microencapsulation*, 14, 409-426.

Jantzen, G.W., Robinson, J.R., 2002. Sustained- and controlled-release drug-delivery systems. In: Banker, G.S., Rhodes, C.T., (Eds.), *Modern Pharmaceutics*, 1st Ed., Marcel Dekker, New York.

Jashnani, R.N., Dalby, R.N., Byron, P.R., 1993. Preparation, characterisation, and dissolution kinetics of two novel albuterol salts. *J. Pharm. Sci.*, 82, 613-616.

Johnson, W., Slaga, T.J., 2000. Final report on the safety assessment of *Elaeis Guineensis* (Palm) oil, *Elaeis Guineensis* (Palm) kernel oil, hydrogenated palm oil and hydrogenated palm kernel oil. *Int. J. Toxicol.*, 19(S2), 7-28.

Jones, B.G., Dickinson, P.A., Gumbleton, M., Kellaway, I.W., 2002. Lung surfactant phospholipids inhibit the uptake of respirable microspheres by the alveolar macrophage NR8383. *J. Pharm. Pharmacol.*, 54, 1065-1072.

Jones, D.S., 2002. *Pharmaceutical Statistics*, 1st Ed., Pharmaceutical Press, London.

Juliano, R.L., McCullough, H.N., 1980. Controlled delivery of an antitumour drug: localized action of liposome encapsulated cytosine arabinoside administered via the respiratory system. *J. Pharmacol. Exp. Ther.*, 214, 381-387.

Jung, J., Perrut, M., 2001. Particle design using supercritical fluids: Literature and patent review. *J. Supercritical Fluids*, 20, 179-219.

Kachrimanis, K., Malamataris, S., 1999. Crystallization of paracetamol from ethanol-water solutions in the presence of polymers. *J. Pharm. Pharmacol.*, 51, 1219-1227.

Karabulut, I., Kayahan, M., Yaprak, S., 2003. Determination of changes in some physical and chemical properties of soybean oil during hydrogenation. *Food Chemistry*, 81, 453-456.

Kaş. H.S., 1997. Chitosan: properties, preparations and application to microparticulate systems. *J. Microencapsulation*, 14, 689-711.

Kawashima, Y., Yamamoto, H., Takeuchi, H., Fujioka, T.H., 1999. Pulmonary delivery of insulin with nebulised DL-lactide/glycolide copolymer (PLGA) nanospheres to prolong hypoglycaemic effect. *J. Controlled Release*, 62, 279-287.

Kellaway, I.W., Cook, R.O., 2003. Process for formulating water-soluble compounds. UK Patent Application, GB0323003.4.

Kellaway, I.W., Farr, S.J., 1990. Liposomes as drug delivery systems to the lung. *Adv. Drug Del. Rev.*, 5, 149-161.

Knoch, M., Finlay, W., 2003. Nebulizer technology. In: Rathbone, M.J., Hadgraft, J., Roberts, M.S., (Eds.), *Modified-release drug delivery technology*, 1st Ed., Marcel Dekker, New York.

Kreyling, W.G., Blanchard, J.D., Godleski, J.J., Haessermann, S., Heyder, J., Hutzler, P., Schulz, H., Sweeney, T.D., Takenaka, S., Ziesenis, A., 1999. Anatomical localization of 24- and 96-h particle retention in canine airways. *J. Appl. Physiol.*, 87, 269-284.

Kreyling, W.G., Scheuch, G., 2000. Clearance of particles deposited in the lungs. In: Gehr, P., Heyder, J., (Eds.), *Particle-lung interactions*, 1st Ed., Marcel Dekker, New York.

Labiris, N.R., Dolovich, M.B., 2003a. Pulmonary drug delivery. Part I: Physiological factors affecting therapeutic effectiveness of aerosolised medications. *Br. J. Clin. Pharmacol.*, 56, 588-599.

Labiris, N.R., Dolovich, M.B., 2003b. Pulmonary drug delivery. Part II: The role of inhalant delivery devices and drug formulations in therapeutic effectiveness of aerosolised medications. *Br. J. Clin. Pharmacol.*, 56, 600-612.

Lai, Y-L., Mehta, R.C., Thacker, A.A., Yoo, S-D., McNamara, P.J., DeLuca, P.P., 1993. Sustained bronchodilation with isoproterenol poly(glycolide-co-lactide) microspheres. *Pharm. Res.*, 10, 119-125.

Langer, K., Balthasar, S., Vogel, V., Dinauer, N., von Briesen, H., Schubert, D., 2003. Optimisation of the preparation process for human serum albumin (HSA) nanoparticles. *Int. J. Pharm.*, 257, 169-180.

Larhrib, H., Martin, G.P., Prime, D., Marriott, C., 2003. Characterisation and deposition studies of engineered lactose crystals with potential use as a carrier for aerosolised salbutamol sulphate form dry powder inhalers. *Eur. J. Pharm. Sci.*, 19, 211-221.

Leach, C.L., Davidson, P.J., Boudreau, R.J., 1988. Improved airway targeting with the CFC-free HFA-beclomethasone metered-dose inhaler compared with CFC-beclomethasone. *Eur. Resp. J.*, 12, 1346-1353.

Lee, K.Y.C., Lipp, M.M., Zasadzinski, J.A., Waring, A.J., 1997. Effects of lung surfactant specific protein SP-B and model SP-B peptide on lipid monolayers at the air-water interface. *Colloids Surfaces A: Physicochem. Eng. Aspects*, 128, 225-242.

Lee, P.I., Good, W.R., 1987. Controlled release technology: Pharmaceutical applications, 1st Ed., American Chemical Society, Washington DC.

Lee, V.H.L., Robinson, J.R., 1978. Methods to achieve sustained drug delivery. In: Robinson, J.R. (Ed.) Sustained and controlled release drug delivery systems, 1st Ed., Marcel Dekker, New York.

Li, F.Q., Hu, J.H., Lu, B., Yao, H., Zhang, W.G., 2001. Ciprofloxacin-loaded bovine serum albumin microspheres: preparation and drug release in vitro. *J. Microencapsulation*, 18, 825-829.

Lin, W.-J., Lee, H.-G., 2003. Design of a microporous controlled delivery system for theophylline tablets. *J. Controlled Release*, 89, 179-187.

Lipworth, B.J., 1999. Modern drug treatment of chronic asthma. *Brit. Med. J.*, 318, 380-384.

Liversidge, G.G., Conzentino, P., 1995. Drug particle size reduction for decreasing gastric irritancy and enhancing absorption of naproxen in rats. *Int. J. Pharm.*, 125, 309-313.

Liversidge, G.G., Grant, D.J.W., Padfield, J.M., 1981. Influence of physicochemical interactions on the properties of suppositories I: Interactions between the constituents of suppository bases. *Int. J. Pharm.*, 7, 211-223.

Lumry, W., Noveck, R., Weinstein, S., Barnhart, F., Vandermeer, A., Murray, A., Resiner, C., 2001. Switching from Ventolin CFC to Ventolin HFA is well tolerated and effective in patients with asthma. *Annals. Allergy, Asthma Immunology.*, 86, 297-303.

Lutton, E.S., Fehl, A.J., 1970. The polymorphism of odd and even saturated single acid triglycerides, C₈-C₂₂. *Lipids*, 5, 90-99.

Ma, X., Taw, J., Chiang, C.-M., 1996. Control of drug crystallization in transdermal matrix system. *Int. J. Pharm.*, 142, 115-119.

Mackellar, A.J., Buckton, G., Newton, J.M., Chowdhry, B.Z., Orr, C.A., 1994. The controlled crystallization of a model powder: 1. The effects of altering the stirring rate and the supersaturation profile, and the incorporation of a surfactant (Poloxamer 188). *Int. J. Pharm.*, 112, 65-78.

Makino, K., Yamamoto, N., Higuchi, K., Harada, N., Ohshima, H., Terada, H., 2003. Phagocytic uptake of polystyrene microspheres by alveolar macrophages: effects of the size and surface properties of the microspheres. *Colloids and Surfaces B: Biointerfaces*, 27, 33-39.

Malcolmson, R.J., Embleton, J.K., 1998. Dry powder formulations for pulmonary delivery. *Pharm. Sci. Tech. Today*, 1, 394-398.

Malo, J.L., Cartier, A., Merland, N., Ghezzi, H., Burek, A., Morris, J., Jennings, B.H., 1989. Four-times-a-day dosing frequency is better than twice-a-day regimen in subjects requiring a high-dose inhaled steroid, budesonide to control moderate to severe asthma. *Am. Rev. Resp. Dis.*, 140, 624-628.

Malton, A., Sumbly, B.S., Dandiker, Y., 1996. A comparison of the in-vitro drug delivery from salbutamol Diskus and terbutaline Turbuhaler inhalers. *J. Pharm. Med.*, 6, 35-48.

Mann, M., Eliasson, O., Patel, K., Zuwallack, R.L., 1992. A comparison of the effects of bid and qid dosing on compliance with inhaled flunisolide. *Chest*, 101, 496-499.

Martini, F.H., 2004., (Ed.), *Fundamentals of anatomy and physiology*, 6th Ed., Pearson Education International, San Francisco, CA.

Martonen, T., Yang, Y., 1996. Deposition mechanisms of pharmaceutical particles in human airways. In: Hickey, A.J., (Ed.) *Inhalation Aerosols: Physical and Biological basis for therapy*, 1st Ed., Marcel Dekker, New York.

Masters, K., 2002. *Spray drying in practice*. 1st Ed., SprayDryConsult International, Denmark.

Matthews, C.K., van Holde, K.E., 1996. *Biochemistry*, 2nd Ed., Benjamin-Cummings Publishing Company, Menlo Park, CA.

McCalden, T.A., Fielding, R.M., Mihalko, P.J., Kaplan, S.A., 1969. Sustained bronchodilator therapy using inhaled liposomal formulations of beta-2 adrenergic agonists. In: Prescott, L.F., Nimmo, W.S., (Eds.), *Novel drug delivery and its therapeutic application*, 1st Ed., John Wiley and Sons, Chichester.

McConville, J.T., Patel, N., Ditchburn, N., Tobyn, M.J., Staniforth, J.N., Woodcock, P., 2000. Use of a novel modified TSI for the evaluation of controlled-release aerosol formulations. *Drug Dev. Ind. Pharm.*, 26, 1191-1198.

McDonald, K.J., Martin, G.P., 2000. Transition to CFC-free metered dose inhalers - into the new millennium. *Int. J. Pharm.*, 201, 89-107.

McFadden, E.R., Hejal, R., 1995. Asthma. *Lancet*, 345, 1251-1219.

Mercer, R.R., Russell, M.L., Crapo, J.D., 1992. Mucous lining layers in the human and rat airways. *Ann. Rev. Am. Resp. Dis.*, 145, 355.

Mehnert, W., Mader, K., 2001. Solid Lipid Nanoparticles: Production, characterization and applications. *Adv. Drug Deliv. Rev.*, 47, 165-196.

Miers, H.A., Isaac, F., 1907. The spontaneous crystallization of binary mixtures. *Proceedings of the Royal Society*, A79, 322-351. (cited in Mullin, 1993)

Miller, N.C., Ross, D.L., Nasr, M.M., 1998. Effect of formulation factors on the observed bounce in cascade impactors used to measure the spray particle size of metered dose inhalers. *Int. J. Pharm.*, 173, 93-102.

Milqvist-Fureby, A., 2003. Characterisation of spray-dried emulsions with mixed fat phases. *Colloids and Surfaces B: Biointerfaces*, 31, 65-79.

Moss, O.R., 1979. Simulants of lung interstitial fluid. *Health Phys.*, 36, 447-448.

Mulders, H., 2003. The use of a SEM/FIB dualbeam applied to biological samples. *G.I.T. Imaging Microscopy*, 2, 8-10.

Muller, R.H., Maaßen, H., Weyhers, F., Specht, F., Lucks, J.S., 1996. Cytotoxicity of magnetite-loaded polylactide, polylactide/glycolide particles and solid lipid nanoparticles. *Int. J. Pharm.*, 138, 85-94.

Muller, R.H., Mader, K., Gohla, S., 2000. Solid Lipid nanoparticles (SLN) for controlled drug delivery – a review of the state of the art. *Eur. J. Pharm. Biopharm.*, 50, 161-177.

Mullin, J.W., 1993. *Crystallization*, 3rd Ed., Butterworth-Heinemann, Oxford.

Muramatsu, M., Kanada, K., Nishida, A., Ouchi, K., Saito, N., Yoshida, M., Shimoaka, A., Ozeki, T., Yuasa, H., Kanaya, Y., 2000. Application of Carbopol® to controlled release preparations I. Carbopol® as a novel coating material. *Int. J. Pharm.*, 199, 77-83.

Needham, M., 2000. Determination of the concentration of terbutaline sulphate in pressurised metered dose inhalers by high performance liquid chromatography. *AstraZeneca Test Method*, AS165.003-1.0.

Newhouse, M.T., 1998. The current laboratory determination of 'respirable mass' is not clinically relevant. *J. Aerosol. Med.*, 11, S122-S132.

Newman, S.P., Pavia, D., Moren, F., Sheahan, N.F., Clarke, S.W., 1981. Deposition of pressurised aerosols in the human respiratory tract. *Thorax*, 36, 52-55.

Newman, S.P., Pellow, P.G.D., Clarke, S.W., 1987. In vitro comparison of deVilbriss jet and ultrasonic nebulisers. *Chest*, 92, 991-994.

Newton, J.M., 1996. Spray Drying and its Application in Pharmaceuticals. *Man. Chem. Aerosol News.*, April, 33-36.

Ng, K., Stringer, K.A., Cohen, Z., Serraro, R., Tian, B., Meyer, J.D., Falk, R., Randolph, T., Manning, M.C., Thompson, D.C., 1998. Alveolar macrophage cell line is not activated by exposure to polymeric microspheres. *Int. J. Pharm.*, 170, 41-49.

Obaidat, A.A., Obaidat, R.M., 2001. Controlled Release of tramadol hydrochloride from matrices prepared using glyceryl behenate. *Eur. J. Pharm. Biopharm.*, 52, 231-235.

Okada M., 1970. Whisker-like growth of triglyceride. *J. Crystal Growth.*, 7, 371-374.

O'Hara, P., Hickey, A.J., 2000. Respirable PLGA microspheres containing rifampicin for the treatment of tuberculosis: Manufacture and Characterization. *Pharm. Res.*, 17, 955-961.

Ostrander, K.D., Bosch, H.W., Bondanza, D.M., 1999. An in-vitro assessment of a NanoCrystal™ beclomethasone dipropionate colloidal dispersion via ultrasonic nebulization. *Eur. J. Pharm. Biopharm.*, 48, 207-215.

Palmieri, G.F., Wehrle, P., Stamm, A., 1994. Evaluation of spray-drying as a method to prepare microparticles for controlled drug release. *Drug Dev. Ind. Pharm.*, 20, 2859-2879.

Parry-Billings, M., Boyes, R.N., Clisby, L.M., Braithwaite, P., Williams, S., Harper, A.E., 1999. Design, development and performance of a novel multidose dry powder inhaler. *Pharm. Tech.*, 23, 70-81.

Patton, J.S., Mechanisms of macromolecule uptake by the lungs., 1996. *Adv. Drug Deliv. Rev.*, 19, 3-36.

Patton, J.S., Bukar, J., Nagarajan, S., 1999. Inhaled insulin. *Adv. Drug Deliv. Rev.*, 35, 235-247.

Pepin, X., Blanchon, S., Couarraze, G., 1999. Powder dynamic contact angle data in the pharmaceutical industry. *Pharm. Sci. Tech. Today*, 2, 111-118.

Perrut, M., 2002. Method for encapsulating fine solid particles in the form of microcapsules. World Patent WO0205944.

Phaneuf, M.W., 1999. Applications of focused ion beam microscopy to materials science specimens. *Micron*, 30, 277-288.

Pillai, R.S., Yeates, D.B., Miller, I.F., Hickey, A.J., 1998. Controlled Dissolution from wax-coated particles in canine lungs. *J. Appl. Physiol.*, 84, 717-725.

Polatli, M., Dayanir, V., Polatli, O., Ozkan, S.B., Cildag, O., 2002. The effect of ipratropium bromide on intraocular pressure in patients with chronic obstructive pulmonary disease: An open label study. *Curr. Ther. Res.*, 63, 380-387.

Polli, G.P., Grim, W.M., Bacher, F.A., Yunker, M.H., 1969. Influence of formulation on aerosol particle size. *J. Pharm. Sci.*, 58, 484-486.

Porte, H., Courraze, G., 1998. Microencapsulation processes for the manufacture of systems providing modified release of active constituent. In: Chulia, D., Deleuil, M., Pourcelot, Y., (Eds.), Powder technology and pharmaceutical processes., 2nd Ed., Elsevier Science, Amsterdam.

Price, D., Thomas, M., Mitchell, G., Niziol, C., Featherstone, R., 2003. Improvement of asthma control with a breath actuated pressurised metered dose inhaler (BAI): a prescribing claims study of 5556 patients using a traditional pressurised metered dose inhaler (MDI) or a breath actuated device. *Resp. Med.*, 97, 12-19.

Puchelle, E., Vargaftig, B.B., 2001. Chronic Obstructive pulmonary disease: an old disease with novel concepts and drug strategies. *Trends in Pharmacol. Sci.*, 22, 495-497.

Raghavan, S.L., Trividic, A., Davis, A.F., Hadgraft, J., 2001. Crystallization of hydrocortisone acetate: influence of polymers. *Int. J. Pharm.*, 212, 213-221.

Ranga Rao, K.V., Padmalatha, D.K., Buri, P., 1990. Influence of molecular size and water solubility of the solute on its release from swelling and erosion controlled polymeric matrices. *J Controlled Release*, 12, 133-141.

Rathbone, M.J., Hadgraft, J., Roberts, M.S. (Eds.), Modified-release drug delivery technology, 1st Ed., Marcel Dekker, New York.

Rees, P. J., Clark, T.J., Moren, F., 1982. The importance of particle size in response to inhaled bronchodilators. *Eur. J. Resp. Dis.*, 119, 73-78.

Ribeiro Dos Santos, I., Richard, J., Pech., B., Thies, C., Benoit, J.P., 2002. Microencapsulation of protein particles within lipids using a novel supercritical fluid process. *Int. J. Pharm.*, 242, 69-78.

Robinson, J.R., 1978. Sustained and controlled release drug delivery systems, 1st Ed., Marcel Dekker, New York.

Roche, N., 1999. Pulmonary Medicine. *Brit. Med. J.*, 318, 171-176.

Rodrigues, M. Peirico, N., Matos, H., Gomes de Azevedo, E., Lobato, M.R., Almeida, A.J., 2003. Microcomposites theophylline/hydrogenated palm oil from a PGSS process for controlled drug delivery systems. *J. Supercritical Fluids*, 1-11. (Article in press, from www.sciencedirect.com)

Rosario, D., Otulana, B., 2003. Regulatory issues for pulmonary delivery systems. In: Rathbone, M.J., Hadgraft, J., Roberts, M.S., (Eds.), Modified-release drug delivery technology, 1st Ed., Marcel Dekker, New York.

Rowe, R.C., Sheskey, P.J., Weller, P.J., 2002. Handbook of pharmaceutical excipients, 4th Ed., Pharmaceutical Press, London.

Rudolph, G., Kobrich, R., 1994. A mathematical model of mass deposition in man. *Am. Occup. Hyg.*, 38, 15-23.

Sacchetti, M., van Oort, M.M., 1996. Spray-drying and supercritical fluid particle generation techniques. In: Hickey, A.J., (Ed.), *Inhalation Aerosols: Physical and Biological basis for therapy*, 1st Ed., Marcel-Dekker, New York.

Saks, S.R. and Gardner, L.B., 1997. The pharmacoeconomic value of controlled release dosage forms. *J Controlled Release*, 48, 237-242.

Saleki-Gerhardt, A., Ahlneck, C., Zografi, G., 1994. Assessment of disorder in crystalline solids. *Int. J. Pharm.*, 101, 237-247.

Sawayanagi Y., Nambu, N., Nagai, T., 1982. Permeation of drugs through chitosan membranes. *Chem. Pharm. Bull.*, 30, 3297-3301.

Schulz, H., 1998. Mechanisms and factors affecting intrapulmonary particle deposition: implications for efficient inhalation therapies. *Pharm. Sci. Tech. Today*, 1, 336-344.

Selek, H., Sahin, S., Ercan, M.T., Sargon, M., Hincal, A.A., Kas, H.S., 2003. Formulation and in vitro/in vivo evaluation of terbutaline sulphate incorporated in PLGA (25/75) and PLA microspheres. *J. Microencapsulation*, 20, 261-271.

Shanker, R.M., Baltusis, P.J., Hruska, R.M., 1994. Development of a new technique for the assessment of wettability of powders. *Pharm. Res.*, 11, S243.

Sharma, R., Saxena, D., Dwivedi, A.K., Mira, A., 2001. Inhalable microparticles containing drug combinations to target alveolar macrophages for treatment of pulmonary tuberculosis. *Pharm. Res.*, 18, 1405-1410.

Shekunov, B.Y., Feeley, J.C., Chow, A.H.L., Tong, H.H.Y., York, P., 2003. Aerosolisation behaviour of micronised and supercritically-processed powders. *Aerosol Sci.*, 34, 553-568.

Shekunov, B.Y., York, P., 2000. Crystallization processes in pharmaceutical technology and drug design. *J Crystal Growth*, 211, 122-136.

Sherwood, L., 1993. *Human physiology: from cells to systems*, 2nd Ed., West Publishing Company, St. Paul, MN.

Sievers, R.E., Karst, U., Schaeffer, J.D., Stoldt, C.R., Watkins, B.A., 1996. Supercritical CO₂-assisted nebulization for the production and administration of drugs. *J. Aerosol Sci.*, 27, S497-S498.

Simonelli, A.P., Mehta, S.C., Higuchi, W.I., 1970. Inhibition of sulfathiazole crystal growth by polyvinylpyrrolidone. *J Pharm Sci.*, 59, 633-638.

Singh, R.K., Kim, W-S., Ollinger, M., Craciun, V., Coowantwong, I., Hochhaus, G., Koshizaki, N., 2002. Laser based synthesis of nanofunctionalised particulates for pulmonary based controlled drug delivery applications. *Appl. Surface Sci.*, 197/198, 610-614.

Sjostrom, B., Kronberg, B., Carlfors, J., 1993a. A method for the preparation of submicron particles of sparingly water-soluble drugs by precipitation in oil-in-water emulsions. I: Influence of emulsification and surfactant concentration. *J. Pharm. Sci.*, 82, 579-583.

Sjostrom, B., Bergenstahl, B., Kronberg, B., 1993b. A method for the preparation of submicron particles of sparingly water-soluble drugs by precipitation in oil-in-water emulsions. II: Influence of the emulsifier, the solvent and the drug substance. *J. Pharm. Sci.*, 82, 584-589.

Sjostrom, B., Kaplun, A., Talmon, Y., Cabane, B., 1995. Structures of nanoparticles prepared from oil-in-water emulsions. *Pharm. Res.*, 12, 39-48.

Smith, I.J., 2002. Developments in Inhalation technology. *Drug Deliv. Sys. Sci.*, 2, 63-65.

Smolensky, M.H., D'Alonzo, G.E., Kunkel, G., Barnes, P.J., 1987. Day-night patterns in bronchial patency and dyspnoea: Basis for one daily and unequally divided twice daily dosing schedules. *Chronobiol. Int.*, 4, 303-307.

Staniforth, J.N., 1996. Carrier particles for use in dry powder inhalers. *World Patent WO9623485*.

Steckel, H., Muller, B.W., 1997. In vitro evaluation of dry powder inhalers II: influence of carrier particle size and concentration on in vitro deposition. *Int. J. Pharm.*, 154, 31-37.

Steckel, H., Resenack, N., Muller, B.W., 2003a. In-situ-micronization of disodium cromoglycate for pulmonary delivery. *Eur. J Pharm. Biopharm.*, 55, 173-180.

Steckel, H., Resenack, N., Villax, P., Muller, B.W., 2003b. In vitro characterization of jet-milled and In-situ-micronized fluticasone-17-propionate. *Int. J. Pharm.*, 258, 63-75.

Stone, K.C., Merler, R.R., Gehr, P., Stockstin, B., Crapo, J.D., 1992. Allometric relationships of cell numbers and size in the mammalian lung. *Am. Resp. Cell. Mol. Biol.*, 6, 235-243.

Sudo, E., Boyd, W.A., King, M., 2000. Effects of dextran sulphate on tracheal mucocilliary velocity in dogs. *J. Aerosol Med. - Deposition Clearance & Effects in the lung*, 13, 87-96.

Summers, Q.A., Nesbit, M.R., Levin, R., Holgate, S.T., 1991. A non-bronchoconstrictor bacteriostatic preservative for nebuliser solutions. *Br. J. Clin. Pharmacol.*, 31, 204-206.

Sutananta, W., Craig, D.Q.M., Newton, J.M., 1994. An investigation into the effect of preparation conditions on the structure and mechanical properties of pharmaceutical glyceride bases. *Int. J. Pharm.*, 110, 75-91.

Suzuki, H., Sunada, H., 1998. Influence of water-soluble polymers on the dissolution of nifedipine solid dispersions with combined carriers. *Chem. Pharm. Bull.*, 46, 482-487.

Takeuchi, H., Yamamoto, H., Kawashima, Y., 2001. Mucoadhesive nanoparticulate systems for peptide drug delivery. *Adv. Drug Deliv. Rev.*, 47, 39-59.

Tamulinas, C.B., Leach, C.L., 2000. Routes of exposure: Inhalational and Intranasal. In: Weiner, M.L., Kotkoski, L.A., (Eds.), *Excipient toxicity and safety*, 1st Ed., Marcel-Dekker, New York.

Tanninen, V.P., Luhtala, S., Yliruusi, J., 1992. X-ray-powder diffraction line-profile analysis in the study on the effect of surface-active agent on the crystal properties of carbamazepine. *Acta. Pharmaceutica Nordica*, 4, 277-282.

Task Group on Lung Dynamics, 1966. *Health Phys.*, 12, 173-207.

Taylor, G., Gumbleton, M., 2002 Predicting the effects of mucocilliary clearance on systemic bioavailability from the lung. In: Byron, P.R., Dalby, R.N., Preat, V., (Eds.) *Respiratory Drug Delivery VIII, Vol 2*, 863-806.

Taylor, J., Arthur Kotch, A., Rice, K., Ghafouri, M., Kurland, C.L., Fagan, N.M., Witek Jr, T.J., Ipratropium Bromide HFA Study Group., 2001. Ipratropium Bromide Hydrofluoroalkane Inhalation Aerosol Is Safe and Effective in Patients With COPD. *Chest*, 120, 1253-1261.

Taylor, K.M.G., Farr, S.J., 1993. Liposomes for drug delivery to the respiratory tract. *Drug Dev. Ind. Pharm.*, 19, 123-142.

Taylor, K.M.G., Taylor, G., Kellaway, I.W., Stevens, J., 1989. The influence of liposomal encapsulation on sodium cromoglycate pharmacokinetics in man. *Pharm Res.*, 6, 663-636.

Taylor, M.K., van Oort, M., Hickey, A.J., 2002. *In vitro* dissolution screening method for evaluation of drug release properties of engineered, sustained release inhalation particles. In: Byron, P.R., Dalby, R.N., Preat, V., (Eds.) *Respiratory Drug Delivery VIII, Vol 2*, 447-449.

Thanoo, B.C., Sunny, M.C., Jayakrishnan, A., 1992. Cross-linked chitosan microspheres: preparation and evaluation as a Matrix for the controlled release of pharmaceuticals. *J. Pharm. Pharmacol.*, 44, 283-286.

Thien, M., Maitz, A.H., Austin, M.A., 1982. Dissolution rates of airborne uranium in simulated lung fluid. *Health Physics*, 43, 587-590.

Tiwari, D., Goldman, D., Dixit, S., Malick, W.A., Madan, P.L., 1998. Compatibility evaluation of metered dose inhaler valve elastomers with tetrafluoroethane (P134a), a non-CFC propellant. *Drug Dev. Ind. Pharm.*, 24, 345-352.

Urbanski, J.J., 1991. Continuation of tempering after production. *The Manufacturing Confectioner*, 71, 126-130.

USP, United States Pharmacopoeia 24, 2000. US Pharmacopoeial convention, Rockville, MD.

Vasile, M.J., Nassar, R., Xie, J., Guo, H., 1999. Microfabrication techniques using focused ion beams and emergent applications. *Micron*, 30, 235-244.

Venkatraman, S., Gale, R., 1998. Skin adhesives and skin adhesion 1. Transdermal drug delivery systems. *Biomaterials*, 19, 1119-1136.

Verveat, C. Byron, P.R., 1999. Drug-surfactant-propellant interactions in HFA-formulations. *Int. J. Pharm.*, 186, 13-30.

Vidgren, M.T., Vidgren, P.A., Paronen, T.P., 1987. Comparison of physical and inhalation properties of spray dried and mechanically micronised disodium cromoglycate. *Int. J. Pharm.*, 35, 139-144.

Wang, F-J., Wang, C-H., 2002. Sustained release of etanidazole from spray-dried microspheres prepared by non-halogenated solvents. *J. Controlled Release*, 81, 263-280.

Wang, J., Ben-Jebria, A., Edwards, D.A., 1999. Inhalation of estradiol for sustained systemic delivery. *J. Aerosol Med. Deposition, Clearance and Effects in the Lung.*, 12, 27-36.

Ward, G.H., Shultz, R.K., 1995. Process-induced crystallinity changes in albuterol sulfate and its effects on powder physical stability. *Pharm Res.*, 12, 773-779.

Weda, M., Zanen, P., de Boer, A.H., Gjaltema, D., Ajaoud, A., Barends, D.M., Frijlink, H.W., 2002. Equivalence testing of salbutamol dry powder inhalers: in vitro impaction results versus in vivo efficacy. *Int. J. Pharm.*, 249, 247-255.

Weibel, E.R., 1963. *Morphometry of the Human Lung*, 1st Ed., Academic Press, New York.

Wendel, S., Celik, M., 1997. An overview of spray-drying applications. *Pharm. Tech.*, 10, 124-156.

Westesen, K., Bunjes, H., Koch, M.H.J., 1997. Physicochemical characterization of lipid nanoparticles and evaluation of their drug loading capacity and sustained release potential. *J. Controlled Release*, 48, 223-236.

Wetterlin, K., 1988. Turbohaler, a new powder inhaler for administration of drug to the airways. *Pharm Res.*, 5, 506-508.

WHO, World Health Organisation, 2000. *Bronchial Asthma Fact Sheet 206*. (from www.who.org).

Williams, A.S., Taylor, G., 1992. Synthesis, characterization and release of cromoglycate from dextran conjugates. *Int. J. Pharm.*, 83, 233-239.

Williams III, R.O., Barron, M.K., Alonso, A.J., Remunan-Lopez, C., 1998. Investigation of a pMDI system containing microspheres and P134a. *Int. J. Pharm.*, 174, 209-222.

Williams III, R.O., Patel, A.M., Barron, M.K., Rogers, T.L., 2001. Investigation of some commonly available spacer devices for the delivery of glucocorticoids steroids from a pMDI. *Drug Dev. Ind. Pharm.*, 27, 401-412.

Wise, D.L., 2000. *Handbook of pharmaceutical controlled release technology*, 1st Ed., Marcel Dekker, New York.

York, P., 1992. Crystal engineering and particle design for the powder compaction process. *Drug Dev. Ind. Pharm.*, 18, 677-721.

Zanen, P., Go, L.T., Lammers, J.W., 1996. Optimal particle size for β -agonists and anticholinergic aerosols in patients with severe airflow obstruction. *Thorax*, 51, 977-980.

Zeng, X.M., Martin, G.P., Marriott, C., 1995a. The controlled delivery of drugs to the lung. *Int. J. Pharm.*, 124, 149-164.

Zeng, X.M., Martin, G.P., Marriott, C., 1995b. The preparation and in vitro evaluation of tetrandine-entrapped albumin microspheres as an inhalation drug delivery system. *Eur. J. Pharm. Sci.*, 3, 87-93.

Zeng, X.M., Martin, G.P., Marriott, C., 2001. *Particulate interactions in dry powder formulations for inhalation*, 1st Ed., Taylor and Francis, London.

Ziller, K.H., Rupprecht, H.H., 1988. Control of crystal growth in drug suspension. 1. Design of a control unit and application to acetaminophen solutions. *Drug Dev. Ind. Pharm.*, 14, 2341-2370.